AD-A135 409 DAMPING MATERIALS FINITE ELEMENTS AND SPECIAL PROJECTS 1/3
(U) DAYTON UNIV OH RESEARCH INST M RUDDELL ET AL.
DEC 82 UDR-TR-82-110 AFWAL-TR-82-4167 F33615-79-C-5108

UNCLASSIFIED F/G 14/2 NL

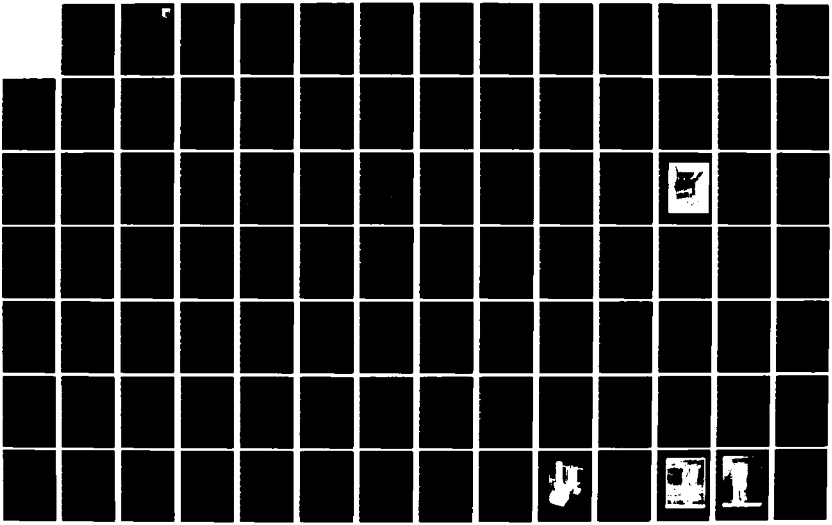

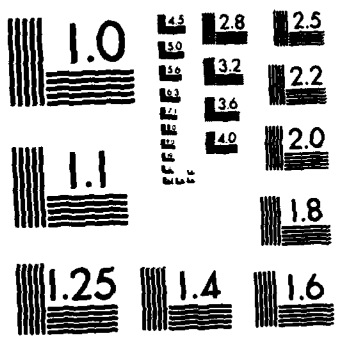

MICROCOPY RESOLUTION TEST CHART
NATIONAL BUREAU OF STANDARDS-1963-A

(12)

AFWAL-TR-82-4167

A135409

DAMPING MATERIALS, FINITE ELEMENTS AND SPECIAL PROJECTS

UNIVERSITY OF DAYTON
RESEARCH INSTITUTE
300 COLLEGE PARK AVENUE
DAYTON, OHIO 45469

DECEMBER 1982

FINAL REPORT FOR PERIOD OCTOBER 1979 - JULY 1982

APPROVED FOR PUBLIC RELEASE; DISTRIBUTION UNLIMITED

MATERIAL LABORATORY
AIR FORCE WRIGHT AERONAUTICAL LABORATORIES
AIR FORCE SYSTEMS COMMAND
WRIGHT-PATTERSON AIR FORCE BASE, OHIO 45433

8

NOTICE

When Government drawings, specifications, or other data are used for any purpose other than in connection with a definitely related Government procurement operation, the United States Government thereby incurs no responsibility nor any obligation whatsoever; and the fact that the government may have formulated, furnished, or in any way supplied the said drawings, specifications, or other data, is not to be regarded by implication or otherwise as in any manner licensing the holder or any other person or corporation, or conveying any rights or permission to manufacture use, or sell any patented invention that may in any way be related thereto.

This report has been reviewed by the Office of Public Affairs (ASD/PA) and is releasable to the National Technical Information Service (NTIS). At NTIS, it will be available to the general public, including foreign nations.

This technical report has been reviewed and is approved for publication.

David I.G. Jones

DAVID I.G. JONES, Project Engineer
Metals Behavior Branch
Metals and Ceramics Division
Materials Laboratory

John P. Henderson

JOHN P. HENDERSON, Chief
Metals Behavior Branch
Metals and Ceramics Division
Materials Laboratory

FOR THE COMMANDER:

LAWRENCE N. HJELM, Asst. Chief
Metals and Ceramics Division
Materials Laboratory

"If your address has changed, if you wish to be removed from our mailing list, or if the addressee is no longer employed by your organization please notify AFWAL/MLLN, *W-PAFB, OH 45433 to help us maintain a current mailing list".*

Copies of this report should not be returned unless return is required by security considerations, contractual obligations, or notice on a specific document.

UNCLASSIFIED

SECURITY CLASSIFICATION OF THIS PAGE (When Data Entered)

REPORT DOCUMENTATION PAGE		READ INSTRUCTIONS BEFORE COMPLETING FORM
1. REPORT NUMBER AFWAL-TR-82-4167	2. GOVT ACCESSION NO. AD-A135 409	3. RECIPIENT'S CATALOG NUMBER
4. TITLE (and Subtitle) DAMPING MATERIALS, FINITE ELEMENTS AND SPECIAL PROJECTS		5. TYPE OF REPORT & PERIOD COVERED Final Report for Period October 1979 - July 1982
		6. PERFORMING ORG. REPORT NUMBER UDR-TR-82-110
7. AUTHOR(s) Mark Ruddell, Philip A. Graf, Matthew F. Kluesener, David M. Hopkins, William Goddard, Robert J. Dominic, Mohan Soni		8. CONTRACT OR GRANT NUMBER(s) F33615-79-C-5108
9. PERFORMING ORGANIZATION NAME AND ADDRESS University of Dayton Research Institute, 300 College Park Avenue, Dayton, Ohio 45469		10. PROGRAM ELEMENT, PROJECT, TASK AREA & WORK UNIT NUMBERS 62102F 24180312
11. CONTROLLING OFFICE NAME AND ADDRESS Materials Laboratory(AFWAL/MLLN) Air Force Wright Aeronautical Laboratories (AFSC) Wright-Patterson Air Force Base, Ohio 45433		12. REPORT DATE December 1982
		13. NUMBER OF PAGES 209
14. MONITORING AGENCY NAME & ADDRESS(if different from Controlling Office)		15. SECURITY CLASS. (of this report) Unclassified
		15a. DECLASSIFICATION/DOWNGRADING SCHEDULE

16. DISTRIBUTION STATEMENT (of this Report)

Approved for public release; distribution unlimited.

17. DISTRIBUTION STATEMENT (of the abstract entered in Block 20, if different from Report)

18. SUPPLEMENTARY NOTES

19. KEY WORDS (Continue on reverse side if necessary and identify by block number)

Damping Materials
Test Techniques
Transducers
Turbine Blades
Finite Elements
Data Reduction

20. ABSTRACT (Continue on reverse side if necessary and identify by block number)

This report denotes work under the subject contract in the area of polymeric and enamel material damping properties measurement, finite element analsyis of damped components and some special projects, including state-of-the-art mobility measurement evaluations and development of a unique high temperature, high driving force electro-magnetic transducer.

DD FORM 1 JAN 73 1473 EDITION OF 1 NOV 65 IS OBSOLETE

UNCLASSIFIED

SECURITY CLASSIFICATION OF THIS PAGE (When Data Entered)

TABLE OF CONTENTS

TABLE OF CONTENTS
(concluded)

LIST OF ILLUSTRATIONS

LIST OF ILLUSTRATIONS
(continued)

LIST OF ILLUSTRATIONS
(continued)

LIST OF ILLUSTRATIONS
(continued)

LIST OF ILLUSTRATIONS
(continued)

LIST OF ILLUSTRATIONS
(continued)

LIST OF ILLUSTRATION
(concluded)

LIST OF TABLES

SECTION 1
MATERIALS

1.1 POLYMERIC MATERIALS

1.1.1 New Materials

The dynamic damping properties were determined for eleven commercial materials and two materials compounded by UDRI. The materials are listed in Table 1.1. The materials were tested by the resonant beam technique as discussed in AFWAL-TR-80-4093, "Polymeric Material Testing Procedures to Determine Damping Properties and the Results of Selected Commercial Materials." Nomograms for twelve of the materials are shown in Figures 1.1 through 1.12. Tabular data for these materials are in Appendix A.

One free layer material, DAP-1, (Allforce Acoustics) was difficult to test and the nomograph has not yet been produced. Although the raw data was consistent and believable, the reduced data contained negative and ridiculously high loss factor and modulus values for some points at temperatures above the damping peak. This was initially attributed to improper thickness and stiffness ratios of the composite beam. As a result, DAP-1 was tested in seven different configurations, using both steel and aluminum beams(Table 1.2) However, all of these combinations produced similar results. It is possible that DAP-1 becomes soft enough at temperatures above the damping peak to use in a sandwich configuration.

1.1.2 E•A•R C-1002

A representative of the E•A•R division of the Cabot Corporation questioned the validity and test method used to determine the damping properties of their vinyl-based damping material, C-1002.

C-1002 was tested by UDRI in a free-layer beam configuration because of its relatively high stiffness at room temperature. According to E•A•R, C-1002 should have been tested in a sandwich beam (shear) configuration. The results from the first beam test (Figure 1.13) indicate that near the high end of the test temperature range, the modulus of C-1002 approaches the upper limit for sandwich beam materials (100 MPa, as defined by the ASTM E-33 standard).

TABLE 1.1

NEW MATERIALS TESTED

Material	Manufacturer	Test Configuration
NPE-9047	3M	Shear (sandwich)
NPE-9046	3M	" "
ISD-468	3M	" "
MN	Soundcoat	" "
D	"	" "
N	"	" "
M	"	" "
LT	"	" "
C-1002	E•A•R (Cabot Corp.)	Free Layer (Oberst)
C-2003	" " "	" " "
DAP-1	Allforce Acoustics	Oberst & Modified Oberst
Butyl 268	UDRI	Shear (sandwich)
Butyl 268+ 60% carbon black	"	" "

TABLE 1.2

DAMPING LAYER AND BEAM COMBINATIONS USED TO TEST DAP-1

DAP-1 Thickness	Beam Thickness	Beam Material	Configuration
0.060-inch	0.080-inch	Aluminum	Oberst
0.060-inch	0.060-inch	Aluminum	Oberst
0.060-inch	0.068-inch	Steel	Oberst
0.060-inch	0.080-inch	Aluminum	Modified Oberst
0.020-inch	0.080-inch	Aluminum	Oberst
0.020-inch	0.068-inch	Steel	Oberst
0.020-inch	0.068-inch	Steel	Modified Oberst

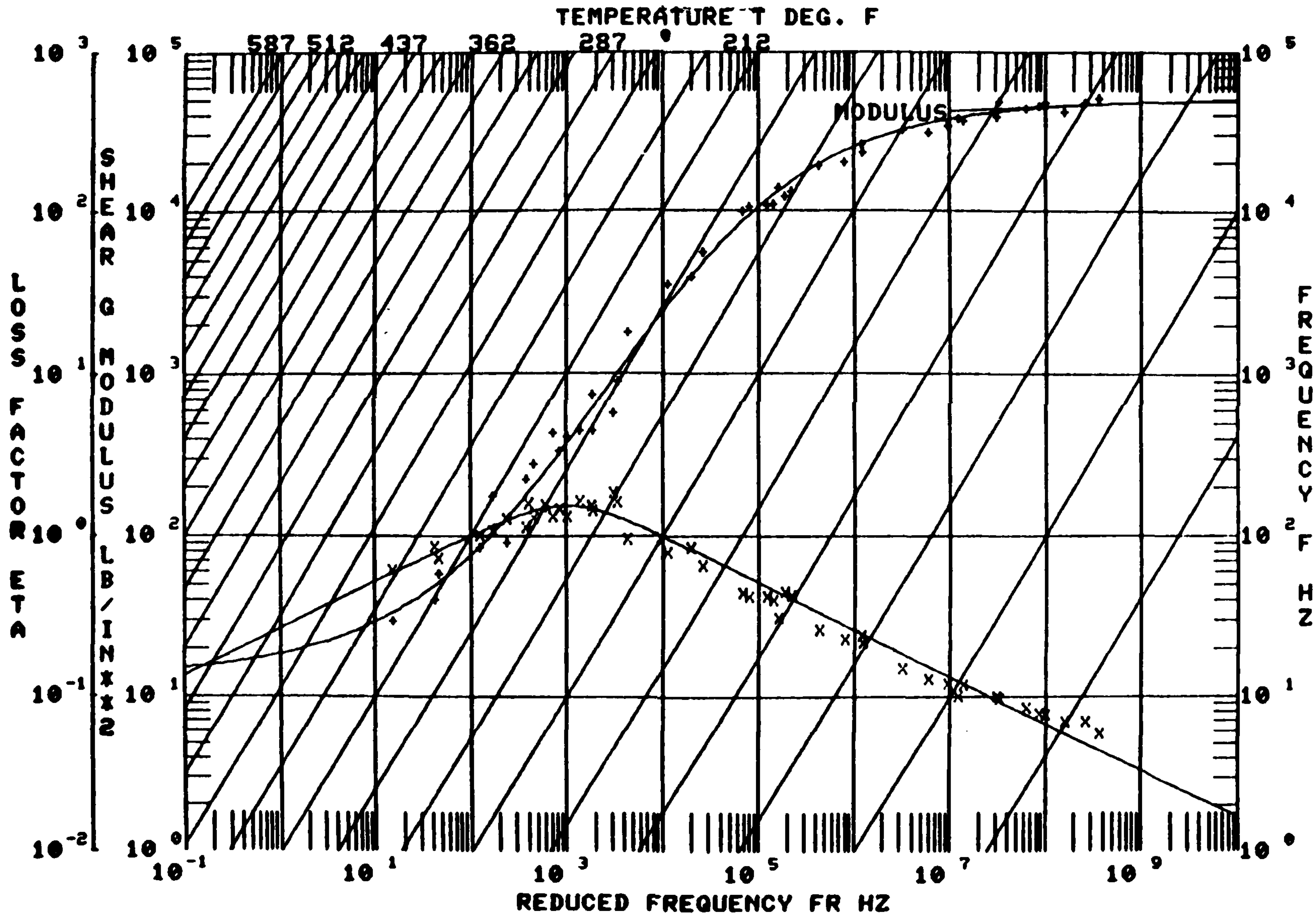

Figure 1.1. Nomogram for 3M NPE-9047 (NBN-51914-50-2).

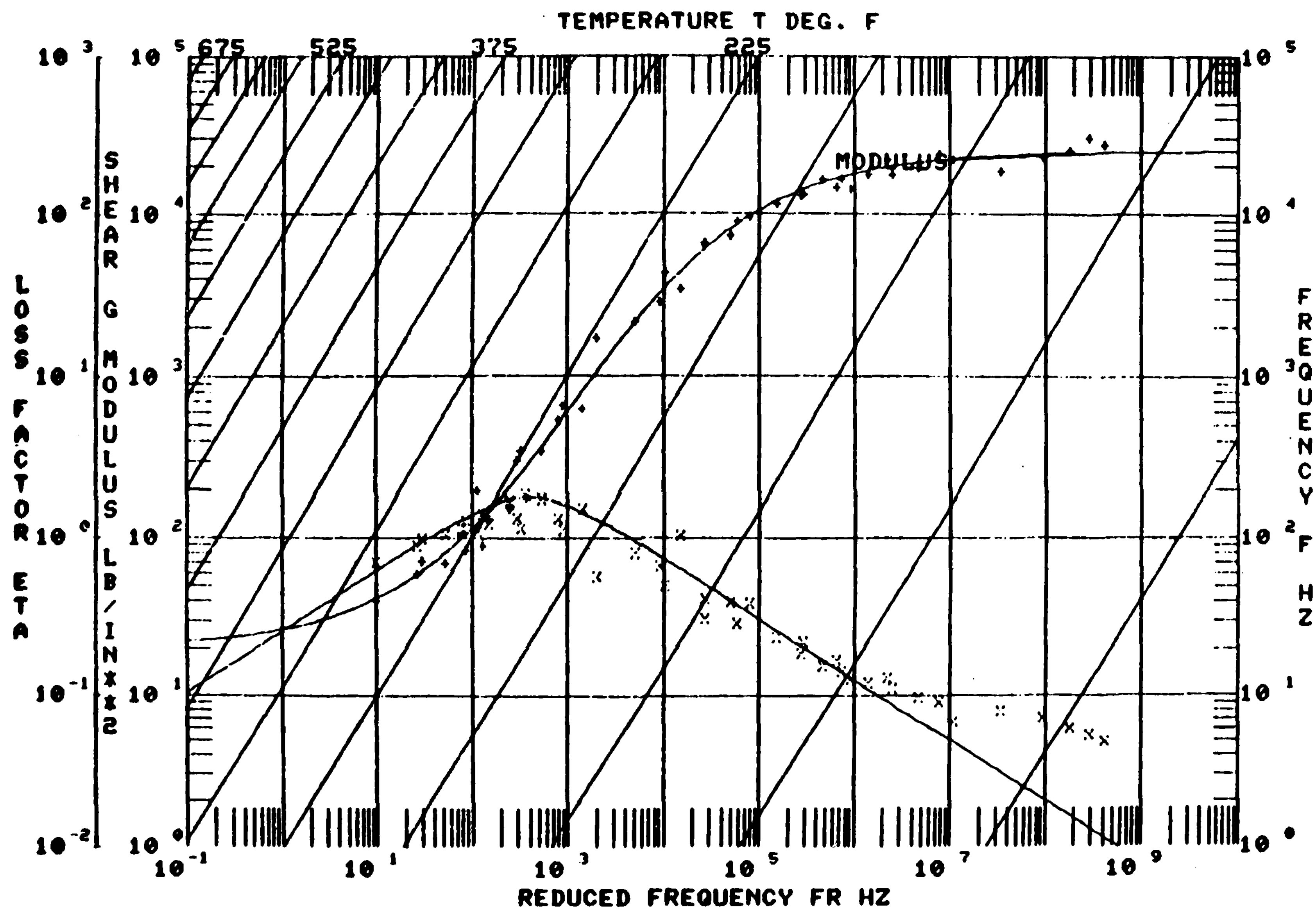

Figure 1.2. Nomogram for 3M NPE-9046 (NBN -51914-50-8).

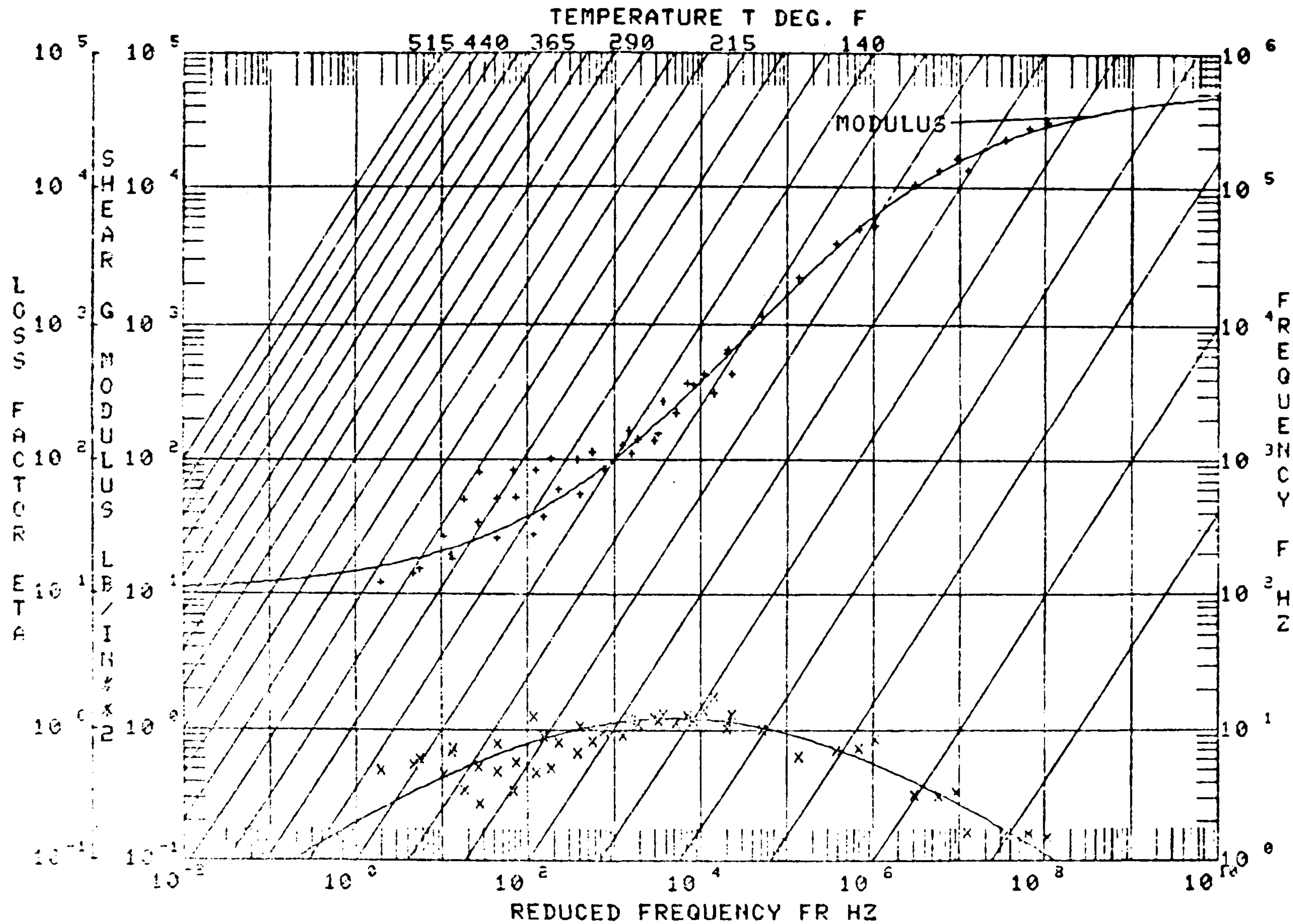

Figure 1.3. Nomogram for 3M ISD-468.

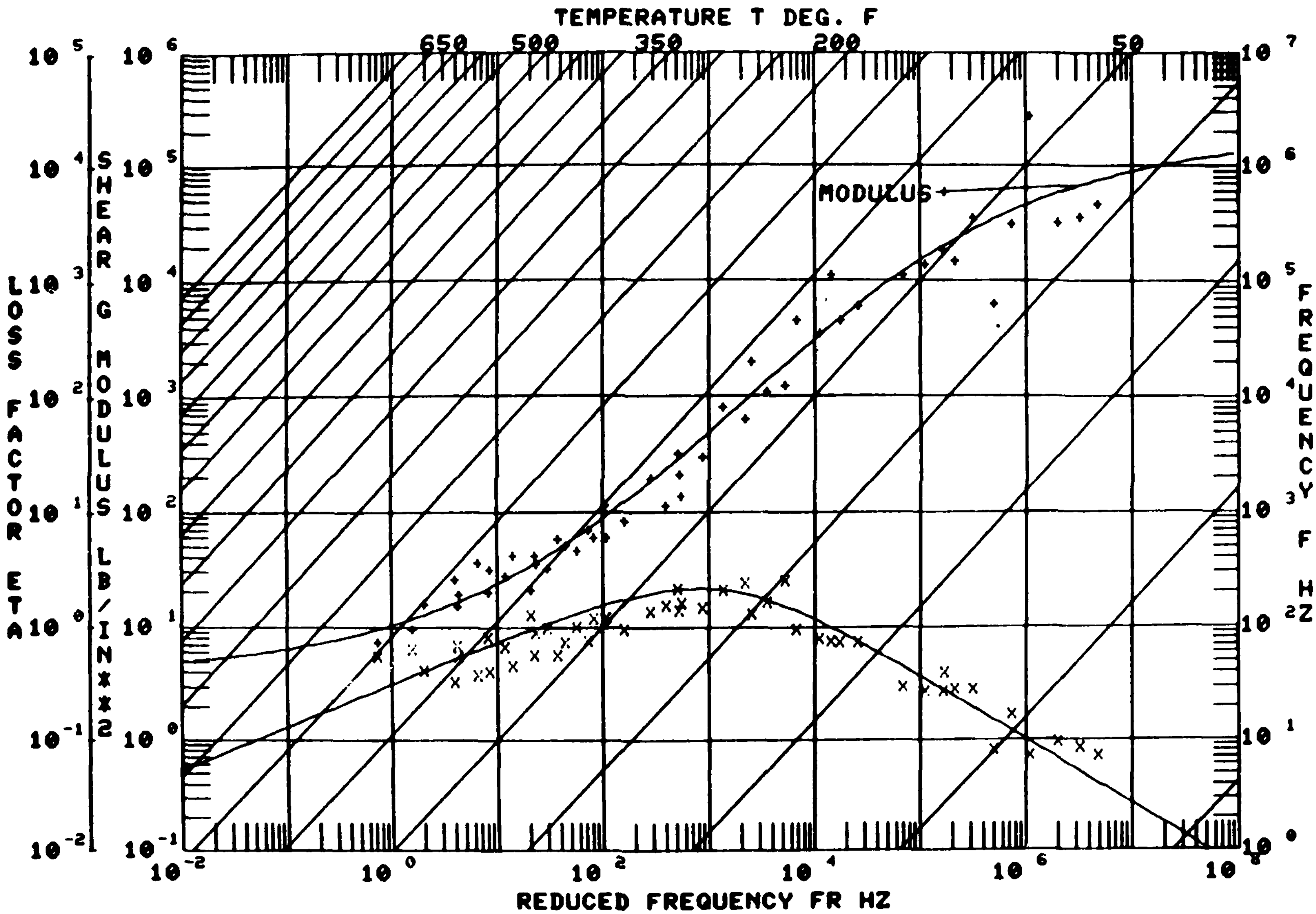

Figure 1.4. Nomogram for Soundcoat MN (121580).

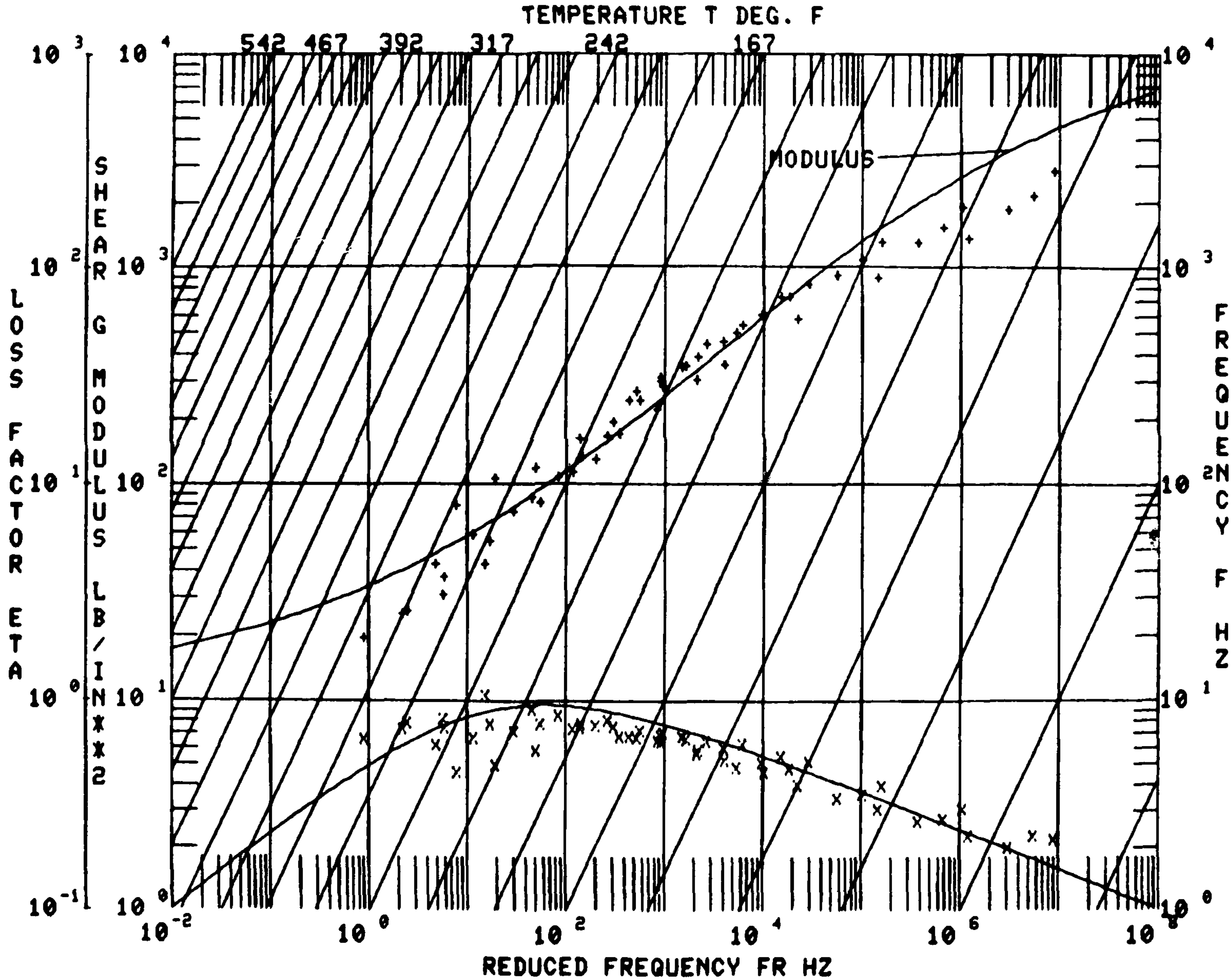

Figure 1.5. Nomogram for Soundcoat D.

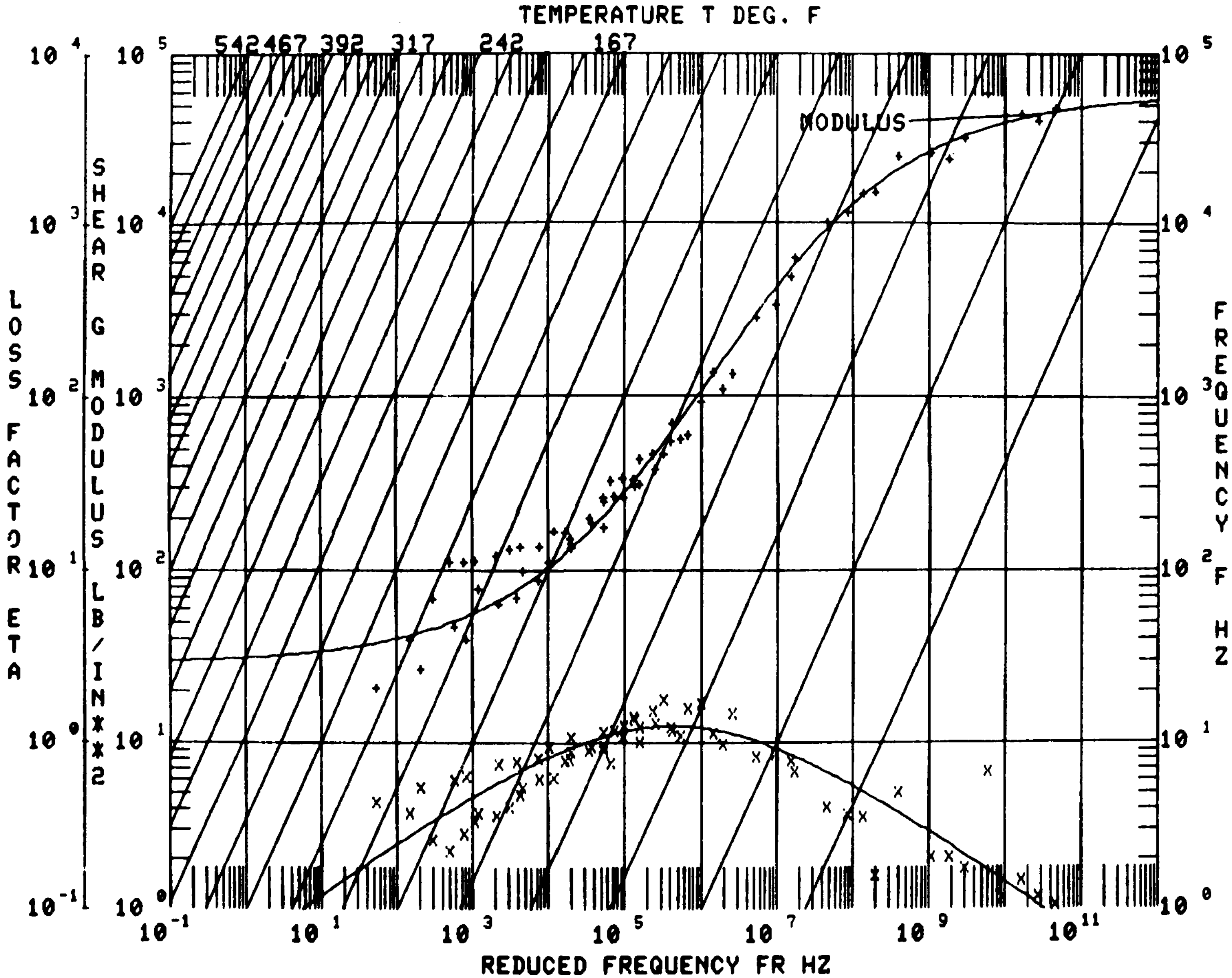

Figure 1.6. Nomogram for Soundcoat N

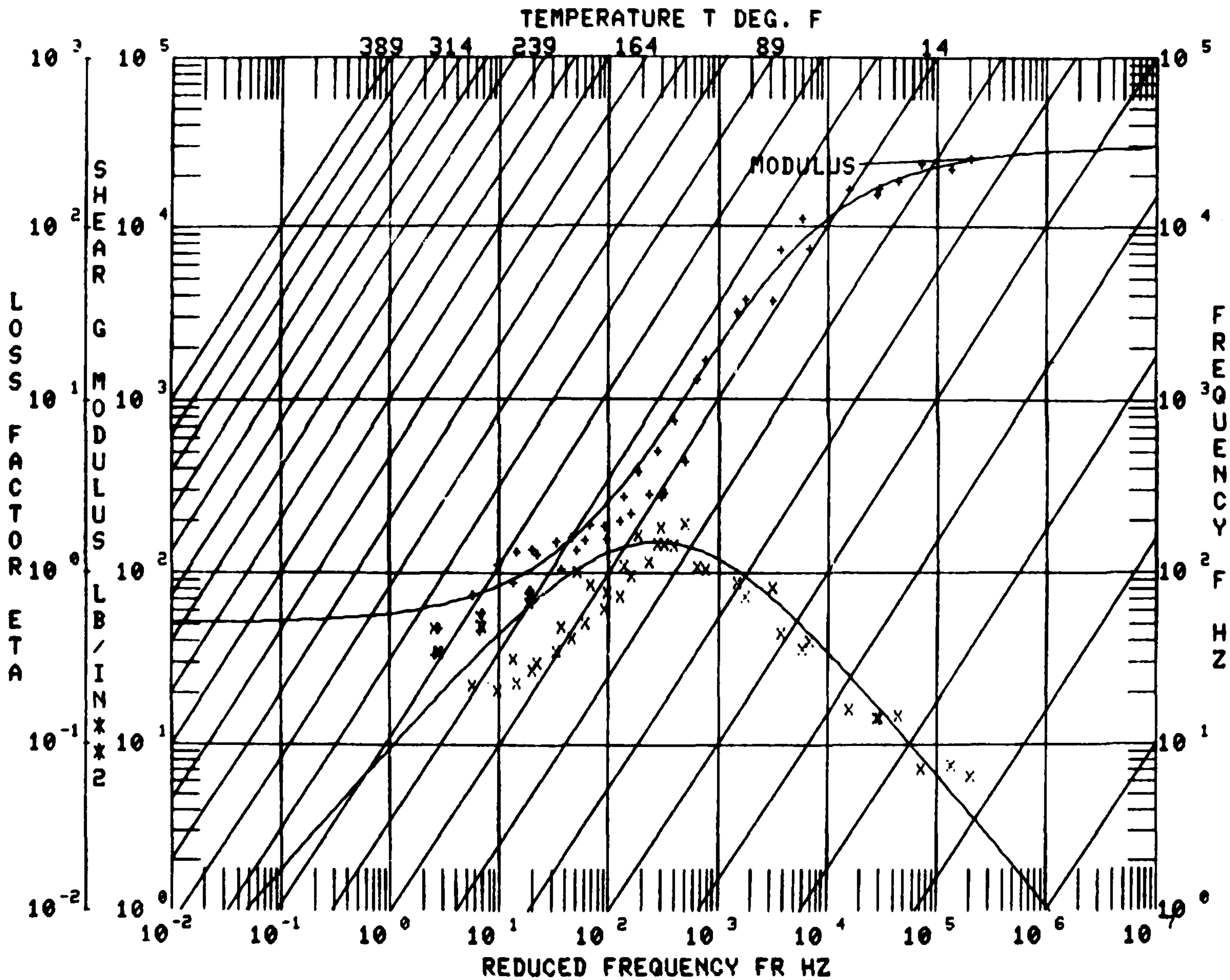

Figure 1.7. Nomogram for Soundcoat M

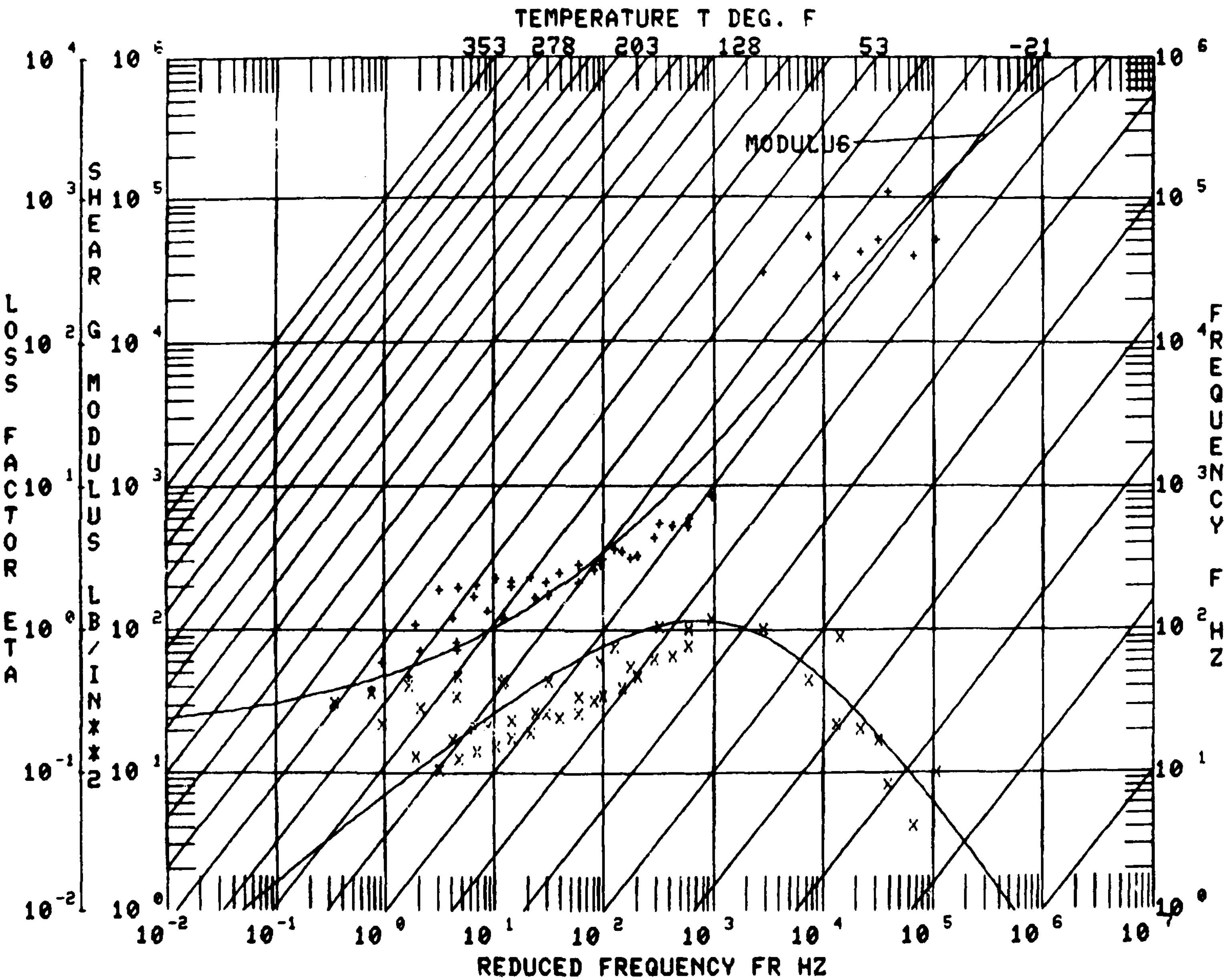

Figure 1.8. Nomogram for Soundcoat LT

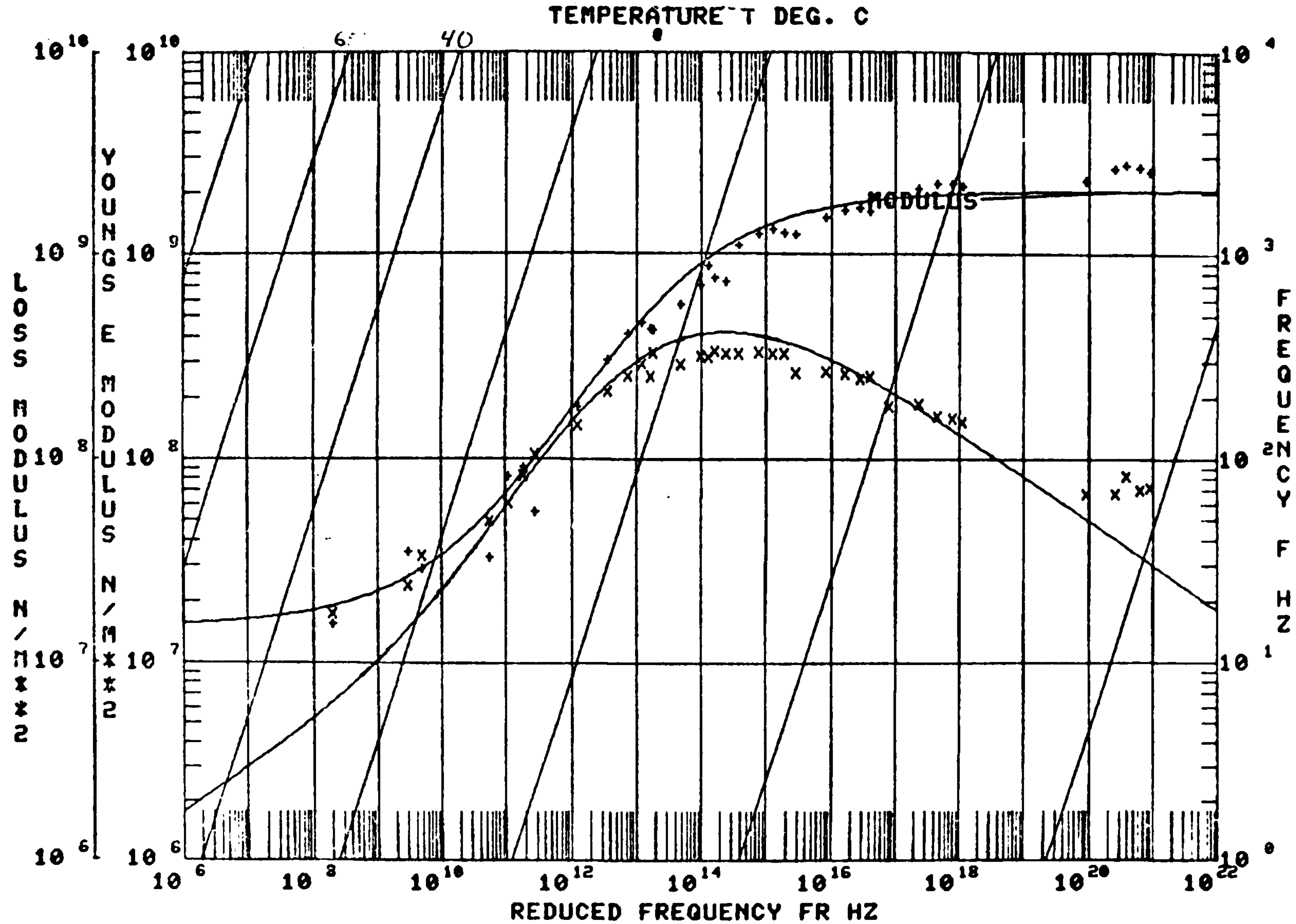

Figure 1.9. Nomogram for E·A·R C-1002

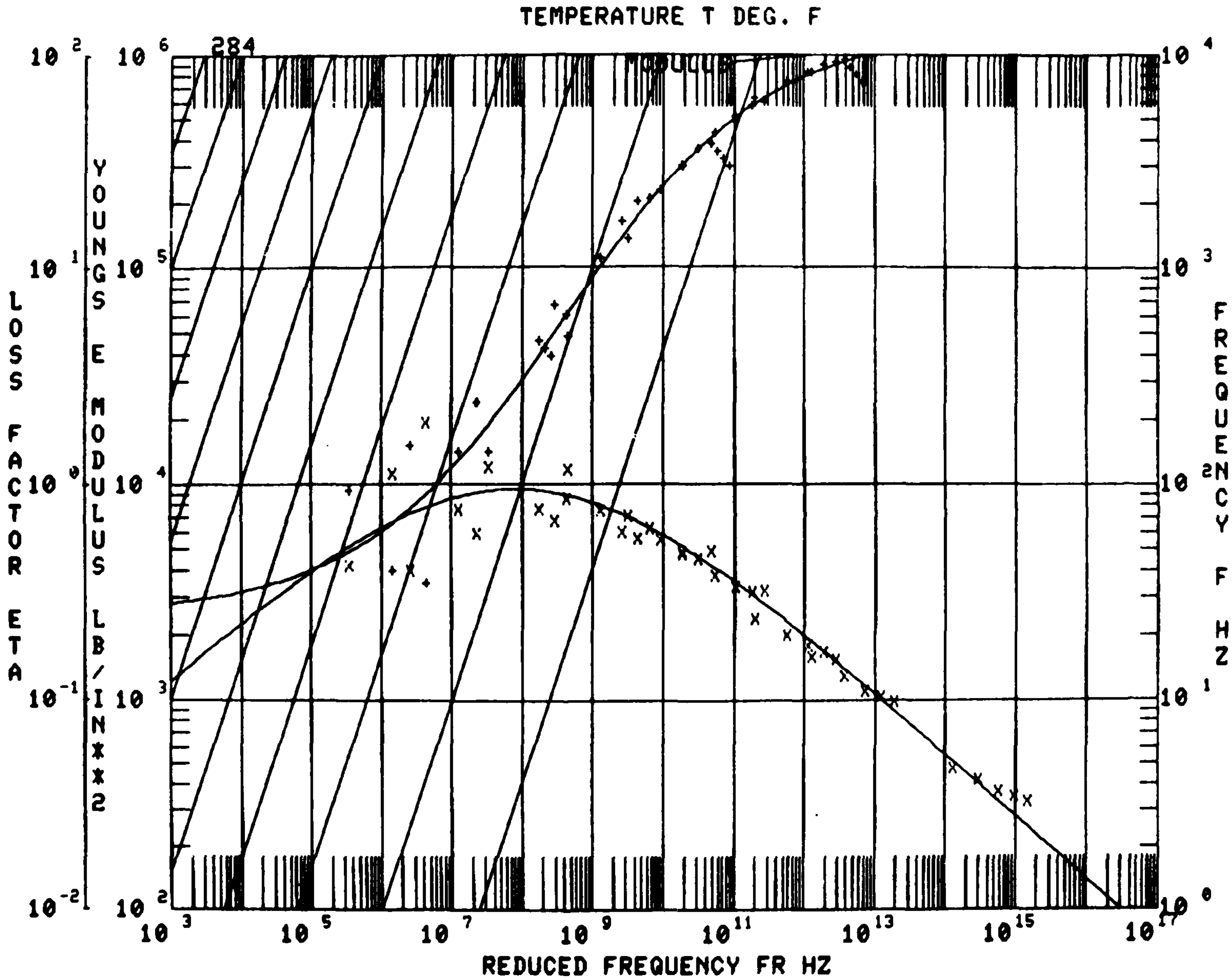

Figure 1.10. Nomogram for E·A·R C-2003

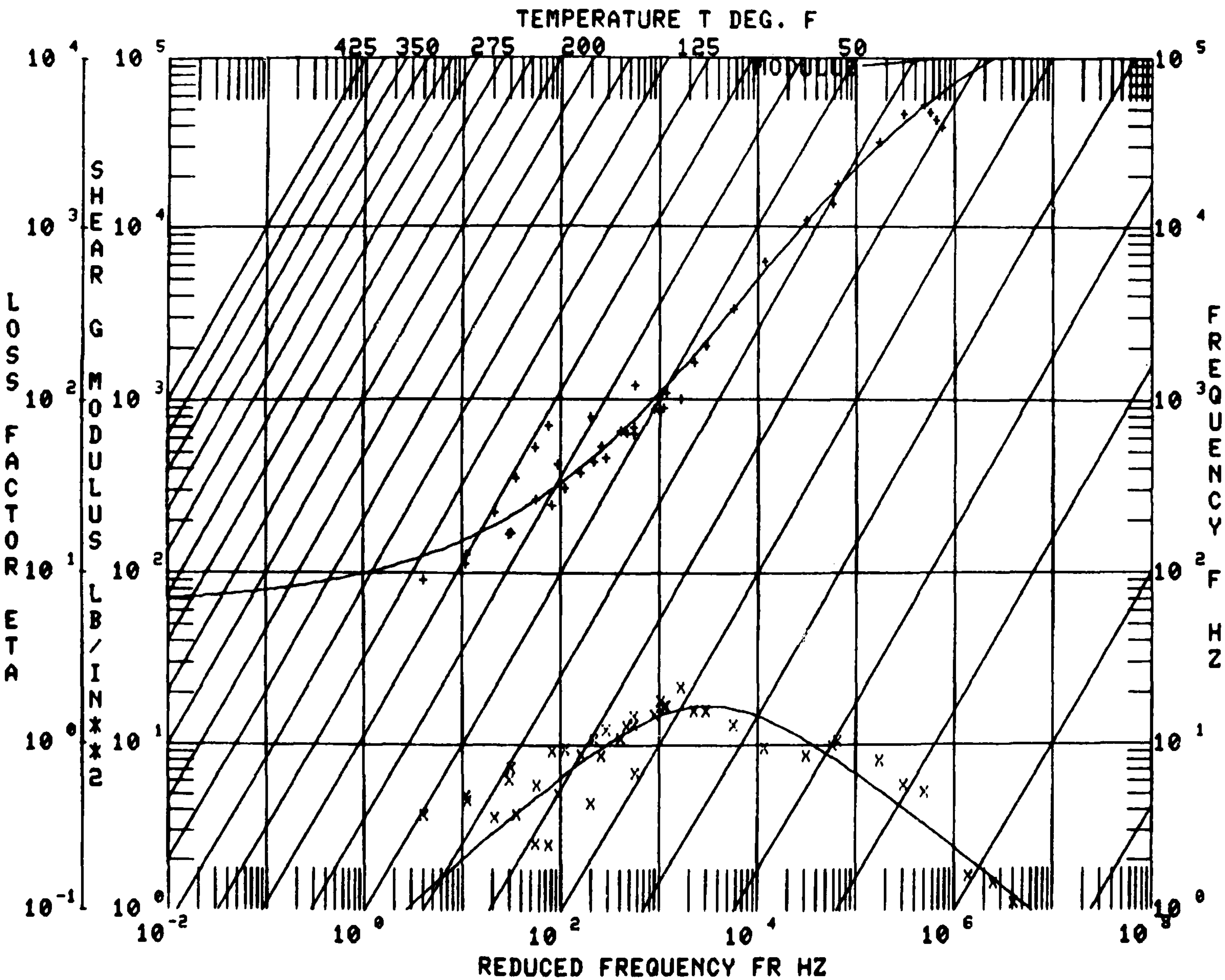

Figure 1.11. Nomogram for UDRI Butyl 268

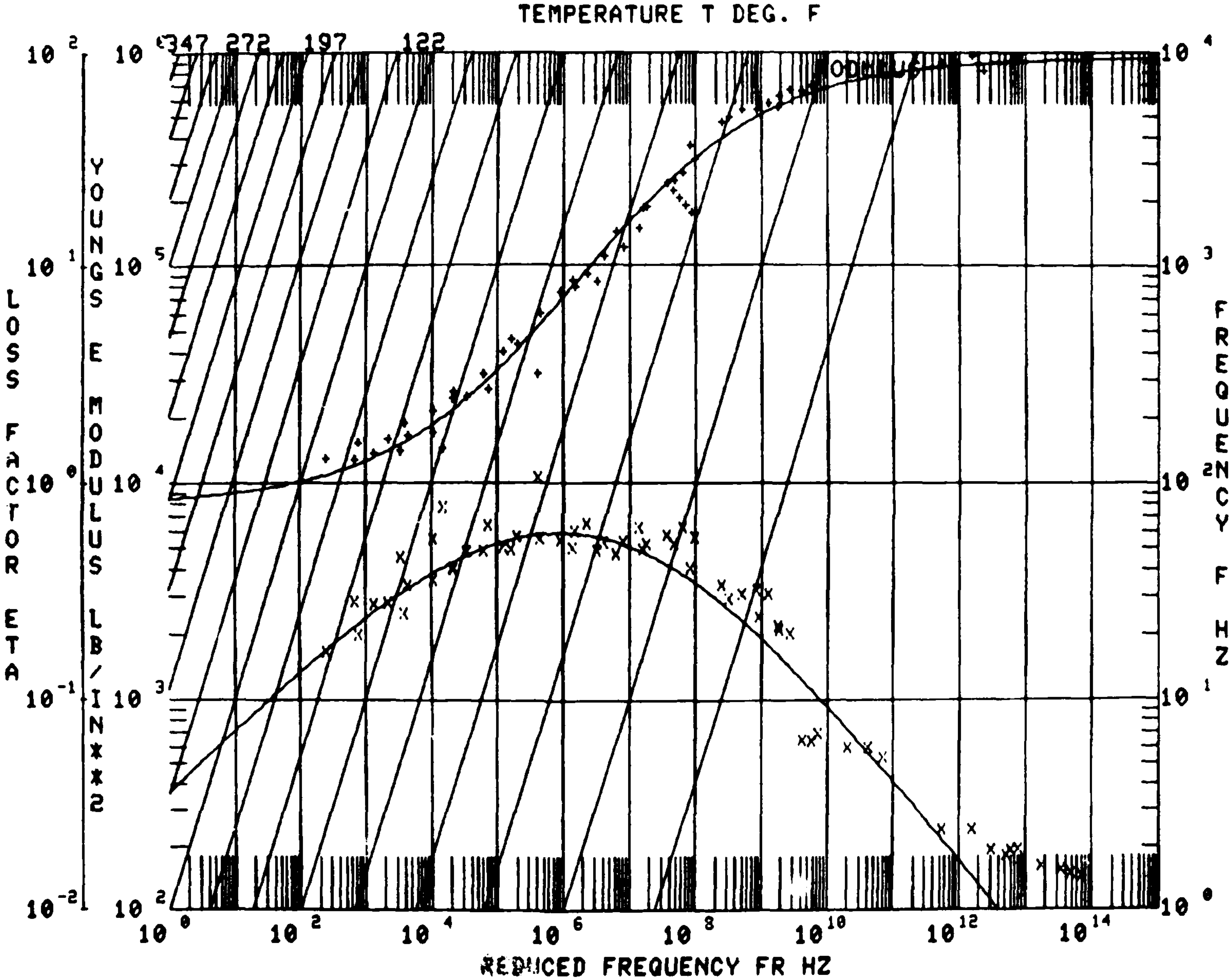

Figure 1.12. Nomogram for UDRI Butyl 268 + 60% Carbon Black

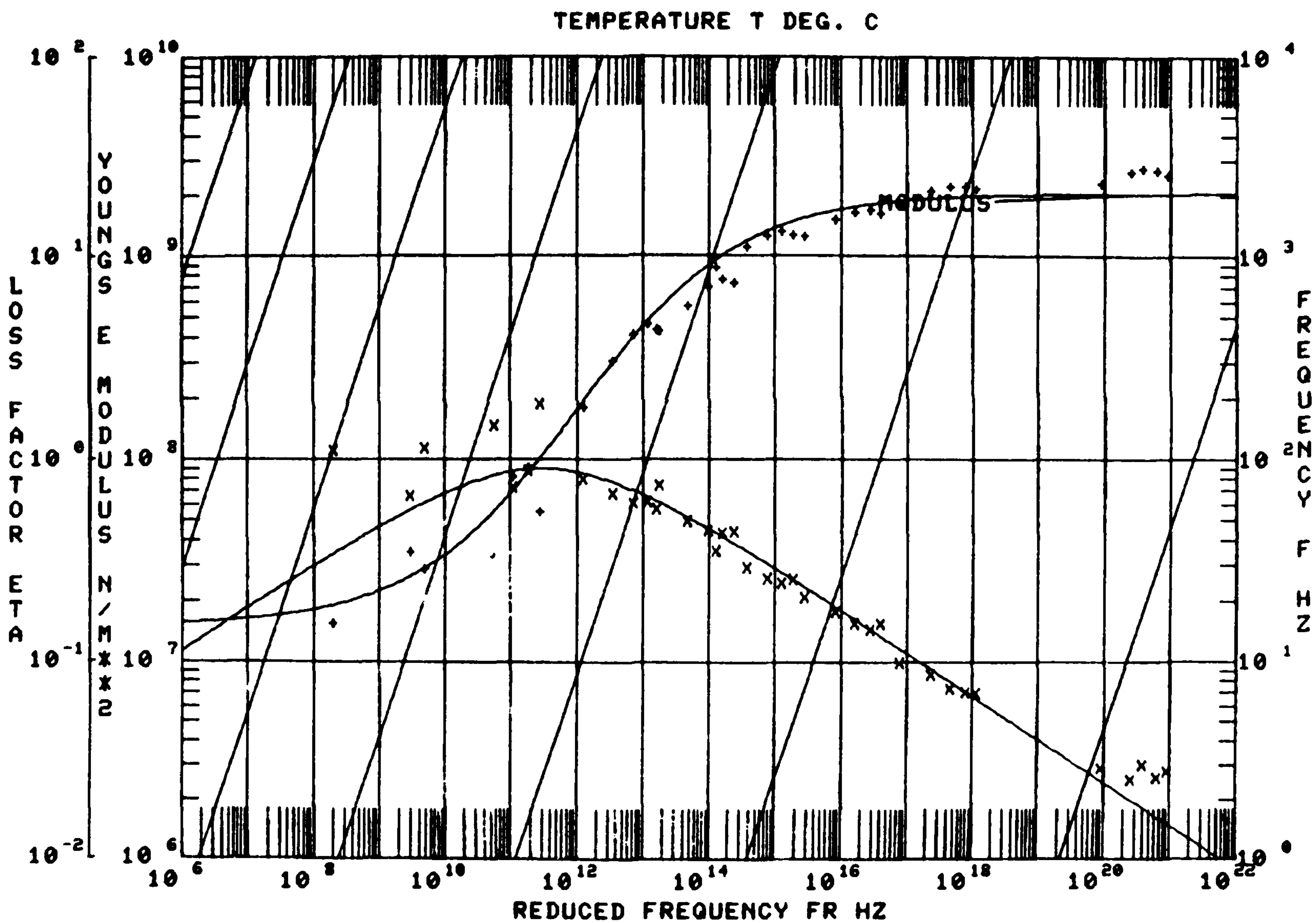

Figure 1.13. Nomograph of E·A·R C-1002.

To verify our beam test, a Dynamic Mechanical Analysis (DMA) was conducted on C-1002 to check the modulus and glass transition temperature. According to the DMA data (Figure 1.14) the glass transition occurred at -2°C (28.4°F), and the modulus drops to 100 MPa at approximately -8°C (17.6°F). The maximum modulus of C-1002 is about 4410 MPa, well above the upper limit for a sandwich beam test. The UDRI feels, therefore, that a free-layer beam test was the proper method of testing E•A•R C-1002.

1.1.3 ISD-110

It was suggested that ISD-110 should be retested in a sandwich beam configuration having a maximum structural loss factor of 0.2. The UDRI was supplied with a sample of 0.058 inch thick ISD-110. Computer predictions based on available beam pairs indicated that the test should be done with 0.068 inch stainless steel beams.

In addition to the stainless steel beam test, ISD-110 was tested on 0.080 inch aluminum beams, the Dynamic Mechanical Analyzer and the Reovibran. Due to the limitations of the Reovibran, the test sample was 0.002 inch thick ISD-110, and from a different batch than that used for the beam and DMA tests.

Figure 1.15 is the nomogram for ISD-110 which is commonly used at UDRI. Figures 1.16 through 1.19 are nomographs of the stainless steel beam, aluminum beam, DMA, and Reovibran tests of ISD-110. All of the nomographs show good correlations between loss factors, but some significant differences in modulus. Tabular data for these materials are in Appendix B.

1.1.4 ASTM E-33 Committee Testing

The UDRI participated in a "round robin" testing program conducted by the ASTM E-33 committee to aid in developing a national standard for evaluating polymeric materials. This involved the characterization of eight bare beams and the evaluation of six materials by the resonant beam technique. Raw data, reduced data, and reduced temperature nomograms were forwarded to the E-33 committee on completion.

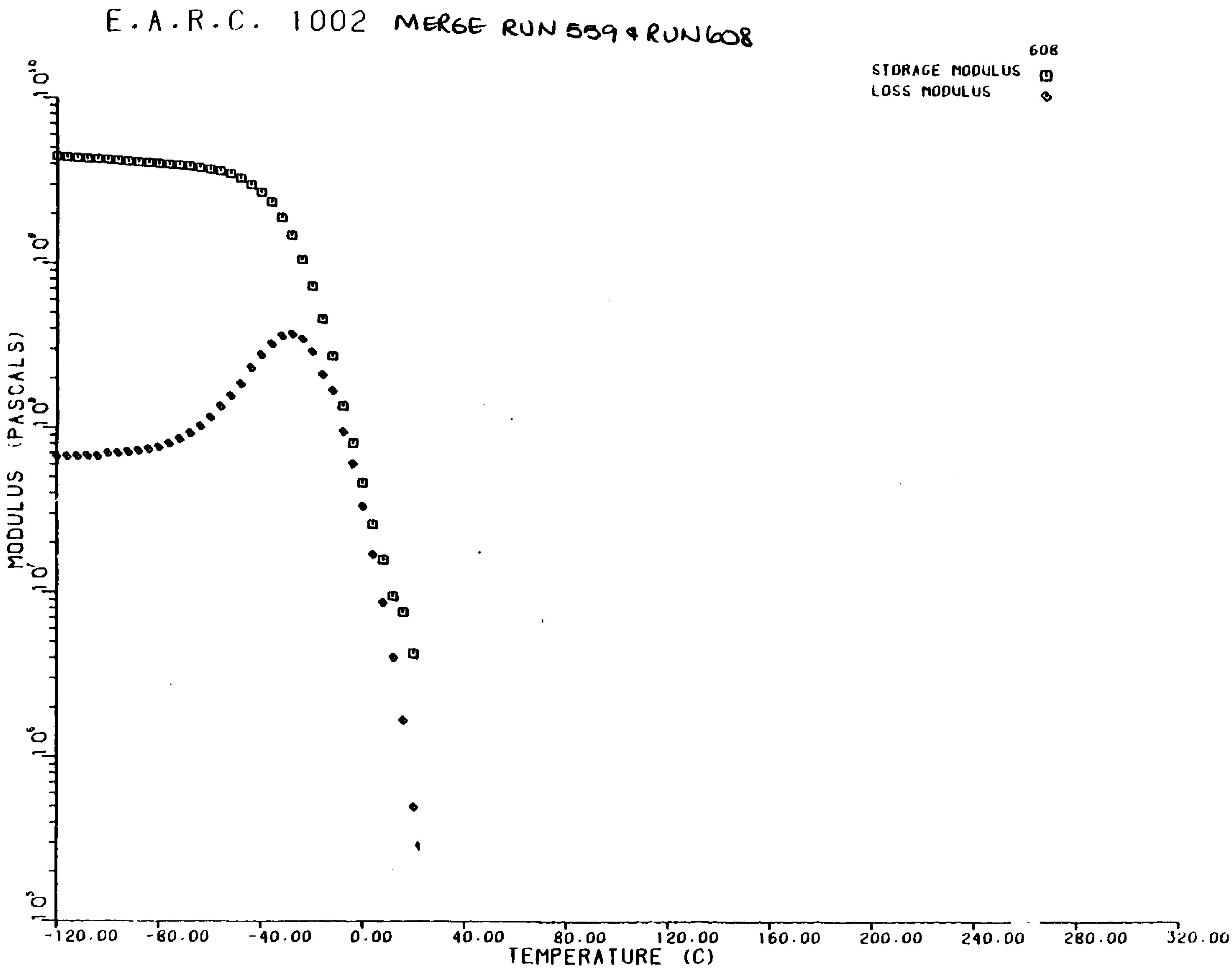

Figure 1.14. Data from DMA Test of E·A·R C-1002.

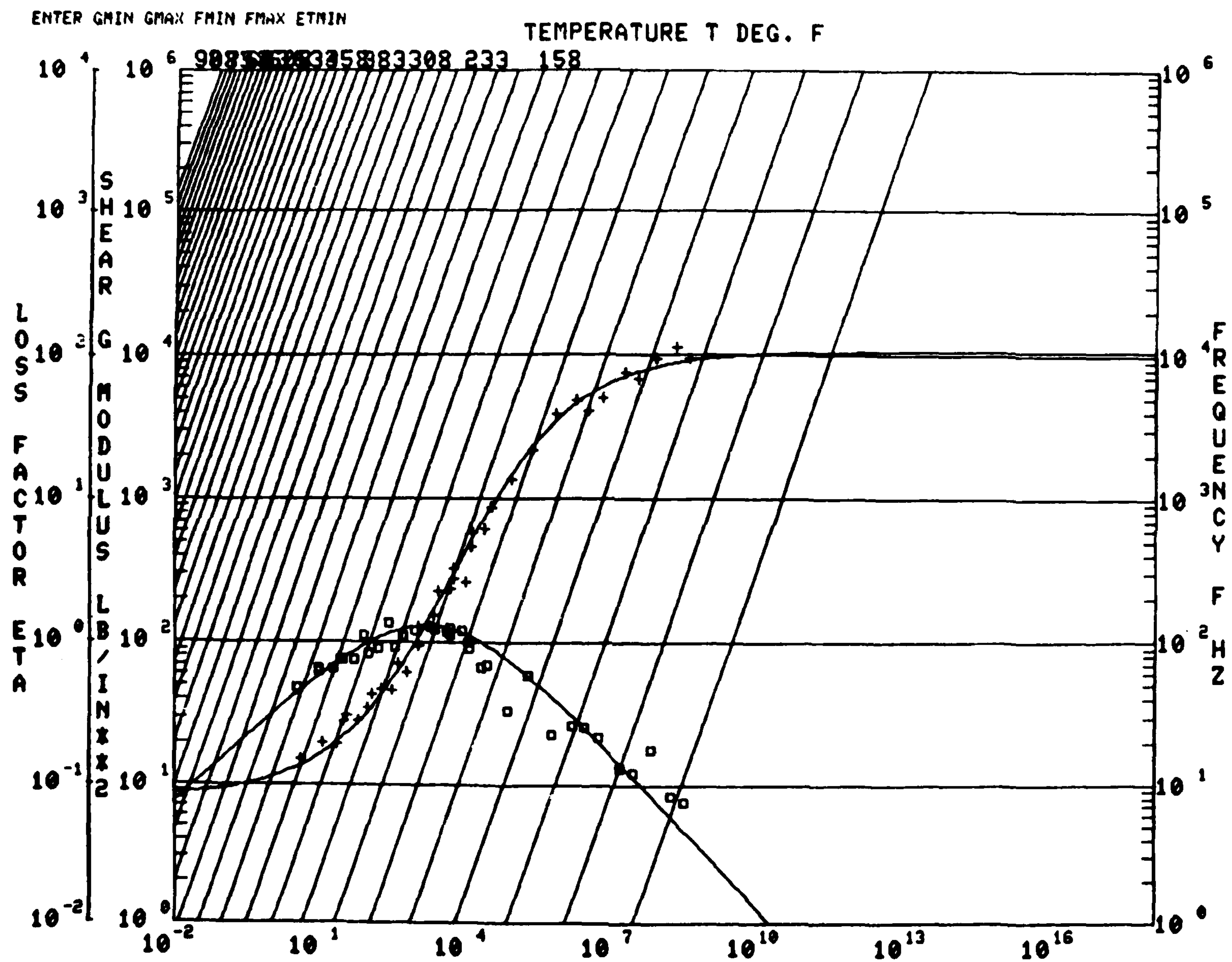

Figure 1.15. 0.005" ISD-110 on 0.060" Aluminum Beams.

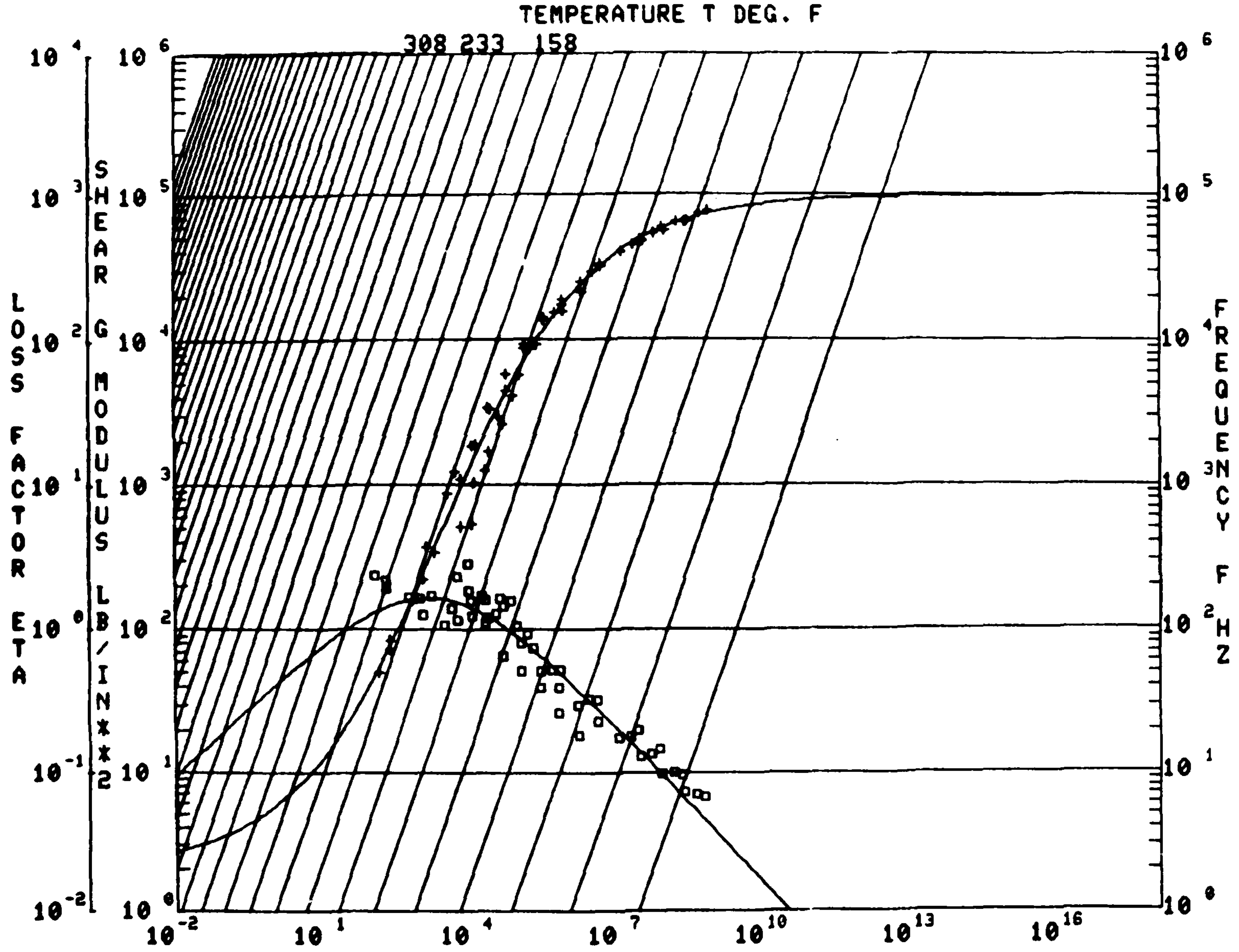

Figure 1.16. 0.058" ISD-110 on 0.068" Stainless Steel Beams

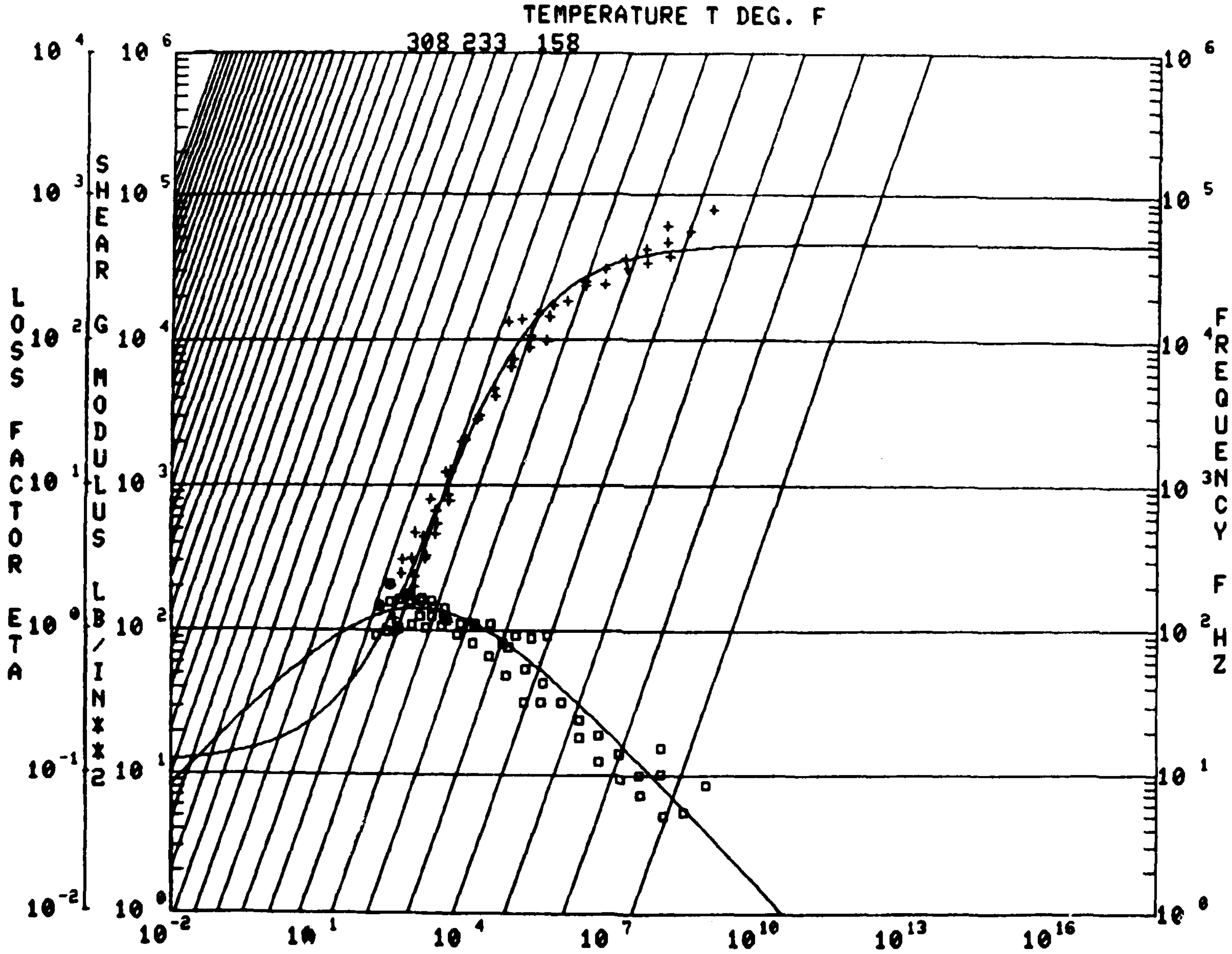

Figure 1.17. 0.058" ISD-110 on 0.080" Aluminum Beams

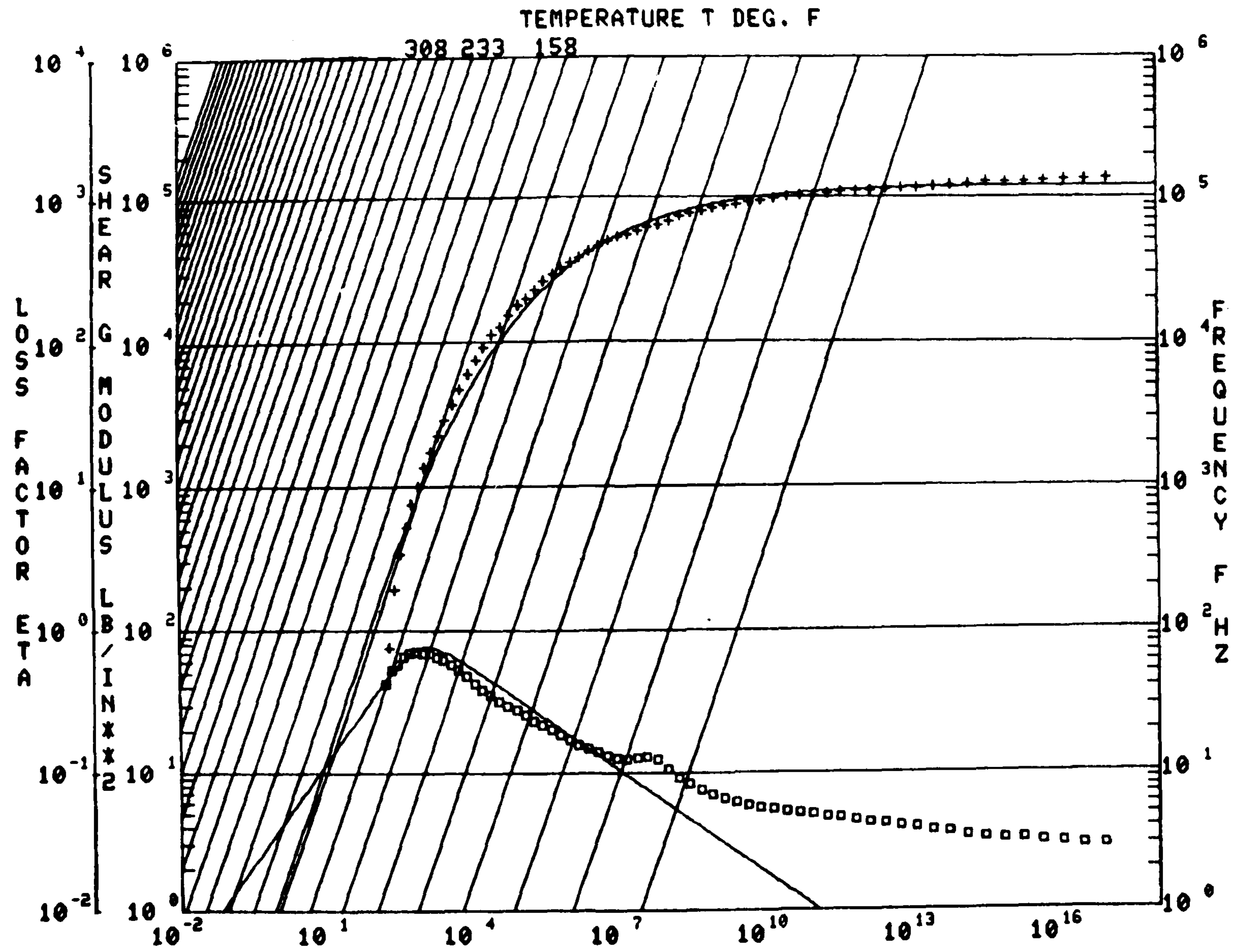

Figure 1.18. 0.058" ISD-110, DMA Test

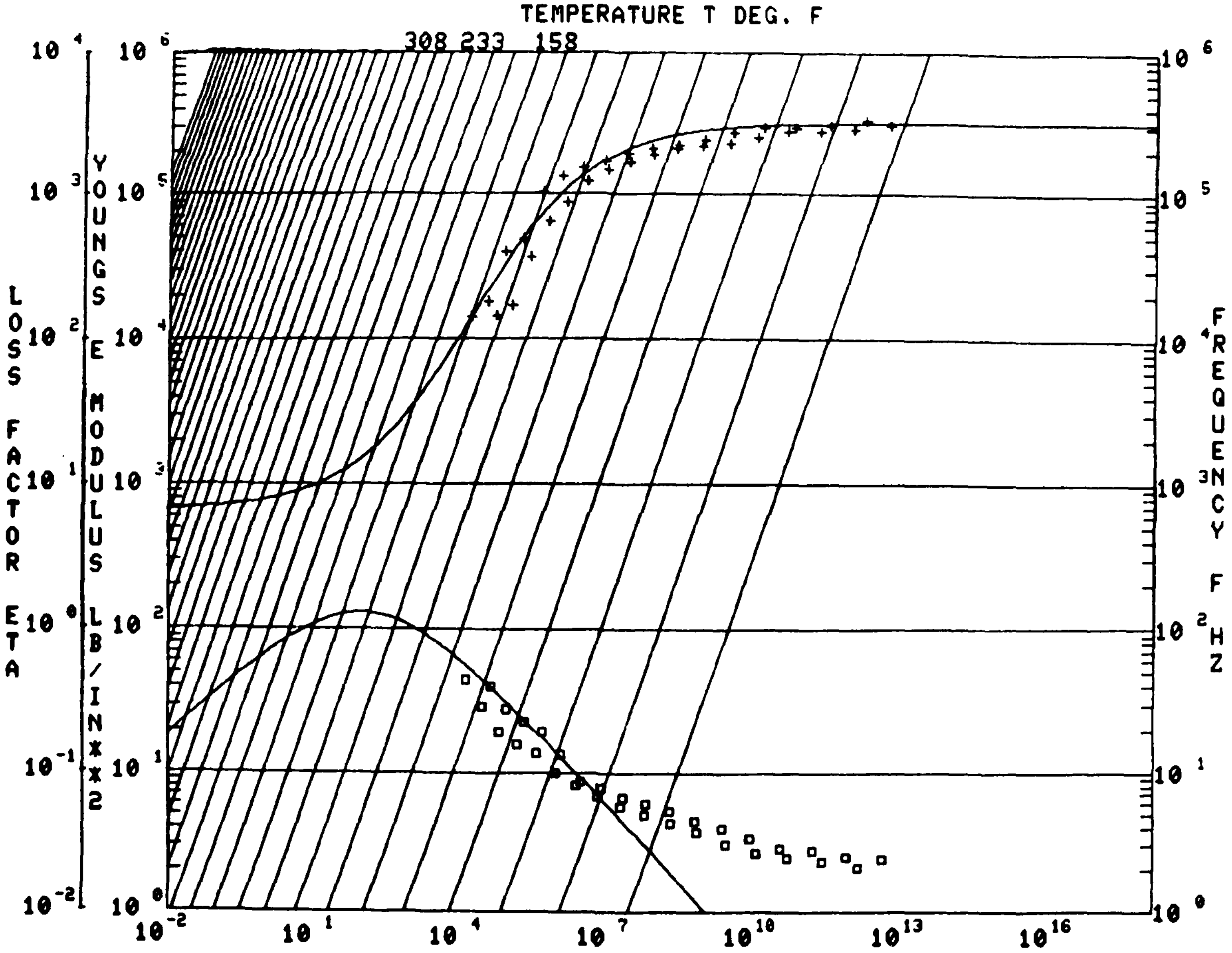

Figure 1.19. 0.002" ISD-110, Reovibran Test

1.2. VITREOUS ENAMELS TESTING

Testing of vitreous enamels was conducted in support of several research and developmental efforts sponsored by AFWAL/MLLN. The testing effort was expended on high temperature characterization of damping properties of a variety of formulations, and the investigation of the effects on some formulations of extended exposure to hostile environments such as jet engine exhaust gases and/or high temperatures.

High temperature characterization was accomplished using the half-power bandwidth method to measure the structural damping of several bending modes, usually the second through sixth, over the appropriate temperature range. The test data were reduced to nomographs of material loss factor, material loss modulus, and Young's modulus versus reduced frequency and temperature using routines documented in Section 1.3 .

Environmental exposure studies were conducted in the Exhaust Gas Simulator or high temperature furnaces. Results were evaluated by the half-power bandwidth method, visual inspection, X-ray diffraction, scanning electron microscopy, or optical microscopy as appropriate. This section presents descriptions of the testing facilities used and the procedures followed, and brief discussion of the projects supported.

1.2.1. Determination of Material Properties

The definition of vibration damping properties by the Oberst beam testing technique involves four main steps. The damping characteristics of the uncoated beam specimen are determined by the resonant beam technique. After the base line data for the test beam is known, the beam is then coated with the high temperature damping material to be evaluated. The composite beam is then tested to obtain the damping characteristics of the coated specimen. The data from the uncoated and coated beam tests are then combined and entered into a computer program which defines the material's storage modulus, loss modulus, and loss factor of the specific temperatures and modes as determined from the beam tests. A reduced frequency nomograph is developed from these material properties by means of another computer program. This nomograph displays the vibration damping properties of the materials as a function of temperature and frequency for a temperature and frequency range which extends beyond that of the test data.

1.2.1.1. High Temperature Enamels Test Apparatus

The apparatus used for high temperature characteristics testing consists of a constant pressure cantilever test fixture, a controlled modified tube furnace, an excitation system consisting of an electromagnetic transducer (refrigerant cooled) with its driving and monitoring circuitry, and a response force measuring system.

High Temperature Cantilever Test Fixture

The high temperature enamels cantilever test fixture was developed to maintain a constant clamping force on the test specimen as the temperature is varied over the test range, and to transmit the motion of the test specimen to the force gage located outside the high temperature furnace. The high temperature enamels damping fixture number one is illustrated in Figure 1.20. The fixture consists of an isolated table, clamping fixture, force couple, force gage, and air cylinder. The table is a platform mounted to a wooden frame by isolation mounts. A metal plate is attached to the table. The clamping fixture is two blocks machined from Inconel Alloy Number 625. Two bolts machined from Inconel Alloy 625 pass through grooves along the side of the blocks and through the table and are attached to the top of a force link. The test specimen is inserted between the blocks and approximately 50 psi applied to the air cylinder providing a constant clamping force to the root of the specimen. The air cylinder is a major innovation for this system. Any bolting system used to apply clamping pressure lost torque at the higher temperatures. The air cylinder takes into account any thermal expansion and this results in a constant clamping pressure over the entire temperature range. Vibrations in the beam are mechanically transmitted to the force link via the fixture block and bolts. Fixture number two (illustrated in Figure 1.21) is

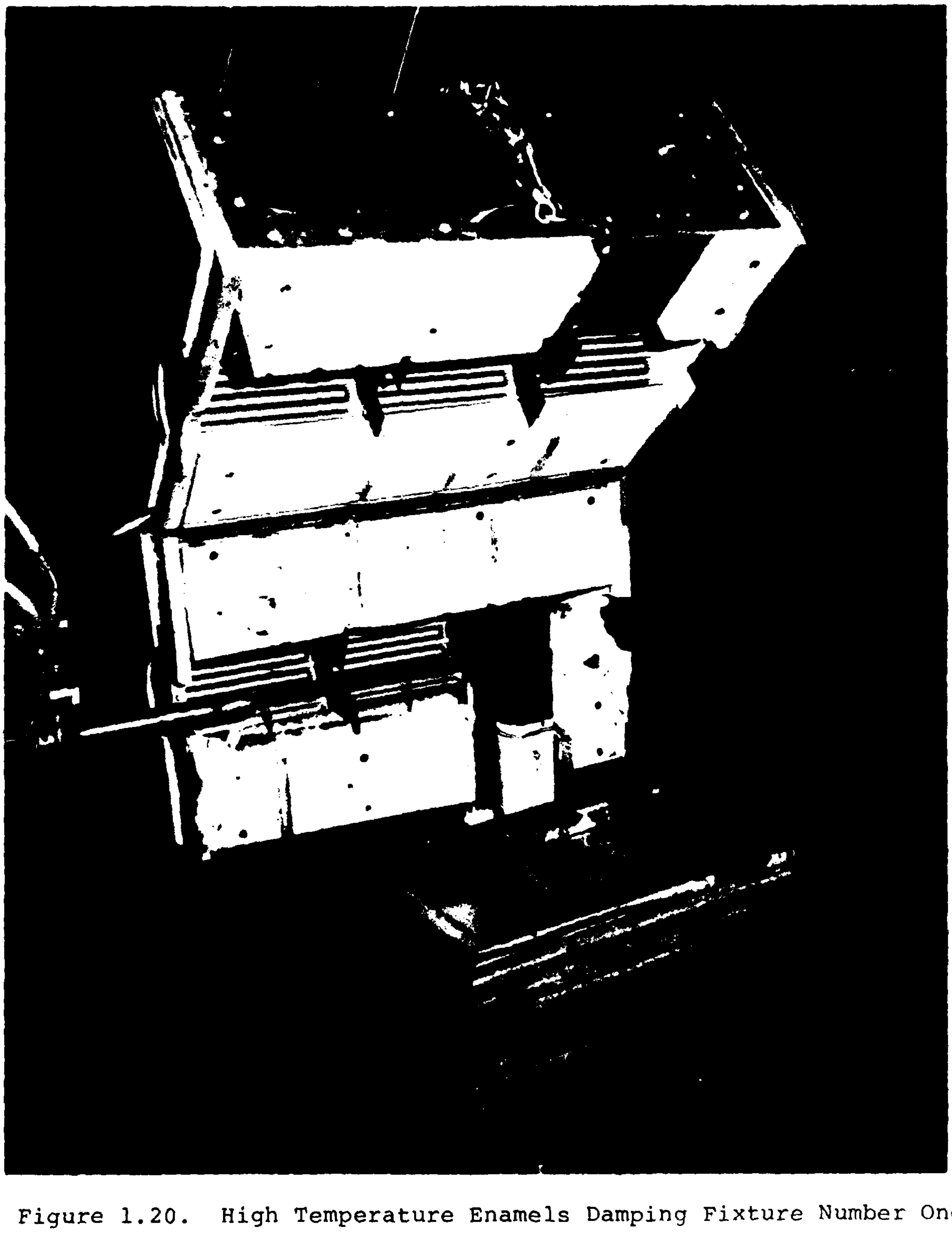

Figure 1.20. High Temperature Enamels Damping Fixture Number One.

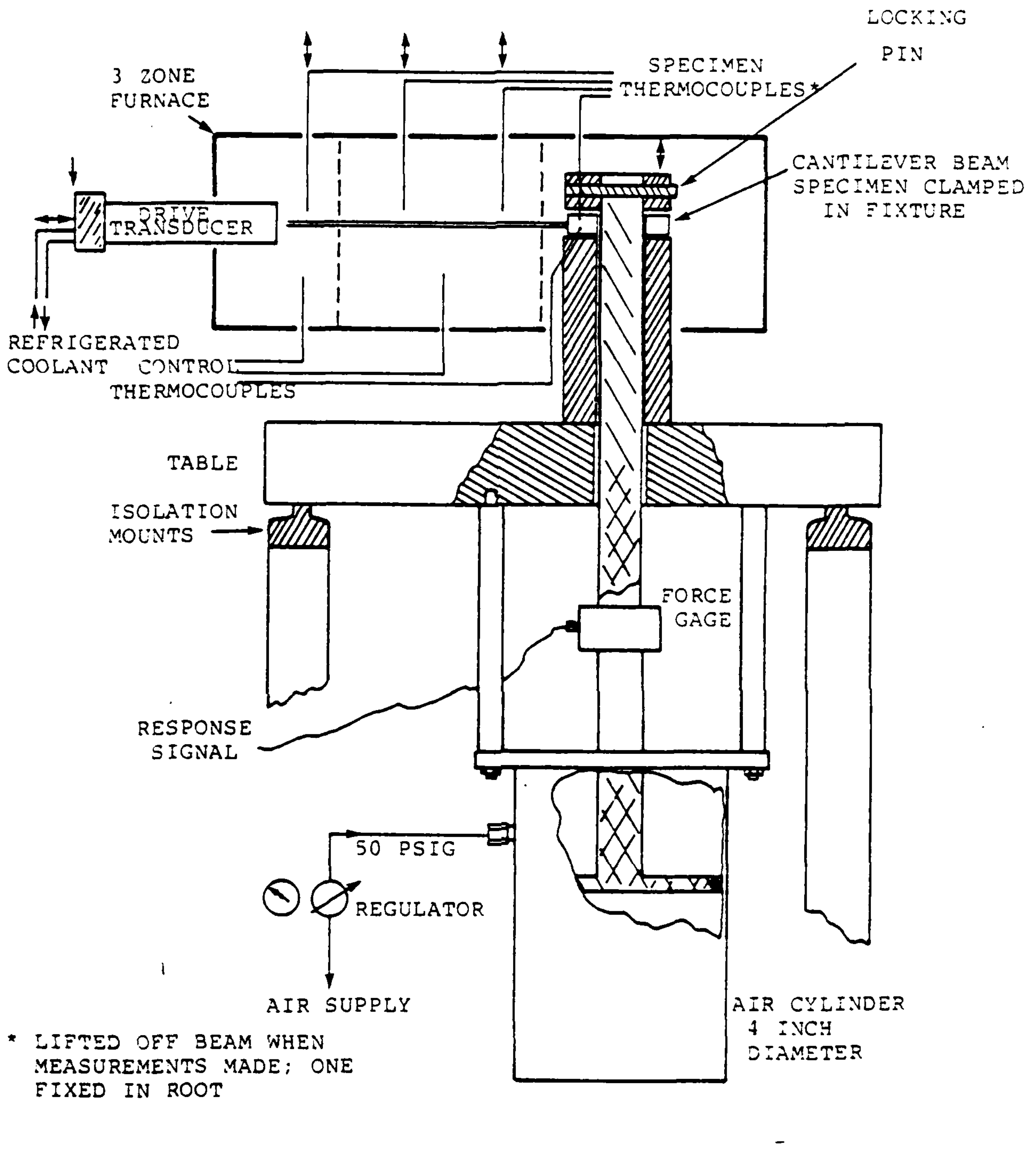

Figure 1.21. High Temperature Enamels Damping Fixture Number Two.

similar, except the blocks and bolts are made of Hastalloy X. Only one bolt is used and it is passed through the center of the block and specimen root. This arrangement reduces background interference as seen by the force link.

Temperature Control

To achieve the high temperature necessary for the evaluation of high temperature vibration damping materials, a three-zone tube furnace was modified to accept the enamels test fixture and the electromagnetic drive transducer. Baffles are used to separate the zones for more precise temperature control. The temperature in each zone is independently controlled by a proportional temperature controller. Control thermocouples provide the signals to the proportional controllers. The controllers are manually adjusted to achieve the desired temperature as read on monitoring thermocouples. Figure 1.22 is a schematic of the enamels testing furnace showing the location of the control thermocouples (TM-1, TM-2A, TM-2B, and TC-3). Zone one (fixture end) thermocouples are inserted into holes in the root of the test specimen. Zones two and three control thermocouples are inserted through the bottom of the furnace to about one-half inch below the test specimen. Zones two and three monitoring thermocouples are set down onto the surface of the test specimen measuring the temperature of the enamel coating. The temperature is set and allowed to stabilize. When the temperature is at the desired level, the zone two and zone three monitoring thermocouples are lifted and modal damping data is taken. Even with baffles separating the zones, there is considerable interaction between the zones. To achieve more accurate control of the temperature, two monitoring thermocouples are used in zone two. Table 1.3 shows typical temperature variance between monitoring thermocouples after the temperature is stabilized at the desired temperature. The test temperature is considered stabilized when the variations in Table 1.3 are maintained for three minutes.

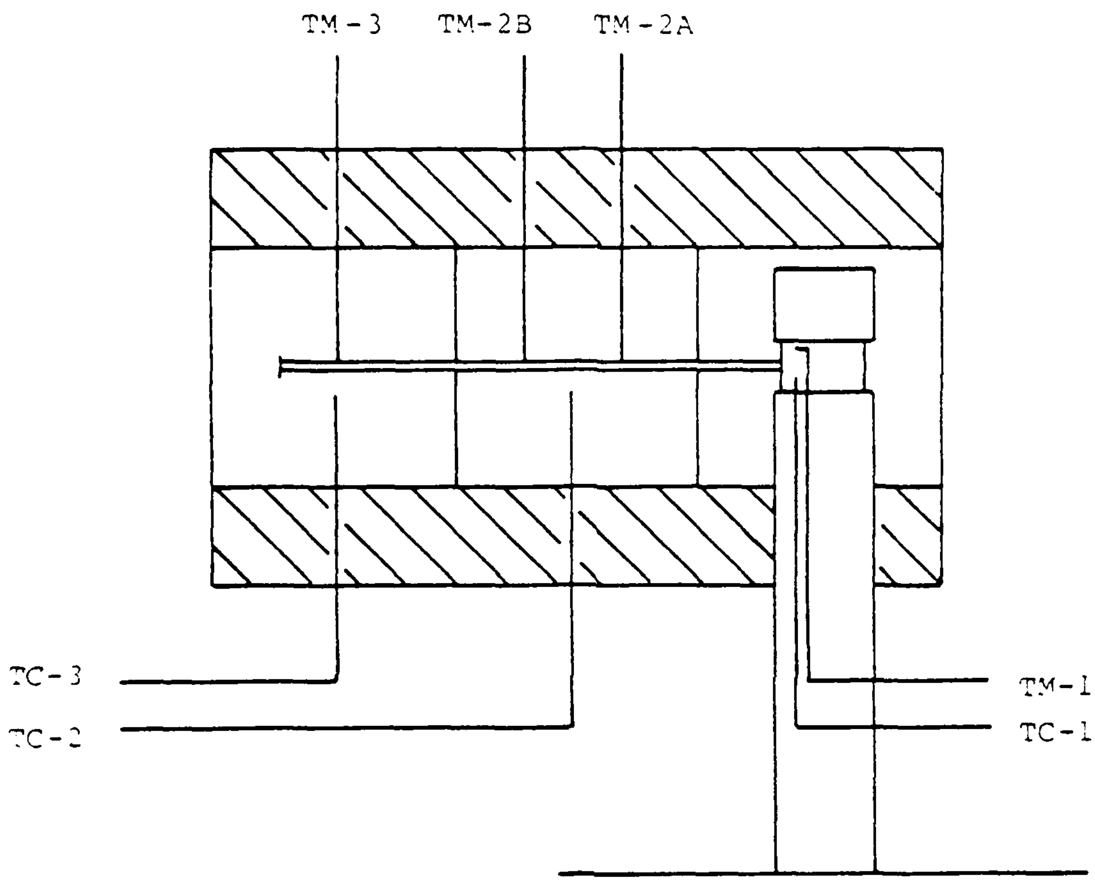

Figure 1.22. Schematic of the Enamels Testing Furnace Showing the Locations of the Control and Monitoring Thermocouples.

TABLE 1.3

TEMPERATURE DEVIATION OF MONITOR THERMOCOUPLES

Thermocouple Number	Furnace Zone	Derivation from Set Temperature
TM-1	1	1.7 to 2.8°C
TM-2A	2	-1.7 to 2.8°C
TM-2B	2	1.7 to 2.8°C
TM-3	3	-2.8 to 3.9°C

Excitation System

Excitation of resonant vibrations in beams in high temperature environments (980°C, 1800°F) requires unique equipment. Because no commercially marketed magnetic transducer capable of operation at these temperatures was available, the UDRI developed and fabricated under a previous contract to AFWAL/MLLN a refrigerant cooled non-contacting electromagnetic transducer.[1] Improvements to the original designs of both the transducer and its cooling system evolved and were implemented during this contractural period.

The transducer body is constructed of mild steel. The end covering the coil and the core is also mild steel but the end cap is non-magnetic stainless steel. A teflon bobbin holds the coil in place. When using this type of transducer, a DC current source is required for the static magnetic field. The required dynamic signal is applied to excite the structure under test. The block diagram in Figure 1.23 shows connection for the transducer.

Standard commercially available electronic equipment is used to produce and monitor the drive transducer input signal. The amplified output of a frequency synthesizer in series with a DC power supply provide the controlled sine power signal which results in the desired magnetic field from the drive transducer. A cobalt disc on the end of the test beam provide the magnetic couple

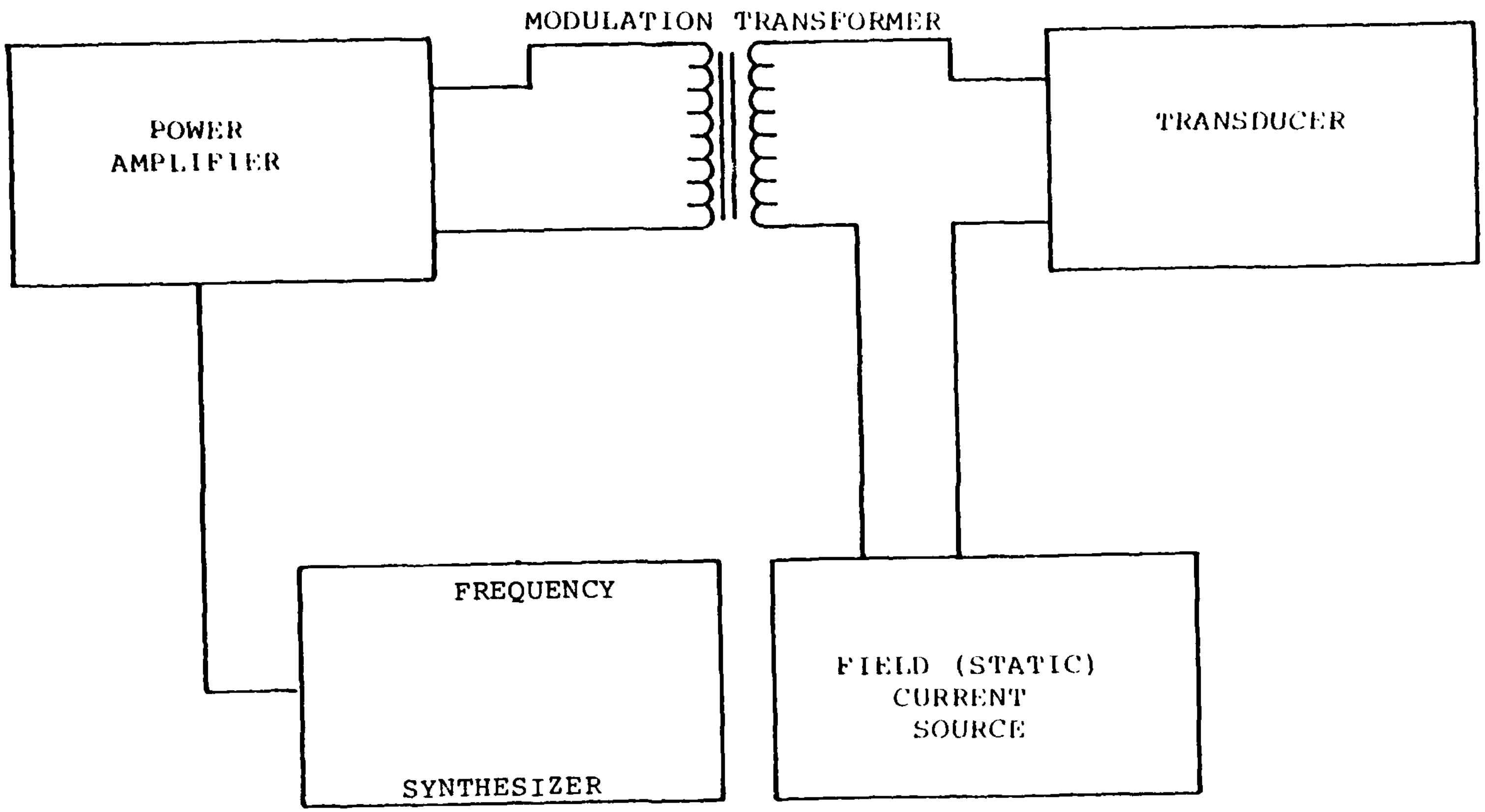

Figure 1.23. Schematic of the Connection of the Drive Transducer.

between the drive transducer and the test beam. By varying the frequency of the synthesizer resonant vibration is induced in the beam.

The equipment used to cool the transducer was in its original form, a 4000 BTU room air conditioner which was modified by replacing the evaporator coil with the transducer. This system operated in satisfactory manner, however, the continuous duty cycle shortened the life of the compressor. The consumer oriented compressor was replaced with a commercial compressor and has operated efficiently since its installation. A schematic of the refrigeration system is presented in Figure 1.24.

Force Response Measuring System

The resonant motion induced in the beam is transmitted mechanically through the high temperature cantilever test fixture to a force link. The output of the force link is amplified and provides the signal for the half-power bandwidth measurement needed to determine the material's damping properties. Figure 1.25 is a block diagram of the high temperature testing apparatus and Table 1.4 lists the electronic equipment used in this experimental set-up.

1.2.1.2. Beam Testing

The method for determining the loss factor and complex Young's modulus properties for high temperature free layer materials is the Oberst beam test [2]. The frequency response and modal damping as a function of temperature are measured for each undamped test beam. Accurate measurements of the resonant frequencies are necessary because the material damping properties calculated from experimental measurements are very sensitive to errors in the ratio of the coated beam resonant frequency to the uncoated resonant frequency (f_c/f_n), expecially for thin coatings.

TABLE 1.4

LIST OF ELECTRONIC EQUIPMENT

Description	Manufacturer	Model Number
Oscilloscope	Ballantine	1066S
Meter, R.M.S.	Hewlett-Packard	3400A
Amplifier, Power	McIntosh	MC50
Drive Transducer, Freon Cooled	UDRI fabricated	
Refrigeration System, Transducer	UDRI fabricated	
Preamplifier, Precision	MB Electronics	N400
Plotter, Graphic X/Y	Hewlett-Packard	7035B
Force Gage, Axial	PCB	233A
Power Supply, Current Source	Harrison	6203A
Impedence Transformer, Line Driver	UDRI fabricated	
Frequency Synthesizer	Hewlett-Packard	3325A

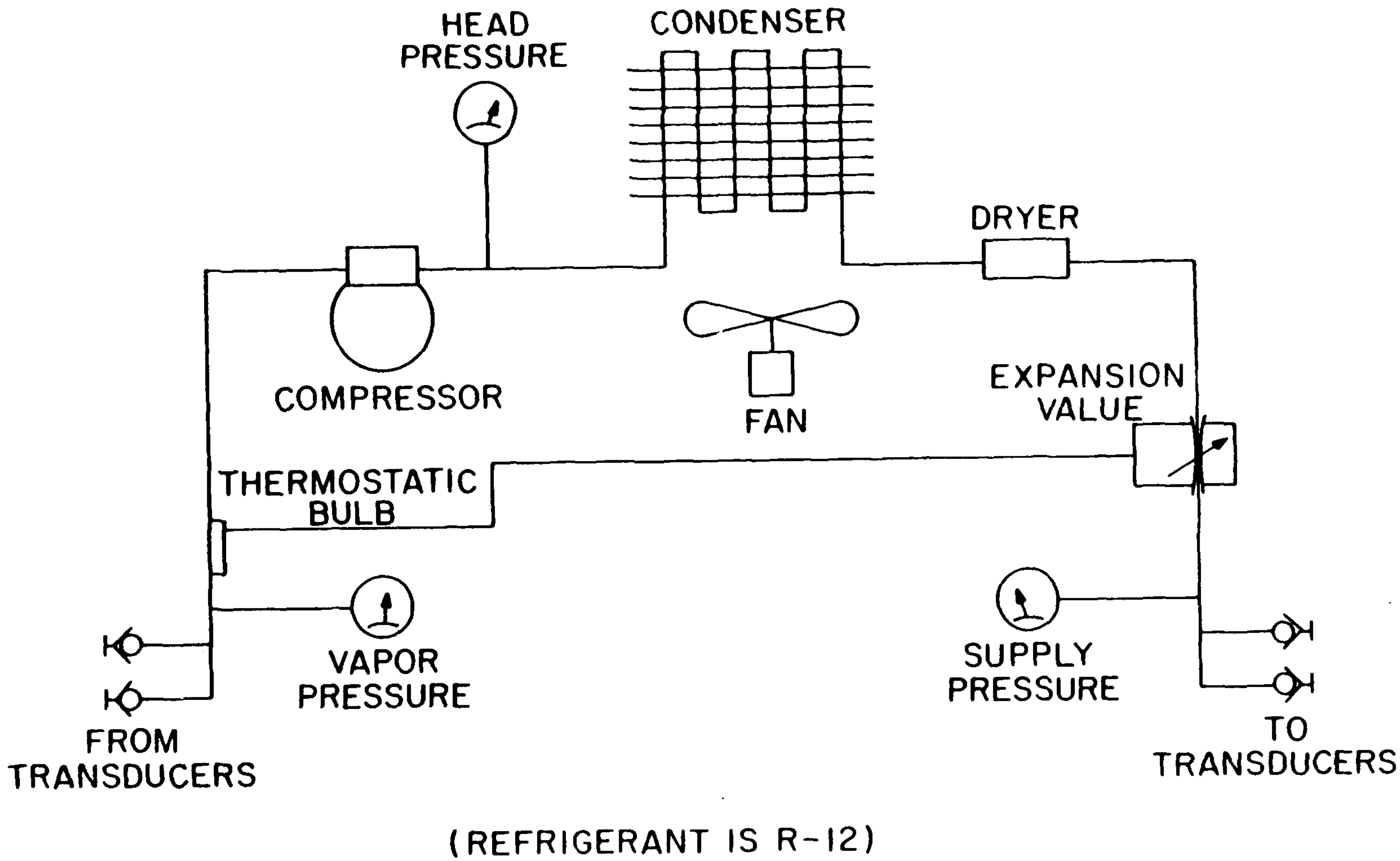

Figure 1.24. Schematic of High Temperature Damping Test Apparatus Cooling System.

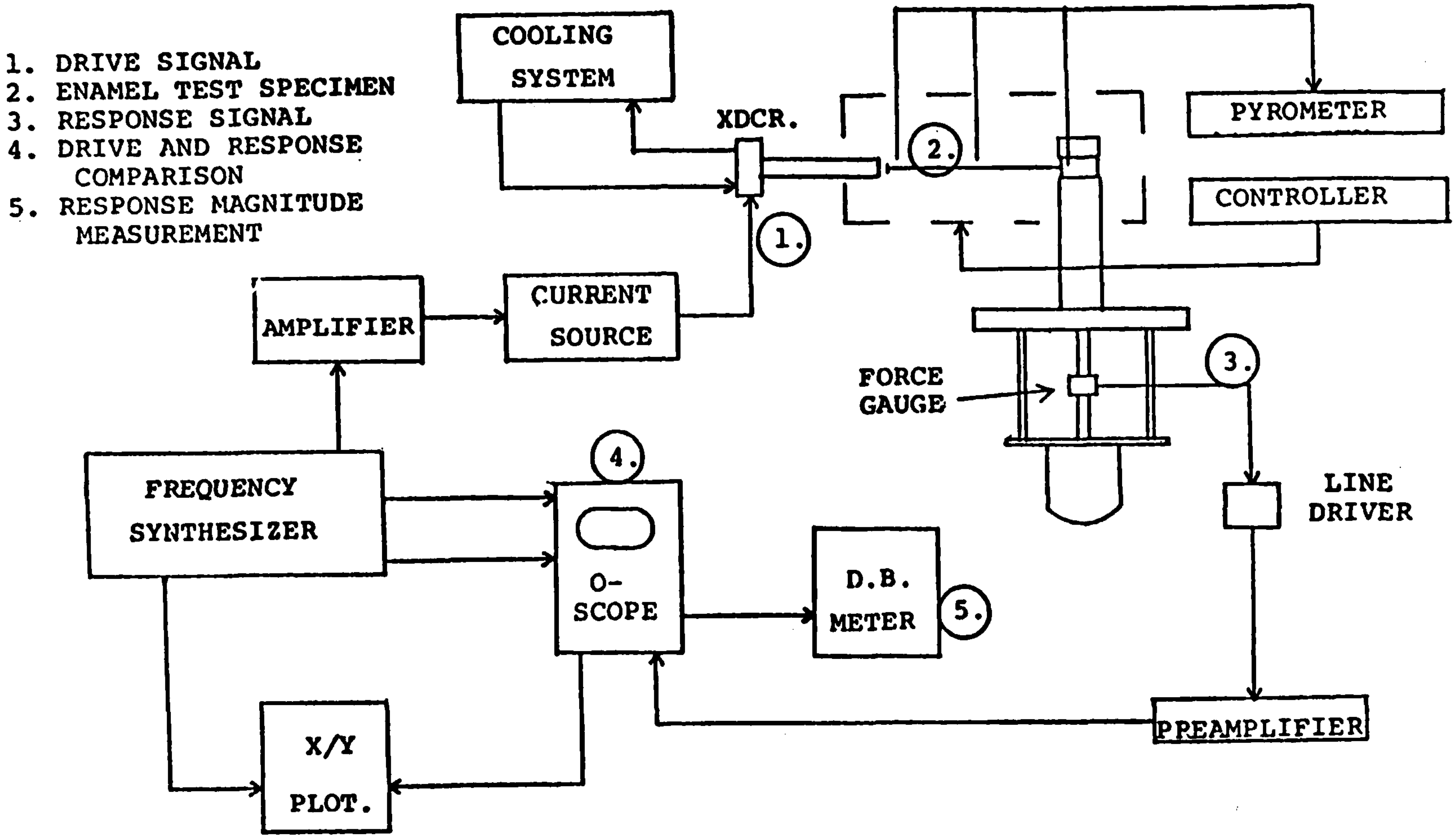

Figure 1.25. Block Diagram of High-Temperature Test Apparatus.

Uncoated Test

The high temperature enamel test specimens are cantilever beams made of either Haynes Alloy Number 188, Hastalloy C, Hastalloy X, or 17-4PH stainless steel Hastalloy X. Figure 1.26 is a schematic of the test specimens with typical dimensions. The top beam is made to be used in test fixture number one, and the bottom in test fixture number two. Both specimens are identical except a one-half inch hole is drilled in the root of the beams to be used in fixture number two. The beams are cut from sheet and machined to the required dimensions. The roots are cut from 0.25 inch Hastalloy X sheets and machined to size. A 0.125 inch hole is drilled into each root to allow the high temperature testing furnace's zone one thermocouples to be inserted into the beam. The roots are then welded onto the top and bottom of the test beam. The beams and roots are welded on three sides to insure adequate clamping. Since Haynes Alloy Number 188 and the Hastalloy alloys are non-magnetic, a high Curie temperature cobalt disc is welded onto the beam to provide a magnetic couple to the electromagnetic drive transducer.

The physical dimensions for the uncoated beam are measured and recorded. To determine the material loss factor and complex Young's modulus, the Oberst equations require the uncoated beam thickness (h_b), length (ℓ), and density (ρ_b). Beam dimensions are illustrated in Figure 1.26.

The cantilever beam test specimen is placed in the apparatus illustrated in Figure 1.21. As mentioned previously, this apparatus compensates for the thermal expansion and high temperature creep of the fixture and ensures a constant clamping pressure over the entire temperature range for which the measurements are obtained.

For the uncoated beams, each beam is stabilized at the highest expected test temperature (usually about 1,000°C) and the resonant frequency and modal damping of the second through sixth modes are measured. The temperature is then reduced in 100°C

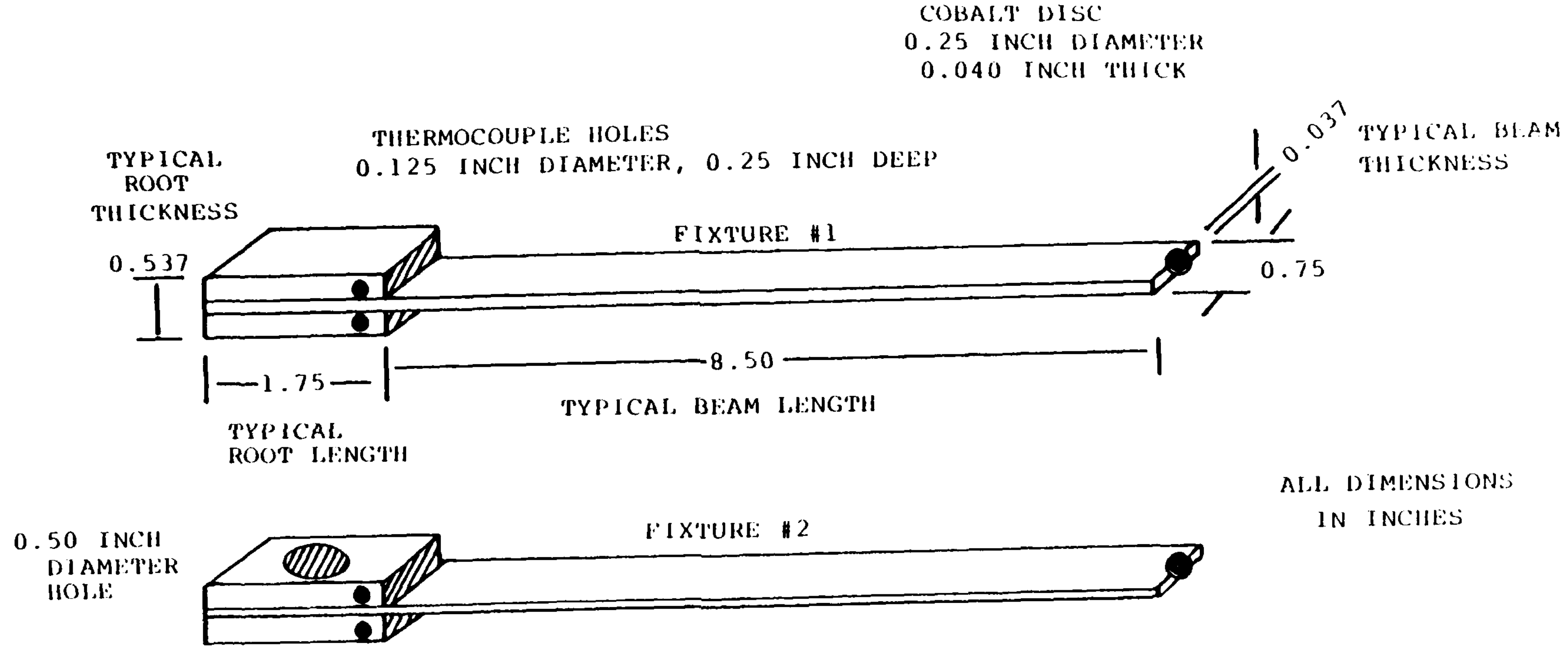

Figure 1.26. Schematic of the Cantilever Beam Test Specimens with Typical Dimensions.

increments, stabilized (refer to Table 1.3), and the response measurements repeated. This procedure is continued to approximately 300°C. The resonant frequency and modal damping versus temperature for each of the modes are then plotted. The resonant frequency versus temperature for each of the modes are then plotted. The resonant frequency versus temperature curve, as illustrated in Figure 1.27, for each of the modes of the uncoated specimens tested is a smooth curve, and accurate resonant frequencies could be picked from this curve for any temperature of interest. The modal damping is determined by measuring the half-power bandwidth of each of the modes ($\eta = \Delta f_n / f_n$) and plotted versus temperature as illustrated in Figure 1.28.

Experience showed it was necessary to heat the specimen to the highest temperature and measure the response of the specimen as it cooled. The resonant frequencies measured on cooling from the highest temperature were higher than the resonant frequencies measured upon heating from room temperature to the highest temperature of interest. Once the specimen was heated to the highest temperature and cooled, the resonant frequencies measured going up in temperature and those measured coming down in temperature were the same, within experimental error, providing the specimen remained in the fixture. Other investigators have also noticed this behavior [3]. It is believed to be caused by the beam "setting in" the fixture and the relief of surface stresses in the beam introduced during fabrication. It is not due to the beam material being annealed. The anneling temperature of the beam material used (Haynes Alloy 188) is greater than 1,100°C.

Coated Beam Test

After the uncoated specimen responses are measured, the beam is then coated on one side with a glass. The coated beam is heated to the expected maximum temperature for the particular coating, and the resonant frequencies and modal damping of the second through sixth modes are measured. The temperature is then reduced in steps of 25°C and the response is again measured. If the modal damping decreased upon cooling, the temperature of the speci

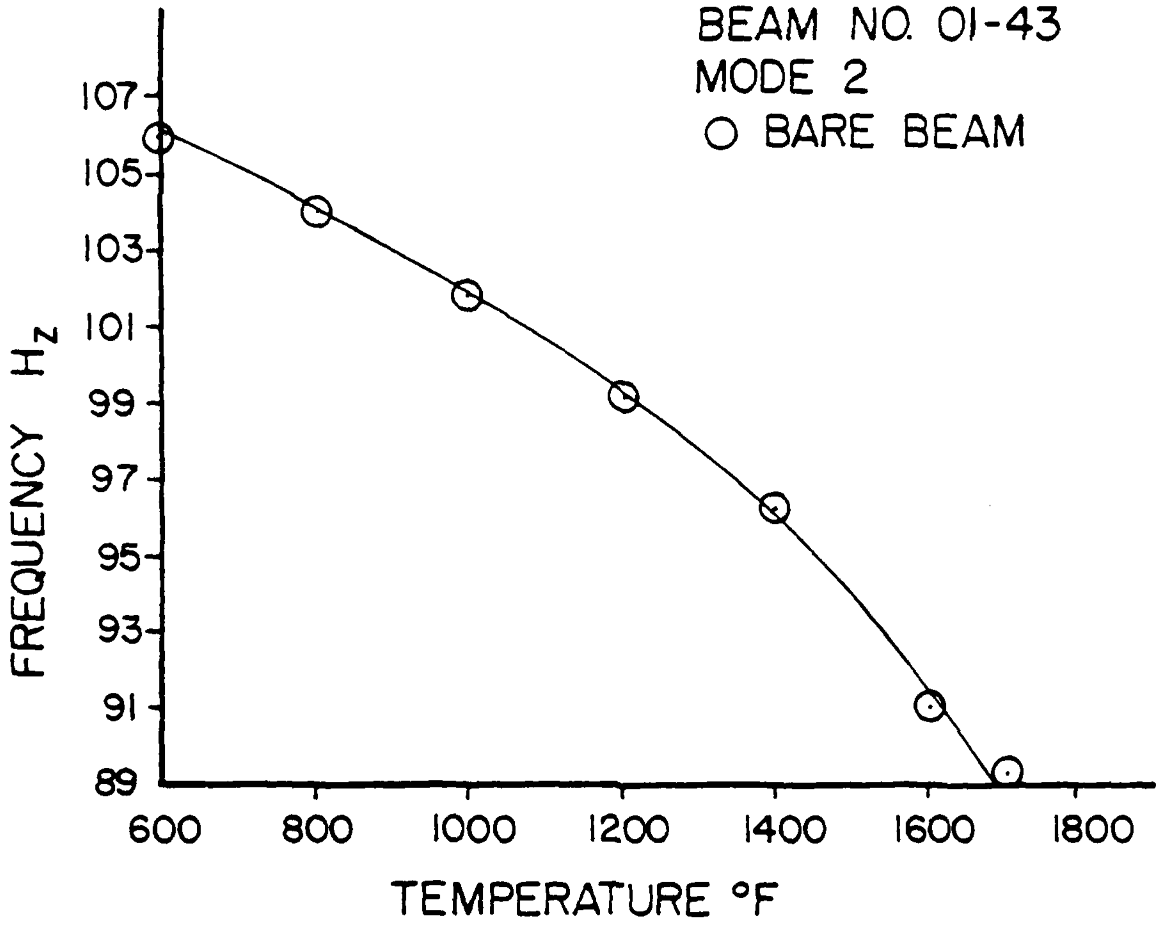

Figure 1.27. Resonant Frequency Versus Temperature Curve of Modes for Bare (Uncoated) Beam.

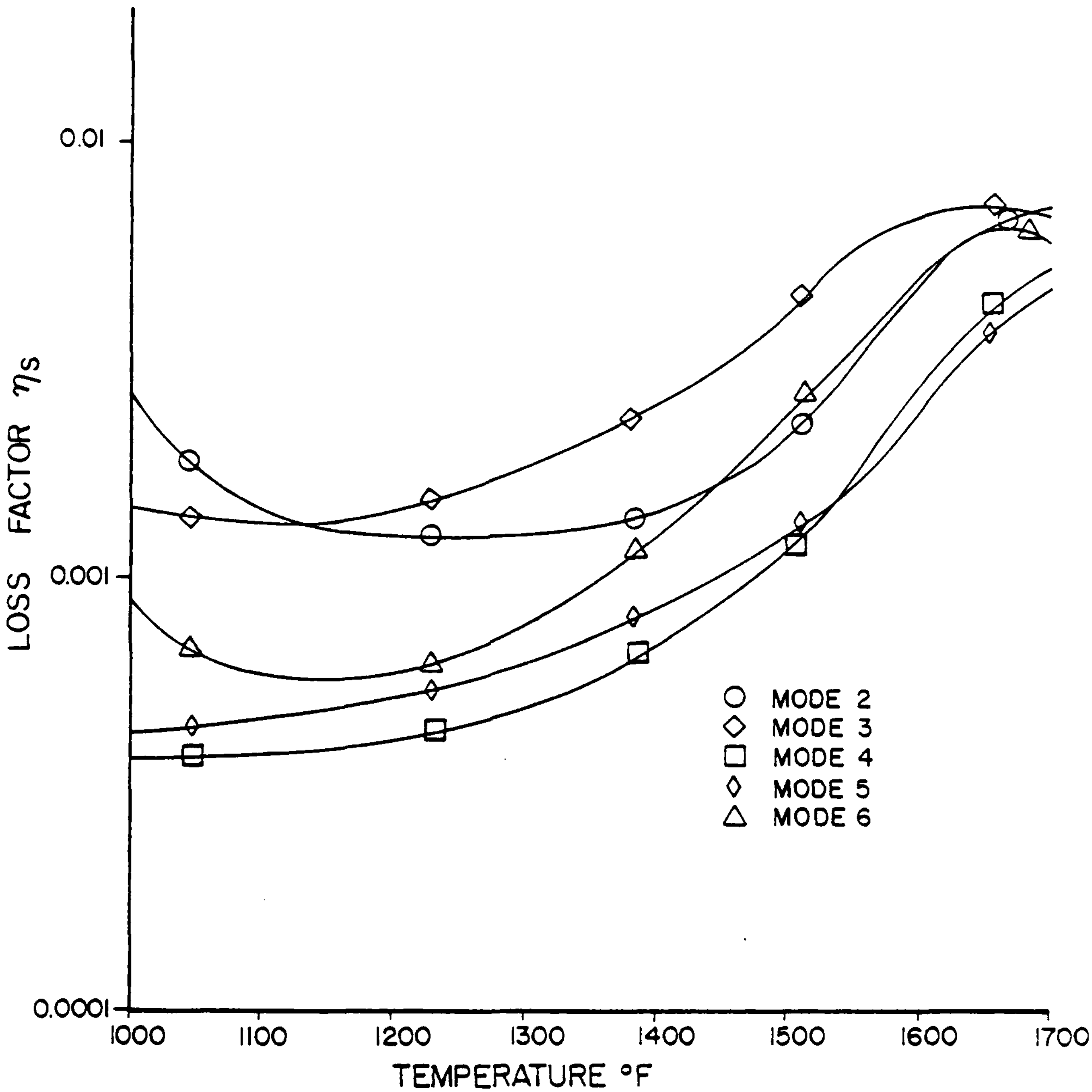

Figure 1.28. Half-power Bandwidth (Modal Damping) of Each Mode Versus Temperature for Bare (Uncoated) Beam.

is increased above the initial test temperature in 25°C increments until the modal damping decreases for two successive increases in temperature. The specimen is then cooled in 25°C steps and new measurements taken. Figure 1.29 is a typical plot of coated beam center frequency versus temperature and Figure 1.30 is a typical plot modal damping versus temperature.

The measurements made upon heating are not used to calculate the damping properties of the coating for the reasons previously mentioned. Another reason is that a glass is sensitive to its previous thermal history, in particular to the rate at which it is cooled from its firing temperature. The specimens tested are fired and then air quenched. This rapid cooling may have caused large residual stresses and some non-equilibrium structure can be frozen in. Heating the glass above its softening temperature and slowly cooling it allows the residual stresses to be relieved and the glass to maintain equilibrium.

The loss factor of the uncoated beam is subtracted from the measured loss factor of the coated beam to obtain a "corrected" modal damping coefficient. Sridharan [3] has shown that for small modal damping

$$\eta_c = \eta_s - \eta_b$$

where

η_b is the modal damping of the uncoated beam;

η_s is the measured modal damping of the coated specimen;

η_c is the modal damping that would have been observed if the uncoated beam damping was zero.

This correction is usually only necessary for temperatures greater than 650°C (1,200°F). The data recorded for each of the modes and temperatures are:

T - the temperature of the specimen;

f_n - the resonant frequency for the n^{th} mode of the uncoated beam;

f_c - the resonant frequency for the n^{th} mode of the coated beam;

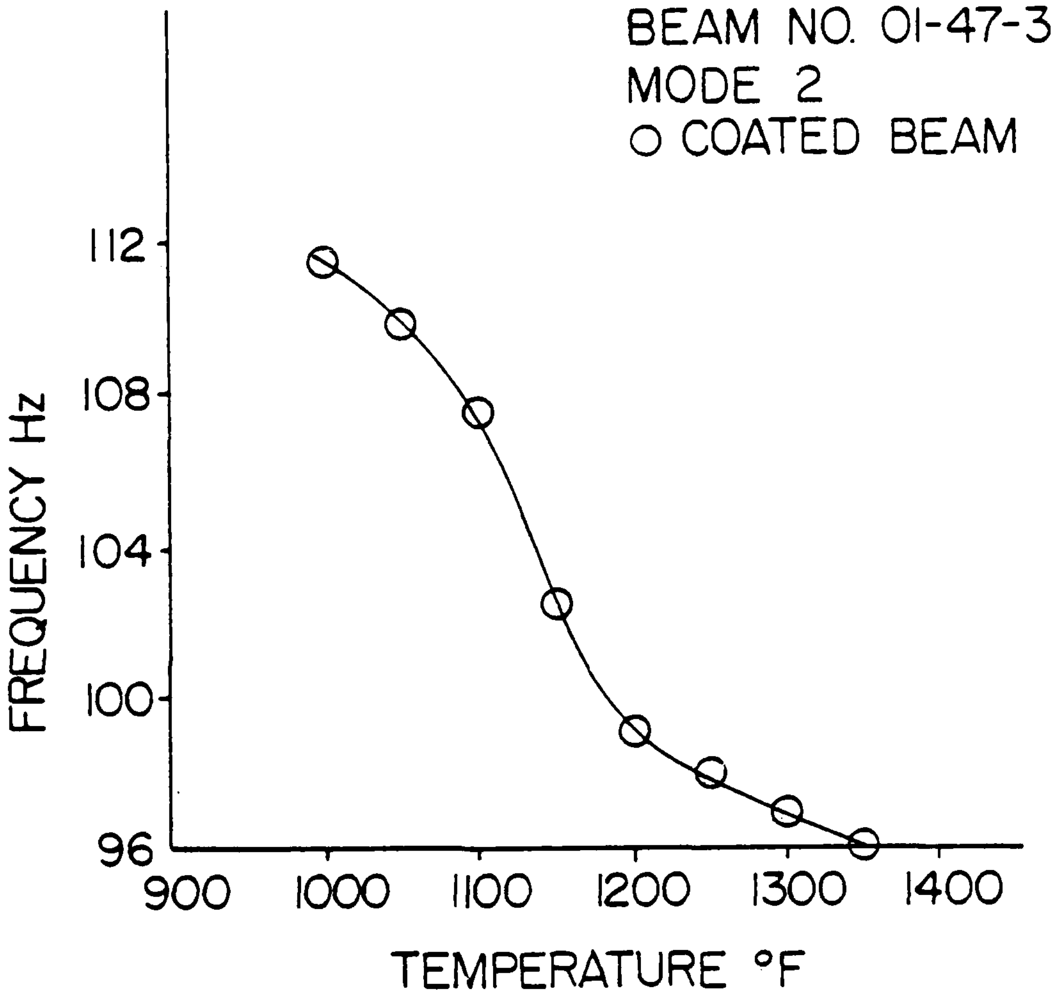

Figure 1.29. Typical Plot of Coated Beam Center Frequency Versus Temperature.

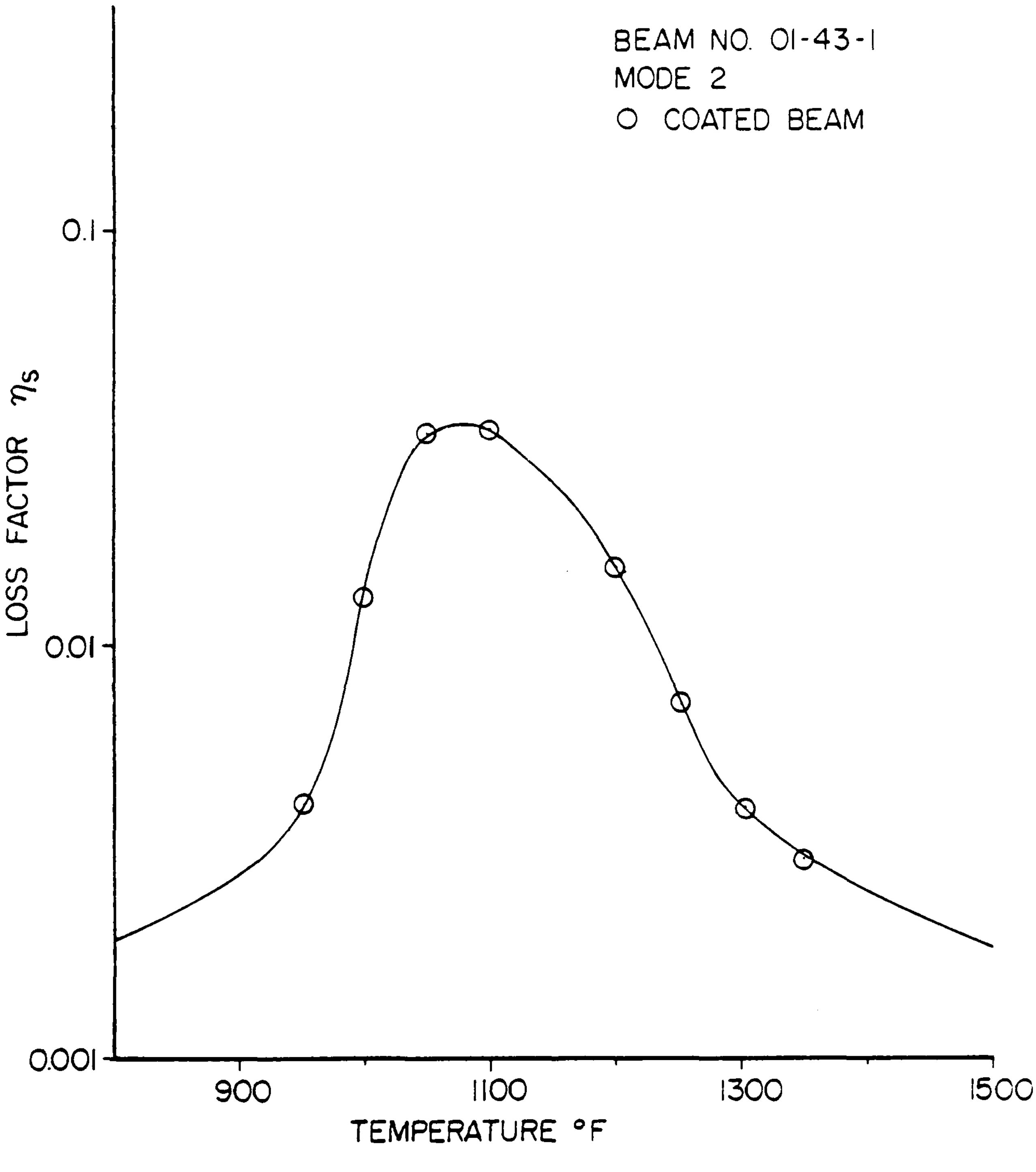

Figure 1.30. Half-power Bandwidth (Modal Damping) Versus Temperature for Coated Beam.

Δf_n - the half-power bandwidth of the n^{th} mode of the uncoated beam;

Δf_c - the half-power bandwidth of the n^{th} mode of the coated beam;

η_s - modal damping of the n^{th} mode of the coated beam;

η_b - modal damping of the n^{th} mode of the uncoated beam.

1.2.1.3. Calculation of Damping Properties

The damping characteristics of the coatings are determined by measuring the vibration response of a composite cantilever beam at varying temperatures over the viscoelastic range. It is assumed that the enamel can be treated as a complex quantity

$$E_D^* = E_D' + iE_D'' = E_D\ (1 + i\ \eta_D)$$

$$\eta_D = E_D''/E_D'$$

where E_D' is the storage or Young's modulus of the enamel and η_D is the ratio of the dissipative modulus, E_D'' to the storage modulus.

Consider the metal beam with enamel coating on one side, as shown in Figure 1.31.

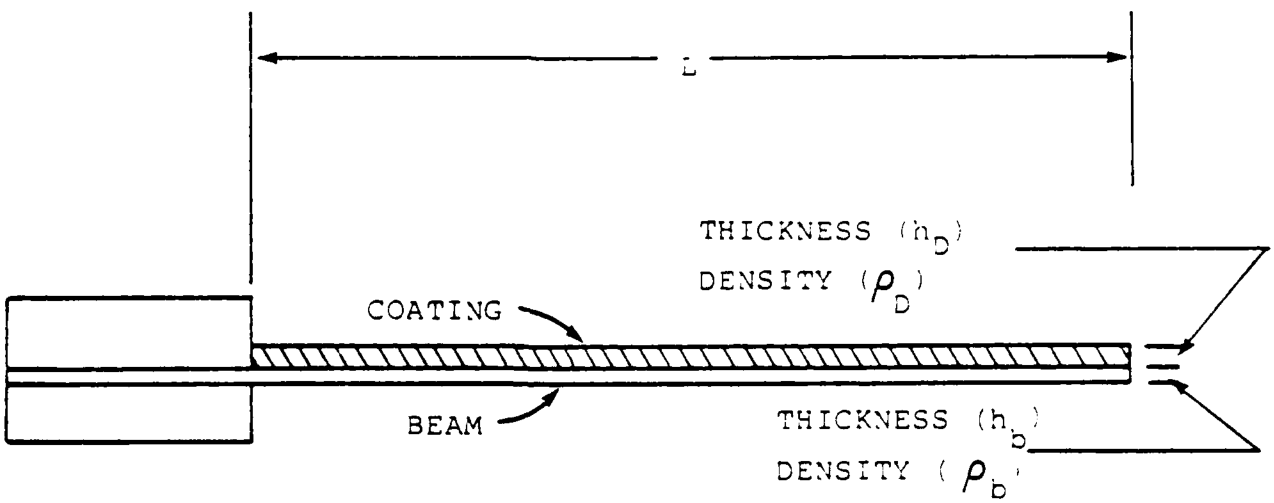

Figure 1.31. Coated Oberst Test Beam.

ξ_n^4 = the eigen value corresponding to the n^{th} mode and is a constant, determined by the boundary conditions;

$\mu_1 = \rho_1 bh_1$ = the mass per unit length of the metal beam;

L = the length of the beam;

I = $1/12\ bh_1^3$ = the second moment of area of the metal beam about its centerline.

The values of ξ_n^4 for beams with classical boundary conditions are well known and can be found in reference [4]. Thus, from the measured resonant frequencies of the coated and bare beams and the measured composite loss factor, the damping properties of the enamel can be determined as a function of temperature and frequency.

The resonant frequencies and modal damping of five to six modes of the coated beam, covering a frequency range of 100 Hz to 1,500 Hz can usually be measured for each temperature. Thus, the damping properties of the vitreous coating over a decade of frequency at a given temperature can be easily and quickly determined.

1.2.1.4. Material Properties Presentation

A nomograph developed by Jones [5] is used to present both the temperature and frequency dependence of the enamel coating. A computer program developed by King [6], using the technique of Rogers and Nashif [7], is used to plot the properties on the nomograph. There are two graphs for a coating. One plot is the storage modulus and loss modulus versus reduced frequency which is illustrated in Figure 1.32, and the other plot is the storage modulus and loss factor versus reduced frequency which is shown in Figure 1.33. These plots readily illustrate the variation of the damping properties of the material with frequency and temperature.

The plot is read by choosing the temperature of interest and following the oblique temperature isotherm until it intersects the horizontal constant frequency line of interest (frequency is the right vertical axis of the plot).

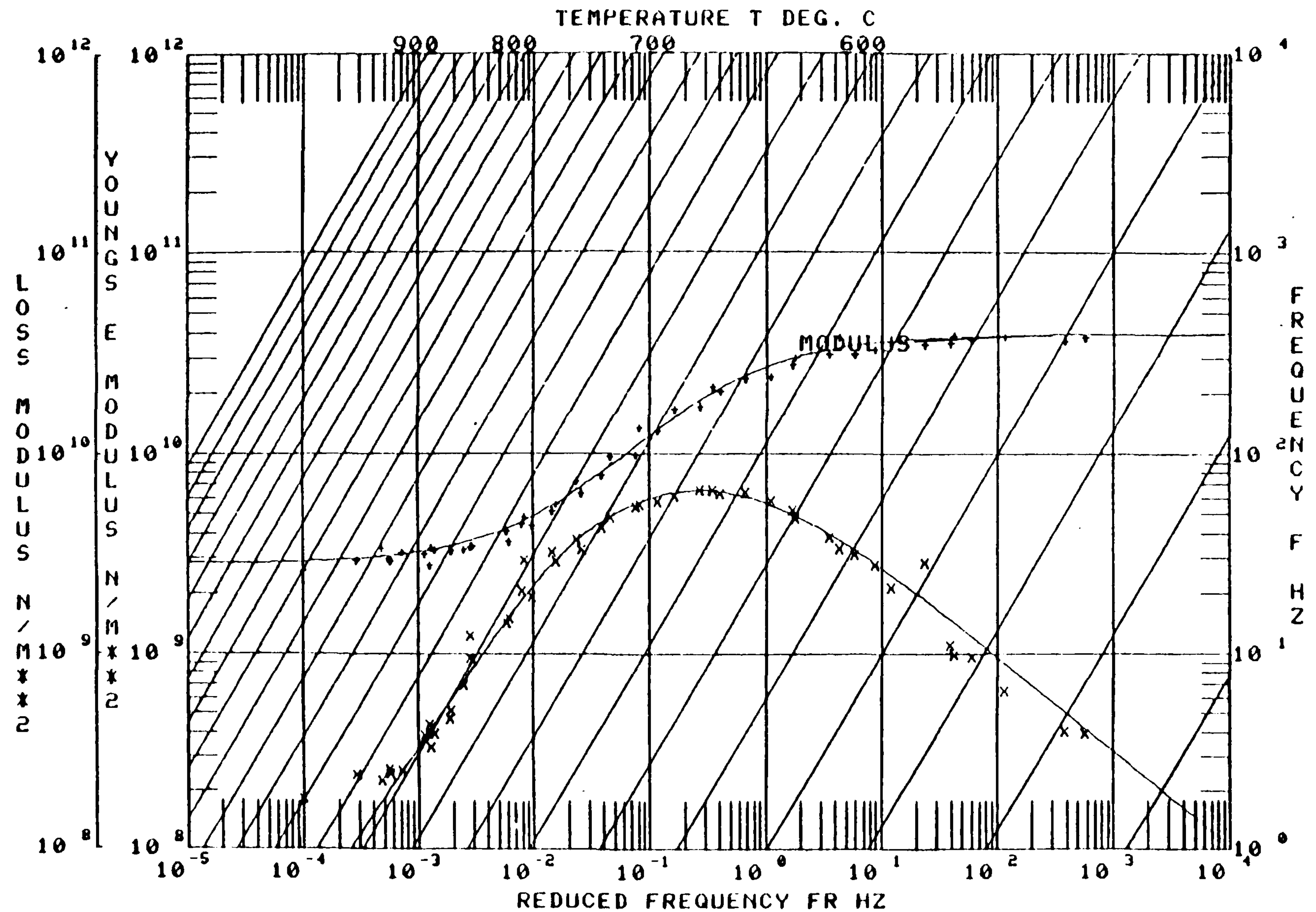

Figure 1.32. Storage Modulus and Loss Modulus Versus Reduced Frequency.

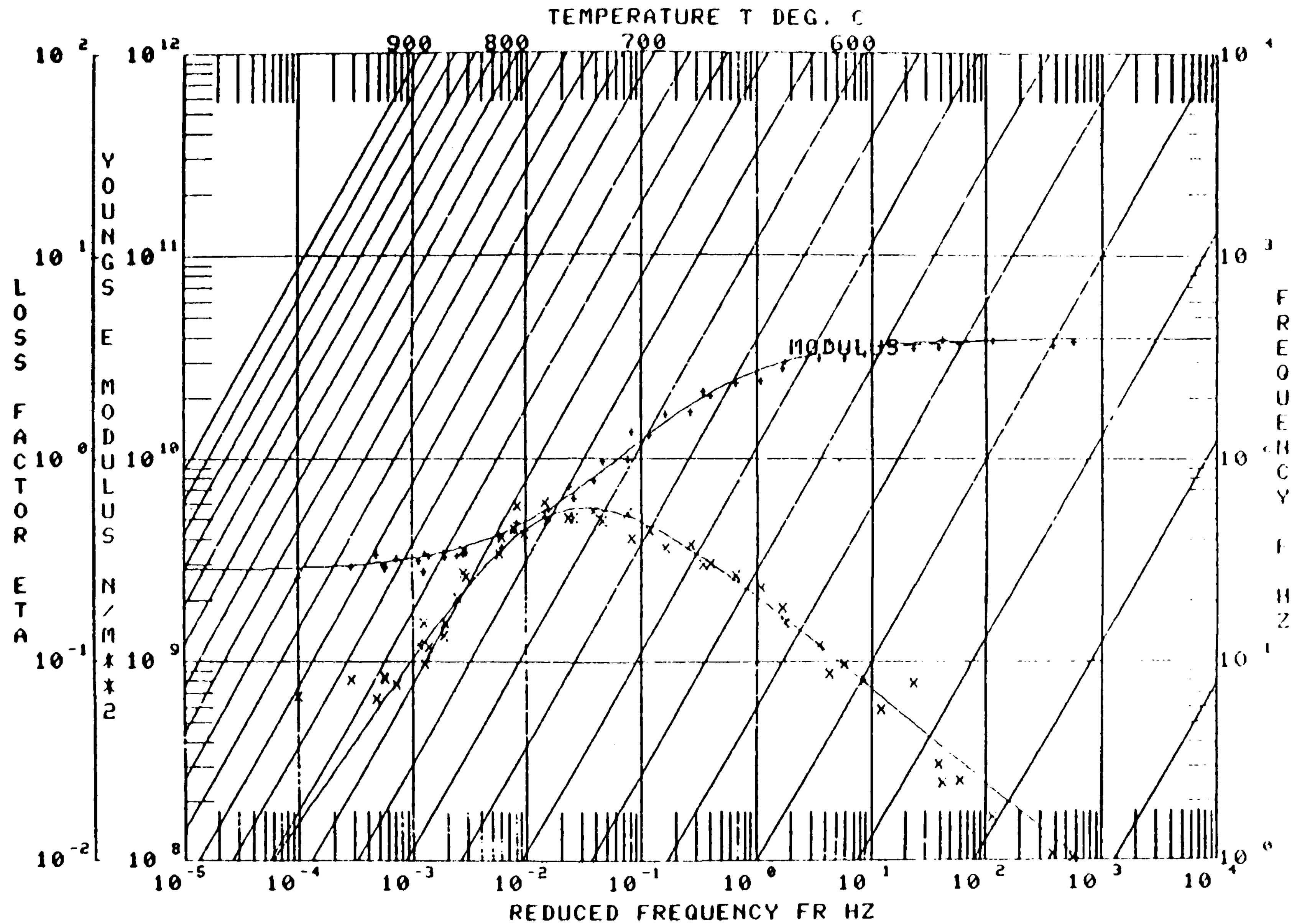

Figure 1.33. Storage Modulus and Loss Factor Versus Reduced Frequency.

The formulas developed by Oberst [2] and used by many other investigators were used to determine the damping properties of the enamel as a function of frequency and temperature. These formulae are:

$$(\omega_n/\omega_{1n})^2(1+h_D\rho_D/h_1\rho_1) = \frac{1+2(E_D/E_1)(H_D/h_1)A + (E_D/E_1)^2(h_D/h_1)^4}{1 + (E_D/E_1)(h_D/h_1)} \qquad (1)$$

and

$$\frac{\eta_D}{\eta_c} = \frac{(E_D/E_1)(h_D/h_1)[2A + 2(E_D/E_1)(h_D/h_1)^3 + (E_D/E_1)^2(h_D/h_1)^{-4} - 1]}{[1 + (E_D/E_1)(h_D/h_1)][1 + 2A(E_D/E_1)(h_D/h_1) + (E_D/E_1)^2(h_D/h_1)^4]} \qquad (2)$$

where

$$A = 2 + 3(h_D/h_1) + 2(h_D/h_1)^2 \qquad (3)$$

ω_n = natural frequency of the n^{th} mode of the composite beam, $2\pi f_n$, rad/sec;

ω_{1n} = natural frequency of the n^{th} mode of the metal beam, $2\pi f_{in}$, rad/sec;

h_D = thickness of enamel coating applied to composite beam;

h_1 = thickness of metal beam;

ρ_D = density of enamel coating;

ρ_1 = density of metal beam;

E_D = real part of the modulus of enamel coating;

E_1 = Young's modulus of metal beam;

η_c = effective loss factor of composite beam;

η_D = loss factor of enamel coating.

The quantities of h_D, h_1, ρ_D, and ρ_1 are known and are assumed to remain constant with temperature. The parameters ω_n, ω_{1n}, and η_c are experimentally measured. The value of η_D is determined from

$$\eta_c = \frac{\Delta\omega_n}{\omega_n} = \frac{\Delta f_c}{f_c} \qquad (4)$$

where Δf_c is the bandwidth at the half-power points of the response peak for the nth mode. The value of E_1 can be determined from the measured response of the uncoated metal beam using

$$\xi_n^4 = \mu_1\omega_{1n}^2 L^4/E_1I_1 \qquad (5)$$

vertical line at that point until it intersects the curve of interest, and read the properties of interest. Figures 1.34 and 1.35 illustrate this method to identify the damping properties at 500 Hz and 600°C. By reversing this process, the temperature of peak damping can be determined as illustrated in Figure 1.36. By defining the effective temperature range of material damping is above 1.707 peak damping (Figure 1.37), a description of the shape of the damping peak can be made. These methods were used to develop the summary of damping properties on the material damping properties evaluation summary sheet used in the data presentation Appendix of this report.

It can easily be seen from the nomographs that the data in this format is amenable to the development of analytical equations which would represent the data. The equations used to fit the material properties are those suggested by Rogers in reference [7].

The ability to represent the dynamic material properties in equation form greatly facilitates the use of this data in analytical structural design. A short discussion of the equations and parameters used in the curve fitting routine follows. More detailed information is in references [6] and [7].

The curves fit to the data on the nomographs were calculated by the computer program previously in this Section. The basic form for these equations are as follows:

Storage Modulus

$$\log_{10}(E_D') = \log 10(M_f) + \frac{2 \log_{10}\left(\frac{M_{rom}}{M_\ell}\right)}{1 + \left(\frac{f_{rom}}{f_r}\right)^N} \tag{6}$$

where:

E_D' is the material storage modulus;

f_r is the reduced frequency;

M_{rom} is the inflection point of the storage modulus curve as read on the Young's modulus scale;

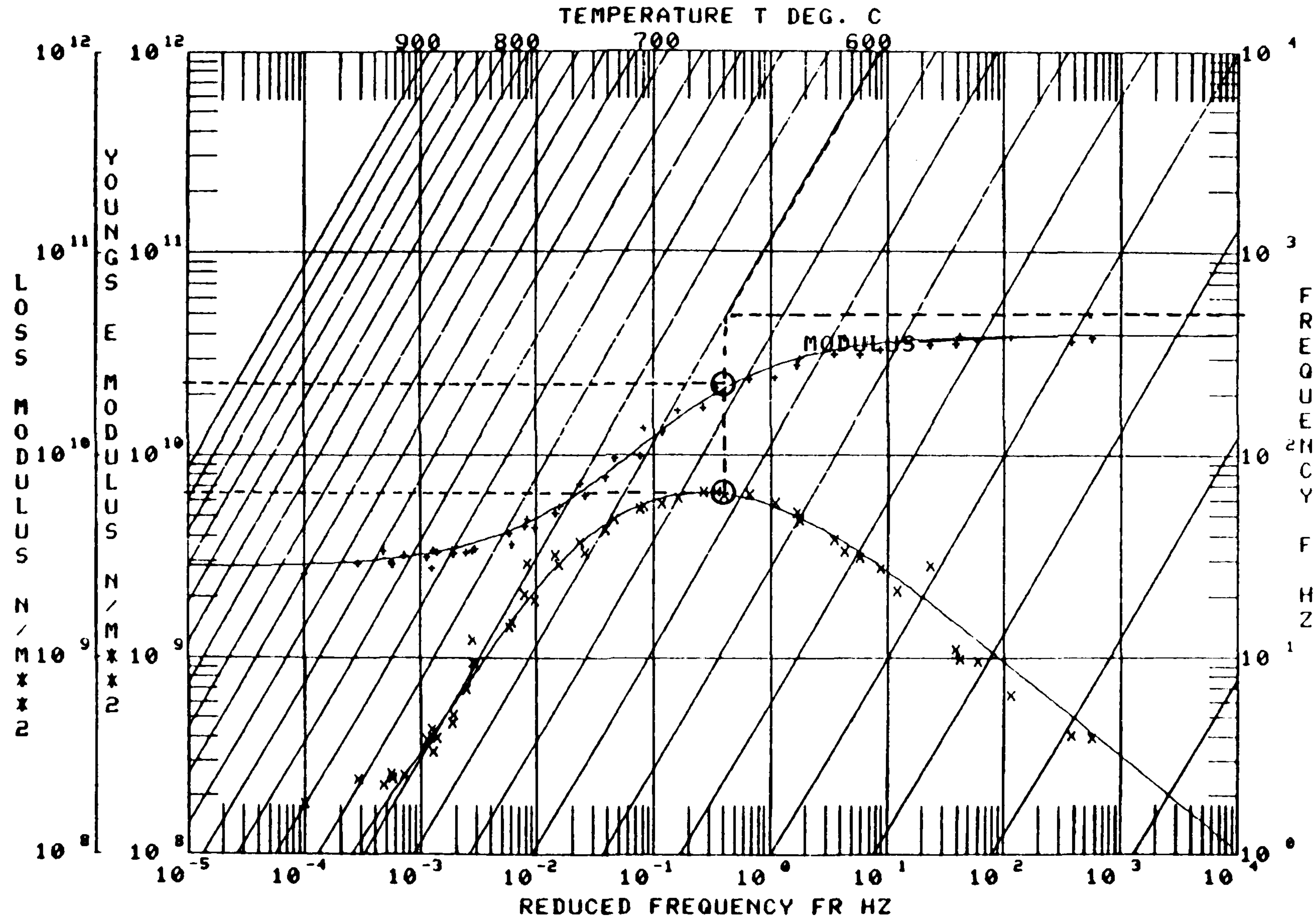

Figure 1.34. Example for Determining Loss Factor and Storage Modulus at 500 Hz and 600°C.

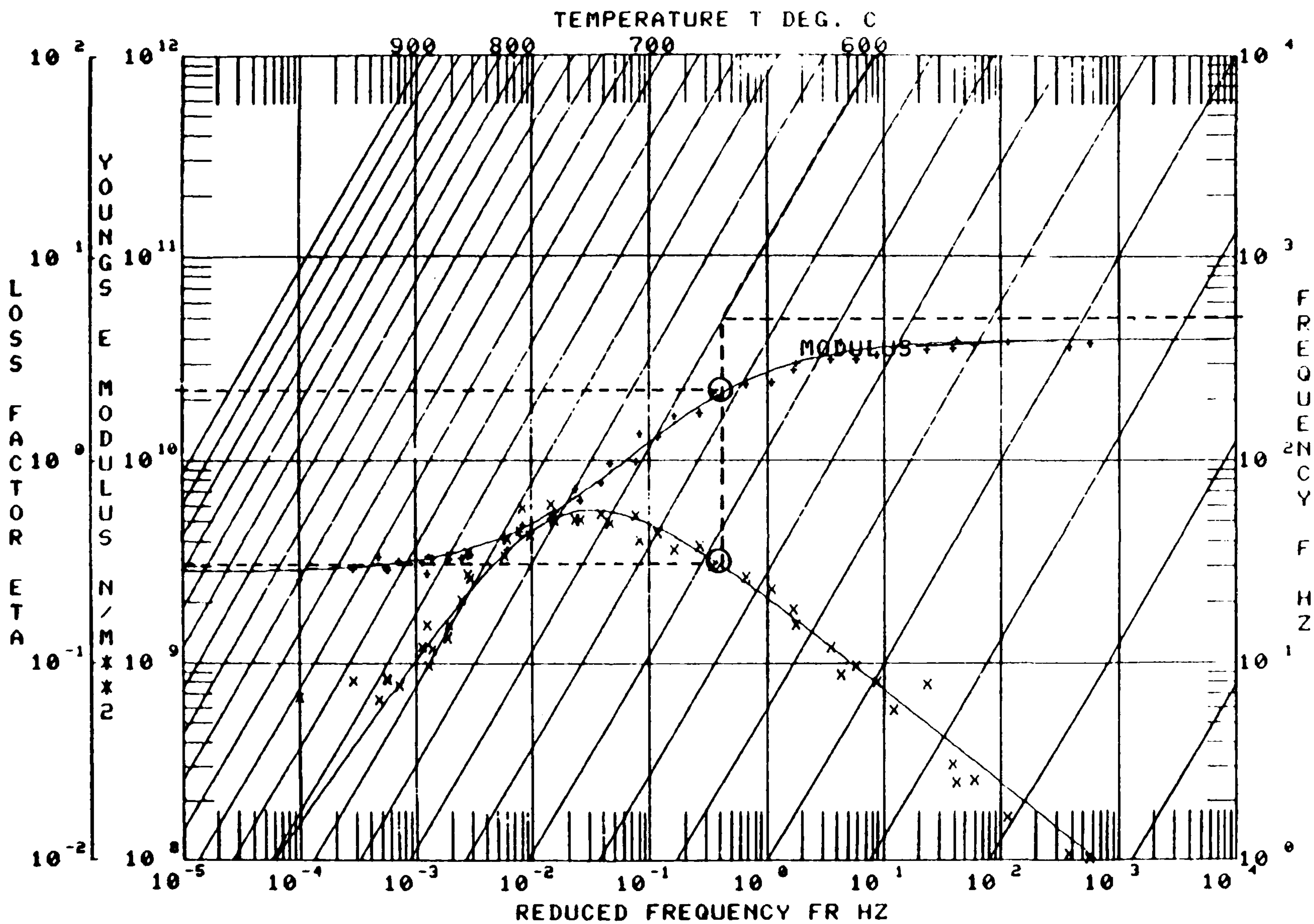

Figure 1.35. Example for Determining Loss Modulus and Storage Modulus at 500 Hz and 600°C.

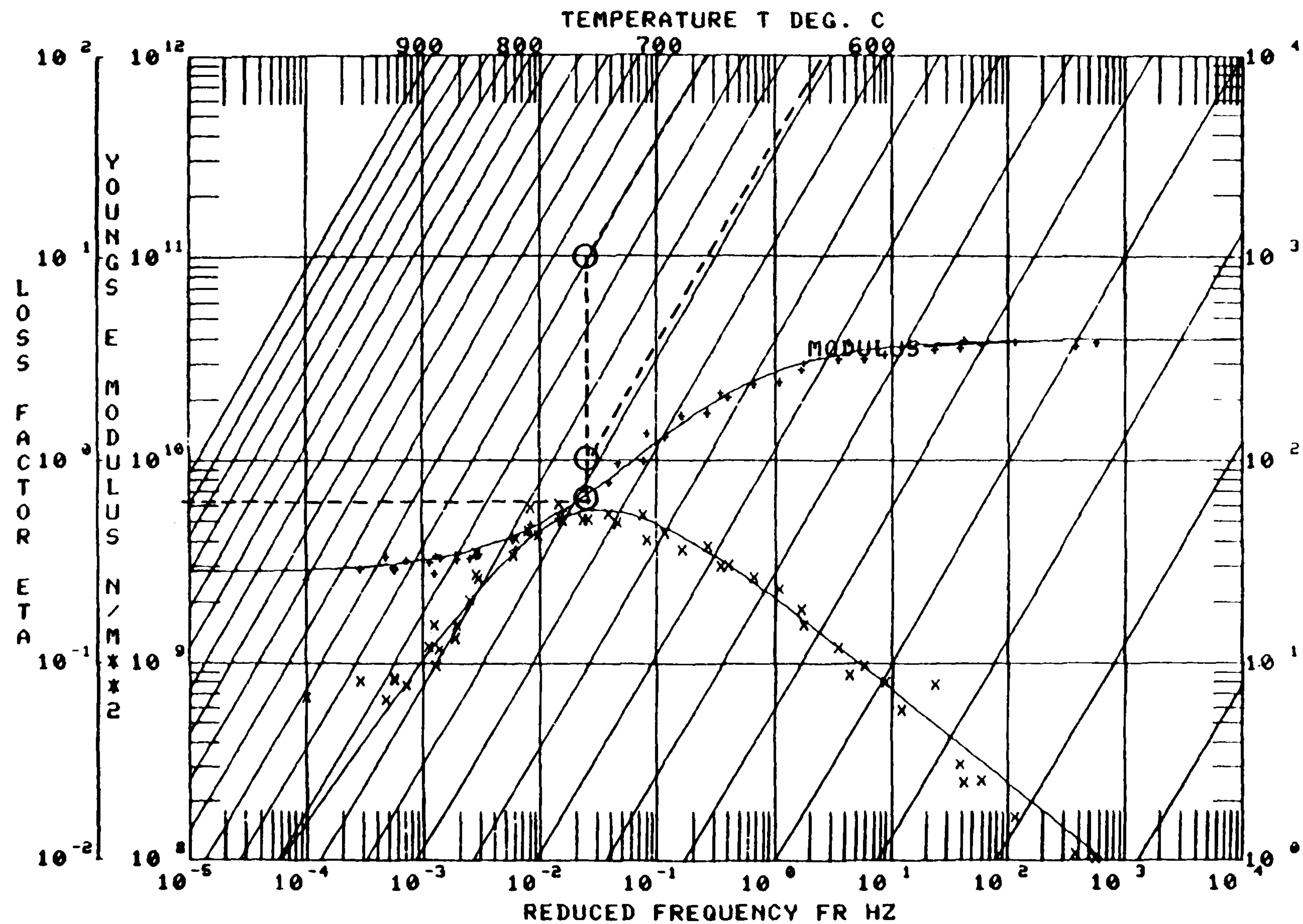

Figure 1.36. Example for Determining Peak Damping Temperature for 100 and 1,000 Hz.

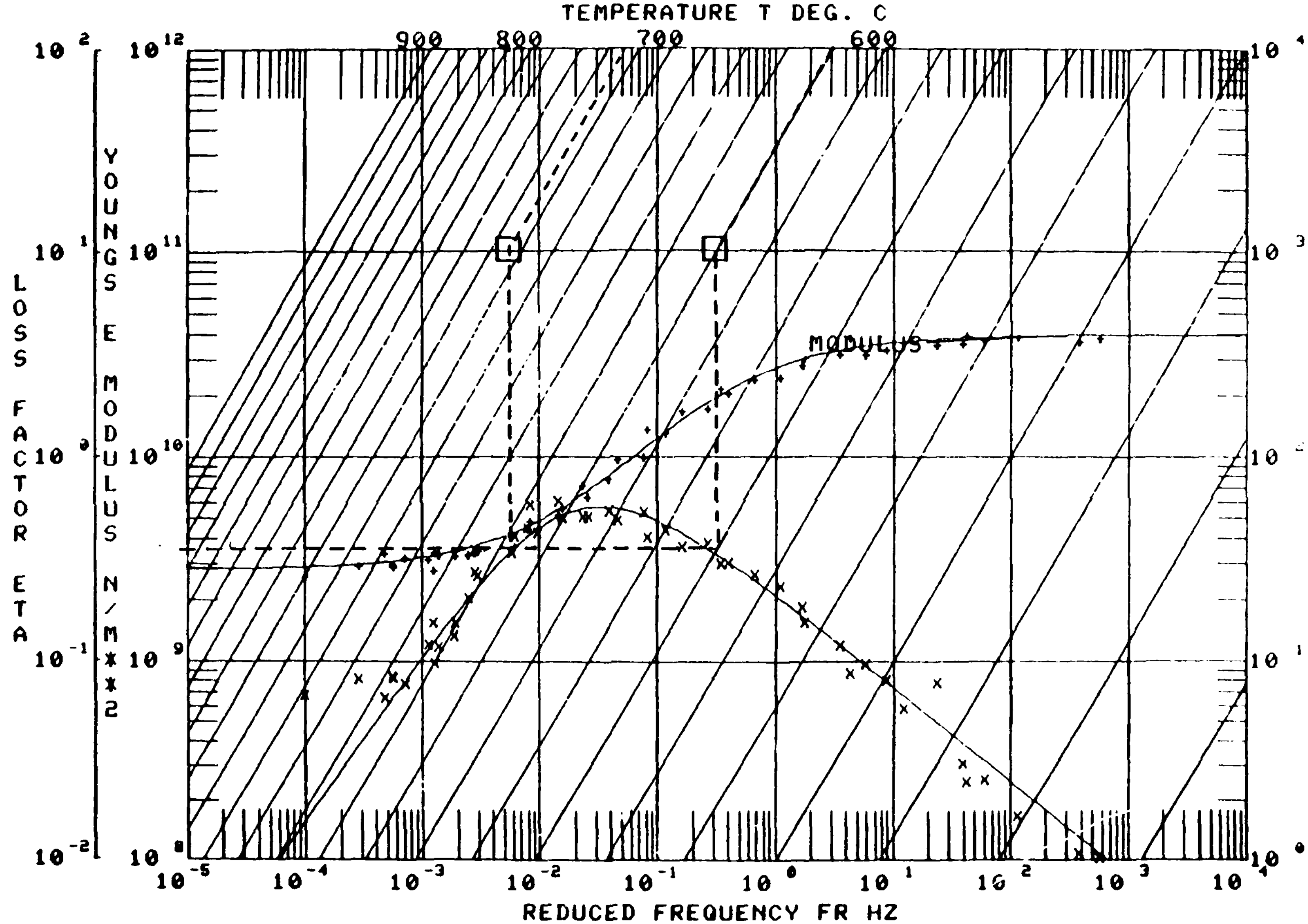

Figure 1.37. Example for Determining Material Damping Temperature Range at 1,000 Hz.

f_{rom} is the reduced frequency value of this inflection point;

N is the slope of the curve at the inflection point;

M_ℓ is the Young's modulus value of the lower horizontal assymptope of this curve.

Figure 1.38 illustrates the curve fit parameters M_{rom}, f_{rom}, N, and M_ℓ.

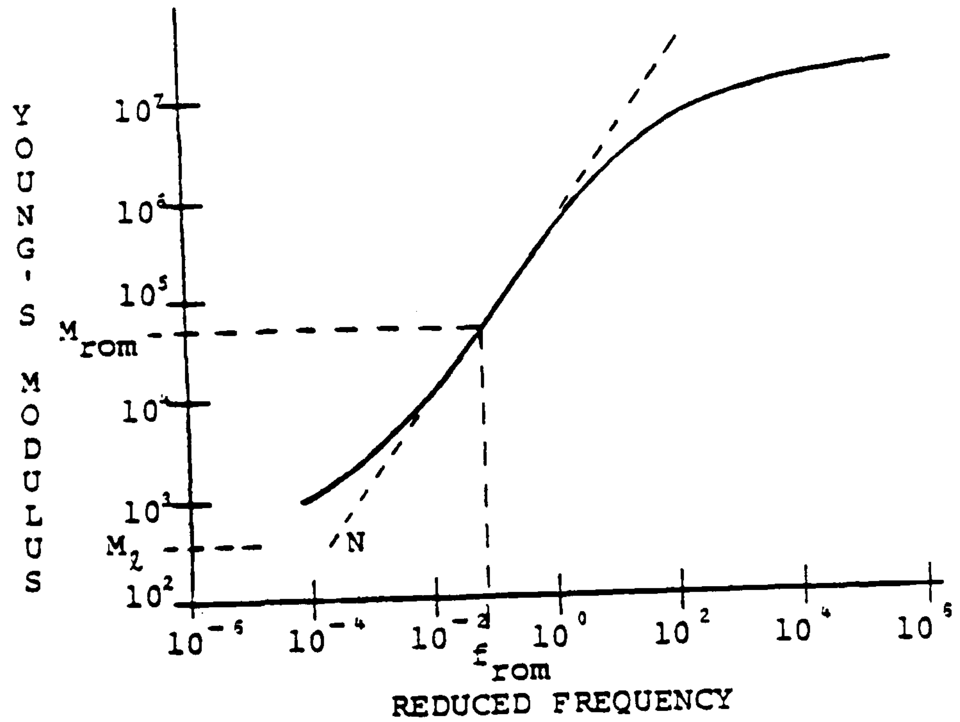

Figure 1.38. Curve Fit Parameters for Storage Modulus.

Loss Factor

$$\log_{10}(\eta) = \log_{10}(\eta_{fro\ell}) + \frac{C}{2}\left[\left(\frac{S_\ell + S_h}{C}\right)\log_{10}\left(\frac{f_\ell}{f_{ro\ell}}\right) + (S_\ell + S_h)\left(1 - \sqrt{1 + \left(\frac{\log_{10}\left(\frac{f_r}{f_{ro\ell}}\right)}{C}\right)^2}\right)\right] \tag{7}$$

where:

η is the loss factor;

f_r is the reduced frequency;

$\eta_{fro\ell}$ is the loss factor value of the damping peak;

$f_{ro\ell}$ is the reduced frequency value of the damping peak;

S_ℓ is the slope of assymptotic line for low values of reduced frequency;

S_h is the slope of assymptotic line for high values of reduced frequency;

C is a paramenter which defines the curvature of the damping peak.

Figure 1.39 illustrates the curve fit parameters $\eta_{fro\ell}$, $f_{ro\ell}$, S_ℓ, S_h, and C.

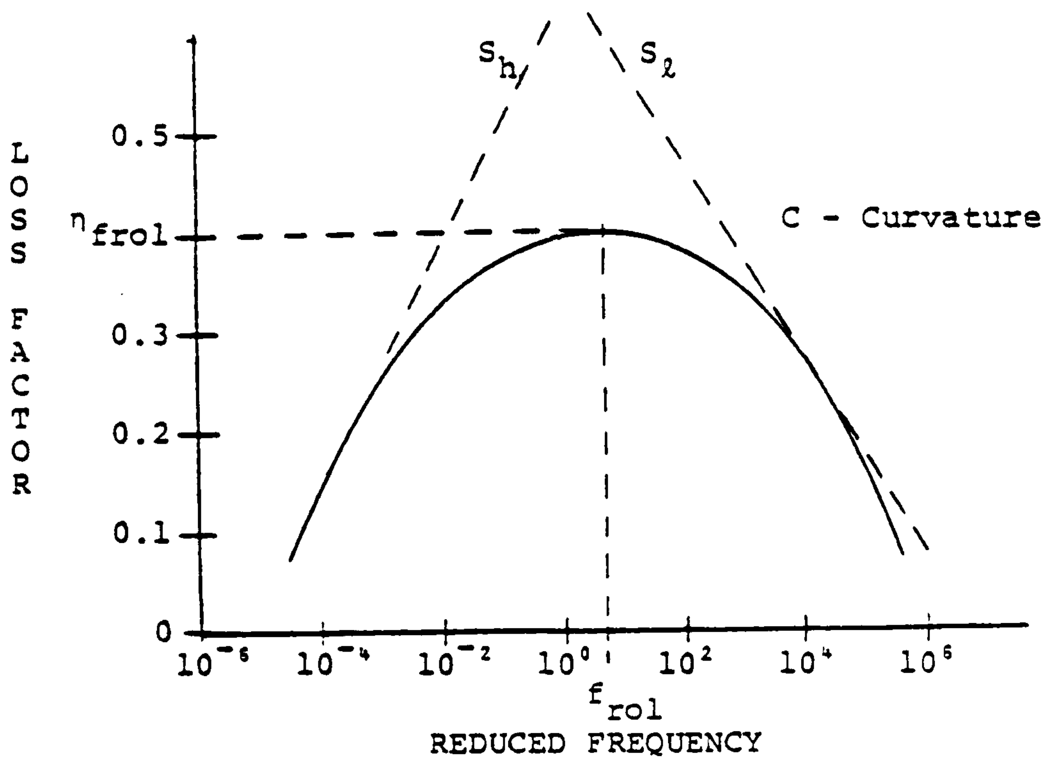

Figure 1.39. Curve Fit Parameters for Loss Factor

The curve fit equations for each material are included in the materials damping properties evaluation summary sheets.

1.2.1.5. Data Files Maintenance

A file of high temperature beam test data compiled between February, 1977 and November, 1979 were completely reorganized and have been updated as additional tests were conducted. The format used to tabulate the results of these enamels tests are shown in Figures 1.40 through 1.45 as follows:

Figure 1.40: A Brief Summary of Each Beam Test

Figure 1.41: Bare Beam Test Data

Figure 1.42: Composite Beam Test Data

Figure 1.43: Reduced Data (Computer Print-out)

Figure 1.44: Reduced Temperature Nomograph with Young's Modulus and Loss Factor Plotted (Computer Print-out)

Figure 1.45: Reduced Temperature Nomograph with Young's Modulus and Loss Modulus Plotted (Computer Print-out)

Material properties of all materials characterized to date are currently available upon request.

A beam test number is assigned to each beam test and includes a two digit beam material code followed by a two digit specimen number and the test run number of this beam. The test run number is a chronological count indicating the number of coated beam tests run on that particular beam. An example of this system follows.

01	01	-1
Material Code Haynes Alloy #188	Specimen Number First beam made of Haynes #188	First coated beam test of specimen 01-01

The bare beam tests are indicated in the same manner with no test number. The bare beam test number of the beam example above would be 01-01.

The results of the beam tests have been reported in appropriate technical reports. These results are available upon request.

Beam No. 01-48-4 Date: 4/25/79

Damping Material Corning 7570 + 2% Na_2O + 2% $KHCO_3$

Material Thickness 0.0186 in. Material Density 0.1876 lb/in^3 Fixture No. 2

Beam Thickness .0371 in. Beam Density 0.33 lb/in^3 Length 8.28 in.

Temperature Test Range: Between 925 °F and 650 °F

Frequency Test Range: Between N/A Hz and N/A Hz

Loss Factor η_D:

Peak	100 Hz	η_D 0.5	Temperature 800 °F	
	1000 Hz	η_D 0.5	Temperature 842 °F	
Range	100 Hz	830 °F	770 °F	
	1000 Hz	860 °F	810 °F	

Complex Modulus: E_D^*

Peak	100 Hz	7.2×10^6 psi	Temperature 760 °F
	1000 Hz	7.2×10^6 psi	Temperature 810 °F
Range	100 Hz	820 °F	740 °F
	1000 Hz	852 °F	770 °F

Vibe 2 Index 70 Cufit Index 119

Project: F107-2

Remarks: Coating smooth and glossy with no visible signs of deterioration at completion of test.

Figure 1.40. Vitreous Enamel Evaluation Sheet.

Bare Beam No. 01-48

Temp.	Mode	f_C	f_L	f_R	Δf	η
°F		Hz	Hz	Hz	Hz	
1700	2	91.32	91.02	91.66	.64	.00701
1700	4	504.87	503.52	506.16	2.64	.00523
1700	5	837.31	835.14	839.00	3.86	.00461
1700	6	1253.24	1249.93	1256.41	6.48	.00517
1650	2	91.93	91.63	92.30	.67	.00729
1650	4	508.85	507.85	509.92	2.07	.00407
1650	5	843.49	841.81	844.88	3.07	.00364
1650	6	1261.49	1258.07	1265.05	6.98	.00553
1600	2	93.01	92.69	93.35	.66	.00710
1600	4	513.40	512.77	514.08	1.31	.00255
1600	5	850.77	849.74	851.78	2.04	.00240
1600	6	1272.71	1271.91	1274.40	2.49	.00196
1600	2	92.94				
1600	3	260.95				
1600	4	512.97				
1600	5	849.68				
1600	6	1272.57				
1550	2	94.01	93.73	94.27	.54	.00574
1550	4	517.68	517.28	518.15	.88	.00170
1550	5	857.57	856.97	858.44	1.47	.00171
1550	6	1283.32	1282.16	1284.41	2.25	.00175
1500	2	94.73	94.55	94.95	.40	.00422
1500	3	265.34	265.07	265.61	.54	.00204
1500	4	521.54	521.32	521.92	.60	.00115
1500	5	864.06	863.55	864.62	1.07	.00124
1500	6	1293.12	1292.28	1294.04	1.76	.00136
1400	2	96.07				
1400	3	268.96				
1400	4	528.72				
1400	5	875.72				
1400	6	1310.02				

Page 1 of 2

Figure 1.41. Bare Beam Test Data.

Beam No. 01-48-4

°F Temp.	Mode	f_c	f_n	f_L	f_R	Δf	η_s	η_c	1dB
925	2	93.39	102.18	93.29	93.53	.24	.0026		
	3	260.45	285.60	260.06	260.87	.81	.0031		
	4	511.48	562.90	510.44	512.52	2.08	.0041		
	5	843.11	932.10	840.91	845.69	4.78	.0057		
	6	1257.30	1394.90	1252.52	1263.12	10.60	.0084		
900	2	93.66	102.44	93.51	93.81	.30	.00033	.0033	
	3	261.34	286.35	260.79	262.07	1.28	.0049		
	4	513.42	564.40	511.33	515.51	4.18	.0081		
	5	846.36	934.50	842.14	851.93	9.79	.0116		
	6	1263.65	1398.60	1256.23	1276.54	20.31	.0161		
900	2	93.83	102.44	93.62	93.95	.33	.0035		
	3	261.34	286.35	260.92	261.58	1.30	.0050		
	4	512.82	564.40	510.84	515.00	4.16	.0081		
	5	846.51	934.50	841.32	853.46	12.14	.0143		
	6	1264.88	1398.60	1253.80	1276.25	22.45	.0177		
875	2	94.11	102.71	93.84	94.36	.52	.0055		
	3	262.51	287.15	260.99	263.66	2.67	.0102		
	4	515.82	565.60	511.31	520.64	9.33	.0181		
	5	855.12	937.00	843.72	868.02	24.30	.0284		
	6	1279.14	1402.00	1267.14	1286.53	38.11	.0298		

Figure 1.42. Composite Beam Test Data.

EXPERIMENTAL CODE : 70
MATERIAL :BEAM NO. 01-48
DATA SOURCES
MANUFACTURER :N
AFML :UDRI BEAM COATED ONE SIDE 4/27
OTHER :7570 + 2% NA2O + 2% KHCO3

NO.	MODULUS N/M**2	LOSS FACTOR	TEMP. DEG. C	FREQ. HZ	MODE NO.	BEAM MOD. N/M**2	COMPOSITE LOSS FAC.	BEAM FREQ. HZ	COMPLEX MOD. N/M**2
1	1.85229E+10	.1465	426.7	1416.4	6.	2.14025E+11	.0318	1412.5	2.71414E+09
2	2.62775E+09	.2005	496.1	1257.3	6.	2.08724E+11	.0084	1394.9	5.26924E+08
3	3.04803E+09	.1175	496.1	843.1	5.	2.07201E+11	.0057	932.1	3.58177E+08
4	3.61045E+09	.0720	496.1	511.5	4.	2.06498E+11	.0041	562.9	2.59796E+08
5	6.99095E+09	.0298	496.1	266.5	3.	2.04129E+11	.0031	285.6	2.08000E+08
6	4.38865E+09	.0483	482.2	93.7	2.	2.05898E+11	.0033	102.4	2.11870E+08
7	4.14538E+09	.0753	482.2	261.3	3.	2.05203E+11	.0049	286.3	3.12080E+08
8	3.77388E+09	.1371	482.2	513.4	4.	2.07600E+11	.0081	564.4	5.17506E+08
9	3.22566E+09	.2279	482.2	846.4	5.	2.08270E+11	.0116	934.5	7.35106E+08
10	2.94341E+09	.3471	482.2	1263.6	6.	2.09833E+11	.0161	1398.6	1.02157E+09
11	4.21818E+09	.4620	468.3	1279.1	6.	2.10855E+11	.0298	1402.0	1.94863E+09
12	4.22356E+09	.4369	468.3	855.1	5.	2.09386E+11	.0284	937.0	1.84543E+09
13	4.11645E+09	.2840	468.3	515.8	4.	2.08483E+11	.0181	565.6	1.16898E+09
14	4.38351E+09	.1497	468.3	262.5	3.	2.06351E+11	.0102	287.2	6.56116E+08
15	4.69146E+09	.0761	468.3	94.1	2.	2.06985E+11	.0055	102.7	3.56979E+08
16	4.85578E+09	.1617	454.4	94.4	2.	2.08034E+11	.0120	103.0	7.85002E+08
17	1.49710E+10	.2294	440.6	1383.7	6.	2.12996E+11	.0428	1409.1	3.43393E+09
18	1.00193E+10	.4016	440.6	895.7	5.	2.11447E+11	.0550	941.6	4.02414E+09
19	8.35547E+09	.4903	440.6	534.8	4.	2.10701E+11	.0579	568.6	4.09673E+09
20	6.47196E+09	.5157	440.6	268.1	3.	2.08657E+11	.0493	288.7	3.33770E+09
21	6.56370E+09	.3726	440.6	95.9	2.	2.09046E+11	.0360	103.2	2.44556E+09
22	2.38791E+10	.0152	343.3	108.3	2.	2.16112E+11	.0039	104.9	3.63991E+08
23	2.57155E+10	.0097	343.3	306.6	3.	2.16755E+11	.0026	294.3	2.49801E+08
24	1.39311E+10	.3338	426.7	920.9	5.	2.12436E+11	.0591	943.8	4.64952E+09
25	1.41140E+10	.3324	426.7	557.0	4.	2.11740E+11	.0596	570.0	4.69183E+09
26	1.00539E+10	.3968	426.7	98.5	2.	2.10019E+11	.0548	103.5	3.98986E+09
27	1.58110E+10	.3008	412.8	286.8	3.	2.10830E+11	.0589	290.2	4.75671E+09
28	1.93269E+10	.2094	412.8	576.1	4.	2.12818E+11	.0470	571.4	4.04737E+09
29	1.77205E+10	.1756	412.8	944.4	5.	2.13427E+11	.0370	946.0	3.11120E+09
30	2.28657E+10	.0922	412.8	1454.4	6.	2.15087E+11	.0230	1416.0	2.10762E+09
31	2.22034E+10	.0775	398.9	970.7	5.	2.14421E+11	.0190	948.2	1.72009E+09
32	2.20047E+10	.1089	398.9	585.9	4.	2.13788E+11	.0266	572.7	2.39610E+09
33	2.07313E+10	.1448	398.9	295.9	3.	2.11921E+11	.0342	291.0	3.00266E+09
34	1.95730E+10	.1490	398.9	105.0	2.	2.12135E+11	.0338	104.0	2.91563E+09
35	2.46712E+10	.0415	385.0	1473.6	6.	2.17096E+11	.0108	1422.6	1.02287E+09
36	2.40522E+10	.0404	385.0	982.3	5.	2.15463E+11	.0104	950.5	9.71278E+08
37	2.39989E+10	.0477	385.0	593.4	4.	2.14797E+11	.0123	574.1	1.14553E+09
38	2.35885E+10	.0640	385.0	301.2	3.	2.13088E+11	.0164	291.8	1.51021E+09
39	2.20721E+10	.0795	385.0	106.7	2.	2.13075E+11	.0195	104.2	1.75449E+09
40	2.33755E+10	.0418	371.1	107.6	2.	2.14098E+11	.0106	104.5	9.75940E+08
41	2.52756E+10	.0307	371.1	304.5	3.	2.14185E+11	.0082	292.5	7.76941E+08
42	2.53510E+19	.0230	371.1	990.7	5.	2.16416E+11	.0061	952.6	5.82382E+08
43	2.59255E+10	.0265	371.1	1485.7	6.	2.18074E+11	.0071	1425.8	6.86834E+08
44	2.65727E+10	.0181	357.2	1493.1	6.	2.19054E+11	.0049	1429.0	4.79794E+08
45	2.61380E+10	.0111	357.2	996.4	5.	2.17371E+11	.0030	954.7	2.90523E+08
46	2.58026E+10	.0168	357.2	602.1	4.	2.17725E+11	.0045	578.0	4.34107E+08
47	2.63258E+10	.0161	357.2	306.8	3.	2.15285E+11	.0044	293.3	4.24723E+08
48	2.46949E+10	.0225	357.2	108.6	2.	2.15083E+11	.0059	104.7	5.55689E+08
49	2.56967E+10	.0101	343.3	602.1	4.	2.18102E+11	.0027	578.5	2.60344E+08

Figure 1.43. Reduced Data (Computer Print-Out).

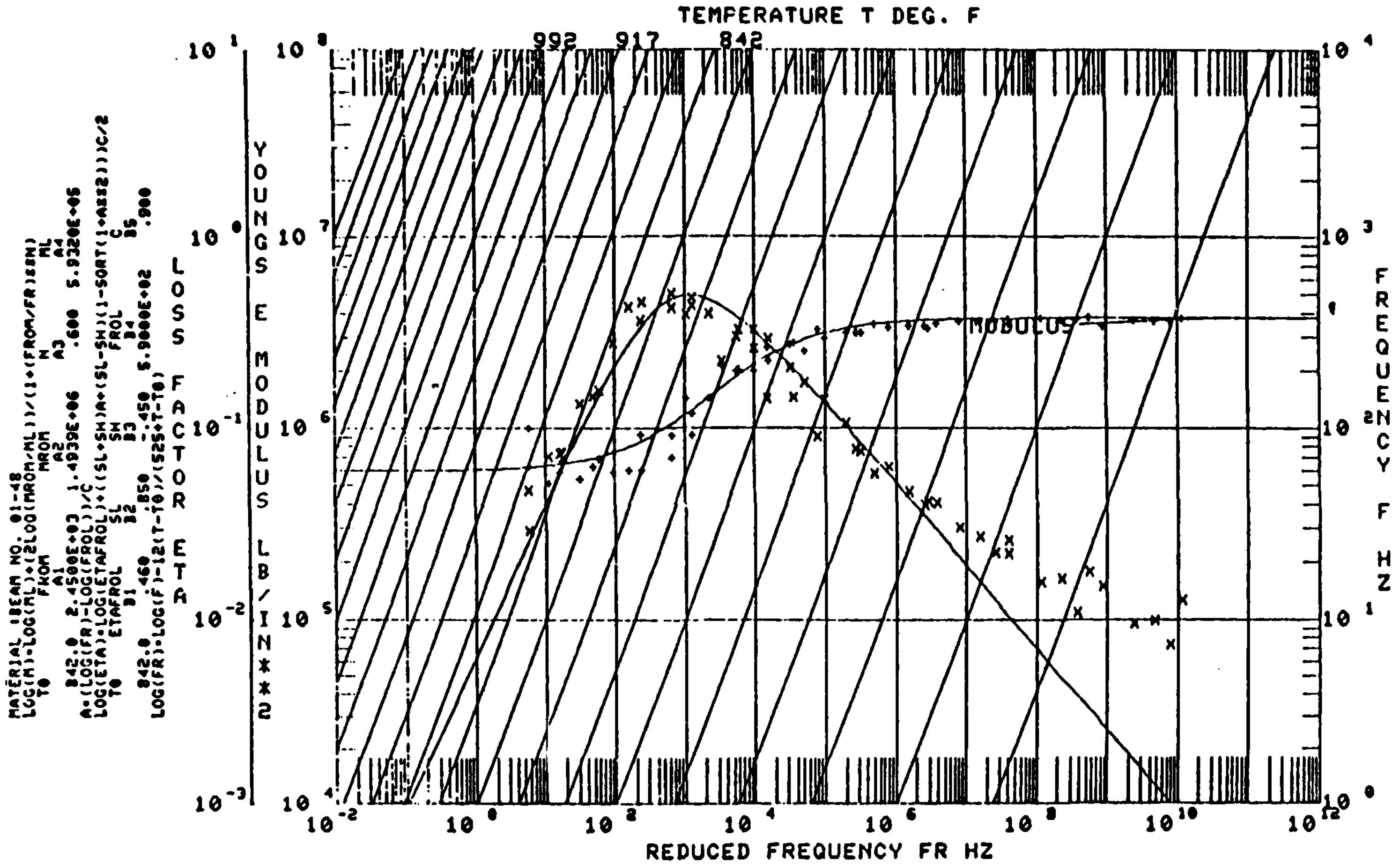

Figure 1.44. Reduced Temperature Nomograph with Young's Modulus and Loss Factor Plotted (Computer Print-Out).

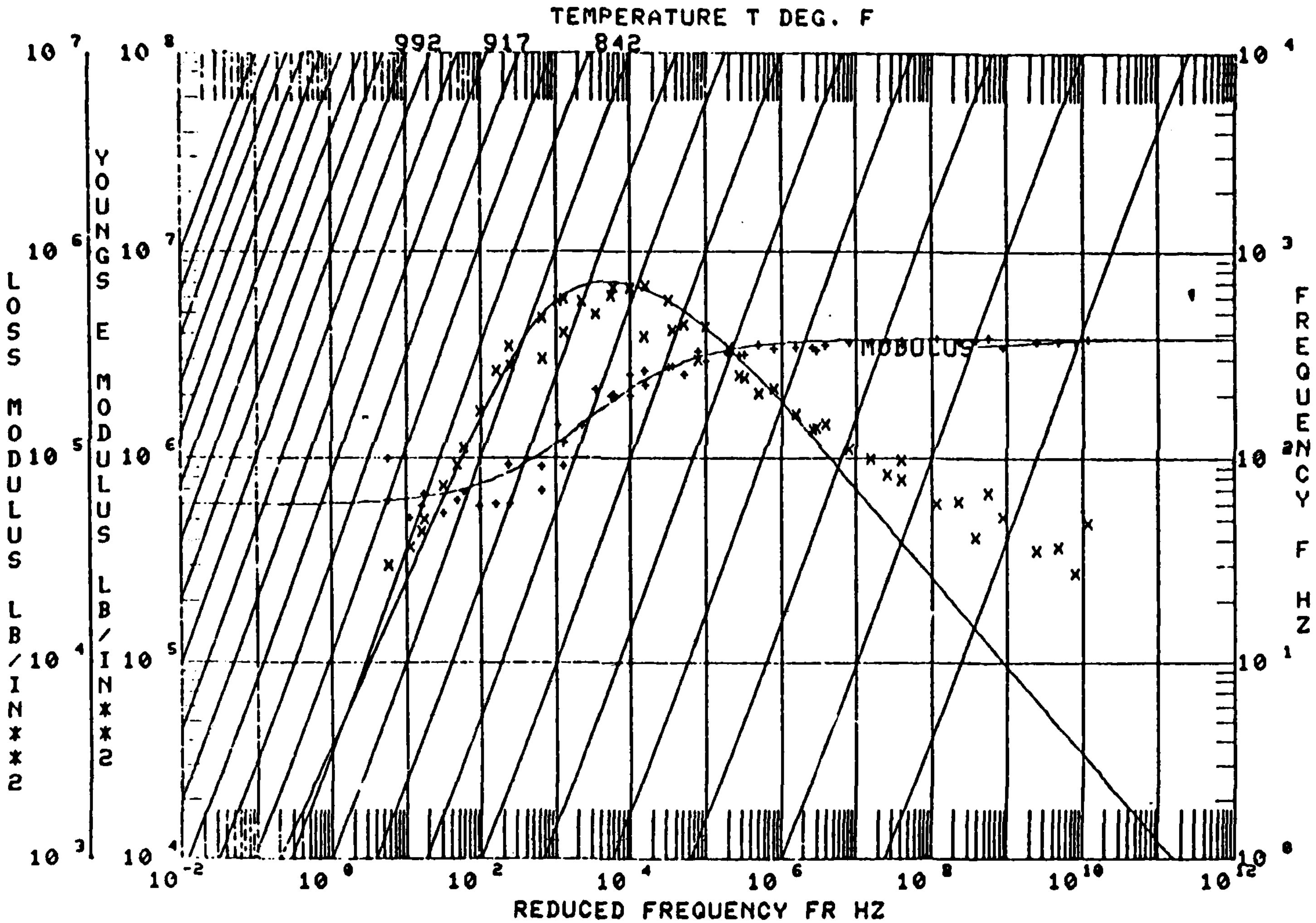

Figure 1.45. Reduced Temperature Nomograph with Young's Modulus and Loss Modulus Plotted (Computer Print-Out).

1.2.1.6. Materials Tested

Magnesia-Alumina Spinel

UDRI and Detroit Diesel Allison Division of the General Motors Corporation (DDA), conducted a cooperative effort to characterize a DDA proprietary temperature damping material.

The UDRI supplied two 17-4PH steel beam specimens, serial number 03-05 and 03-06, to DDA for coating. Baseline damping measurements obtained for the second through sixth modes in the 700°F to 1,000°F (371.11°C to 537.78°C) range and the data were stored before the beams were transported to DDA.

The beams were coated with METCO 212-NS Magnesia-Alumina Spinel (Mag-Spinel) and tested at DDA. The procedures and test results were reported by Mr. David R. Oeth, DDA, in a letter report dated 14 March 1981. The coated beams were returned to UDRI for testing at elevated temperatures.

Room temperatures were conducted on the beam using three level of excitation while the force gage output and strain gage output were monitored. The relative outputs were plotted as strain gage output versus force gage output for the lowest four bending modes. It was planned to use these relationships to conduct the high temperature tests at the three desired levels of excitation. The procedures followed during these tests were as previously described with the exception of the strain gage monitoring. The circuit used to monitor bending strain is illustrated in Figure 1.46.

As testing at elevated temperatures commenced it was apparent that the system was not capable of driving the beam at the desired excitation levels. It was decided to drive the system at three levels of excitation; 25, 50, and 75 mv rms output at the frequency synthesizer (1.70, 3.40, and 5.10 volts rms into the transducer).

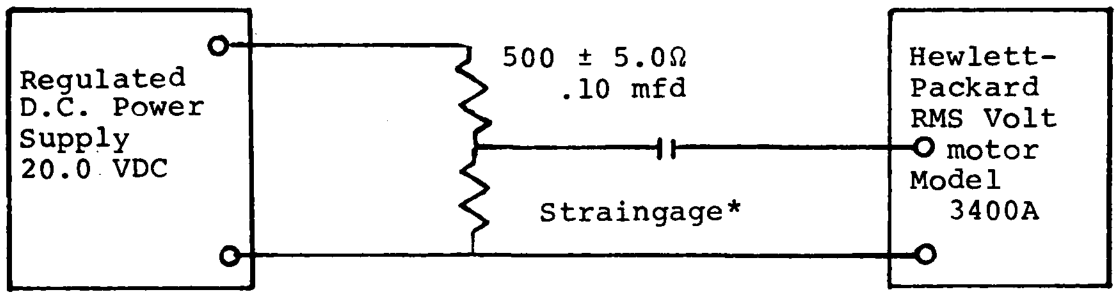

*Straingage: M-M type ED-DY-062-AK-350

Figure 1.46. Bending Strain Monitoring Circuit

Sine frequency sweeps of the force gage output at each temperature were recorded for the second bending mode of beam 03-06. These are presented in Figures 1.47 through 1.53. These curves reflect the expected tendency toward increasing asymmetry about the center frequency as the intensity of excitation is increased. The expected decrease in center frequency related to the increased excitation intensity is also demonstrated.

The reduced material properties are presented in Figures 1.54 through 1.59. Curves of loss modulus and loss factor versus temperature and reduced frequency could not be fit to these data as the temperature at which peak damping occurs was not clearly defined. It would appear that the loss factor is fairly constant over a very wide temperature range, certainly over the range at which the 17-4PH stainless steel beams could be tested.

Serious discrepancy was noted between the structural loss factors derived from the room temperature tests and those reported by DDA. These differences have not been reconciled.

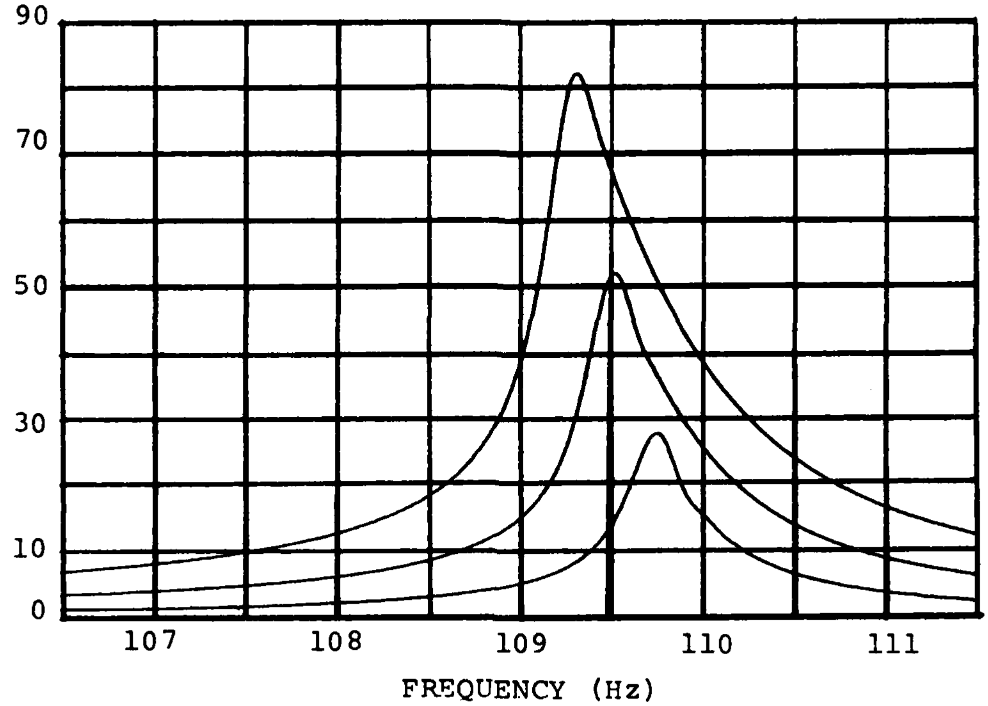

Figure 1.47. Second Bending Mode Responses of Beam 03-06 at 800°F.

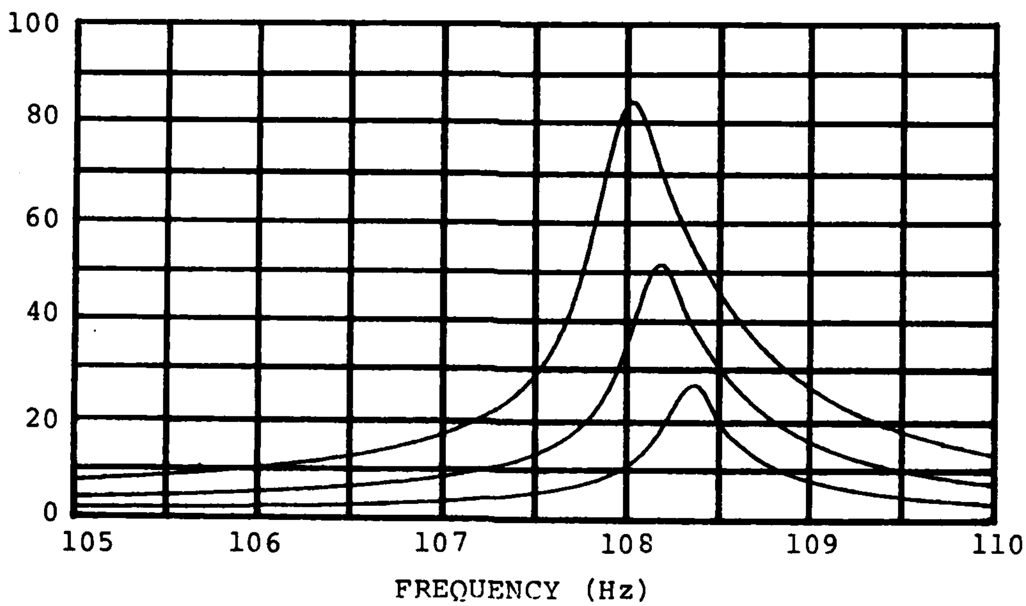

Figure 1.48. Second Bending Mode Responses of Beam 03-06 at 850°F.

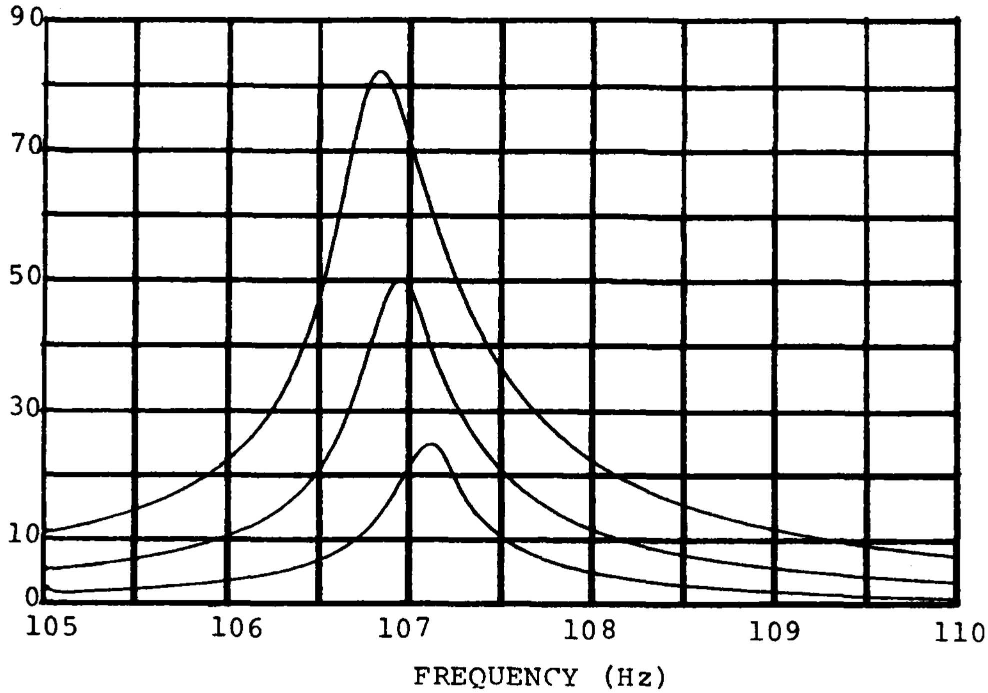

Figure 1.49. Second Bending Mode Responses of Beam 03-06 at 900°F.

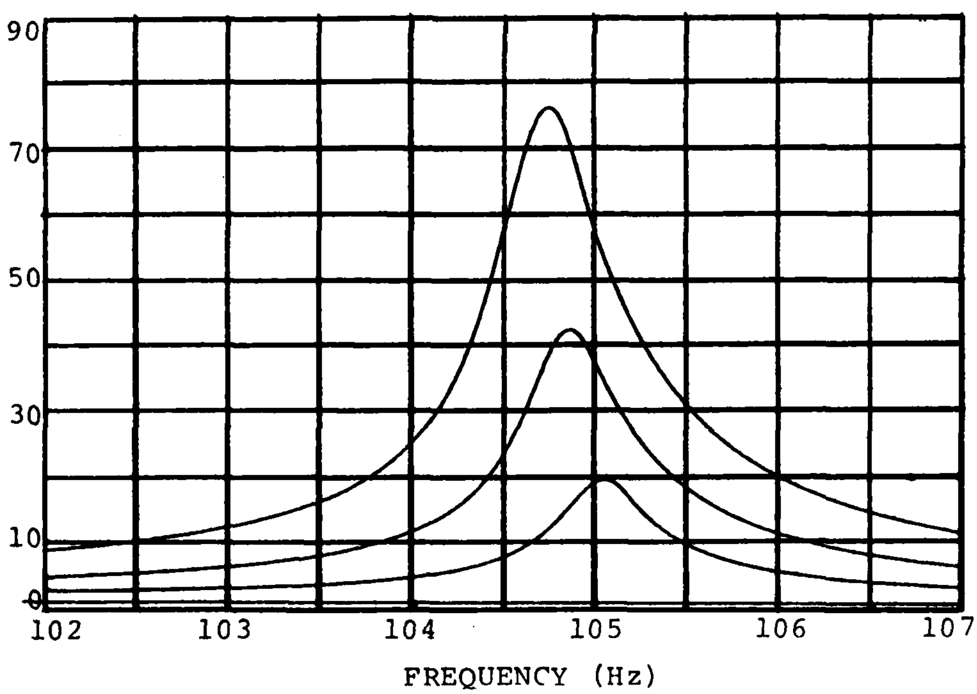

Figure 1.50. Second Bending Mode Response of Beam 03-06 at 1002°F.

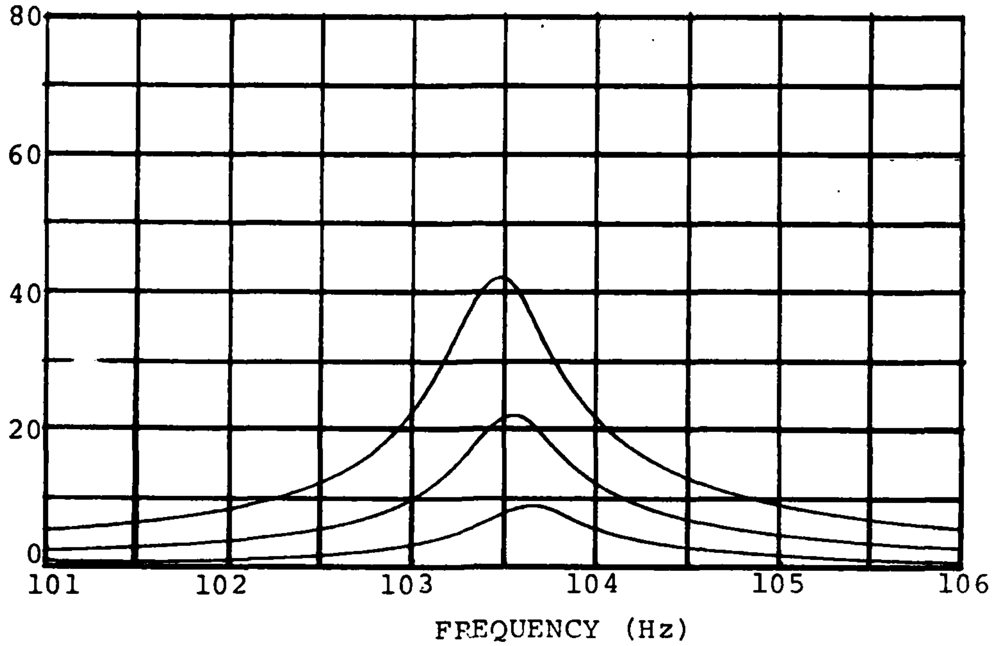

Figure 1.51. Second Bending Mode Responses of Beam 03-06 at 1053°F.

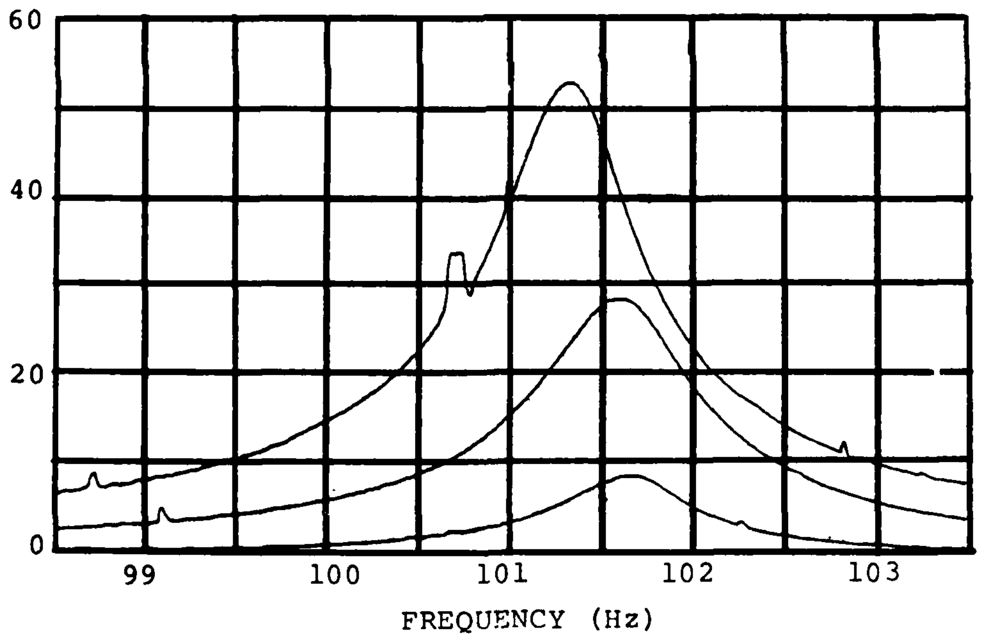

Figure 1.52. Second Bending Mode Responses of Beam 03-06 at 1093°F.

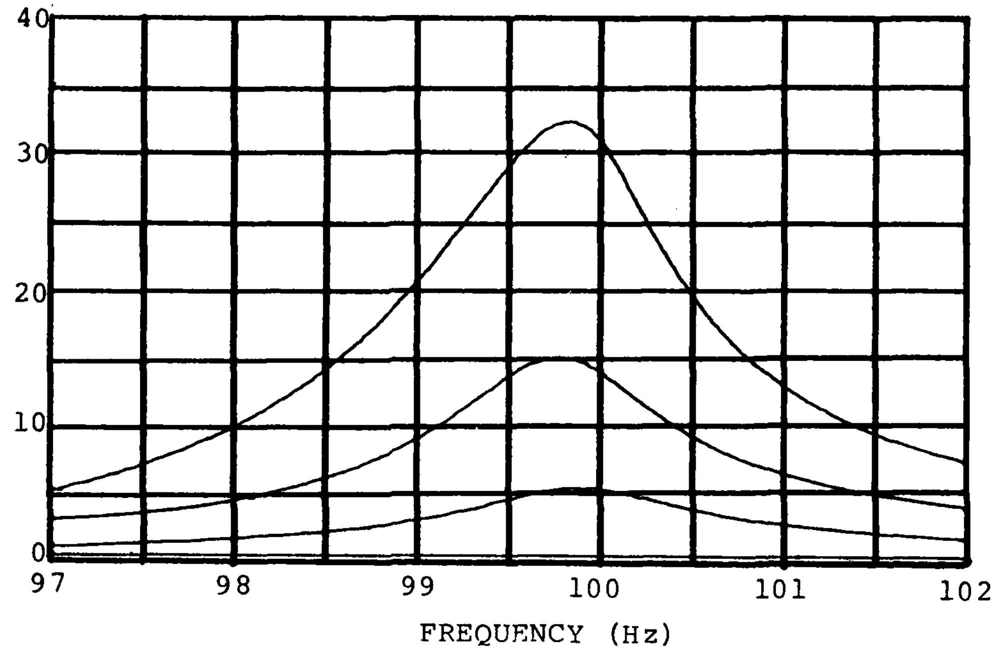

Figure 1.53. Second Bending Mode Responses of Beam 03-06 at 1147°F.

CONFIGURATION TYPE 2
DAMPING LAYER THICKNESS .00400 DENSITY .10838
BEAM LENGTH 8.75000 THICKNESS .04400 DENSITY .28100

NO.	MODULUS N/M**2	LOSS FACTOR	TEMP. DEG. C	FREQ. HZ	MODE NO.	BEAM MOD. N/M**2	COMPOSITE LOSS FAC.	BEAM FREQ. HZ	LOSS MOD. N/M**2
1	1.54161E+10	.1749	537.8	101.1	2.	1.51634E+11	.0055	101.2	2.69666E+09
2	1.46041E+10	.1451	537.8	283.8	3.	1.52530E+11	.0043	234.4	2.11858E+09
3	1.66624E+10	.1284	537.8	558.3	4.	1.53362E+11	.0043	558.3	2.13961E+09
4	1.60785E+10	.1414	510.0	102.6	2.	1.56139E+11	.0045	102.7	2.27337E+09
5	1.77883E+10	.0917	510.0	228.3	3.	1.56798E+11	.0032	283.1	1.63175E+09
6	1.78499E+10	.1061	510.0	565.3	4.	1.57340E+11	.0037	565.5	1.89324E+09
7	1.97643E+10	.0873	482.2	104.2	2.	1.60057E+11	.0033	103.9	1.72612E+09
8	2.22754E+10	.0643	482.2	293.3	3.	1.61044E+11	.0027	291.9	1.43124E+09
9	2.39362E+10	.0669	482.2	576.1	4.	1.61345E+11	.0030	572.6	1.60095E+09
10	1.82887E+10	.0818	454.4	105.4	2.	1.64369E+11	.0028	105.3	1.49514E+09
11	2.24973E+10	.0507	454.4	297.0	3.	1.65255E+11	.0021	295.7	1.14109E+09
12	2.36381E+10	.0509	454.4	583.2	4.	1.65670E+11	.0022	580.3	1.20222E+09

Figure 1.54(a) Reduced Test Data .004 Inch Mag-Spinel, 25mv$_{rms}$ Excitation.

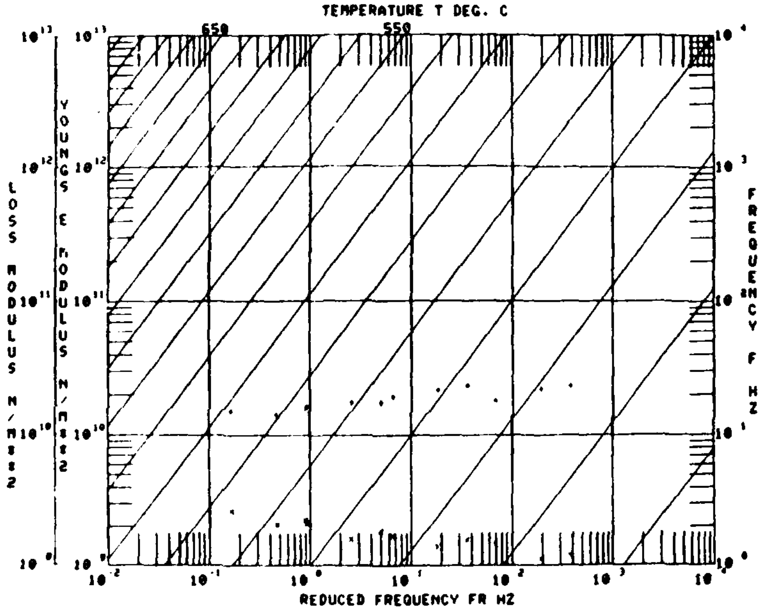

Figure 1.54(b) Loss Modulus-Reduced Frequency Nomograph 0.004 Inch Mag-Spinel 25mv$_{rms}$ Excitation.

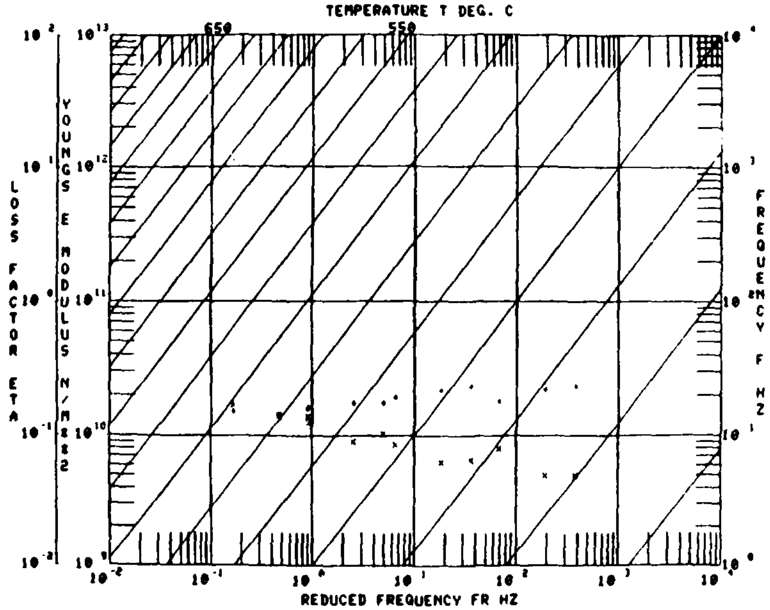

Figure 1.54(c) Loss Factor-Reduced Frequency Nomograph 0.004 Inch Mag-Spinel 25mv$_{rms}$ Excitation.

CONFIGURATION TYPE 2
DAMPING LAYER THICKNESS .00400 DENSITY .10830
BEAM LENGTH 8.75000 THICKNESS .04400 DENSITY .28100

NO.	MODULUS N/M**2	LOSS FACTOR	TEMP. DEG. C	FREQ. HZ	MODE NO.	BEAM MOD. N/M**2	COMPOSITE LOSS FAC.	BEAM FREQ. HZ	LOSS MOD. N/M**2
1	1.72687E+10	.1457	537.8	101.2	2.	1.51634E+11	.0051	101.2	2.51549E+09
2	1.43373E+10	.1270	537.8	283.7	3.	1.52830E+11	.0037	284.4	1.82141E+09
3	1.69301E+10	.0912	537.8	558.4	4.	1.53362E+11	.0031	558.3	1.54382E+09
4	1.58741E+10	.1463	510.0	102.6	2.	1.56139E+11	.0046	102.7	2.32240E+09
5	1.79251E+10	.0825	510.0	289.3	3.	1.56798E+11	.0029	285.1	1.47940E+09
6	1.84677E+10	.0861	510.0	566.2	4.	1.57340E+11	.0031	565.5	1.58927E+09
7	1.81580E+10	.1147	482.2	104.0	2.	1.60057E+11	.0040	103.9	2.08209E+09
8	2.14322E+10	.0691	482.2	293.0	3.	1.61044E+11	.0022	291.9	1.48049E+09
9	2.33730E+10	.0639	482.2	575.5	4.	1.61345E+11	.0028	572.6	1.49172E+09
10	1.69543E+10	.1104	454.4	105.2	2.	1.64369E+11	.0035	105.3	1.86098E+09
11	2.11994E+10	.0536	454.4	296.6	3.	1.65255E+11	.0021	295.7	1.13676E+09
12	2.32767E+10	.0446	454.4	583.1	4.	1.65670E+11	.0019	580.3	1.03719E+09

Figure 1.55(a) Reduced Test Data, 0.004 Inch Mag-Spinel, 50mv$_{rms}$ Excitation.

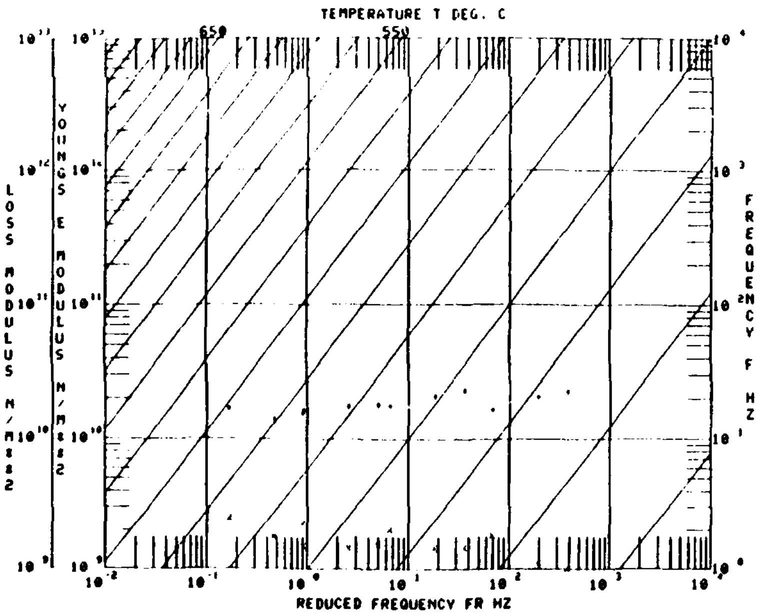

Figure 1.55(b) Loss Modulus-Reduced Frequency Nomograph 0.004 Mag-Spinel 50mv$_{rms}$ Excitation.

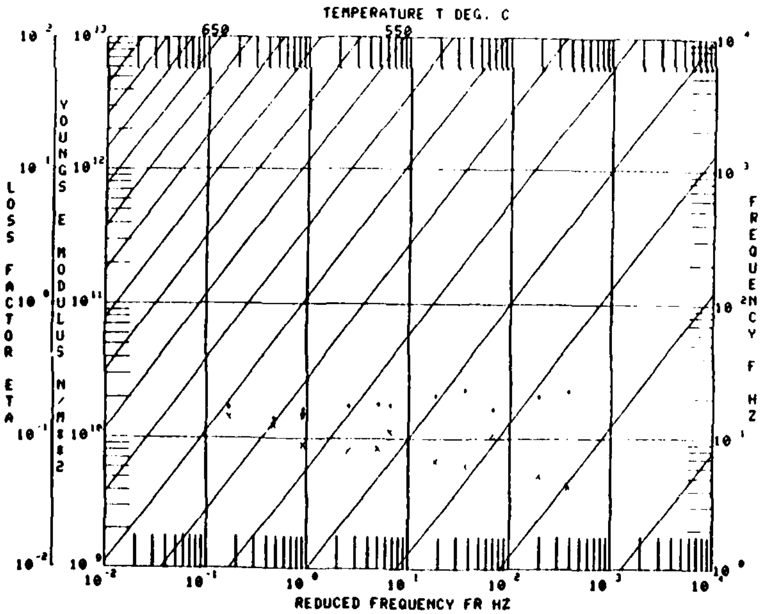

Figure 1.55(c) Loss Factor-Reduced Frequency Nomograph 0.004 Mag-Spinel 50mv$_{rms}$ Excitation.

CONFIGURATION TYPE 2
DAMPING LAYER THICKNESS .00400 DENSITY .10832
BEAM LENGTH 8.75000 THICKNESS .04400 DENSITY .28100

NO.	MODULUS N/M**2	LOSS FACTOR	TEMP. DEG. C	FREQ. HZ	MODE NO.	BEAM MOD. N/M**2	COMPOSITE LOSS FAC.	BEAM FREQ. HZ	LOSS MOD. N/M**2
1	1.73348E+10	.1480	537.8	101.3	2.	1.51634E+11	.0052	101.2	2.56536E+09
2	1.47375E+10	.1304	537.8	283.9	3.	1.52830E+11	.0039	234.4	1.92233E+09
3	1.67294E+10	.1190	537.8	558.3	4.	1.53362E+11	.0040	558.3	1.99076E+09
4	1.58741E+10	.1654	510.0	102.6	2.	1.56139E+11	.0052	102.7	2.62532E+09
5	1.80620E+10	.1017	510.0	238.3	3.	1.56798E+11	.0036	223.1	1.83728E+09
6	1.82618E+10	.0757	510.0	566.1	4.	1.57340E+11	.0027	565.5	1.38332E+09
7	1.76692E+10	.1206	482.2	104.0	2.	1.60057E+11	.0041	103.9	2.13096E+09
8	2.05889E+10	.0769	482.2	292.8	3.	1.61044E+11	.0030	291.9	1.58223E+09
9	2.31617E+10	.0667	482.2	575.7	4.	1.61345E+11	.0029	572.6	1.54402E+09
10	1.54199E+10	.1339	454.4	105.1	2.	1.64363E+11	.0039	105.3	2.06482E+09
11	1.97572E+10	.0655	454.4	296.2	3.	1.65255E+11	.0024	295.7	1.29366E+09
12	2.23369E+10	.0439	454.4	582.6	4.	1.65670E+11	.0018	580.3	9.79909E+08

Figure 1.56(a) Reduced Test Data, 0.004 Mag-Spinel $75mv_{rms}$ Excitation.

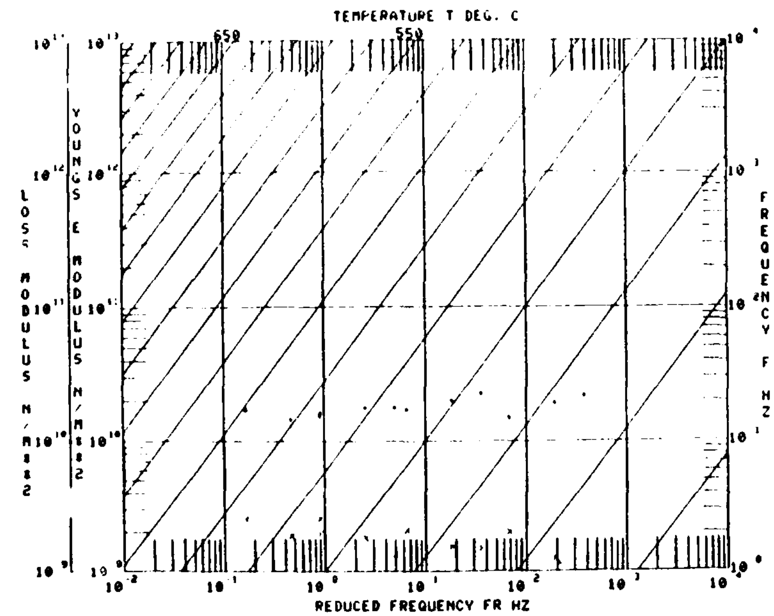

Figure 1.56(b) Loss Modulus-Reduced Frequency Nomograph 0.004 Mag-Spinel $75mv_{rms}$ Excitation.

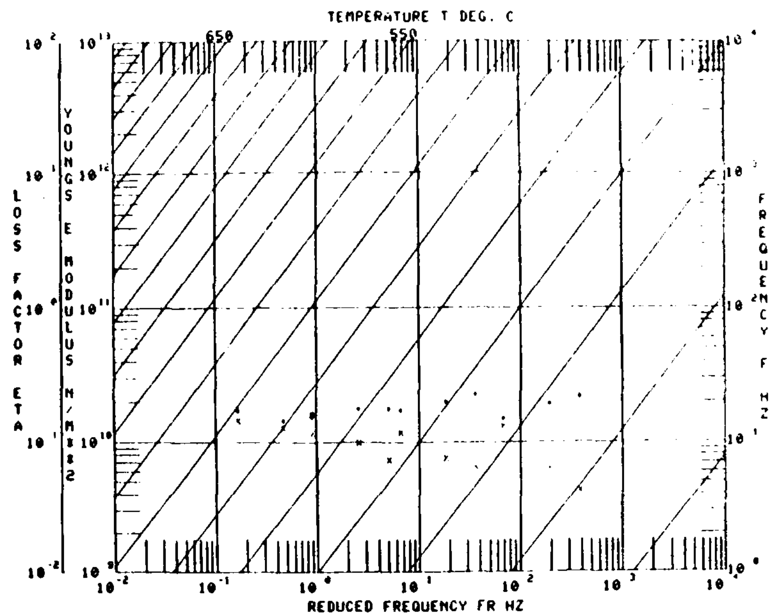

Figure 1.56(c) Loss Factor-Reduced Frequency Nomograph 0.004 Mag-Spinel $75mv_{rms}$ Excitation.

CONFIGURATION TYPE 2
DAMPING LAYER THICKNESS .01000 DENSITY .10832
BEAM LENGTH 8.75000 THICKNESS .04400 DENSITY .28100

NO.	MODULUS N/M**2	LOSS FACTOR	TEMP. DEG. C	FREQ. HZ	MODE NO.	BEAM MOD. N/M**2	COMPOSITE LOSS FAC.	BEAM FREQ. HZ	LOSS MOD. N/M**2
1	2.66636E+10	.0326	538.9	105.0	2.	1.50963E+11	.0047	100.9	8.68644E+08
2	2.85088E+10	.0321	538.9	294.6	3.	1.49937E+11	.0049	281.7	9.14663E+08
3	2.92018E+10	.0213	538.9	579.2	4.	1.50470E+11	.0033	553.0	6.21187E+08
4	2.54101E+10	.0285	510.0	105.6	2.	1.54120E+11	.0039	102.0	7.25028E+08
5	2.63943E+10	.0277	510.0	296.4	3.	1.54117E+11	.0039	285.6	7.30926E+08
6	2.68267E+10	.0232	510.0	582.3	4.	1.54645E+11	.0033	560.6	6.22317E+08
7	2.58623E+10	.0266	482.2	107.0	2.	1.58625E+11	.0036	103.5	6.87295E+08
8	2.66823E+10	.0180	482.2	300.2	3.	1.58486E+11	.0025	289.6	4.80071E+08
9	2.70738E+10	.0143	482.2	569.6	4.	1.58956E+11	.0020	568.4	3.86147E+08
10	2.42775E+10	.0240	454.4	108.3	2.	1.64504E+11	.0030	105.4	5.82383E+08
11	2.57999E+10	.0167	454.4	303.7	3.	1.63716E+11	.0022	294.4	4.30504E+08
12	2.61712E+10	.0128	454.4	596.7	4.	1.64302E+11	.0017	577.9	3.34573E+08
13	2.47620E+10	.0192	426.7	109.5	2.	1.68398E+11	.0024	106.6	4.76613E+08
14	2.51395E+10	.0143	426.7	307.3	3.	1.68760E+11	.0018	298.9	3.59112E+08
15	2.56575E+10	.0094	426.7	603.5	4.	1.69143E+11	.0012	586.3	2.40785E+08

Figure 1.57(a) Reduced Test Data, 0.010 Mag-Spinel $25mv_{rms}$ Excitation.

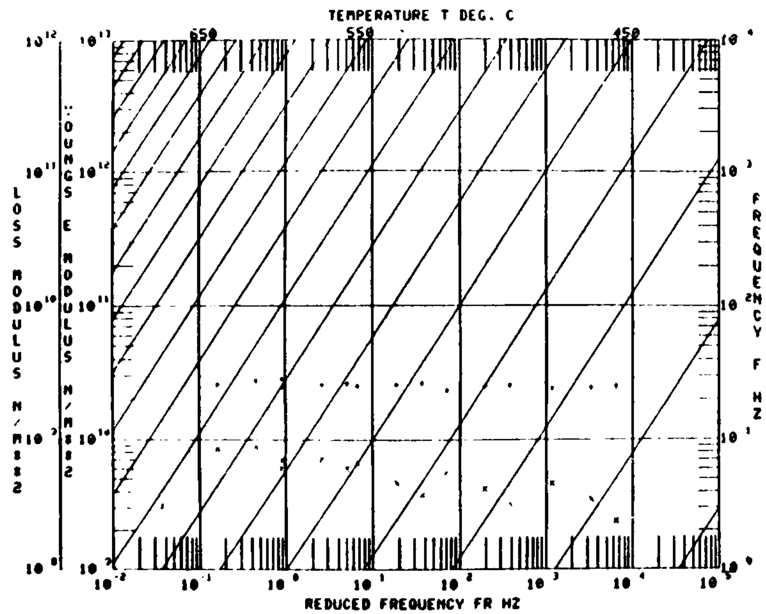

Figure 1.57(b) Loss Modulus-Reduced Frequency Nomograph 0.010 Mag-Spinel $25mv_{rms}$ Excitation.

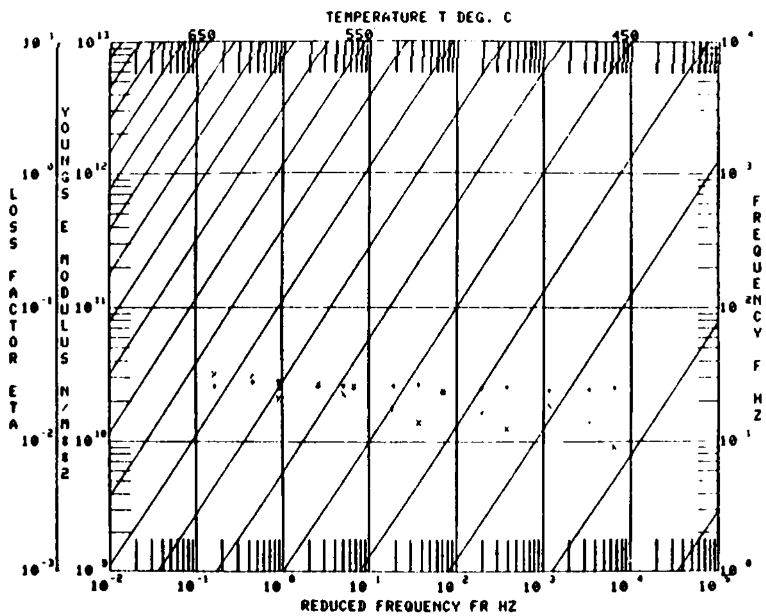

Figure 1.57(c) Loss Factor-Reduced Frequency Nomograph 0.010 Mag Spinel $25mv_{rms}$ Excitation.

CONFIGURATION TYPE 3
DAMPING LAYER THICKNESS .01000 DENSITY .10838
BEAM LENGTH 8.25000 THICKNESS .04400 DENSITY .27100

NO.	MODULUS N/M**2	LOSS FACTOR	TEMP. DEG. C	FREQ. HZ	MODE NO.	BEAM MOD. N/M**2	COMPOSITE LOSS FAC.	BEAM FREQ. HZ	LOSS MOD. N/M**2
1	2.61746E+10	.0359	538.9	104.9	2.	1.50963E+11	.0051	100.9	9.38761E+08
2	2.84318E+10	.0303	538.9	294.5	3.	1.49937E+11	.0047	281.7	8.76774E+08
3	2.92018E+10	.0213	538.9	579.2	4.	1.50470E+11	.0033	553.0	6.21187E+08
4	2.50933E+10	.0355	510.0	105.5	2.	1.54120E+11	.0048	102.0	8.90103E+08
5	2.63186E+10	.0313	510.0	296.3	3.	1.54117E+11	.0044	285.6	8.24126E+08
6	2.68267E+10	.0190	510.0	582.3	4.	1.54645E+11	.0027	560.6	5.09168E+08
7	2.54370E+10	.0307	482.2	106.9	2.	1.58625E+11	.0041	103.5	7.80090E+08
8	2.65690E+10	.0224	482.2	300.1	3.	1.58486E+11	.0031	289.6	5.94752E+08
9	2.70099E+10	.0157	482.2	589.5	4.	1.58956E+11	.0022	563.4	4.24547E+08
10	2.36675E+10	.0310	454.4	108.1	2.	1.64504E+11	.0038	105.4	7.34188E+08
11	2.56609E+10	.0168	454.4	303.6	3.	1.63716E+11	.0022	294.4	4.30040E+08
12	2.61712E+10	.0128	454.4	596.7	4.	1.64302E+11	.0017	577.9	3.34573E+08
13	2.42202E+10	.0269	426.7	109.4	2.	1.68398E+11	.0033	106.6	6.52640E+08
14	2.50415E+10	.0151	426.7	307.2	3.	1.68760E+11	.0019	298.9	3.78781E+08
15	2.55214E+10	.0079	426.7	603.3	4.	1.69143E+11	.0010	586.3	2.00451E+08

Figure 1.58(a) Reduced Test Data, 0.010 Mag-Spinel 50mv$_{rms}$ Excitation.

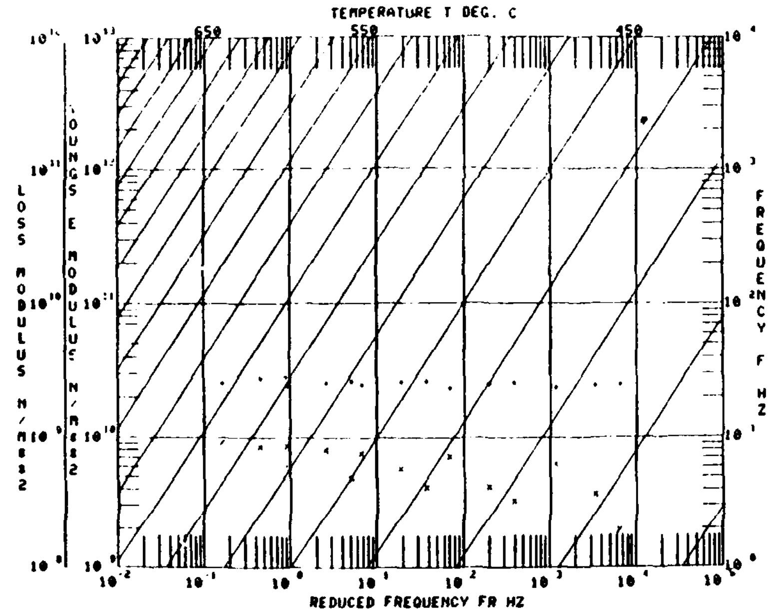

Figure 1.58(b) Loss Modulus-Reduced Frequency Nomograph 0.010 Mag-Spinel 50mv$_{rms}$ Excitation.

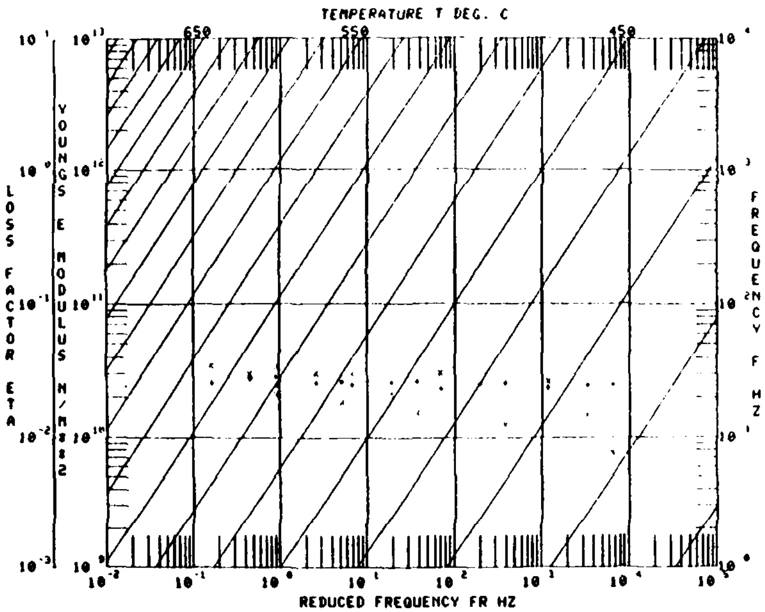

Figure 1.58(c) Loss Factor-Reduced Frequency Nomograph 0.010 Mag-Spinel 50mv$_{rms}$ Excitation.

CONFIGURATION TYPE 2
DAMPING LAYER THICKNESS .01000 DENSITY .10838
BEAM LENGTH 9.75000 THICKNESS .04400 DENSITY .28100

NO.	MODULUS N/M**2	LOSS FACTOR	TEMP. DEG. C	FREQ. HZ	MODE NO.	BEAM MOD. N/M**2	COMPOSITE LOSS FAC.	BEAM FREQ. HZ	LOSS MOD. N/M**2
1	2.55777E+10	.0444	538.9	104.7	2.	1.50963E+11	.0062	100.9	1.13559E+09
2	2.81772E+10	.0324	538.9	294.3	3.	1.49937E+11	.0049	231.7	9.12168E+08
3	2.91379E+10	.0213	538.9	579.1	4.	1.50470E+11	.0033	553.0	6.20863E+08
4	2.61189E+10	.0308	510.0	296.2	3.	1.54117E+11	.0043	285.6	8.04086E+08
5	2.66920E+10	.0219	510.0	582.1	4.	1.54645E+11	.0031	560.6	5.83963E+08
6	2.46857E+10	.0444	482.2	106.7	2.	1.58625E+11	.0058	103.5	1.09693E+09
7	2.63282E+10	.0233	482.2	299.9	3.	1.58496E+11	.0032	289.6	6.12765E+08
8	2.70099E+10	.0179	482.2	589.5	4.	1.58956E+11	.0025	563.4	4.82440E+08
9	2.30942E+10	.0391	454.4	107.9	2.	1.64504E+11	.0047	105.4	9.04007E+08
10	2.54122E+10	.0200	454.4	303.4	3.	1.63716E+11	.0026	294.4	5.07248E+08
11	2.59804E+10	.0129	454.4	596.4	4.	1.64302E+11	.0017	577.9	3.34081E+08
12	2.36409E+10	.0350	426.7	109.2	2.	1.68398E+11	.0042	106.6	8.26959E+08
13	2.46569E+10	.0177	426.7	306.9	3.	1.68760E+11	.0022	298.9	4.37308E+08
14	2.54610E+10	.0102	426.7	603.2	4.	1.69143E+11	.0013	586.3	2.60467E+08
15	2.47766E+10	.0381	510.0	105.4	2.	1.54120E+11	.0051	102.0	9.43278E+08

Figure 1.59(a) Reduced Test Data, 0.010 Mag-Spinel 75mv$_{rms}$ Excitation.

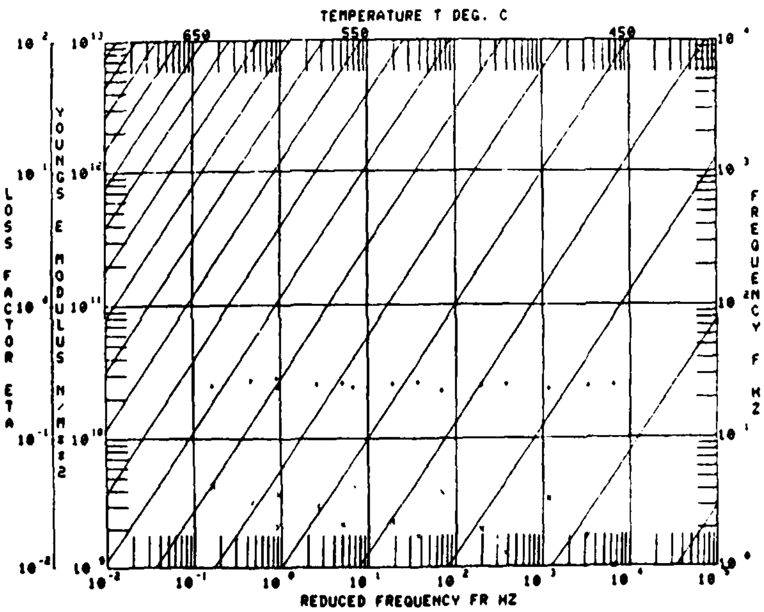

Figure 1.59(b) Loss Factor-Reduced Frequency Nomograph, 0.010 Mag-Spinel 75mv$_{rms}$ Excitation.

1.3. MATERIAL DATA COMPUTER PROGRAMS

1.3.1. Vibration Damping Material Property Reduction and Display Computer Program

The computer programs for determining and displaying the dynamics modulus properties of vibration damping materials have been updated and expanded as required. To keep these programs small enough to run on the Hewlett-Packard 2100 they were subdivided into four stand alone routines as described in Table 1.5 and Figure 1.60.

Figure 1.60 shows the interrelationship between the computer programs "REDUC", "CURVE", "MPROP", and "PREDC", and Table 1.5 lists the input, function, and output of the programs. Beam test data are entered into the data reduction program "REDUC", where material modulus, loss factor, and loss modulus are calculated. The reduced data is stored in a data file on disc where it is accessible by "REDUC" (for data editing and displaying test and/or reduced data), "CURVE", and "MPROP". Reduced data may be plotted on a reduced temperature nomogram, and curves fit to the data in the program "CURVE". Curve parameters are stored in data files on the disk where they are accessible to "CURVE" (for nomogram manipulation), "MPROP", and "PREDC". Program "MPROP" may be used to display the reduced data, nomograms, or material properties at any temperature and frequency. Program "PREDC" may be used to predict the structural dynamics of composite structures. The predictions are based on 4th beam theory.

User manuals with sample input/output for these four manuals are available upon request as listed in Table 1.6.

1.3.2. Additional Material Computer Programs

The following computer programs were developed to operate on the HP2100 minicomputer.

(1) "BECK 1"

"BECK 1" is a computer program written for the 2100 DOS-III System to allow several materials to be plotted in nomogram form on a single nomogram. To accomplish this the temperature scale was converted to temperature relative to T(zero) e.g. $T_0 + 10$.

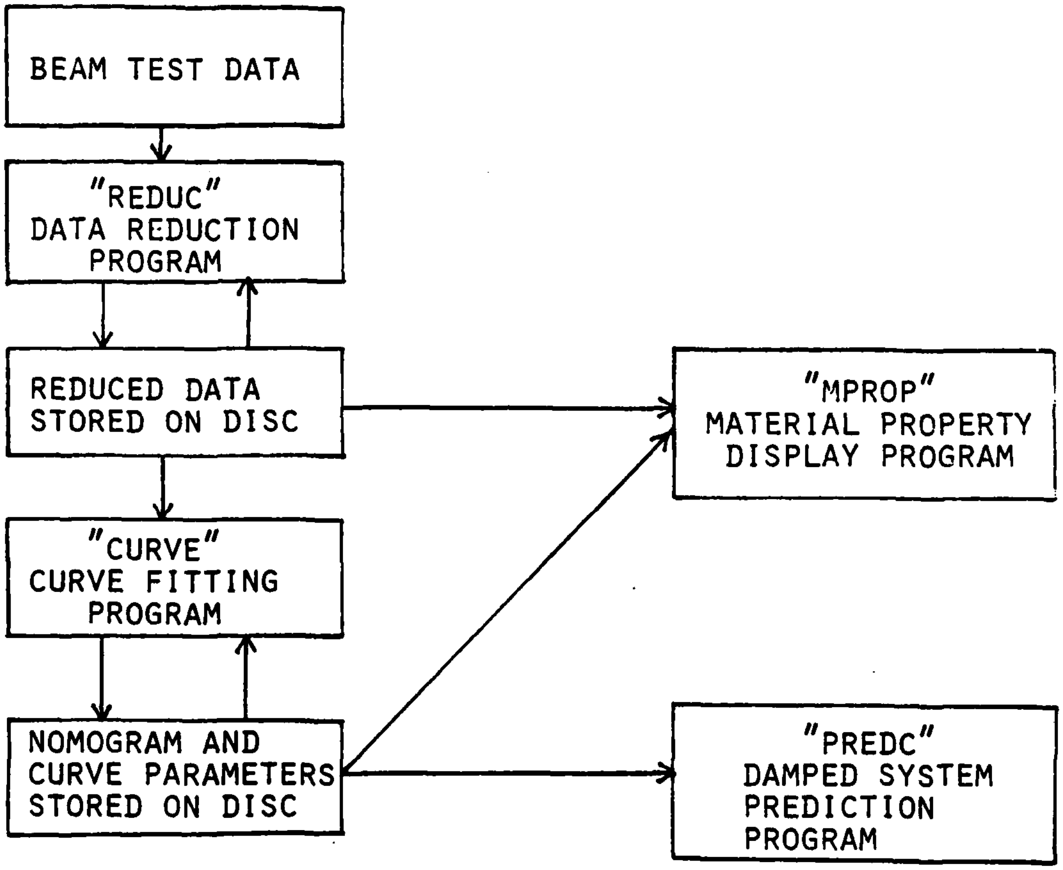

Figure 1.60. The Interrelationship Between the Computer Programs "REDUC", "CURVE", "MPROP" and "PREDC".

(2) "SETTϕ"

"SETTϕ" is a program which allows T zero to be defined rapidly. This time for defining the Dynamic Modulus Equations in the "CURVE" program is greatly reduced by running "SETTϕ" before Curve fitting T zero.

(3) "HOP99"

"HOP99" allows up to four combinations of material and temperature to be plotted in material loss factor versus frequency form.

TABLE 1.5

CAPABILITIES OF MATERIAL EVALUATION AND STRUCTURAL PREDICTION PROGRAMS

Program	Input	Function	Output
REDUC	Damping Material Beam Test Data	Reduce experimental test data to material properties	Material property data for specifice temperatures and frequencies; data files VIBE
CURVE	Material property data for specific temperatures and frequencies; data files VIBE	Develop reduced temperature nomogram material property, and equation paramaters	Reduced temperature nomogram and equation parameter; data files VIBR
MPROP	Reduced temperature nomogram equation parameters; data file VIBR	Display material properties in any form	Material property lists and plots
PREDC	Reduced temperature nomogram equation parameters, strucural configuration; data files VIBR	Predict damping design effectiveness for simple beam and plate structures	Structural loss factor for various design parameters

TABLE 1.6

USER PROGRAM MANUALS

Program	UDRI-TR Number	Title
REDUC	UDR-TR-82-12	User Manual with Sample Input/Output for Material Data Reduction Program (REDUC)
CURVE	UDR-TR-82-13	User Manual with Sample Input/Output for Material Data Curve Fit Program (CURVE)
MPROP	UDR-TR-82-14	User Manual with Sample Input/Output for Material Property Display Program (MPROP)
PREDC	UDR-TR-82-15	User Manual with Sample Input/Ourput for Damped System Prediction Program (PREDC)

1.4 TESTING OF DAMPED SPACE SHUTTLE TEST BEAMS

Several small damped sandwich beams were sent to UDRI to be tested as part of a program to evaluate the effects of the space environment on damping materials. The beams were to be evaluated before being carried aboard the space shuttle, then again after the return. The beams consisted of various combinations of aluminum, graphite-epoxy, and damping materials, as shown in Table 1.8.

The beams were difficult to evaluate because of their small size (3.5 inches long) and poor design (no integral roots, no place to attach roots).

A pin-free test set-up was developed for testing the damped beams. This test set-up is shown in Figure 1.61. The beams are glued to an aluminum rod, which rests on two knife edges. Drive is provided by a noncontacting magnetic transducer at the free end. Initially, the response was measured with an accelerometer, but it was determined that mass loading could be a problem, due to the extremely small size of the beams. To eliminate this problem, the accelerometer was replaced with a non-contacting capactance probe. Table 1.7.

TABLE 1.7

PREDICTED AND MEASURED CENTER FREQUENCIES
OF ALUMINUM SHUTTLE BEAM

MODE	PREDICTED FREQUENCY	MEASURED FREQUENCY	
		ACCELEROMETER	NON-CONTACTING
1	539	536	540
2	1748	1715	1724

All of the test beams were characterized at room temperature using the pin-free test system. There are eight damping configurations each with five identical beams. The two most closely matched beams from each group of five were selected for further testing.

TABLE 1.8

CONSTRUCTION OF SHUTTLE TEST BEAMS

Beam Material	Damping Material	Damping Layer Thickness
graphite-epoxy	ISD-113	0.002"
" "	ISD-113	0.010"
" "	ISD-112	0.002"
" "	ISD-110	0.010"
aluminum	ISD-112	0.002"
"	ISD-113	0.010"
"	ISD-110	0.010"
"	ISD-113	0.002"

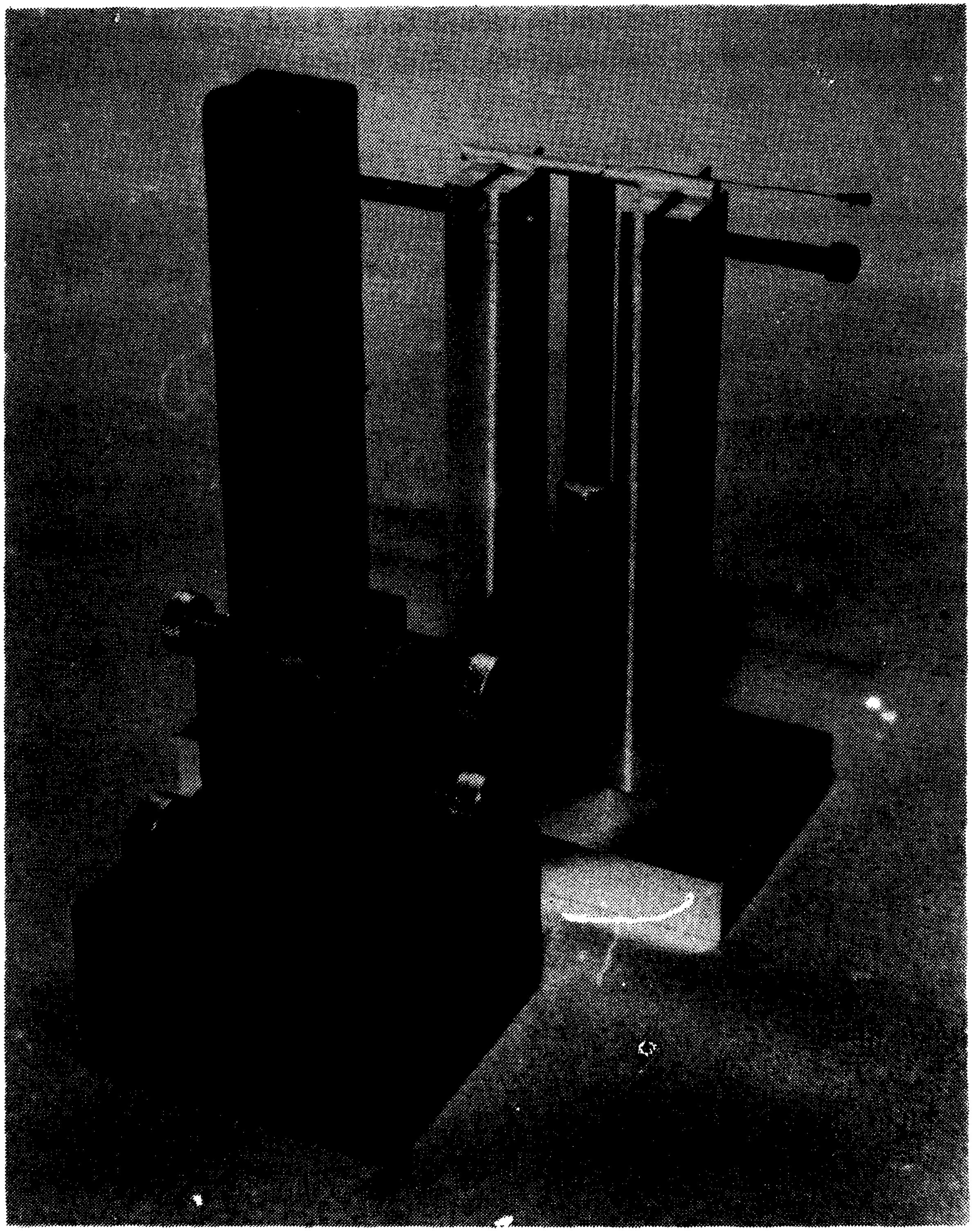

Figure 1.61. Test Set-Up for Pin-Free Beam Test

A computer analysis was performed to determine the temperature of peak damping and the temperatures of 70 percent peak damping, for each configuration. The two selected beams from each was tested at the appropriate three temperatures, then the first beam was retested to check repeatability.

A considerable amount of difficulty was encountered in collecting data caused by transducer positioning. The pin-free test set-up was modified such that the drive and response transducers were mounted directly to the test fixture to ensure more accurate positioning of the transducers.

Although this change helped, it was decided that more accurate data for comparison could be achieved by mounting the beams in a cantilever configuration. This was accomplished by gluing one end of the beam to an aluminum block attached to the vertical support posts of the fixture (Figures 1.62 and 1.63).

The cantilever test configuration greatly increased the repeatability of the data and the signal to noise ratio.

The results of these pre-flight shuttle beam tests are in Table 1.9.

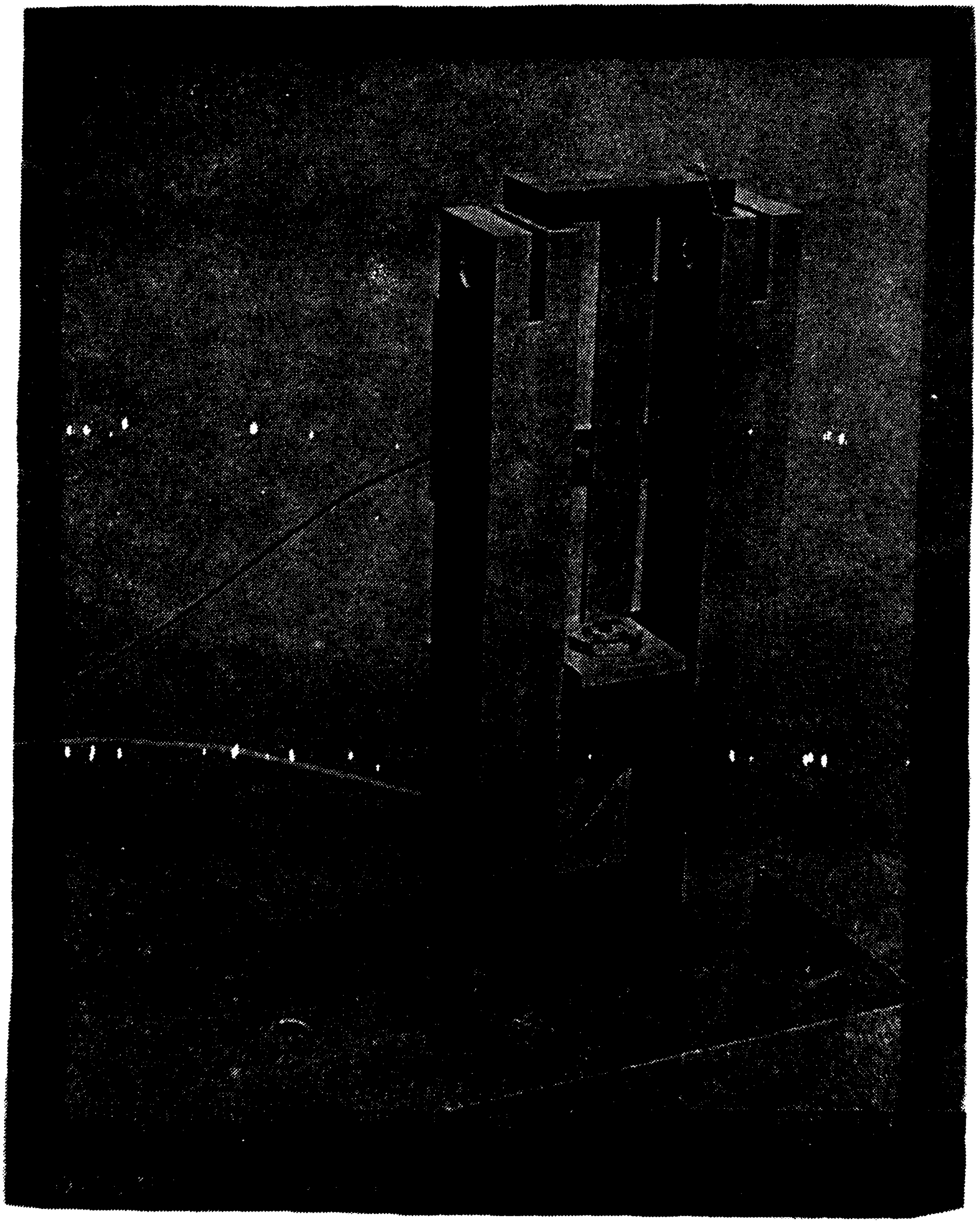

Figure 1.62. Modified Space Shuttle Beam Test Fixture Showing Location of Drive Transducer.

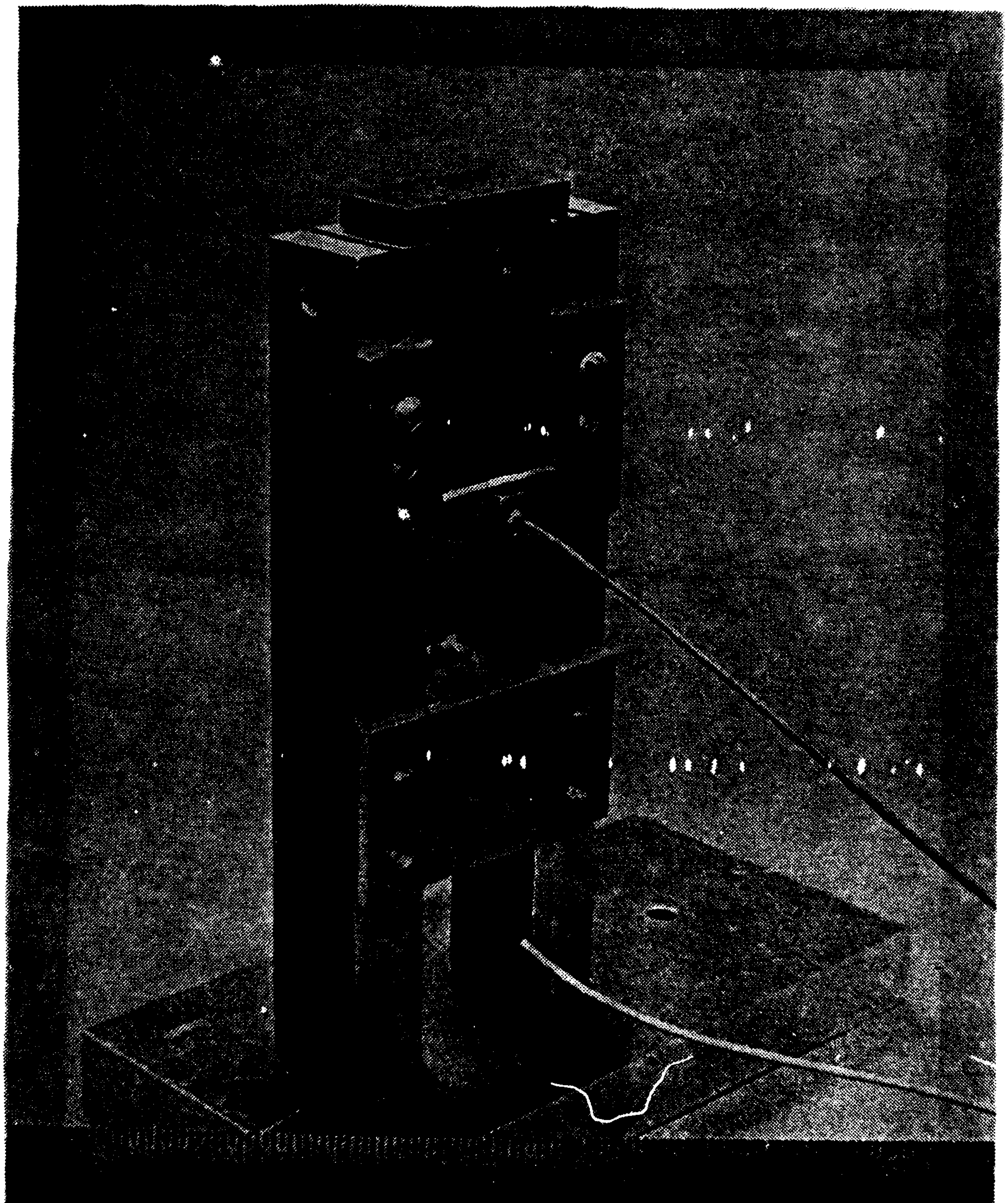

Figure 1.63. Modified Space Shuttle Beam Test Fixture Showing Location of Response Transducer.

TABLE 1.9

SPACE SHUTTLE TEST BEAM DATA

Batch I.D.	Beam No.	°F	Mode	f_c	f_L	f_r	Δf	η
LDEF-1GE 112-2	2	42	1	131.5	128.2	134.5	6.3	.0479
			2	803.3	793.8	816.2	22.4	.0279
			3	2317.7	2310.6	2333.9	23.3	.0101
			4	3923.2	3902.0	3957.5	55.5	.0141
	2	136	1	--	--	--	--	--
			2	434.1	409.5	473.9	64.4	.1484
			3	1147.0	1072.1	1225.7	153.6	.1339
			4	2257.6	2248.8	2270.2	21.4	.0186
	2	70	1	191.0	189,5	193.1	3.6	.0188
			2	1240.1	1227.1	1256.4	29.3	.0236
			3	3347.5	3263.9	3490.0	211.7	.0637
	4	42	1	133.4	131.0	135.5	4.5	.0337
			2	803.5	794.2	829.2	35.0	.0435
			3	2314.4	2304.2	2331.5	27.3	.0118
			4	3928.7	3860.0	3952.8	92.8	.0236
	4	70	1	195.3	193.5	198.4	4.9	.0251
			2	1237.5	1222.1	1254.4	32.3	.0261
			3	3315.4	3220.3	3451.5	231.2	.0697
	4	88	1	188	186	190	4.0	.0213
			2	1210	1189	1231	42	.0347
			3	3223	3099	3350	251	.0779
	4	136	1	--	--	--	--	--
			2	443.9	406.6	475.9	69.3	.1561
			3	1155.0	1143.8	1221.5	77.7	.0673
			4	2299.2	2269.2	2310.3	41.1	.0179
	1	70	1	189.6	187.3	192.2	4.9	.0258
			2	1200.1	1186.2	1219.0	32.8	.0273
			3	3247.3	3161.0	3329.6	168.6	.0519
	3	70	1	201.0	198.4	204.9	6.5	.0323
			2	1242.7	1229.5	1259.0	29.5	.0237
			3	3323.8	3183.4	3395.1	211.7	.0637

AD-A135 409 DAMPING MATERIALS FINITE ELEMENTS AND SPECIAL PROJECTS 2/3
(U) DAYTON UNIV OH RESEARCH INST M RUDDELL ET AL.
DEC 82 UDR-TR-82-110 AFWAL-TR-82-4167 F33615-79-C-5108
UNCLASSIFIED F/G 14/2 NL

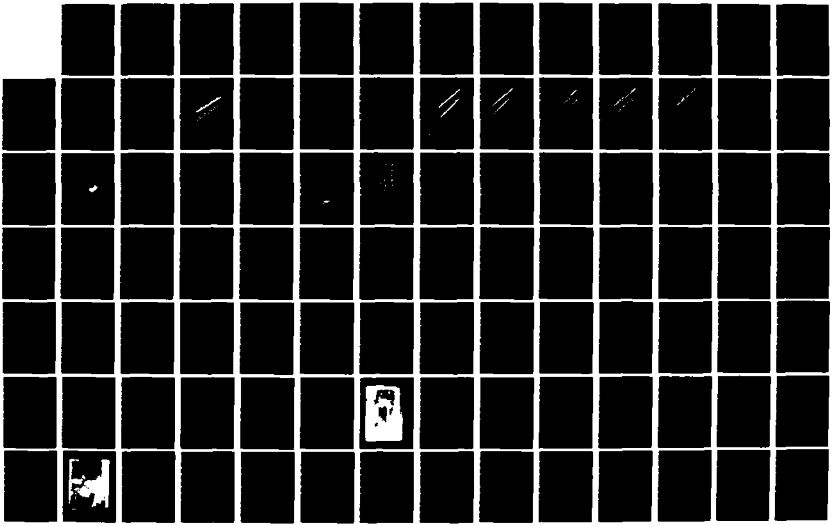

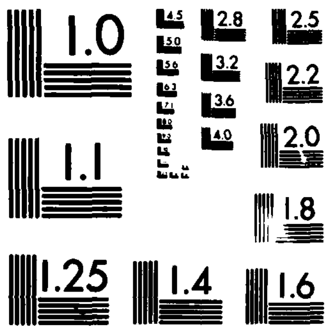

MICROCOPY RESOLUTION TEST CHART
NATIONAL BUREAU OF STANDARDS-1963-A

TABLE 1.9
(continued)

Batch I.D.	Beam No.	°F	Mode	f_c	f_L	f_r	Δf	η
LDEF-1GE 112-2	5	70	1	184.2	182.9	186.2	3.3	.0179
			2	1226.8	1212.5	1245.2	32.7	.0267
			3	3278.9	3156.6	3361.7	205.1	.0625
VEM 113 010	4	-10	1	158.76	156.7	160.83	4.13	.0260
			2	964.69	930.23	993.54	63.31	.0656
			3	2554.69	2414.47	2673.33	258.86	.1013
			4	4618.11	4227.41	4912.65	685.24	.1484
	4	50	1	103.44	91.11	131.78	40.76	.3940
			2	494.23	440.20	534.78	94.58	.1914
			3	1255.87	1141.68	1396.5	254.82	.2029
			4	2382.47	2120.09	2560.28	440.19	.1848
	4	70	1	92.1	87.8	96.5	8.7	.0945
			2	425.3	418.8	434.9	16.1	.0379
			3	1207.5	1164.3	1250.3	86.0	.0712
			4	2308.5	2233.4	2375.6	142.2	.0616
	4	160	1	185.7	168.2	267.8	99.6	.5363
			2	1208.7	1201.4	1220.2	18.8	.0306
			3	2148.5	2116.9	2187.1	70.2	.0328
	5	-10	1	157.54	155.50	160.90	5.4	.0343
			2	900.20	834.80	939.90	105.1	.1167
			3	2481.65	2381.63	2598.43	216.8	.1717
	5	50	1	103.69	91.93	134.34	42.41	.4090
			2	488.50	439.34	526.37	87.03	.1782
			3	1266.58	1151.81	1385.24	233.43	.1843
			4	2331.27	2091.25	2503.39	412.14	.1768
	5	70	1	92.2	86.9	97.0	10.1	.1095
			2	462.4	445.8	474.2	28.4	.0614
			3	1214.6	1175.6	1258.1	82.5	.0680
			4	2299.5	2224.1	2368.7	144.6	.0628
	1	70	1	73.9	67.8	89.8	22.0	.2977
			2	418.4	394.4	447.9	53.5	.1279
			3	1139.3	1088.7	1189.5	100.8	.0885
			4	2186.6	2106.1	2259.2	153.1	.0700

TABLE 1.9
(continued)

Batch I.D.	Beam No.	°F	Mode	f_c	f_L	f_r	Δf	η
VEM 113 010	2	70	1	81.0	73.9	86.7	12.8	.1580
			2	438.2	425.5	450.3	24.8	.0566
			3	1181.3	1127.8	1217.3	89.5	.0758
			4	2209.3	2136.2	2286.3	150.1	.0679
	3	70	1	--	--	--	--	--
			2	435.6	412.9	462.2	49.3	.1132
			3	1158.1	1112.9	1205.5	92.6	.0800
			4	2254.9	2176.1	2335.2	159.1	.0705
VEM 112-002	3	38	1	133.2	131.3	135.4	4.1	.0308
			2	776.9	681.8	811.0	129.2	.1663
	3	70	1	152.5	150.2	156.0	5.8	.0380
			2	659.5	536.3	855.5	319.2	.4840
			3	1575.3	1248.9	1780.2	531.3	.3377
	3	138	2	441.5	398.0	483.2	85.2	.1930
			3	1200.3	1160.4	1267.1	106.7	.0889
			4	2246.7	2221.5	2288.2	66.7	.0297
			5	3739.4	3672.4	3774.2	101.8	.0272
	5	38	1	127.3	124.5	129.4	4.9	.0385
			2	768.8	740.0	793.2	53.2	.0692
			3	2109.2	1983.3	2188.1	204.8	.0971
	5	70	1	122.0	112.6	134.2	21.6	.1770
			2	670.6	623.2	781.4	158.2	.4636
			3	1624.4	1398.5	1766.8	368.3	.4456
	5	88	1	116.0	93.0	130.0	37.0	.3190
			2	580.0	574.0	651.0	77.0	.1328
			3	1510	1495	1540	45	.0298
	5	138	2	442.4	409.7	474.7	65.0	.1469
			3	1171.2	1109.8	1261.6	151.8	.1296
			4	2263.1	2242.1	2338.9	96.8	.0428
			5	3761.2	3701.0	3797.9	96.9	.0258

TABLE 1.9
(continued)

Batch I.D.	Beam No.	°F	Mode	f_c	f_L	f_r	Δf	η
VEM 112-002	1	70	1	118.9	117.1	122.1	5.0	.0421
			2	600.0	529.6	687.9	158.3	.2638
			3	1550.6	1243.5	1724.8	481.3	.3104
	2	70	1	140.5	131.8	151.3	19.5	.1388
			2	672.4	553.3	795.6	242.3	.3604
			3	1730.5	1431.3	1964.6	533.3	.3082
	4	70	1	156.4	153.9	159.0	5.1	.0326
			2	730.5	702.4	787.7	85.3	.2294
			3	1639.4	1455.2	1781.2	326.0	.3908
VEM 110-010	4	70	1	155.7	152.1	161.3	9.2	.0591
			2	919.8	859.7	970.9	111.2	.1209
			3	2395.0	2214.4	2550.4	336.0	.1403
	4	78	1	153.4	149.1	157.9	8.8	.0574
			2	910.4	851.7	962.3	110.6	.1215
			3	2355.4	2183.4	2515.7	332.3	.1411
			4	4024.2	3949.5	4067.8	118.3	.0294
	4	114	1	94.5	92.7	99.2	6.5	.0688
			2	690.0	678.6	749.4	70.8	.1026
			3	1289.8	1280.9	1330.4	49.5	.0384
			4	2628.7	2610.1	2682.5	72.4	.0275
	4	150	3	1125.2	1119.5	1148.2	28.7	.0501
			4	3623.6	3592.7	3647.6	54.9	.0298
			5	5622.11	5171.8	6070.3	898.5	.1598
	5	70	1	151.3	148.0	156.5	8.5	.0562
			2	902.9	858.6	969.5	110.9	.1228
			3	2332.5	2152.4	2486.4	334.0	.1431
	5	78	1	148.4	144.2	153.1	8.9	.0599
			2	895.5	851.6	960.7	109.1	.1218
			3	2305.2	2127.2	2457.2	330.0	.1432
	5	150	4	3809.0	3782.5	3825.4	42.9	.0221
			5	5577.0	4833.4	5927.0	1093.6	.1961

TABLE 1.9
(continued)

Batch I.D.	Beam No.	°F	Mode	f_c	f_L	f_r	Δf	η
VEM 110-010	1	70	1	195.2	190.4	200.8	10.4	.0533
			2	916.4	868.7	963.5	94.8	.1034
			3	2362.7	2187.9	2503.2	315.3	.1334
	2	70	1	159.3	155.7	165.7	10.0	.0628
			2	909.7	826.5	951.9	125.4	.1378
			3	2391.5	2156.6	2665.6	509.0	.2128
	3	70	1	167.6	162.4	175.1	12.7	.0758
			2	919.7	868.4	965.2	96.8	.1053
			3	2394.5	2205.9	2526.2	320.3	.1337
LDEF GE 110-10	2	70	1	218.4	216.1	221.6	5.5	.0252
			2	1394.8	1352.8	1440.6	87.8	.0629
			3	3613.8	3463.9	3742.3	278.4	.0770
	2	77	1	236.9	232.9	241.8	8.9	.0376
			2	1378.4	1335.5	1448.5	113.0	.0819
			3	3795.0	3748.0	3857.9	109.9	.0289
	2	152	2	795.9	784.3	851.9	67.6	.0849
			3	2203.6	2190.7	2231.4	40.7	.0185
			4	3628.8	3573.8	3667.0	93.2	.0257
	4	70	1	210.8	207.5	214.8	7.3	.0346
			2	1360.1	1316.4	1433.0	116.6	.0857
			3	3685.7	3418.3	3802.4	384.1	.1042
	4	77	1	230.6	225.6	235.7	10.1	.0438
			2	1376.4	1338.2	1454.6	116.4	.0846
			3	3822.0	3760.1	3873.6	113.5	.0297
	4	114	1	199.0	180.1	219.4	39.3	.1975
			2	1081.4	941.1	1227.6	286.5	.2649
			3	2716.2	2693.0	2893.6	200.6	.0739
	4	152	2	784.3	779.2	842.7	63.5	.0810
			3	2244.9	2230.0	2263.6	33.6	.0150
			4	3633.4	3547.5	3687.5	140.0	.0385

TABLE 1.9
(continued)

Batch I.D.	Beam No.	°F	Mode	f_c	f_L	f_r	Δf	η
LDEF GE 110-10	1	70	1	356.0	343.4	378.1	34.7	.0975
			2	1420.5	1357.4	1468.5	111.1	.0782
			3	3628.0	3458.7	3769.8	311.1	.0857
	3	70	1	319.2	312.9	325.9	13.0	.0407
			2	1408.6	1366.9	1463.2	96.3	.0684
			3	3663.5	3476.3	3850.5	374.2	.1021
	5	70	1	227.9	215.5	249.2	33.7	.1479
			2	1429.8	1375.3	1473.4	98.1	.0686
			3	3733.0	3541.7	3839.4	297.7	.0797
LDEF-1GE 113 10	3	-10	1	200.5	198.2	202.8	4.6	.0229
			2	1317.5	1289.0	1336.1	47.1	.0357
			3	3606.2	3520.7	3654.1	133.4	.0370
			4	6725.9	6522.8	6854.0	331.2	.0492
	3	48	1	175.4	154.9	195.6	40.7	.2320
			2	896.4	729.0	1094.9	365.9	.4082
			3	2140.7	2071.6	2331.0	259.4	.2381
	3	70	1	145.5	131.9	177.5	45.6	.3134
			2	705.1	606.9	784.5	177.6	.2519
			3	1798.5	1654.8	2003.5	348.7	.1938
			4	3340.0	2910.0	3733.0	823.0	.2464
	4	-10	1	211.4	209.8	213.3	3.5	.0165
			2	1442.6	1424.1	1458.9	34.8	.0241
			3	3819.3	3736.6	3873.3	136.7	.0358
			4	7112.2	6773.8	7303.5	529.7	.0745
	4	16	1	224.8	221.4	228.2	6.8	.0302
			2	1396.6	1355.1	1450.7	95.6	.0684
			3	3624.2	3449.8	3816.6	366.8	.1012
	4	48	1	149.7	140.2	162.9	22.7	.2980
			2	795.4	581.0	957.9	376.9	.4738
			3	2048.1	1626.3	2560.5	934.2	.4561

TABLE 1.9
(continued)

Batch I.D.	Beam No.	°F	Mode	f_c	f_L	f_r	Δf	η
LDEF 1GE 113 10	4	70	1	143.8	129.9	176.8	46.9	.3261
			2	716.5	602.1	817.1	215.0	.3001
			3	1809.0	1682.4	2033.3	350.9	.1939
			4	3404.0	3048.7	3878.7	830.0	.2438
	1	70	1	143.0	130.4	180.7	50.3	.3517
			2	685.1	569.0	768.9	199.9	.2918
			3	1773.9	1541.5	1979.1	437.6	.2479
			4	3287.1	2806.5	3621.3	814.8	.2479
	2	70	1	143.7	136.3	164.1	27.8	.3802
			2	684.8	629.7	725.2	95.5	.2741
			3	1749.0	1618.8	1964.3	345.5	.1975
			4	3413.6	3246.8	3711.0	464.2	.2672
	5	70	1	145.5	130.7	189.5	58.8	.4041
			2	713.7	596.4	804.6	208.2	.2917
			3	1799 1	1655.4	1990.5	335.1	.1863
LDEF-1GE 113-2	3	10	1	191.4	190.2	192.5	2.3	.0120
			2	1209.7	1194.7	1222.0	27.3	.0226
			3	3349.9	3298.2	3387.2	89.0	.0266
			4	6203.0	5969.1	6300.5	331.4	.0534
	3	42	1	164.7	163.2	166.3	3.1	.0188
			2	1202.0	1170.3	1213.6	43.3	.0360
			3	3276.9	3093.7	3419.4	325.7	.0994
			4	6120.2	6082.7	6159.7	77.0	.0126
	3	70	1	164.8	156.5	174.9	18.4	.1117
			2	872.1	749.4	1010.3	260.9	.2992
			3	2323.2	2007.5	2723.2	715.7	.3081
	3	82	1	162.3	154.4	178.6	24.2	.1491
			2	842.8	742.8	950.5	207.7	.2464
			3	2088.3	1841.3	2377.5	536.2	.2567

TABLE 1.9
(continued)

Batch I.D.	Beam No.	°F	Mode	f_c	f_L	f_r	Δf	η
LDEF 1GE 113 2	4	10	1	183.8	182.8	185.1	2.3	.0125
			2	1197.5	1182.6	1207.8	25.2	.0210
			3	3302.0	3260.3	3328.1	67.8	.0205
			4	6285.9	6195.3	6397.5	202.2	.0632
	4	70	1	163.4	155.6	176.7	21.1	.1291
			2	869.4	806.8	943.2	136.4	.3083
			3	2316.0	1997.4	2780.3	782.9	.3380
	4	82	1	158.9	143.9	177.3	33.4	.2102
			2	924.9	911.4	956.7	45.3	.0963
	1	70	1	163.5	155.5	192.0	36.5	.2232
			2	868.2	739.5	989.5	250.0	.2879
			3	2283.8	1965.1	2838.7	873.6	.3825
	2	70	1	161.2	152.3	177.5	25.2	.1563
			2	868.4	716.7	1023.7	307.0	.3535
			3	2230.4	1856.5	2570.9	714.4	.3202
	5	70	1	163.0	156.4	193.5	37.1	.2276
			2	946.5	833.8	1033.5	199.7	.2109
			3	2480.0	2181.9	2882.4	700.5	.2824
VEM 113 002	1	10	1	133.5	132.6	134.6	2.0	.0149
			2	850.8	842.4	857.4	15.0	.0176
			3	2322.7	2291.8	2353.6	61.8	.0266
			4	4446.0	4359.9	4519.5	159.6	.0359
			5	7122.4	6993.6	7337.3	343.7	.0483
	1	44	1	120.9	114.4	130.1	15.7	.1298
			2	738.9	712.0	797.4	85.4	.1156
			3	1656.8	1407.5	1927.5	520.0	.3138
	1	70	2	460.3	411.9	496.9	85.0	.1847
			3	1266.9	1176.1	1403.4	227.3	.1794
	1	82	1	67.3	96.9	119.2	22.3	.2078
			2	546.4	471.7	662.0	190.3	.3482

TABLE 1.9
(concluded)

Batch I.D.	Beam No.	°F	Mode	f_c	f_L	f_r	Δf	η
VEM 113 002	2	10	1	134.3	133.5	135.1	1.6	.0119
			2	836.9	827.0	843.2	16.2	.0193
			3	2687.7	2672.2	2701.5	29.3	.0109
			4	4374.2	4298.7	4400.5	101.8	.0233
			5	7075.5	6910.5	7237.2	326.7	.0461
	2	70	2	479.5	434.7	517.2	82.5	.1721
			3	1282.3	1186.6	1419.6	233.0	.1817
	2	82	1	118.3	108.5	129.9	21.4	.1809
			2	599.4	533.0	720.3	187.3	.3125
	3	70	1	98.9	92.6	112.8	20.2	.2042
			2	562.5	551.6	581.8	30.2	.0537
			3	1282.5	1192.5	1476.2	283.7	.2212
	4	70	1	97.7	92.8	110.8	18.0	.3621
			2	563.6	554.6	580.5	25.9	.0459
			3	1213.7	1199.2	1221.5	22.3	.0184
	5	70	1	98.1	86.1	124.1	38.0	.3874
			2	419.9	405.2	464.1	58.9	.1403
			3	1214.9	1201.3	1342.5	141.2	.1162

1.5 EXHAUST GAS SIMULATOR (EGS)

1.5.1. Background

Previous experience indicated that devising a successful vibration damping vitreous enamel treatment for a given application is not really the end of the design process. The material treatment also has to survive the operational environment. The internal jet engine environment is a highly complex one, which includes such factors as temperature distribution variation and chemical reaction between the enamel treatment and exhaust gases, among others. It was therefore decided at the outset of this contract to design a simple jet engine exhaust gas simulator which could create an accurately duplicated chemical-temperature environment for study purposes.

1.5.2. Simulator Design

Discussions were held with various parties to develop ideas for the design. A literature review by I. T. Osgerby (AIAA Journal, Vol. 12, No. 6, pp. 743-754, June 1974) of turbine combustor modeling and emissions was most helpful. It was decided that a commercially-available 150,000 B.T.U. forced air combustion fuel oil heater designed for free-air heating of large rooms was ideally suited as a base unit. The similarity to a jet engine combustor was very close; and using JP-5 as the fuel base would not require any significant modifications to the basic unit. A stable temperature profile over a relatively wide range would be possible by constructing a simple tubular exhaust extension. It was also decided that since sulfur is the major known reactant, addition of tertiary-butyldisulfide $[(CH_3)_3CSSC(CH_3)_3]$ to the JP-5 (mixture of 0.2 cc per 5 gallons of JP-5) would accurately generate the level of sulfur commonly found in operational engine exhausts.

In order to obtain a relative picture of the emissions to be expected with such a combustion mixture, it was decided to first determine the components of JP-5 fuel (although JP-8 could be used, the ready availability of JP-5 rendered its use more practical).

A sample analysis of JP-5 revealed the following components:

- Percent volatile by volume 96%
  Percent other components by volume 4%
- Percent of volatiles by volume:

Parafins	45.3%
Monocycloparaffins	37.0%
Dicycloparaffins	3.1%
Alkylbenzenes	8.7%
Indans & tetralins	3.2%
Napthalenes	2.7%

1.5.3, Operation

Prior to actual use, the simulator emissions were evaluated. The report is summarized as follows:

- Description of emissive device:
  Simulator: jet engine exhaust gas
  Fuel: JP-5 or JP-8
  Additives: Tertiary-butyldisulfide
  Mixture: 0.2 cc per 5 gallons fuel
- Conclusions of emission test
  Particulate emissions significantly below maximum acceptability. Major pollutant: Sulfur 0.4% total
  Exhaust volume ≈ 30 cfm (free exhaust conditions)
  B.T.U. output ≈ 150,000 (at 250 C.F.M. forced-draft flue exhaust conditions)
- Provisions
  Fuel not to be stored within immediate vicinity
  Approximately 2 C.F.M. fresh air should be provided for each C.F.M. exhaust volume
  CO_2 extinguisher to be provided in close proximity

Initial tests were conducted in free-air conditions behind W-PAFB, building 32. A temperature profile compiled at this time indicated usable temperatures from 1450°F (788°C) to 900°F (482°C)

In the fall of 1979, the Vibration Damping Group moved to a new laboratoy on campus at the Kettering Labs building. The exhaust gas simulator was set-up in a small nearby lab room. This room was provided with a 900 C.F.M. exhaust duct which vented to the roof of the building.

Careful studies indicated that the forced draft of the exhaust gases into the duct caused considerable turbulence of the flow within the extension tube "test chamber". This resulted in an unstable temperature distribution. Various alternative ducting methods were tried until an optimal configuration was devised. A commercially available steel container, approximately 30 inches in diameter, was modified as part of a flue design large enough to reduce the velocity of the forced draft. This then permitted a stable temperature distribution within the chamber ranging from 1330°F (720°C) to 930°F (500°C). With an additional 18-inch extension, temperatures down to 550°F (290°C) were achieved.

1.5.4. Material Evaluation

A data sheet was produced which could be filled out appropriately for each material being evaluated. Provision was made to record material description (including up to 3 overcoats), thermal cycling history, and notes concerning various types of decomposition/degradation, based upon previous experience.

Initial test specimens were materials from the J-85 afterburner liner project, the purpose being to see if the failure condition of the materials exposed to actual exhaust emissions could be duplicated. Also evaluated were "off the shelf" commercial materials, as well as various experimental sulfate materials.

Altogether, the test results were very useful in determining material degradation effects. A total of 16 material exposure tests were conducted in the simulator at various temperatures. A list of the tests are in Table 1.10. The material degradation data sheets for the tests are included, in chronological order, in Appendix C.

TABLE 1.10
COMPLETE SET OF EXPERIMENTS CONDUCTED WITH THE EXHAUST GAS SIMULATOR

Experiment	Project	Material	Exposure °C	Total Time Exposure	Survival
01	J-85-Follow-up	J-85-1	815	8.5 Hours	NO
02	" "	J-85-2	815	8.5 "	PARTIAL
03	" "	J-85-3	815	8.5 "	NO
04	" "	J-85-4	815	8.5 "	NO
05	" "	J-85-5	815	8.5 "	NO
06	Development	8871	540	8.5 "	
07	"	8871 + 3%	540	8.5 "	PARTIAL
08	"	Sulfate 2	399	2.0 "	NO
09	"	Lead 1	635	28.0 "	NO
010	"	Lead 2	635	28.0 "	NO
011	J-85-Follow-up	J-85-14	675	30.0 "	YES
012	Development	AMB5	630	28.0 "	PARTIAL
013	"	Sulfate 3	399	2.0 "	NO
014	"	Sulfate S-7	399	2.0 "	NO
015	"	Sulfate S11	399	2.0 "	NO
016	"	Sulfate S11	399	2.0 "	NO

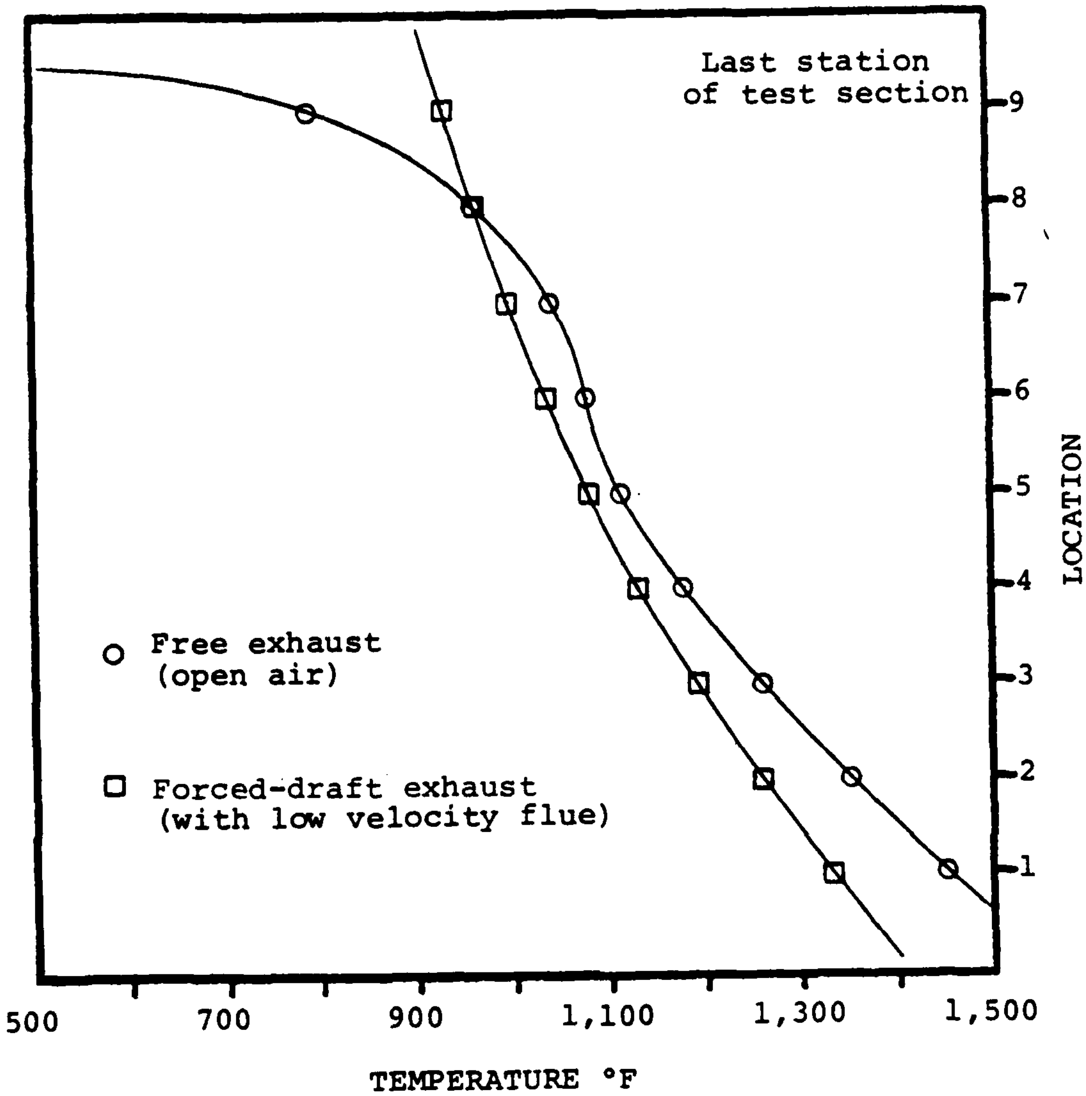

Figure 1.64. Temperature Distribution Versus Exhaust Chamber Position for Both Free-Flow and Forced-Draft Exhaust.

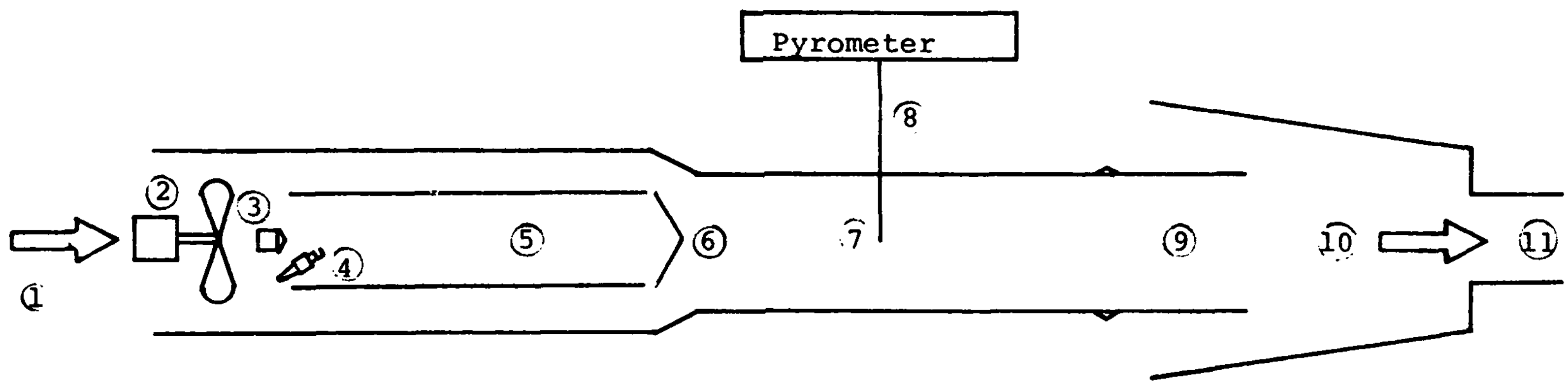

1 Fresh Air Intake
2 Blower
3 Fuel Nozzle
4 Spark Plug Igniter
5 Combustion Chamber
6 Combustion Baffle
7 Main Test Chamber
8 Monitoring Thermocouple
9 Extension Test Chamber
10 Low-Velocity Flue
11 Flue Exhaust, 900 C.F.M.

Figure 1.65. Schematic Cross-Section of Exhaust Gas Simulator.

SECTION 2
FINITE ELEMENT ANALYSES AND DEVELOPMENT

2.1 FINITE ELEMENT ANALYSIS OF STRUCTURES

The finite element program developed under this contract was used to analyze several damped and undamped structures. The following paragraphs contain a detailed discussion of those analyses.

2.1.1 Damped Skin Stringer Panel

To gain experience with the newly developed finite element program, an analysis of a skin stringer panel was conducted. The purpose of the investigation was to lower the stresses in the resonant condition by the use of viscoelastic constrained layer damping. The method and analysis are not limited to aircraft fuselage structures, but are also representative of any general class of structures consisting of stiffened skins or panels.

The model of the skin stringer panel shown in Figure 2.1 consisted of 285 elements and 828 nodes, for a total of almost 2,500 degrees of freedom. Symmetric-symmetric boundary conditions were used in the analysis, yielding the symmetric (odd-odd) modes. The cross section of the structure is shown in Figure 2.2. The panel was 1524 mm (60 inches) long by 813 mm (32 inches) wide, with the boundary conditions chosen. The distance between the stiffening ribs is 254 mm (10 inches).

The ribs and damping material layer were modeled with solid elements. In particular, the damping layer is modeled with 8 node solid elements which are shear deformable. It is important that the damping layer is modeled with shear deformable elements since a constrained layer damping treatment dissipates energy through shear deformation. The ribs were modeled with 16 node elements which have midside nodes (but no nodes through the thickness). Both the 8 node solid and the 16 node solid are formulated according to a full three-dimensional theory of elasticity. The constraining layer and panel were modeled with 8 node thin shell elements. The panel, ribs, and constraining layer were aluminum.

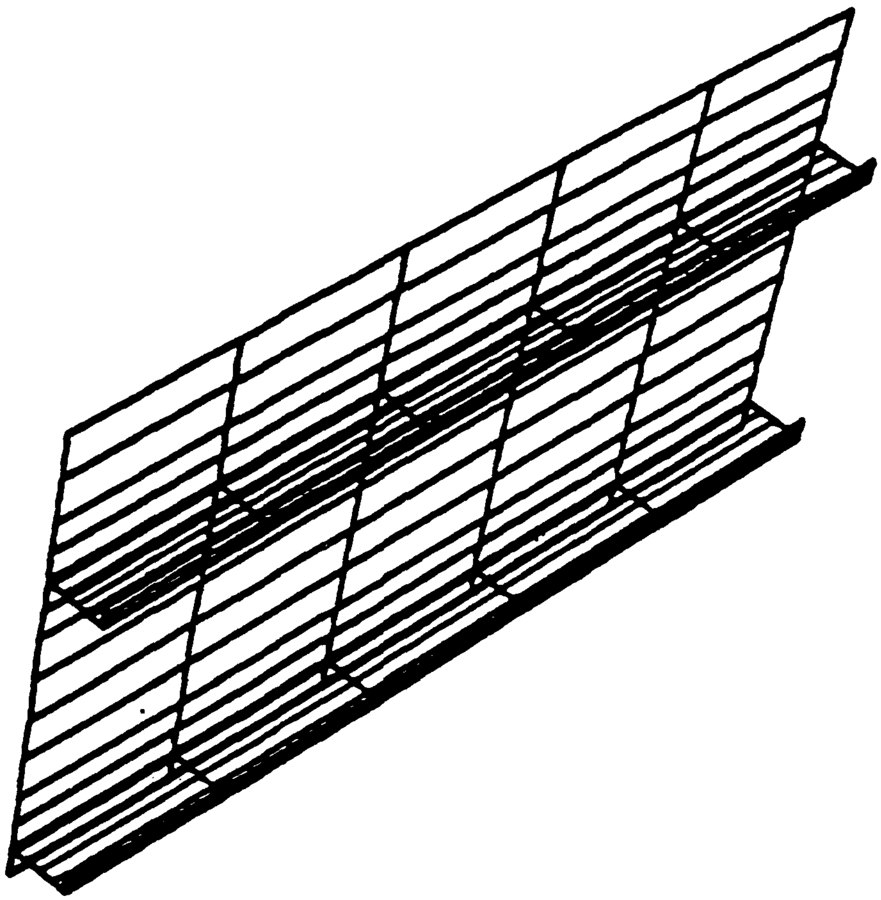

Figure 2.1. Finite Element Model of Stiffened Panel.

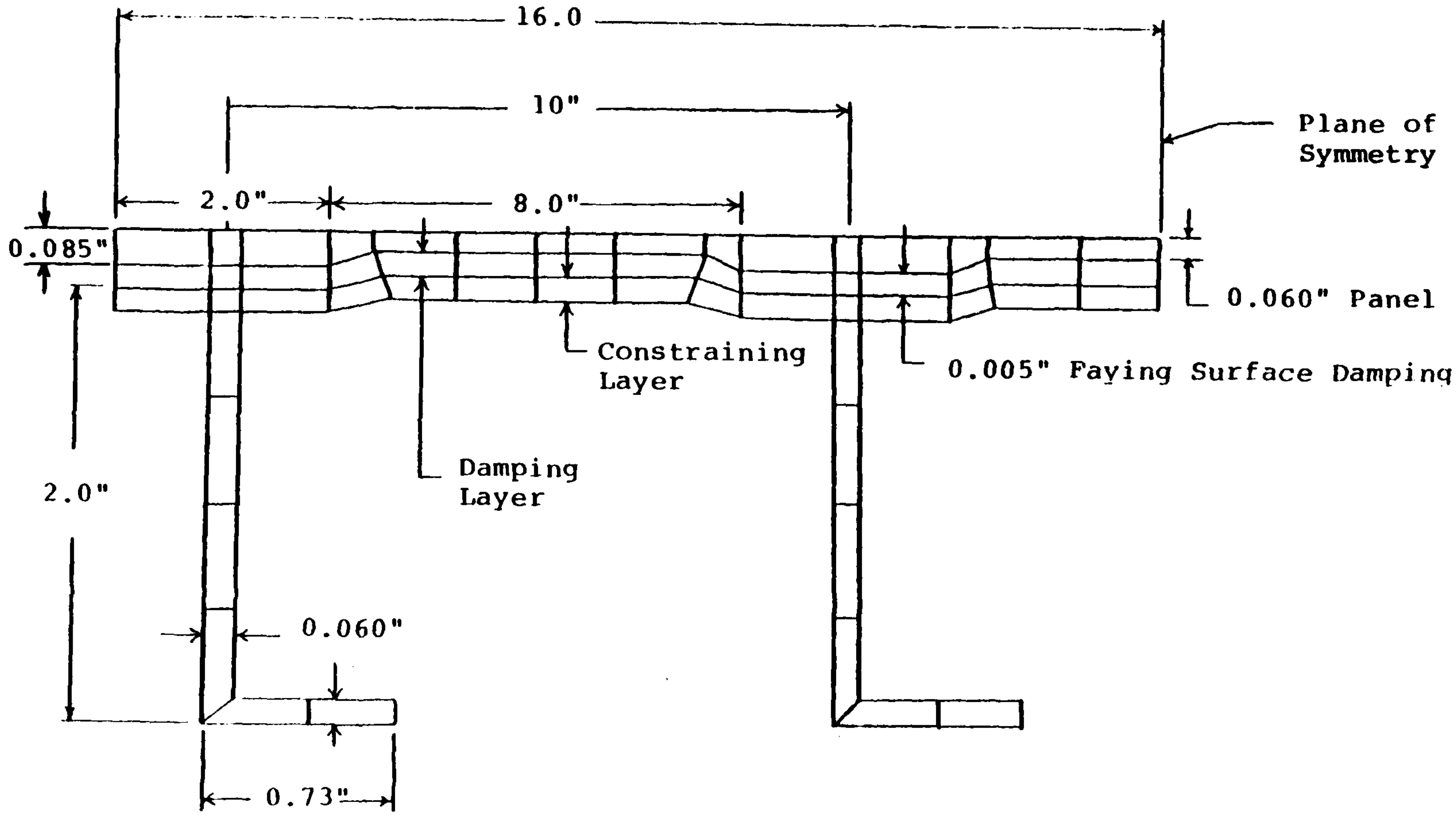

Figure 2.2. Cross-Section of Model.

The stiffeners are 51-mm (2 inches) high, and all sections of the stiffeners are 1.5-mm (0.060 inch) thick. The panel directly under the stiffener web is 2.2-mm (0.085 inch) thick. From this point under the web, the panel tapers to a thickness of 1.5-mm (0.060 inch), in a distance of 25-mm (1-inch). The taper is actually very shallow, and not abrupt as it appears in Figure 2.2. This taper represents a two-step chem-milled panel.

In between the stiffener web and the panel, a very thin element, 0.13-mm (0.005-inch) is incorporated. This element could be used as a faying surface damping treatment. A faying surface damping treatment is a damping layer applied where two surfaces fit together and where relative motion or fretting between the surfaces might occur. For the undamped runs this thin element was given the material properties of aluminum, and it adds little stiffness to the ribs.

In the not too distant past, analysis of skin stringer structures required the use of warping constants to account for the non-uniform torsion that occurs when the stiffening rib is restrained from warping because it is riveted to the skin panel. The non-symmetric ribs displace out of plane when subjected to bending loads that are not applied at the shear center and this in turn induces torsion of the cross-section. These warping constants were needed because the ribs were modeled with one-dimensional beam elements, whose properties were specified by their modulus, moment of inertia, cross-sectional area, and warping constant. However, in the present analysis, the ribs are modeled with 16 node solid elements. The 16 node solid elements encompass the full three-dimensional theory of elasticity with no approximations (other than representing a continuum by a finite number of elements) and hence no special consideration for warping of the ribs is necessary.

In the analysis the "undamped" structure actually included the damping and constraining layers. The stresses for the undamped forced vibration analysis were obtained by giving the damping material a very low loss factor, 0.006, the same loss factor as was used for the aluminum panels and ribs. For the damped force vibration analysis, the damping material was given its normal loss factor of approximately 0.9 at the temperature and frequency of interest, and the stresses were obtained.

The first five modes of the panel for the symmetric-symmetric boundary conditions are listed in Table 2.1 and shown in Figures 2.3 through 2.7. The investigation centered about the third mode, the 3,3 mode at 120.1 Hz, as shown in Figure 2.5.

In the undamped and damped forced vibration analysis, the force was a harmonic pressure loading normal to the surface of the panel. The pressure corresponded to an acoustic sound pressure level of 165 dB. A small amount of inherent damping was included in the base structure (loss factor - 0.006) to simulate actual structural damping and to keep the response at the natural frequency for the undamped case from becoming infinite. The constrained layer damping treatment consists of 0.35-mm (0.014-inch) of 3M Company's ISD 112 damping materials (properties chosen at 29°C(85°F) and 120 Hz and 0.2-mm (0.008-inch) of aluminum constraining layer.

TABLE 2.1

MODES OF UNDAMPED SKIN STRINGER PANEL

Mode	Frequency (Hz)
1,1	48.8
1,3	68.9
3,3	120.1
1,5	149.7
5,3	159.2

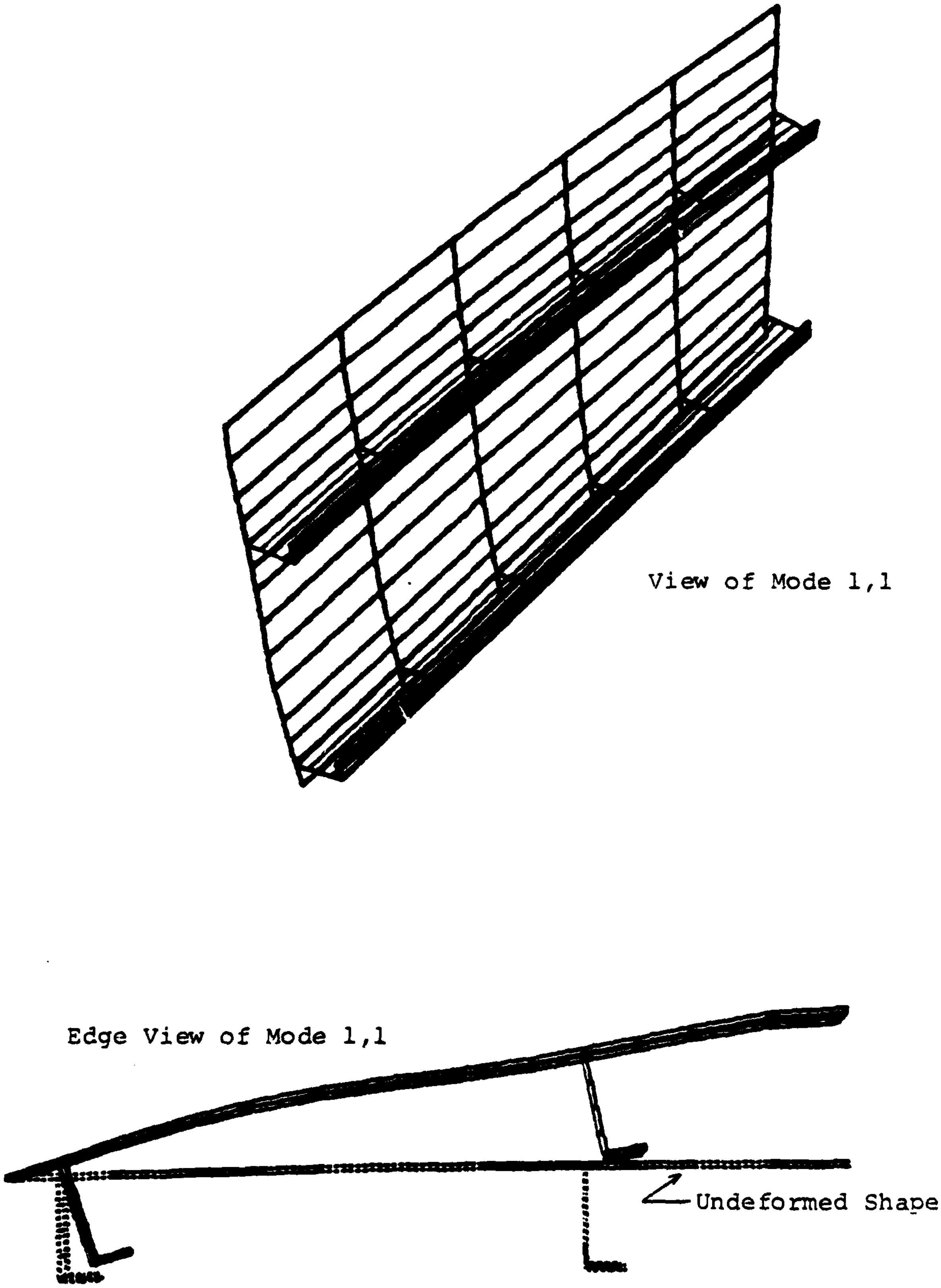

Figure 2.3. Mode 1,1 of Stiffened Panel (48.8 Hz).

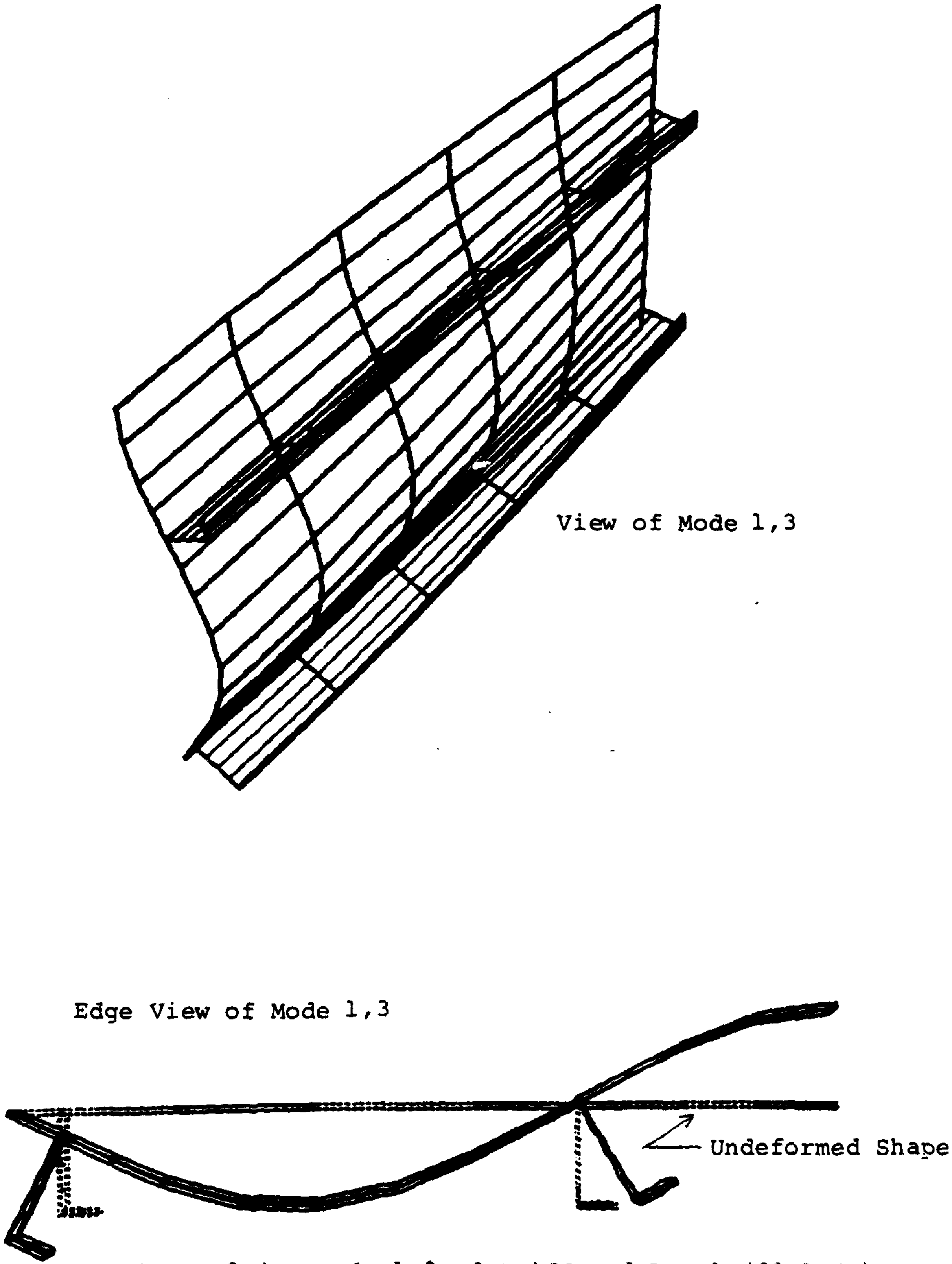

Figure 2.4. Mode 1,3 of Stiffened Panel (68.9 Hz).

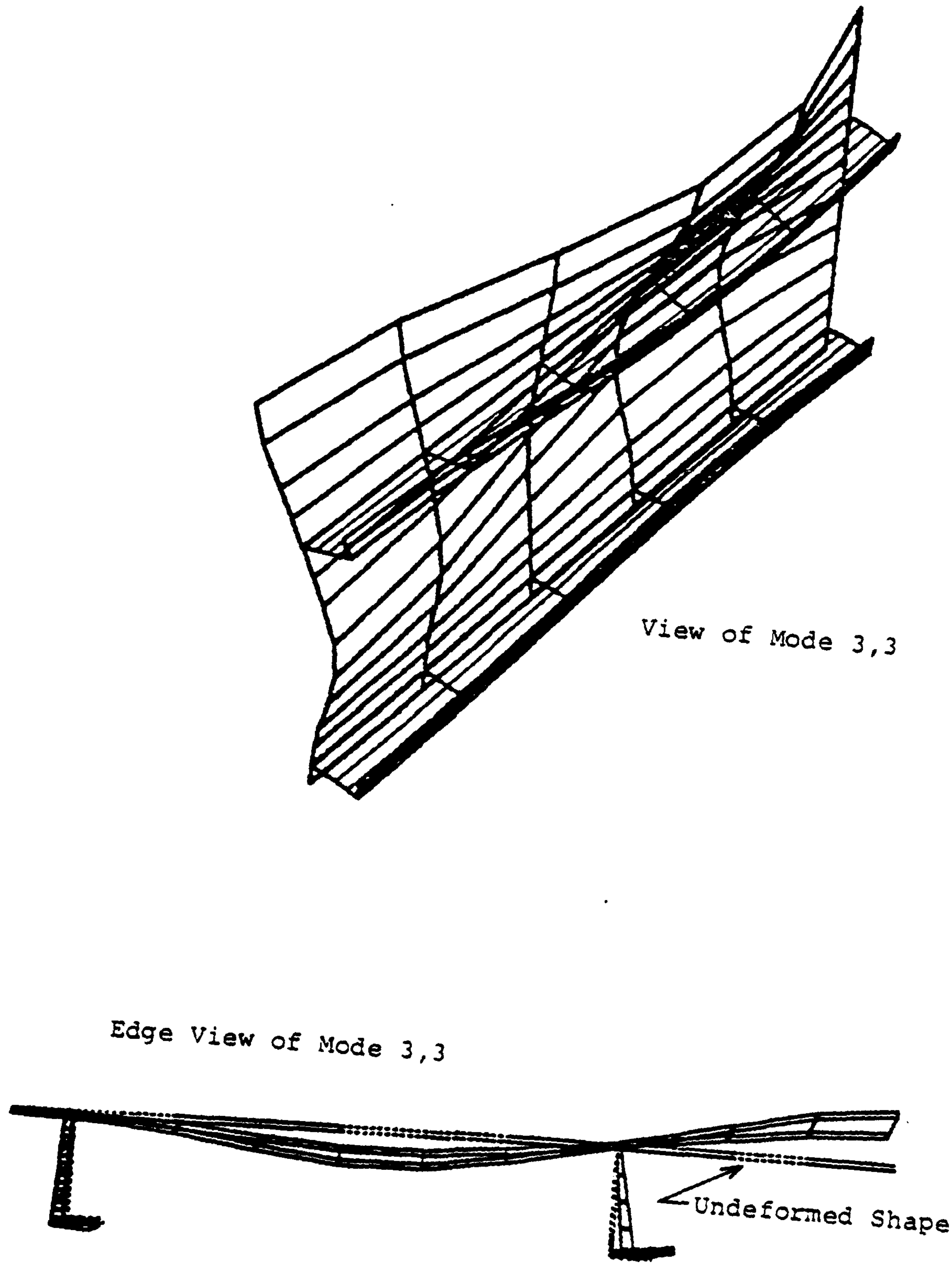

Figure 2.5. Mode 3,3 of Stiffened Panel (120.1 Hz).

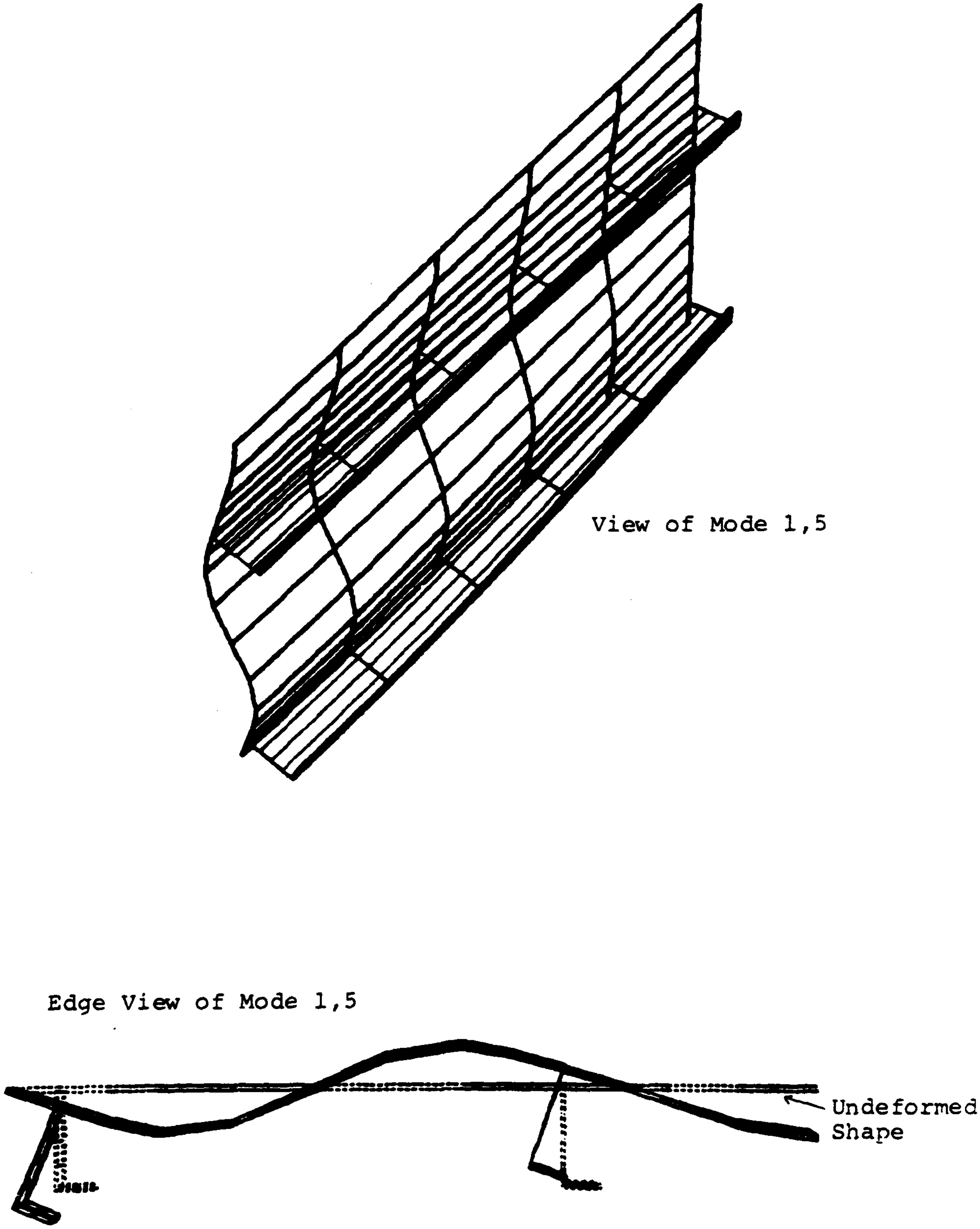

Figure 2.6. Mode 1,5 of Stiffened Panel (149.7 Hz).

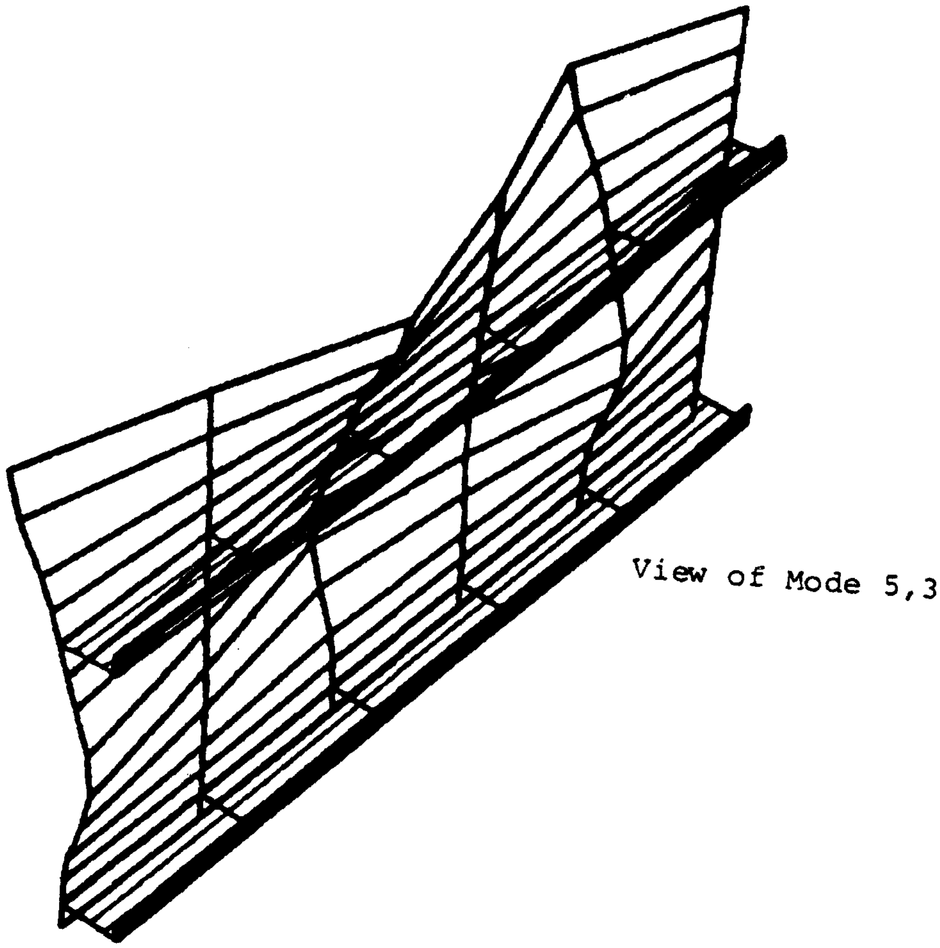

Edge View of Mode 5,3

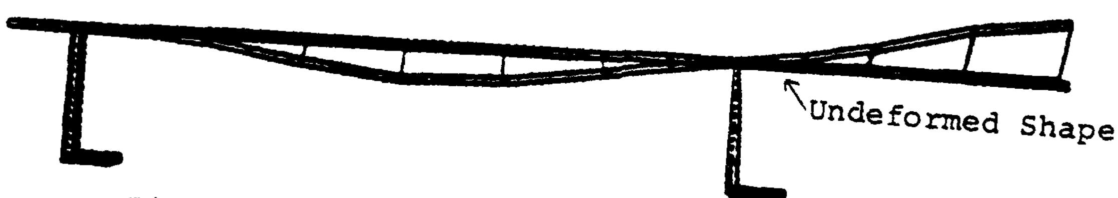

Figure 2.7. Mode 5,3 of Stiffened Panel (159.2 Hz).

The results for the undamped and damped panel are given in Table 2.2. With an inherent loss factor of 0.006, the stress in the undamped panel was 263 MPa (38,000 psi). With the addition of 0.35 mm (0.014 inch) damping layer and a 0.20 mm (0.008 inch) constraining layer, the loss factor increased to 0.029. Stress was reduced by 80 percent to 48.5 MPa (7,030 psi). The addition of the damping treatment represents only a ten percent increase in weight of the structure.

2.1.2. Analyses of F100 2nd Stage Turbine Blade

The UDRI analyzed the F100 2nd stage turbine blade with various damping treatments. The following sections discuss various finite element model of the blade, the results of UDRI analyses of the blade and comparison with NASTRAN models of the blade.

2.1.2.1. F100 2nd Stage Turbine Blade Models

During the course of the turbine blade analyses, card decks of the blade model were made available from two different sources. The UDRI then modified one of the models to use in its analyses. The three finite element models of the F100 2nd stage turbine blade are described below. There are (1) the Kielb, Henderson, and Abell NASTRAN model taken from a 14 July 1975 NASTRAN output file (referred to as the Kielb model); (2) the Pratt and Whitney model, which comes from a NASTRAN card deck supplied from Pratt and Whitney through John Ogg (referred to as P&W model); and (3) the University of Dayton Research Institute model (referred to as UDRI model) which was derived from the P&W model.

The Kielb model includes the platform and neck as shown in Figure 2.8. The model does not include the dovetail section.

An input deck was generated from the Kielb run, and was transmitted to Conor Johnson of Anamet Laboratories, California.

The P&W model also includes the platform and neck, but not the dovetail section. The P&W model is shown in Figure 2.9. It can be seen from the figure that there are errors in the card deck supplied to UDRI. The data file for the P&W model was forwarded to Conor Johnson. The UDRI filled in the missing elements on the airfoil section and used this as the basis for the UDRI model, shown in Figure 2.10.

TABLE 2.2

RESULTS FOR UNDAMPED AND DAMPED PANEL

Condition	Frequency (Hz)	Mode	Damping	Stress	Percent Stress Reduction	Percent Weight Increase
1.5-mm (0.060") panel, undamped	120.1	3,3	0.006	263 MPa (38,000 psi)	0	0
1.5-mm (0.060") panel, 0.35-mm (0.014") damping layer, 0.2-mm (0.008") constraining layer	120.3	3,3	0.029	48.5 MPa (7,030 psi)	80	10

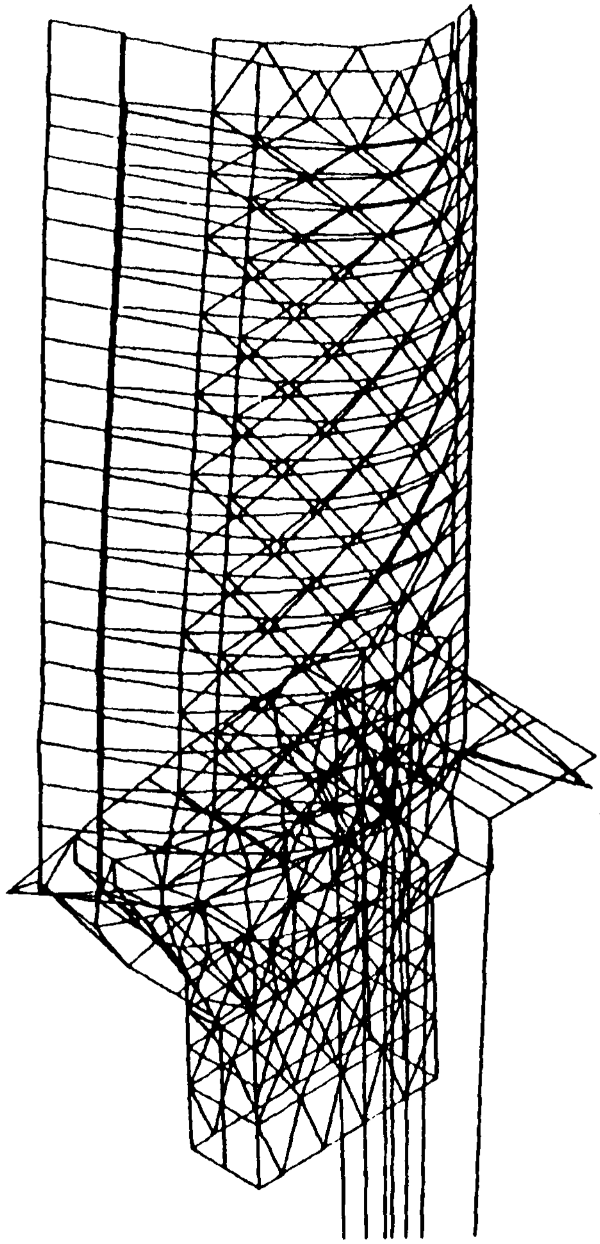

Figure 2.8. Kielb Model, Which Includes the Platform and Neck.

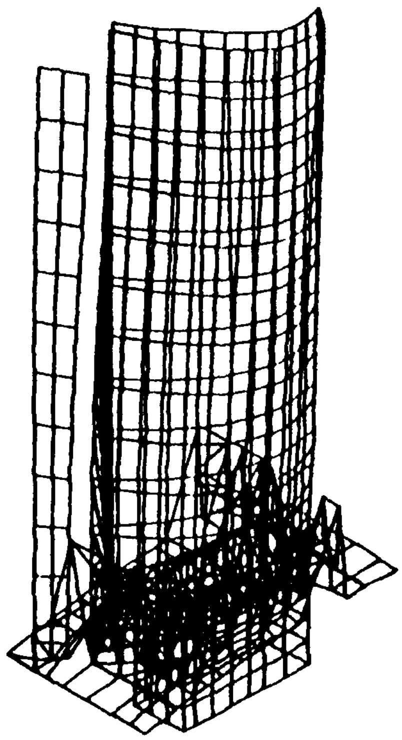

Figure 2.9. Pratt and Whitney Model, Which Includes the Platform and Neck But Not the Dovetail Section.

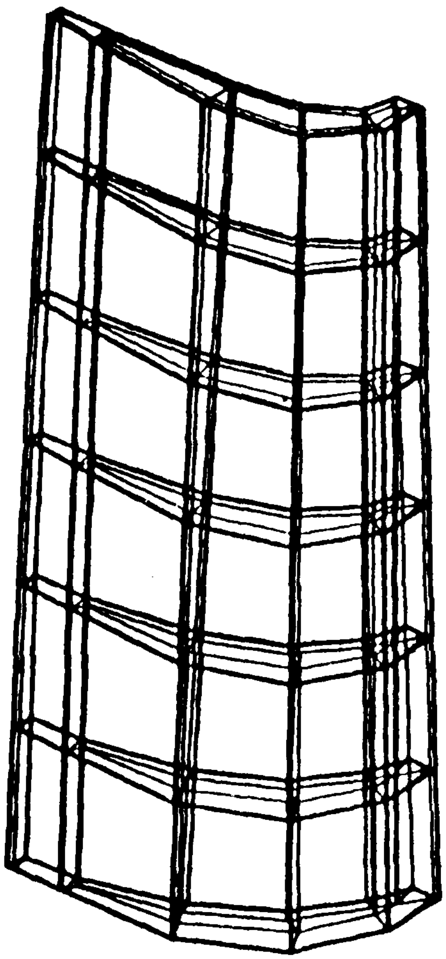

Figure 2.10. The UDRI Model.

2.1.2.2. UDRI Analysis of Damped F100 Turbine Blade

The UDRI conducted an analysis of the F100 2nd stage turbine blade. The analysis consisted of studying the forced harmonic response of the first bending mode of the blade for the following cases: (1) undamped blade; (2) blade with free layer damping treatment; and (3) rotating blade with constrained layer damping treatment. The seven non-rotating cases and the one rotating case are shown in Table 2.3. The first three modes are shown in Figure 2.11.

The model, shown in Figure 2.12, consists of 234 elements. The axial length is divided into six sections, giving 39 elements per section. The cross-section of the blade is also shown in Figure 2.12. The damping treatment consists of a 0.25 mm (0.010 inch) layer of glass covered by a 0.13 mm (0.005 inch) layer of nickel. The glass layer is modeled by twelve elements per section, the nickel by twelve elements per section, and the blade by fifteen elements per section. The platform and root of the blade were not modeled.

The purpose of the forced harmonic response analysis was not to determine absolute stresses and absolute displacements, but was used to show the relative decrease in response with damping as compared to the undamped response, given the same loading condition. This was illustrated by a receptance plots, which were generated by calculating the response at discrete frequencies in the neighborhood of the resonant frequency of interest. From these plots, the half-power bandwidths were determined and structural loss factor computed for that particular mode. Thus, the end results of the forced harmonic response analysis was the structural loss factor. All the receptance plots generated were driving-point measurements, with the load applied at the tip of the blade as shown in Figure 2.13. The eight receptance plots for cases 1 through 8 are shown in Figures 2.14 through 2.17, respectively.

Figure 2.18 shows cases 1, 2, and 3 on the same plot for comparison purposes. Cases 1 and 2 are the undamped blade at room temperature and at 496°C (925°F), respectively. Comparison

TABLE 2.3

ANALYSES OF TURBINE BLADE

Case	Description	First Three Modes (Hz)	Composite Loss Factor
1	Bare, undamped blade, all material properties at room temperature	1,085.1 1,972.0 3,010.4	0.002*
2	Bare, undamped blade, all material properties at 496°C (925°F)	1,002.7 1,822.6 2,782.0	0.002*
3	Damped blade, full blade glass coating with nickel overcoat, material properties at 496°C (925°F)	1,050.7 2,847.4 4,032.9	0.011
4	Damped blade, full glass coating, all material properties at 496°C (925°F)	920.6 1,660.8 2,845.7	0.008
5	Damped blade, full glass coating, all material properties at 427°C (800°F)	940.6 1,690.7 2,917.3	0.0022
6	Damped blade, full glass coating, all material properties at 538°C (1,000°F)	907.3 1,641.0 2,792.2	0.0044
7	Damped blade, full blade glass coating with nickel overcoat, all material properties at 496°C (925°F), 7,500 rpm	1,082.4 2,870.6 4,037.5	0.0083**
8	Damped blade, full blade coating with nickel overcoat, all material properties at 496°C (925°F), glass layer modeled with solid elements	1,058.7 2,874.5 3,999.2	0.0122

*blade material is assumed to have an inherent loss factor of 0.002

**the loss factor is approximate because the peak is non-symmetric; loss factor was estimated by using the left side of the peak and multiplying bandwidth by two. Analysis includes blade rotation effects

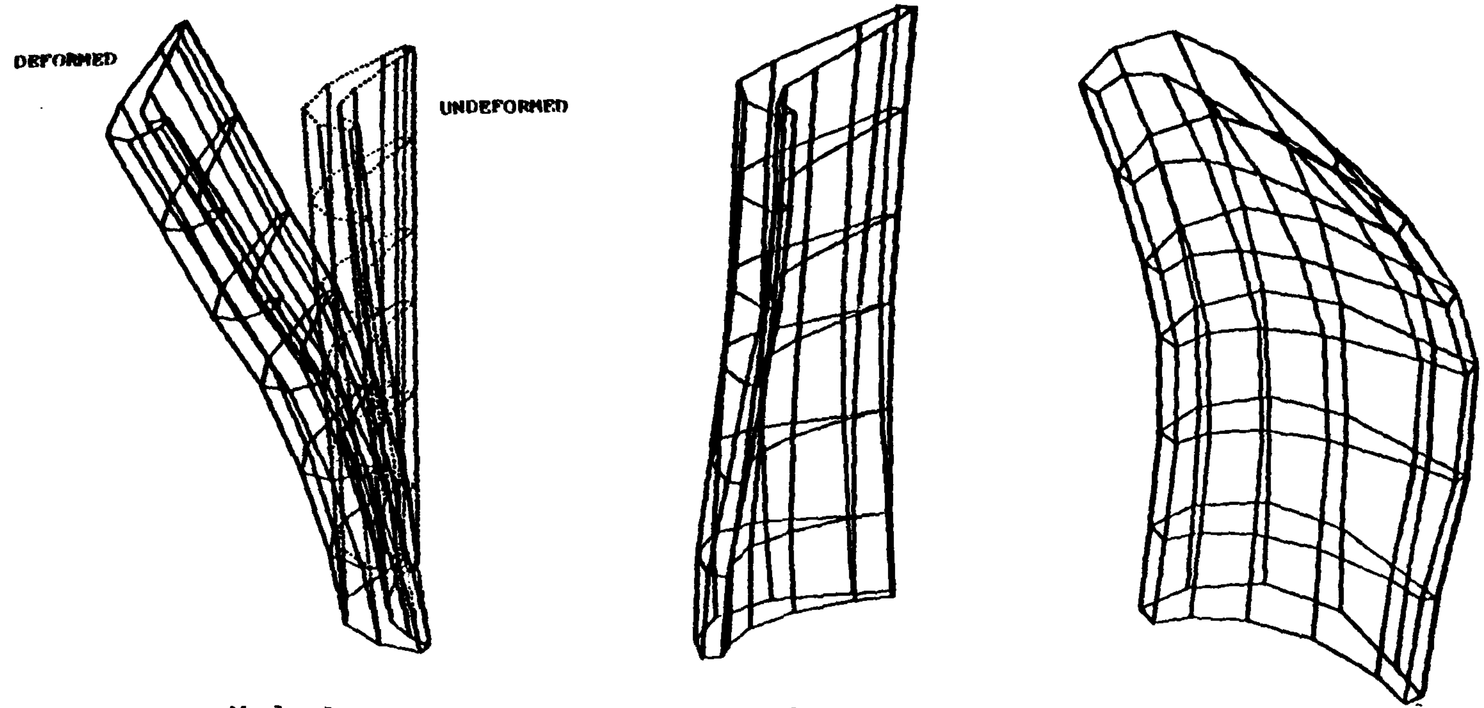

Mode 1
First Bending

Mode 2
First Torsion

Mode 3
Second Bending

Figure 2.11. Deformed Mode Shapes.

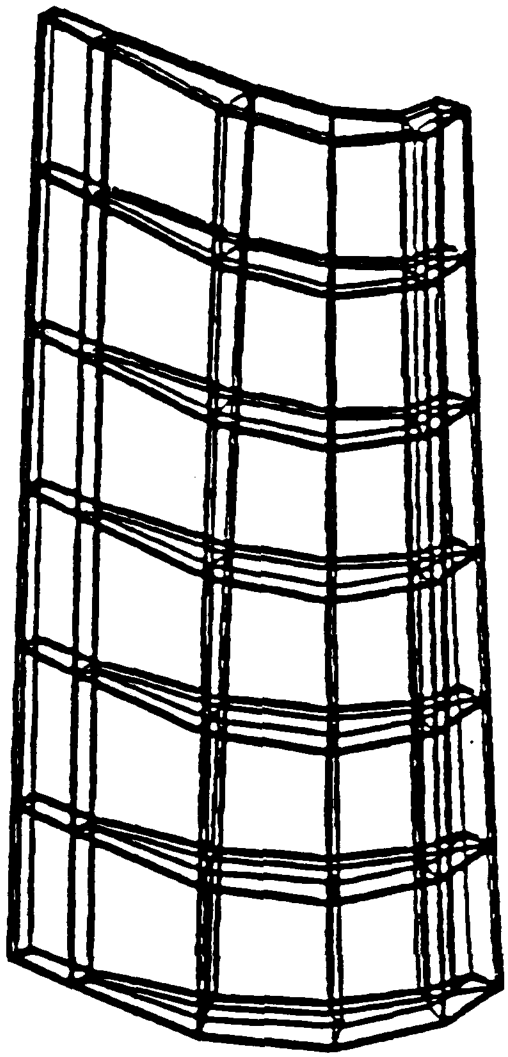

Model of
Turbine Blade

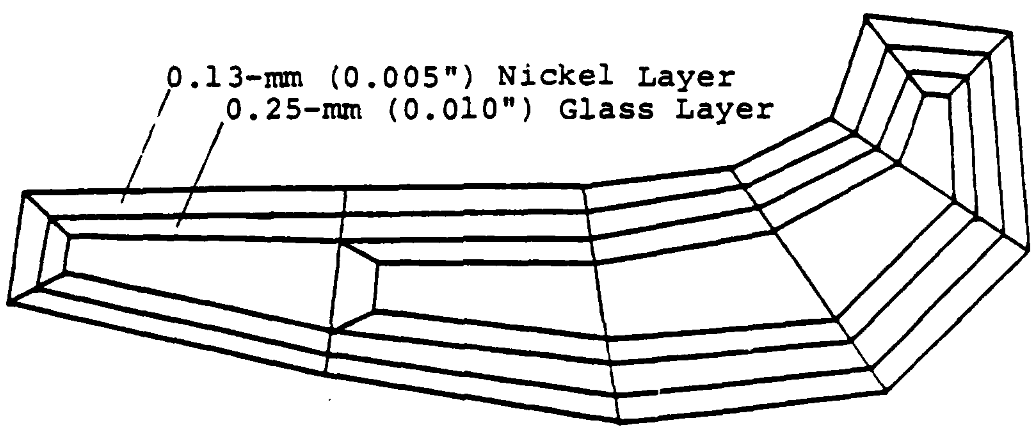

Cross-section of Turbine Blade

Figure 2.12. Finite Element Model of Turbine Blade.

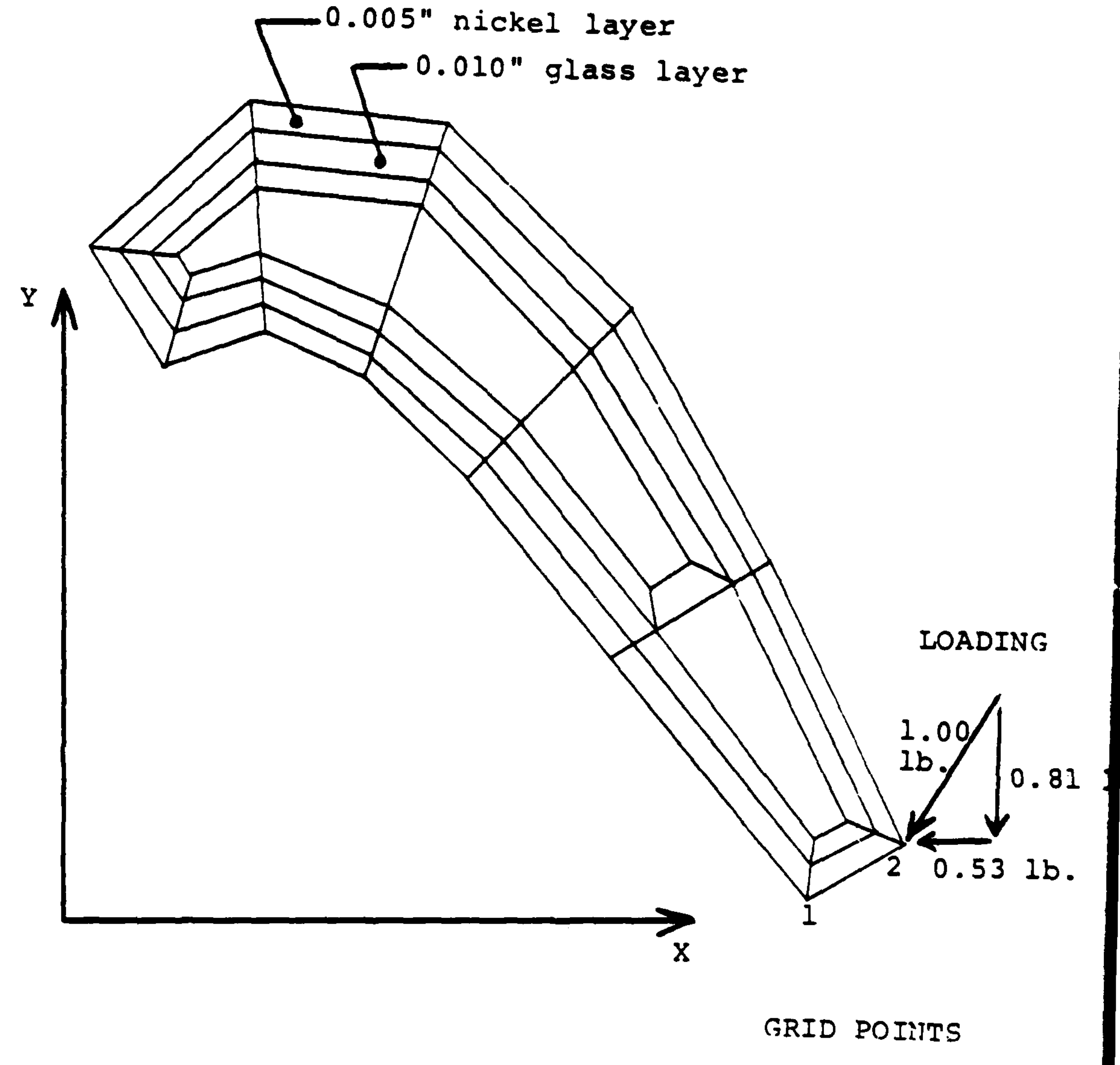

Figure 2.13. Receptance Measurement Points.

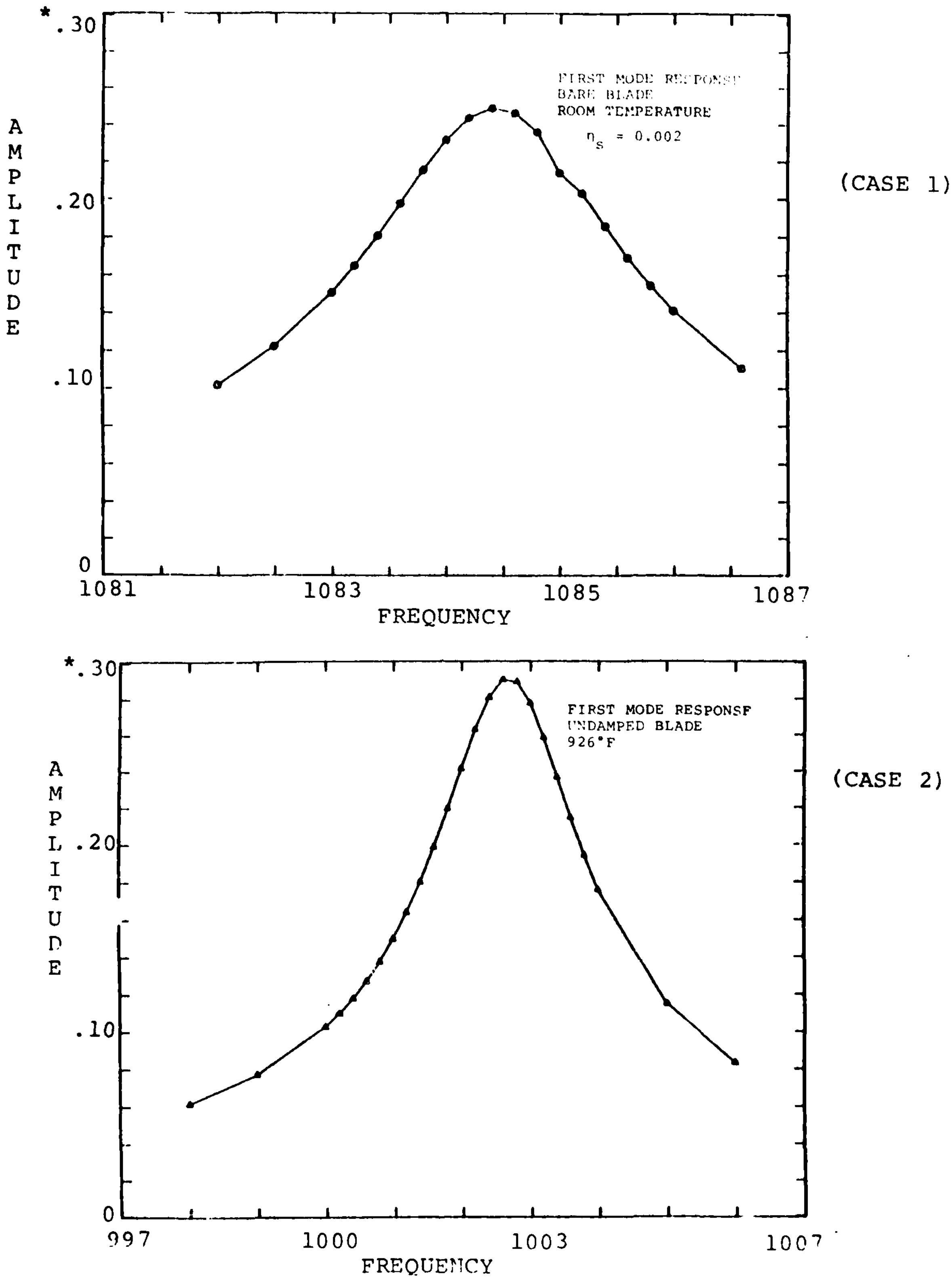

Figure 2.14. Amplitude-Frequency Response.

*amplitude in inches

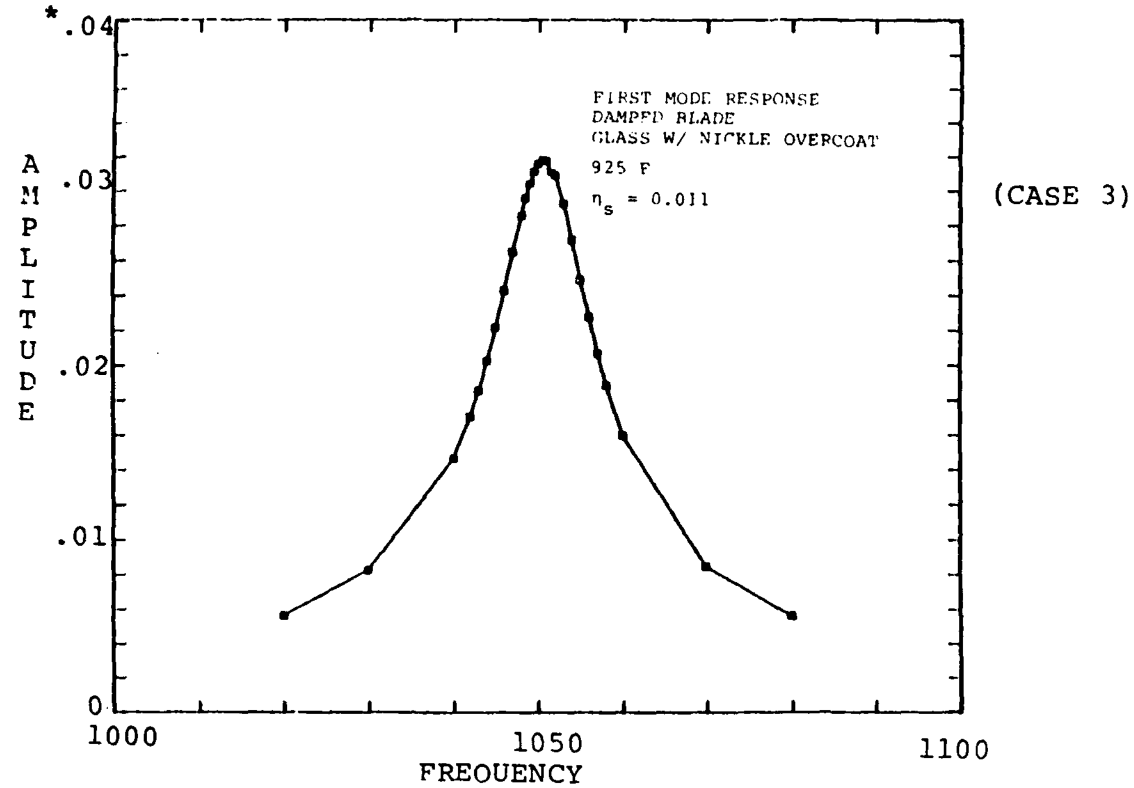

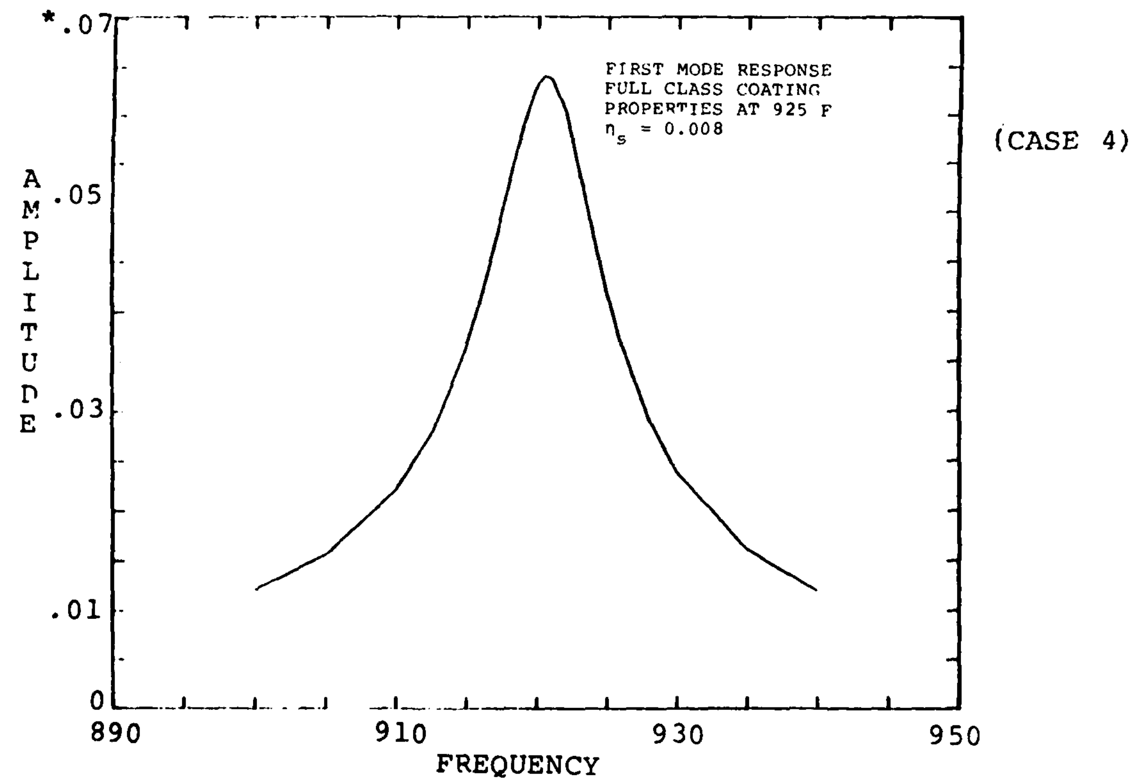

Figure 2.15. Amplitude-Frequency Response.

*amplitude in inches

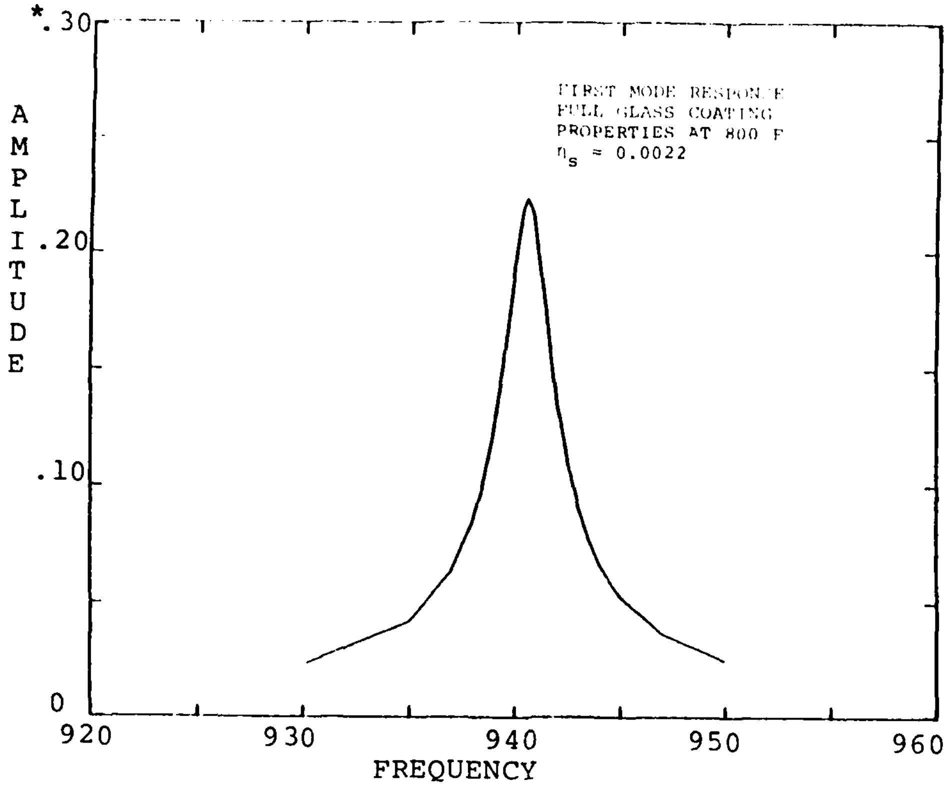

(CASE 5)

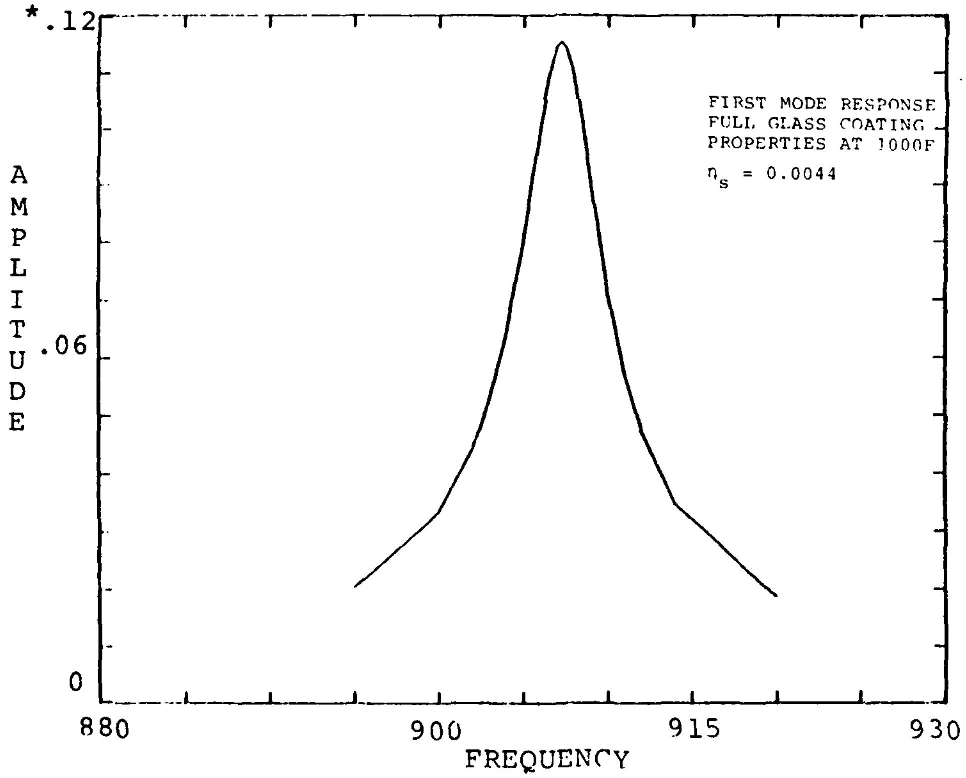

(CASE 6)

Figure 2.16. Amplitude-Frequency Response.

*amplitude in inches

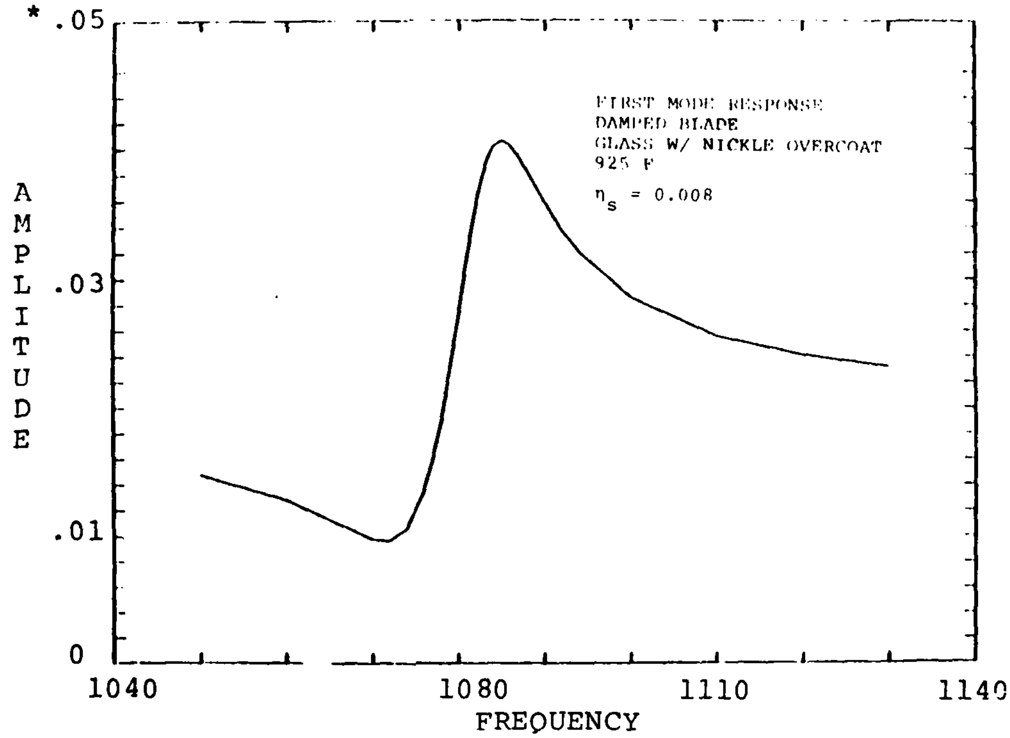

(CASE 7)

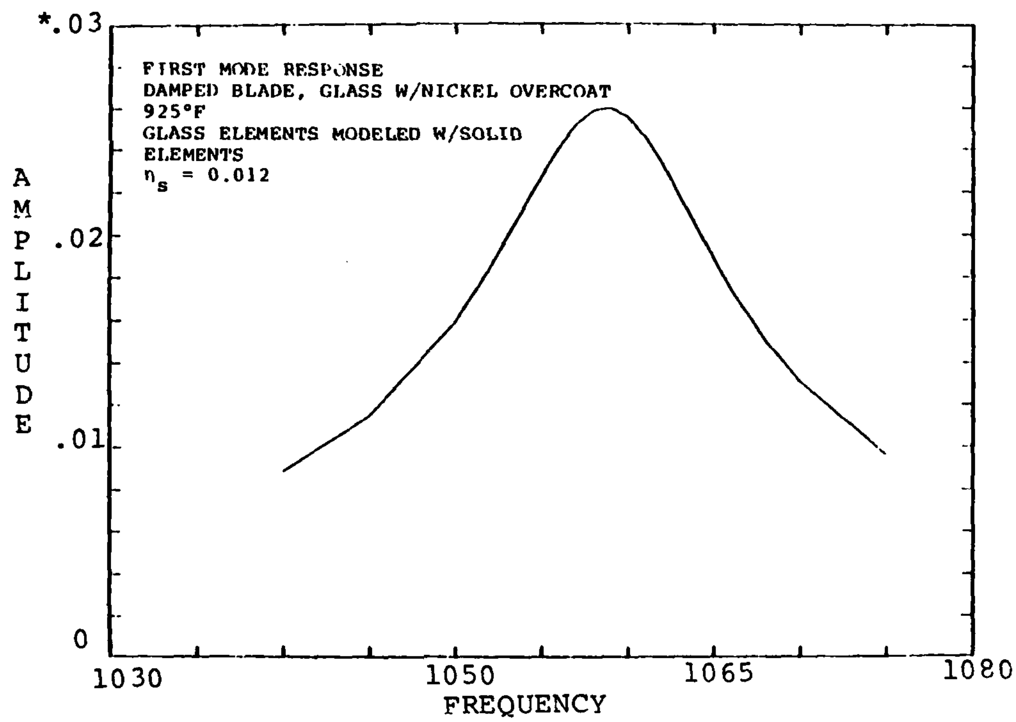

(CASE 8)

Figure 2.17. Amplitude-Frequency Response.

*amplitude in inches

of case 3 with case 2 illustrates the increased first mode frequency of the damped blade due primarily to the stiffness of the nickle overcoat. Of course the most obvious feature is the marked decrease in response of the damped blade compared to the undamped blade. The loss factor increased from .002 to .011.

A series of analyses was completed for a non-rotating blade with an 0.25 mm (0.010 inch) glass free layer coating (full blade coverage (at 427, 496, and 538°C(800, 925, and 1,000°F). The peak structural loss factor occurs at the temperature of 496°C (925°F), at which the loss modulus is also at a maximum. The amplitude-frequency response for the three temperatures is shown in Figure 2.19. This plot shows the reduced response amplitude of the blade at the optimum temperature. The shift in the first mode frequency with temperature can also be seen. The structural loss factors at 427, 496, and 538°C are 0.0022, 0.008, and 0.0044, respectively.

In a structure with a free layer damping treatment, the damping is proportional to the loss modulus. The loss modulus (modulus × loss factor) of Corning Glass 8463 versus temperature is shown in Figure 2.20. Superimposed on this graph is the structural loss factor of the blade with full glass coating. This plot shows that the loss factor predicted by the finite element analysis has the same temperature profile as the loss modulus. For a free layer damping application, these are the trends expected. Also shown on this plot is the experimentally measured structural loss factor for a blade with a half-blade glass coating. The peak structural loss factor is high and occurs at a lower temperature.

Figure 2.21 shows case 3 and case 4 together for comparison purpose. The damped blade with glass coating and nickel overcoat exhibits a lower response than the blade with just a glass coating. Case 4 has a lower first mode frequency because the glass coating adds mass to the blade, but contributes very little stiffness since its modulus is an order of magnitude lower than the modulus of the blade material or nickel overcoat.

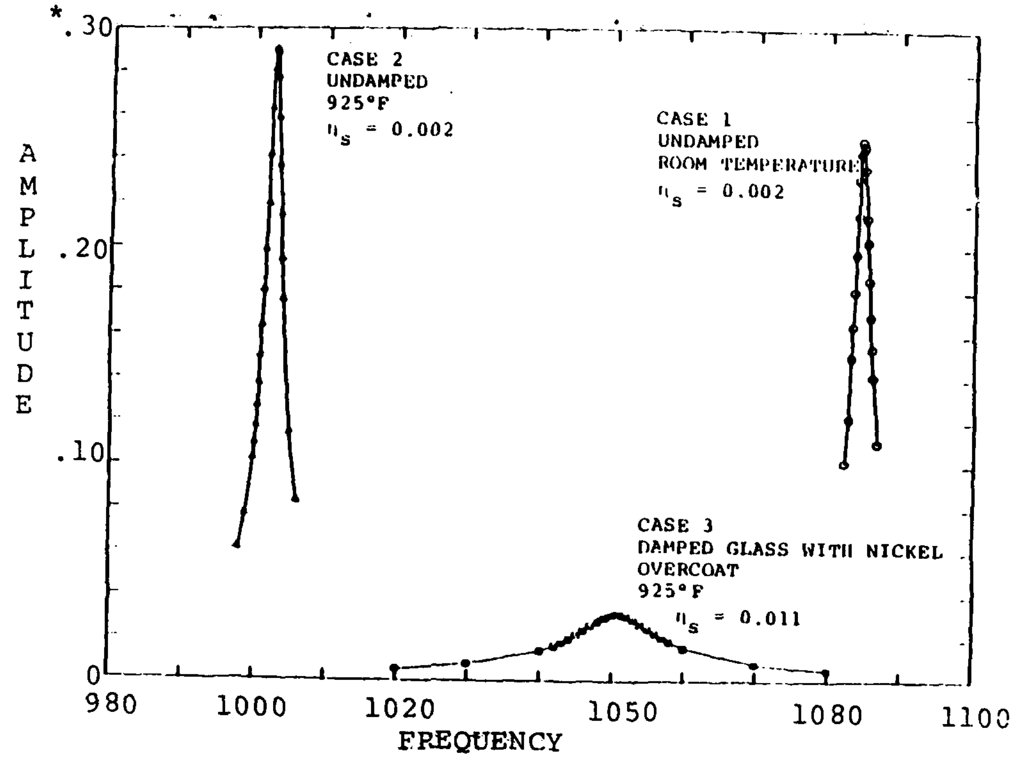

Figure 2.18. Comparison of Damped and Undamped Response.

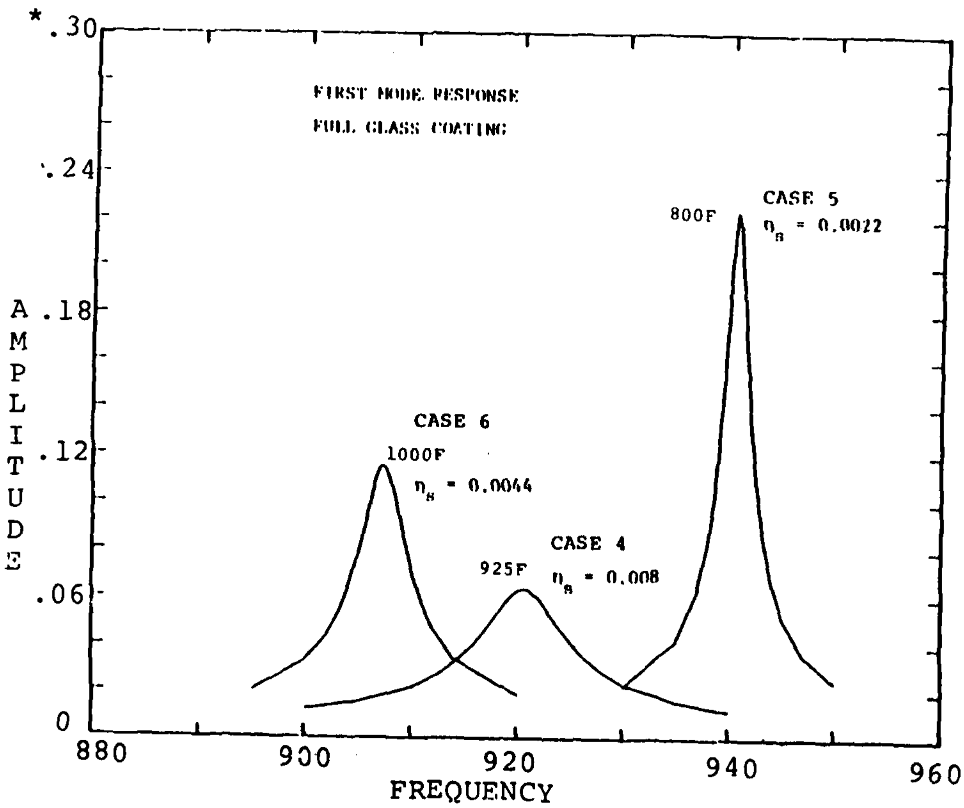

Figure 2.19. First Mode Response of Blade with Full Glass Coating at Three Temperatures.

*amplitude in inches

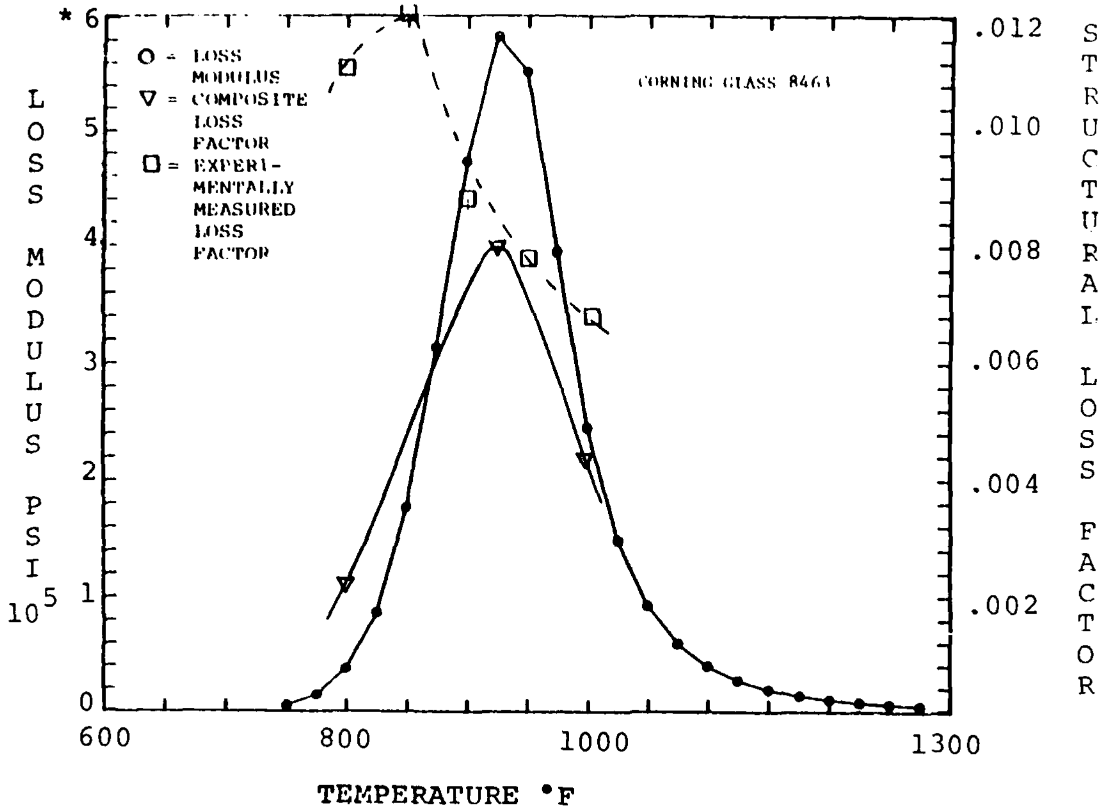

Figure 2.20. Loss Modulus and Composite Factor of Blade with Full Glass Coating versus Temperature.

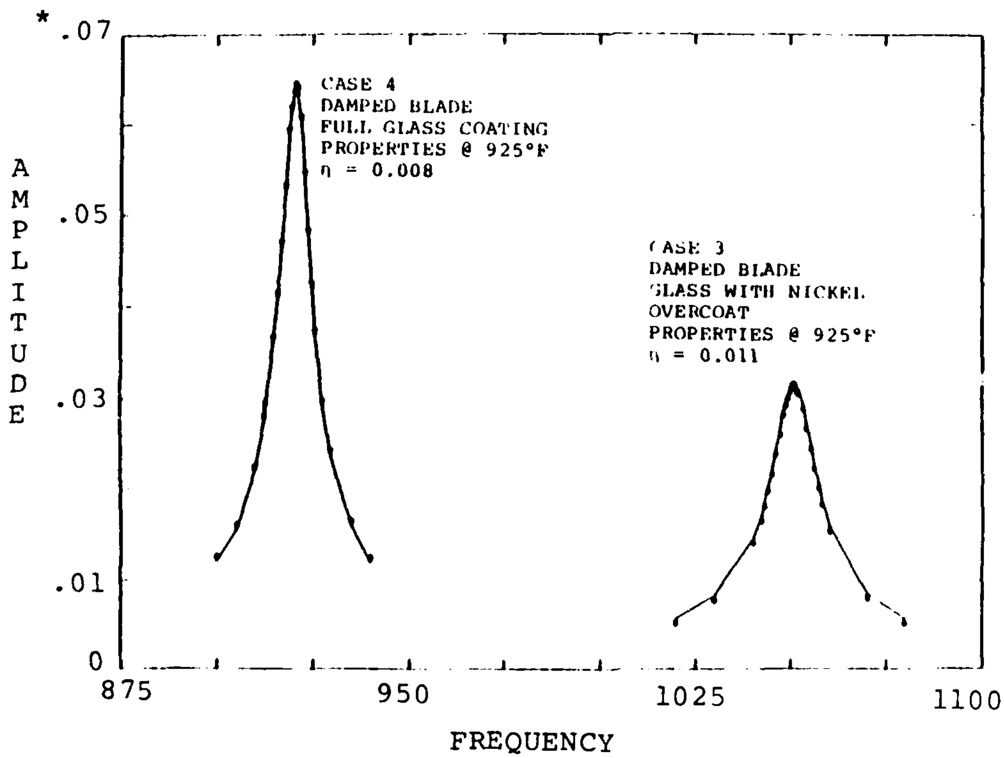

Figure 2.21. Comparison of Blade with Glass and Blade with Glass and Nickel.

*amplitude in inches

Results were obtained for an initially stressed damped blade (case 7, glass coating with nickel overcoat). The initial stress was caused by rotation at 7,500 rpm. The shift in first mode frequency due to rotation can be seen by comparing the rotating and non-rotating cases in Figure 2.22. The width of the peaks in each case are approximately the same, indicating that each has about the same level of damping.

When the blade finite element analysis was initiated, the glass damping layer was modeled with thin-shell (MAGNA-D TYPE 5) elements. This was done because the layer was thin and the glasses ordinarily are applied as free layer damping treatments (extensional deformation). However, the damping layer in constrained layer design is usually modeled with a solid element (TYPE 2). In a constrained layer application, the damping results from shear deformation. The thin-shell element does not accurately model the shear deformation; therefore, the solid elements should be used in these cases. Either element can handle the extensional deformation of a free layer damping application.

To determine the effect of the damping layer element type on the predicted damping, the glass thin-shell elements were changed to solid elements, and a comparison run was made. The test case chosen was the damped blade with glass and a nickel overcoat, non-rotating, at 496°C (925°F). With the glass elements modeled with solid elements, the first mode frequency was 1,058.7 Hz and the composite loss factor was 0.012. With the glass elements modeled with thin-shell elements (as in all previous runs) the first mode frequency was 1,050.7 Hz and the composite loss factor 0.011. The small change in composite loss factor is insignificant since it is determined graphically by the half-power bandwidth method from the amplitude-frequency response plot. The change in frequency is only about 0.8 percent. Both cases are shown in Figure 2.23.

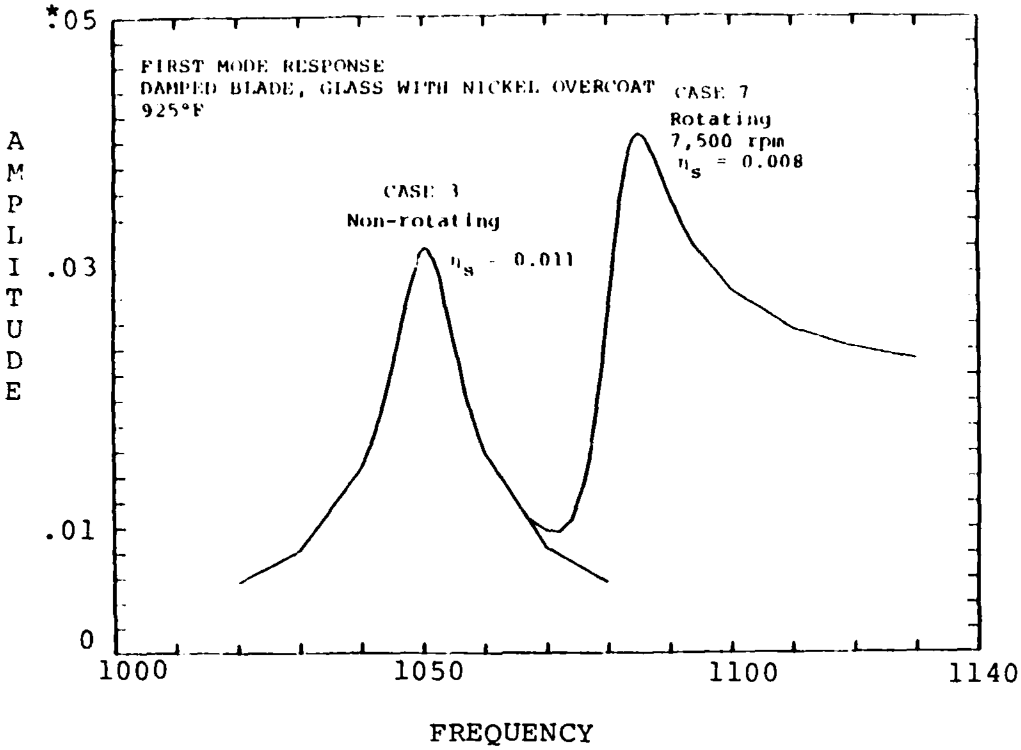

Figure 2.22. First Mode Response of Damped Blade, Rotating and Non-rotating.

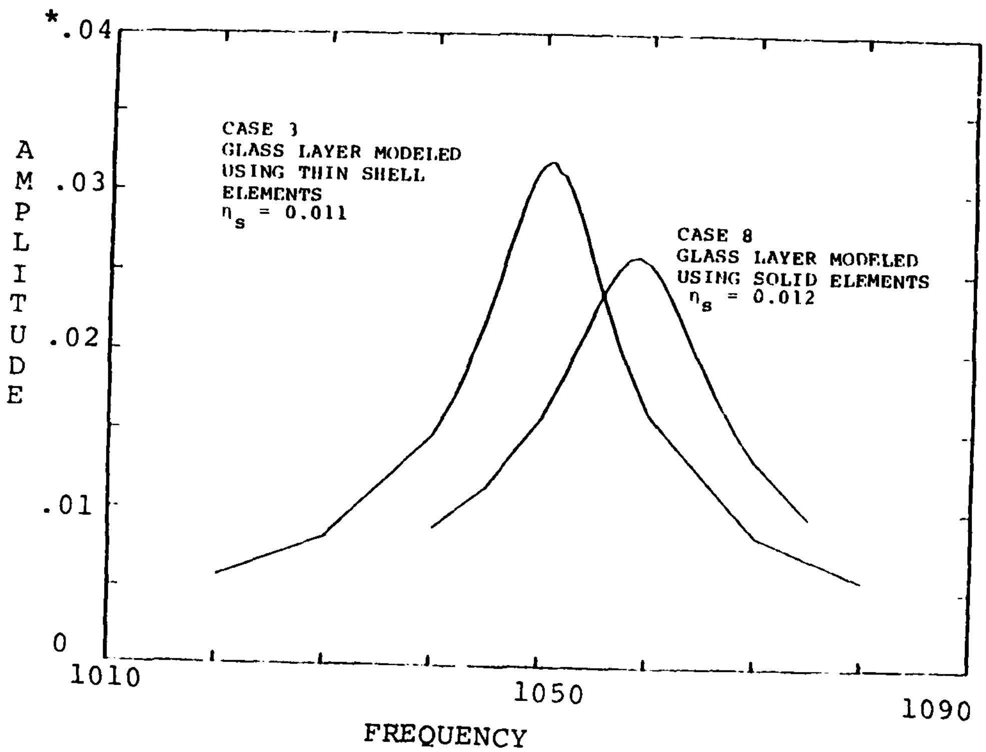

Figure 2. 23. Comparison of Results Using Different Element Types to Model the Glass Damping Layer.

*amplitude in inches

Experimental measurements have shown that a glass with a constraining layer acts as a free layer rather than a constrained layer damping treatment, at temperatures near maximum loss modulus. Therefore, the change in composite loss factor for the two cases may be more significant at higher temperatures, as the glass with nickel overcoat starts to behave more like constrained layer damping.

2.1.2.3. Comparison of NASTRAN and MAGNA-D Results

Interest was expressed in comparing the MAGNA-D results on the turbine blade to results from NASTRAN on the same model. Therefore, Conor Johnson of Anamet Laboratories was supplied with two finite element models of the F100 2nd stage turbine blade; they were the UDRI model and the airfoil section only of the P&W model which is shown in Figure 2.24.

The following free vibration runs were made using NASTRAN: (1) P&W airfoil with thin-shell elements and pins connecting suction and pressure surfaces; (2) P&W airfoil with solid elements and pins connecting suction and pressure surfaces; and, (3) the UDRI model with solid elements and the core modeled as solids. The first three frequencies for the various cases are included in Table 2.4.

The NASTRAN runs used a Young's modulus of 26.5×10^6psi which corresponds to blade material properties at 925°F (496°C). To allow comparison between a NASTRAN run and a MAGNA-D run, the frequencies of the NASTRAN run using the UDRI model and solid elements (case 4) were scaled for a Young's modulus of 31.0×10^6psi, corresponding to the blade material at room temperature. The first mode frequency of the UDRI model using MAGNA-D (case 5) is five percent higher than the corresponding NASTRAN run (case 4), and the second and third modes of the NASTRAN model are 0.5 percent and two percent higher than the MAGNA-D frequencies, respectively.

TABLE 2.4

COMPARISON OF MAGNA-D AND NASTRAN,
FIRST THREE FREQUENCIES OF TURBINE BLADE MODEL

	NASTRAN $E = 26.5 \times 10^6$ Thin-shells	NASTRAN $E = 31.0 \times 10^6$ Thin-shells (Freq. Scaled)	NASTRAN $E = 26.5 \times 10^6$ Solids	NASTRAN $E = 31.0 \times 10^6$ Solids (Freq. Scaled)	MAGNA-D $E = 31.0 \times 10^6$
P&W mesh (air foil only) (1)	CASE 1 1,356 Hz 2,672 Hz 4,062 Hz (2)	CASE 2 1,467 Hz 2,890 Hz 4,393 Hz (2),(4)	CASE 3 1,388 Hz 2,925 Hz 4,461 Hz (2)		
UDRI mesh (air foil only) (1)			CASE 4 1,499 Hz 3,287 Hz 5,025 Hz (3)	CASE 5 1,621 Hz 3,555 Hz 5,435 Hz (4)	CASE 6 1,704 Hz 3,537 Hz 5,311 Hz (5)

(1) All runs undamped, i.e., no damping layers.

(2) Model includes pins connecting suction and pressure side.

(3) Model includes solid core elements.

(4) Frequencies estimated as proportional to square root of the ratio of Young's modulus; case 2 scaled from case 1; case 5 scaled from case 4.

(5) Model includes thin-shell and solids; the thin-shells do not have artificial in-plane shear modulus; run UD5R005 (9/30/80).

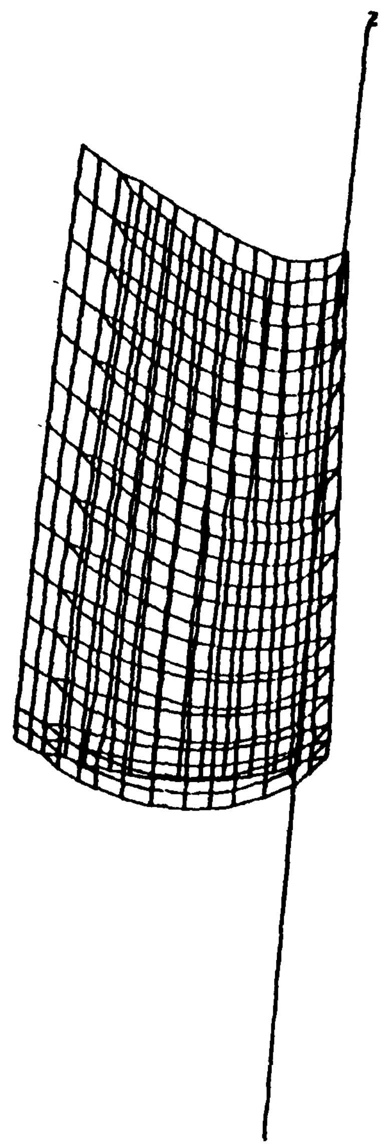

Figure 2.24. Airfoil Section of Pratt and Whitney Model.

The results of the UDRI model using MAGNA-D (case 5) are about 16 percent higher than frequencies of the NASTRAN run with the P&W airfoil and thin-shell elements (case 2). However, this is not surprising since the P&W airfoil has a much finer mesh, which is more flexible and yields lower frequencies.

In general, the MAGNA-D results agree closely with the NASTRAN results for runs using the same model.

2.2. FINITE ELEMENT PROGRAMMING

A capability for predicting the linear damped, steady state response of general three-dimensional structures vibrating about a initially stressed state developed in the program MAGNA-D[1] has been added to the program MAGNA[9]*. This addition extends the damper response analysis capability to include the materially and geometrically nonlinear deformations occurring during initial stressing. Furthermore, the complete element library available in the program MAGNA can be used in the modeling of damped structures. In the following a brief theoretical description of the finite element analyses capability is given.

The finite element formulations is based on the incremental virtual work principle of nonlinear elasticity. It is assumed that the configuration that the initially stressed vibrating structure attains is reached by a succession of two separate motions. First, the structure is subjected to the forces and constraints that are responsible for inducing the initial stresses and deformation. Second, the harmonic motion is superimposed upon this initial deformed state. No further restrictions are made regarding the structural geometry and boundary conditions and the manner in which the initial state of stress is reached. A common initially stressed configuration is that which occurs as a result of rotation.

A summary of the derivation of the finite element equations that govern the forced vibrations of a model is presented in the following paragraphs.

*MAGNA is a proprietary computer program of the UDRI, further details are in Appendix D.

Consider a three-dimensional body in three different stages, as shown in Figure 2.25 state C_o is the undeformed, unstressed state of the body. State C_1 is an intermediate state of deformation, presumed to be known. This configuration represents the state of the body at the most recent state of load incrementation. State C_2 is the "final" state, to be determined upon application of an additional increment of loading. Actually, state C_2 is found by solving for the increment of deformation that occurs, and then adding the increment to the state C_1 deformation.

With a known intermediate or prestressed state C_1, the expression for incremental virtual work between states C_1 and C_2 is given by[7]

$$
\begin{aligned}
&{}_{V_o}[D_{ijkl}e_{kl}\delta e_{ij}+{}_1\sigma_{ij}\delta\eta_{ij}+\rho_o\ddot{u}_i\delta u_i]dV \\
&= {}_{V_o}f_i\delta u_i dV + {}_{\alpha V_o}\bar{t}_i\delta u_i dA \qquad (1)
\end{aligned}
$$

where the repeated indices indicate summation from 1 to 3, and

V_o = volume in state C_o
αV_o = stress boundary in state C_o
ρ_o = mass density in state C_o
${}_1\sigma_{ij}$ = stresses in state C_1
f_i = increments in applied body forces
$\bar{t}_i$ = increments in applied surface tractions
D_{ijkl} = constitutive tensor relating increments of stress and increments of strain
u_i = increments in displacement from state C_1 to C_2
$\ddot{u}_i$ = increments in acceleration
e_{kl} = linear part of the increment in strain
η_{ij} = nonlinear part of the increment in strain
$\delta()$ = virtual change

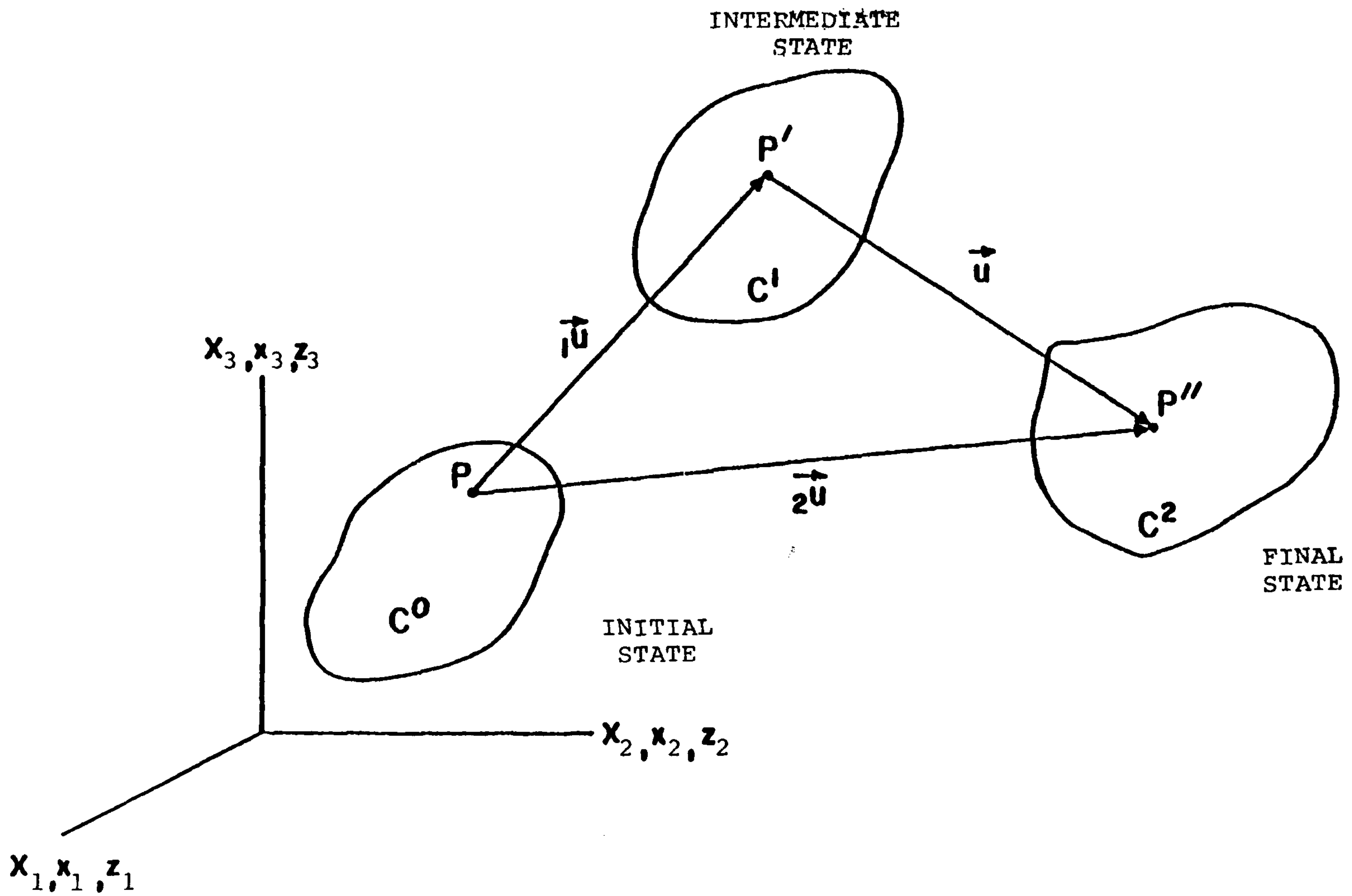

Figure 2.25 **Successive States of Deformation of a Three-Dimensional Body.**

The first two terms on the left-hand side of the above equation represent the strain energy of incremental deformation and the work performed by the initial stress state during the incremental process, respectively. The third term accounts for the increment of work due to the inertial forces of acceleration. The incremental virtual work done by the prescribed increments in body forces and surface tractions appears on the right-hand side of the equation.

Following the usual finite element discretization procedure, the equations governing the time-dependent nonlinear response of the body are obtained as

$$(\underline{\underline{K}}+\underline{\underline{K}}_G)\,\underline{X}+\underline{\underline{M}}\,\ddot{\underline{X}}=\underline{F} \tag{2}$$

where a single underbar denotes a vector and a double underbar indicates a matrix.

As it stands, Equation 2 forms the basis for the development of the MAGNA computer system programs (described in Reference [10]) for transient dynamic analysis of complex three-dimensional structures experiencing large displacements, finite strains, large rotations, and plastic deformation. In this paper we consider a specialization of Equation 2 that permits the development of an analysis method for predicting the linear, damped, steady-state response, of three-dimensional structures, about a nonlinear, initially stressed equilibrium configuration; this method is further specialized to permit the analysis of free vibrations in terms of natural frequencies and normal modes.

Consider that state C_1 of Figure 2.25 is an equilibrium configuration which has been attained by a deformation (possibly nonlinear) from the original state C_o. Analytically, state C_1 is obtained by applying Equation 1 as implemented in a computer program such as MAGNA. In practice, a common form of state C_1 is that of a body rotating about a fixed axis. We consider here a modification of Equation 2 that will permit the prediction of state C_2, the small forced oscillations of a body superposed on state C_1.

Consider the case when the applied forces (increments) in Equation 2 are harmonic in time; that is,

$$F=\bar{\underline{F}}e^{iwt} \tag{3}$$

where w is the forcing frequency, t is the time, and $i = -1$. It is assumed that the response to the harmonic applied forces is also harmonic of the form

$$X=\bar{\underline{X}}e^{iwt} \tag{4}$$

where $\bar{\underline{X}}$ is a vector of nodal displacements that characterizes the spatial form of the response. The elements of $\bar{\underline{X}}$ are, in general, complex owing to possible phase differences (due to damping) between the response quantities and the forcing function. Incorporation of Equations 3 and 4 into Equation 2 leads to (after eliminating e^{iwt} from each term)

$$[\bar{\underline{\underline{K}}}+\underline{\underline{K}}_G-\omega^2\underline{\underline{M}}]\underline{X}=\bar{\underline{F}} \tag{5}$$

This equation yields the small nodal vibrational response about a prestressed equilibrium state predicted by Equation 2. The viscoelastic damping behavior is incorporated through the constitutive law

$$\underline{\sigma}=(\underline{\underline{D}}^R+i\underline{\underline{D}}^1)\underline{e} \tag{6}$$

where D^R and D^1 are the matrices with frequency-dependent coefficients characterizing the energy storage and dissipative behavior of the material, respectively. The stiffness matrix $\bar{\underline{\underline{K}}}$ is thus complex. Equation 5 represents a set of complex, linear algebraic equations. A solution to the equations for a particular value of the forcing frequency ω is obtained by the following steps:

Decomposition: $(\bar{\underline{\underline{K}}}+\underline{\underline{K}}_G-\omega^2\underline{\underline{M}})=\underline{\underline{L}}\,\underline{\underline{D}}\,\underline{\underline{L}}^T$

Forward substitution: $\underline{\underline{L}}\,\underline{\underline{Z}}=\bar{\underline{\underline{F}}}$

Scaling: $\underline{\underline{D}}\,\underline{\underline{Y}}=\underline{\underline{Z}}$

Back substitution: $\underline{\underline{L}}^T\bar{\underline{X}}=\underline{Y}$

These operations have been programed using out-of-core storage techniques so that large-scale systems of equations can be considered.

The above solution can be applied to Equation 5 for a single forcing frequency, or alternatively, a number of solutions can be obtained by sweeping through a number of specified frequencies. This capability is useful for making amplitude and phase angle versus frequency plots of displacements, strains, and stresses. System modal damping factors can be computed in two ways: by the half-power bandwidth method and by the strain energy ratio approach. In the half-power bandwidth method computation of the modal damping factor η_{si} for the ith mode is made by evaluating

$$\eta_{si}=(\omega_2-\omega_1)/\omega_c \tag{7}$$

where ω_c is the frequency corresponding to the maximum amplitude and ω_1 and ω_2 are the frequencies associated with amplitudes $A_{max}/ 2$.

The energy ratio approach to the computation of modal damping factors is expressed as

$$\eta_{si}= \sum_{j=1}^{N} \eta_j W_{jc}^{(i)} \quad \sum_{j=1}^{N} W_{jc}^{(i)} \tag{8}$$

where N is the number of finite elements in the model, η_j is the material damping factor (defined as $\underline{\underline{D}}^I=\eta D^R$) for element j, and $W_{jc}^{(i)}$ is the energy stored in the jth element when the system is being forced at frequency ω_c. A third method of calculating system modal damping based on undamped modal strain energy of the structure is also implemented in the program. In this method the element stored energy $W_{jc}^{(i)}$ appearing in Equation 8 is calculated using the classical normal modes instead of the damped deflection shapes.

The frequency and temperature dependent material properties of the viscoelastic damping materials are input to the program through a user written subroutine.

The program outputs amplitude, phase angles, and stresses at each frequency as well as the system loss factors as calculated using Equation 8. In the normal mode solution procedure the programs output mode shapes, frequencies, stresses, and the system loss factor as calculated using the modal strain energy method.

The program is stored on CDC mass-storage unit is fully operational.

SECTION 3
SPECIAL PROJECTS

3.1. STRUCTURAL ANALYSIS

The portable Hewlett Packard Model Number 5451-B Fast Fourier Analyzer was used to perform frequency and modal analysis on various structures as follows:

TF-30 Vibration Monitoring System Analysis

The Fourier Analyzer was shipped to the Engine Overhaul Facility, Tinker Air Force Base, Oklahoma, to collect data to investigate an excessive rate of post overhaul engine rejection due to high vibration levels. The results of this analysis are presented in University of Dayton technical report UDR-TR-81-27, "Structural Analysis of the TF-30 Engine Vibration Transducers V-1 and V-2." [12]

3.2. DDA ELASTOMERIC TOOLING

In mid-December, 1981, UDRI personnel made a trip to the Detroit-Diesel, Allison (DDA) plant in Indianapolis, Indiana to discuss problems they were having in the bonding of damping wraps to the vanes of the TF-41 low pressure bearing support (LPBS). DDA has fabricated a single vane elastomeric expansion tool which is heated by a hair-dryer-type commercial heat gun. They had set up a switching control unit to the heating element which operated on a thermocouple feedback from near the outlet of the air passage inside the baffling of the fixture. The problem they had encountered were debonds or voids in the ISD-110 layer bond to the outer constraining layer of the wrap. (The TF-41 LPBS damping wrap was epoxy bonds only on the edges and requires damping layer adhesive attachment over the majority of the vane surfaces. It has two damping layers of ISD-110 on one side and two damping layers of ISD-112 on the other with two constraining layers on each side.)

The bond failure of the outer damping layer of ISD-110 seemed quite likely to be a problem of overheating the wrap since the heat flow is from the outside to the inside of the installation set-up for the wrap bonding. We suggested the installation of some thermocouples at the elastomer-outer constraining layer interface to determine the temperature profile over the wrap surface. DDA later reported the temperature survey showed 385°F to be the maximum temperature at the outer surface of the wrap. This temperature is approaching the failure temperature of ISD-110. It is possible the elastomeric tooling configuration was causing some shear between the wrap layers at the failure location. This could quite conceivably cause wrap delamination at maximum stress, maximum temperature locations.

In any case, DDA reported the problem solved by changes to the internal baffling in their bonding. Successful wrap installations, in so far as we know, are now routine. It should be noted that this tooling set-up is a prime candidate for worldwide use in a single vane damping wrap repair kit.

3.3. HIGH FORCE, HIGH TEMPERATURE ELECTROMAGNETIC TRANSDUCER DEVELOPMENT

Development of an electromagnetic transducer having greater force output than those used in the high temperature beam tests was undertaken. These transducers were to excite high frequency modes in bladed disks rotating at high speeds, and were of interest to AFWAL/MLLN and AFWAL/POTA.

The principal concern in the design of this transducer was to maximize the force that it can exert on the target disk or beam. The maximum force results from producing the largest possible magnetic field at the target surface. The biggest single complication in the design arose from the requirement for large force at relatively high frequencies. Several refinements were incorporated to minimize the limiting effects and to maximize power transfer to the magnetic field.

The basic geometry of this transducer is that of a relatively long iron core with a multilayer coil of copper wire wrapped around it. This assembly is contained within a closed, externally threaded housing to allow for cooling and mounting. The actual core is square in cross-section, and is contained within a cylindrical coil form. This configuration allows freon to be circulated between the core and the coil in order to cool the windings. The freon removes much of the heat generated by I^2R losses, permitting a higher current to be driven through the wire coils, thus resulting in a higher magnetic field. Figure 3.1 shows a schematic cross-section of the cooling flow configuration.

At frequencies above several tens of Hertz, eddycurrent losses become significant. These occur in any conductor that is placed within a changing magnetic field, such as the core of a transformer, or the core of this transducer. As the operating frequency is increased, the eddycurrent losses also increase. This eddycurrent effect can be reduced appreciably by constructing the core of thin electrically isolated laminations of the core material, again much as within a transformer. The higher the required operating frequency, the thinner the laminations must be.

The core was constructed from 0.015 inch thick silicon-iron transformer sheet steel to produce a nominal 0.25" x 0.25" x 1 5/8" core, laminated parallel to the long direction (see Figure 3.5). The laminations are pressed into a glass-epoxy coil form with a thin layer of electrical tape to fill in the slight gap which resulted from the core's not having a perfectly square cross-section. The back end of the core is almost in contact with the transducer body, providing a magnetic flux return path through the transducer body. The front of the core is pressed against a ~0.015 inch thick non-magnetic stainless steel membrane. This end provides the external magnetic field to the target disk.

The coil consists of eight layers of 30 gauge enameled wire with a copper-constantan thermocouple embedded between the fourth and fifth layers. The resistance of the coil is nominally 12.5. Fusing current for 30 gauge wire is approximately 10 amperes. To avoid possible damage to the coil, do not exceed 6 amperes peak current under any circumstances. At an ambient temperature of 27°C, the cooling should be adequate for currents up to the above recommended limit. During operation in high temperature environments the coil temperature, monitored by the thermocouple, should not be permitted to exceed 85°C.

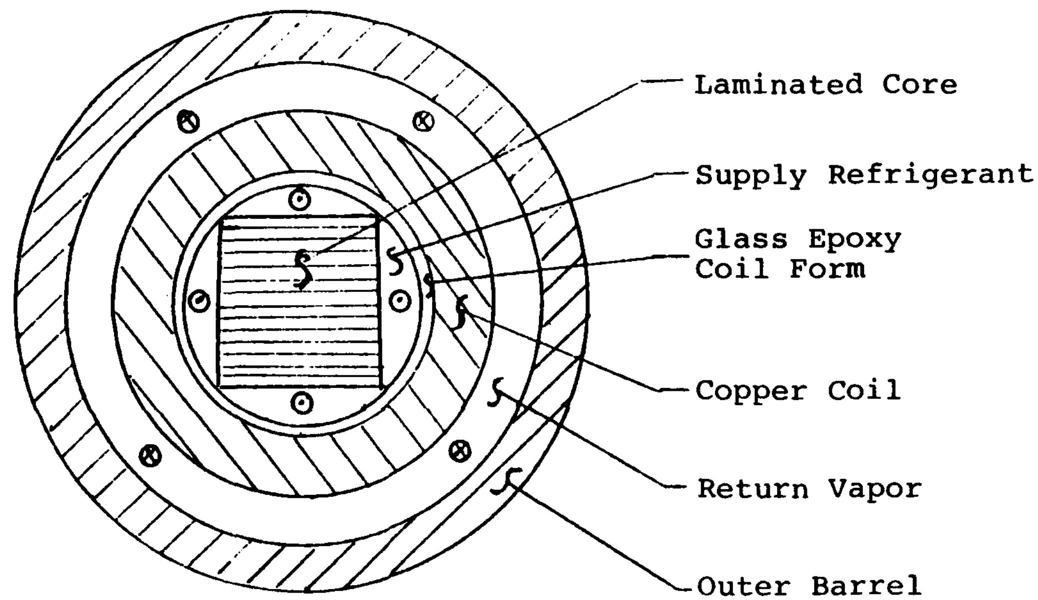

Figure 3.1. Schematic Cross Section of Transducer Showing Coolant Flow

Figures 3.2 through 3.7 show the design drawings of the parts of the transducer assembly.

Performance characteristics of these transducers are shown in Figures 3.8 through 3.12. Figures 3.8 through 3.10 show the Oersteds versus D.C. current input into the transducer. Oersteds are a measure of the magnetic field strength. Figure 3.11 illustrates the increase in power of the transducer as a function of increasing D.C. bias current at a constant A.C. drive voltage. The acceleration output was measured by an accelerometer mounted on a standard aluminum beam. Figure 3.12 illustrates the effect on the drive power an A.C. voltage increase to the transducer with a constant D.C. bias current. Once again the acceleration is monitored on an aluminum beam which is being excited by the transducer.

3.3.1. Cooling System

A cooling system, fabricated to cool the transducers manufactured for the Propulsion Laboratory, was delivered with the transducers. The system was built around a Copeland Model FBAH 0050 1AA compressor/condenser unit. The system is designed to provide cooling for two to eight transducers. Refrigerant flow rate is controlled by metering valves in the supply and return lines, a thermostatic expansion valve, and the amount of freon charge in the system. Distribution of refrigerant among transducers is provided by manifolds (Figure 3.13) between the supply and the return line and the transducers. One set of manifolds was provided with the transducer mounting plate to be used on the bladed disk fixture.

Since it is anticipated that the system will occasionally be subjected to contamination, principally due to connecting and disconnecting transducers, two filter-driers were installed. A filter-drier, having 9 cubic inches desiccant and 21 square inches filter surface, installed in the liquid line, would normally be adequate to provide long-term protection to the system. However, anticipating the probability of refrigerant contamination, not only

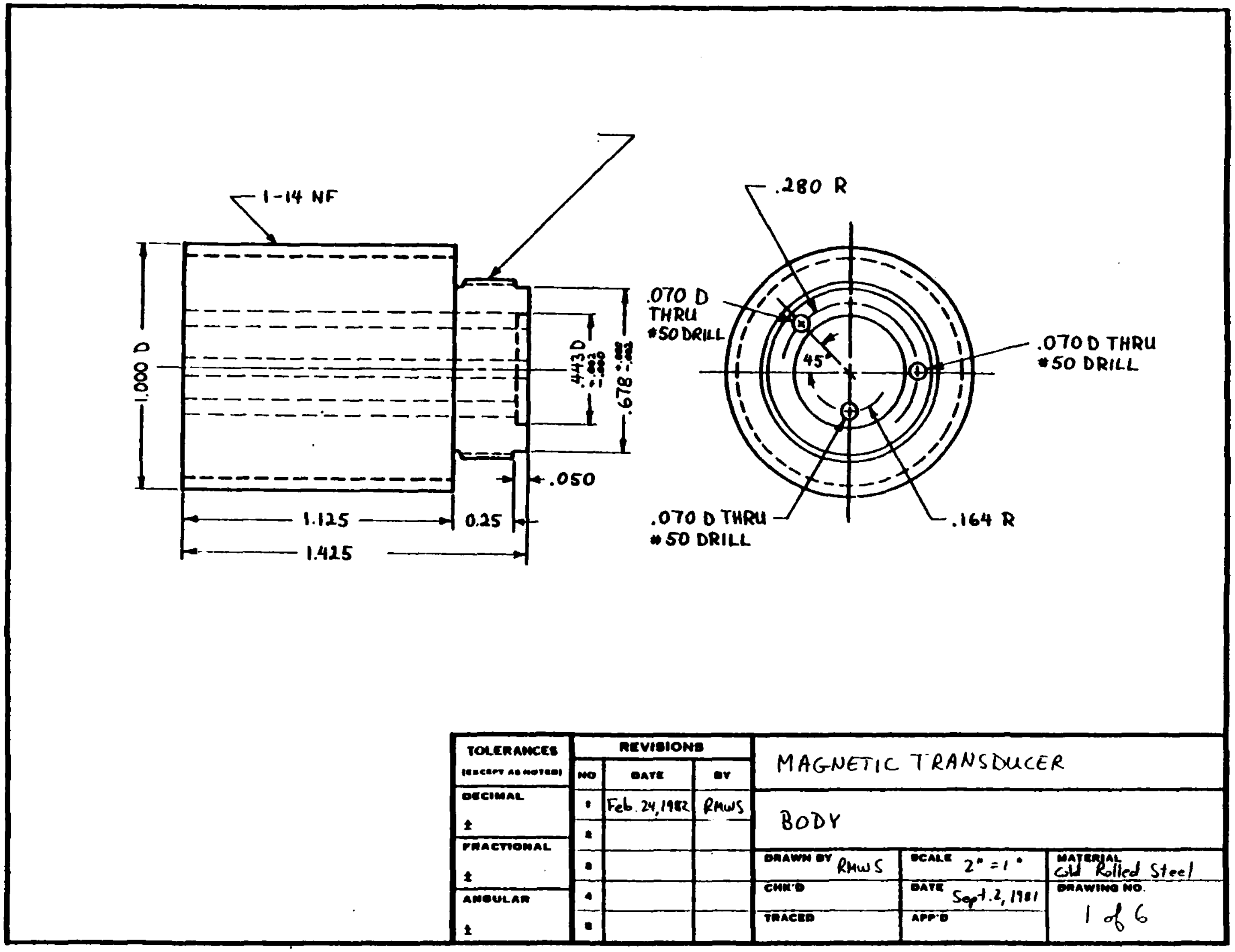

Figure 3.2. Magnetic Transducer Body

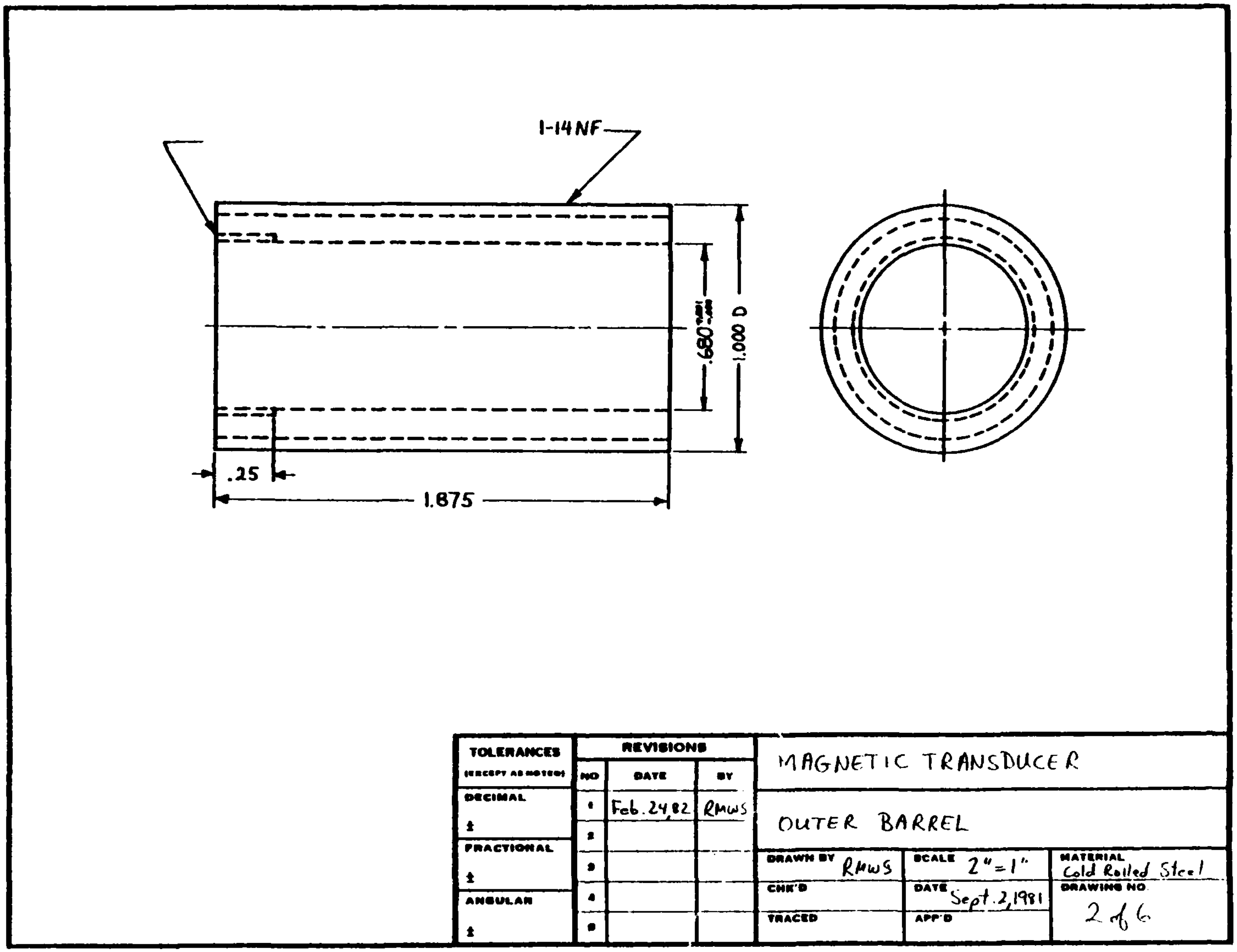

Figure 3.3. Magnetic Transducer Outer Barrel

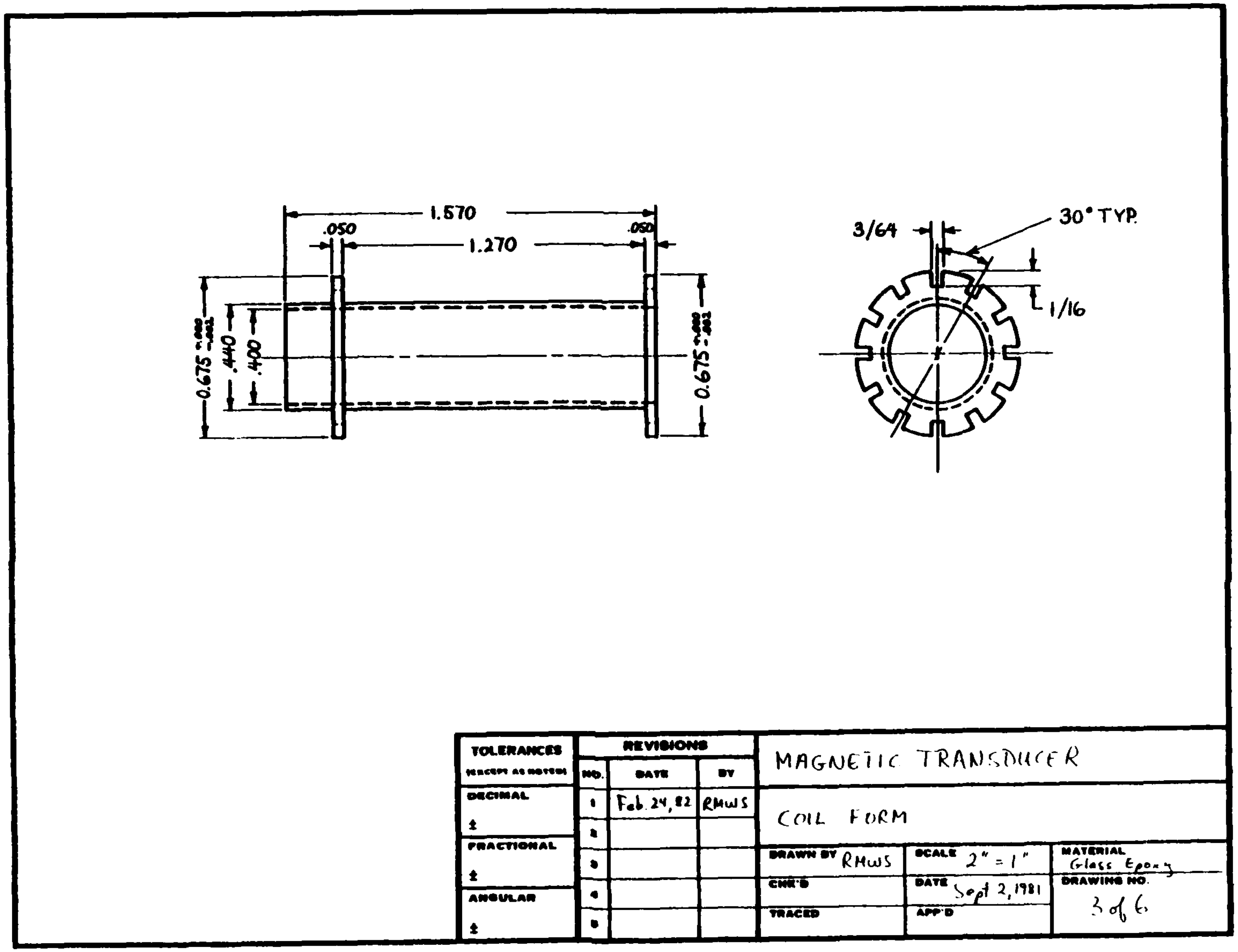

Figure 3.4. Magnetic Transducer Coil Form

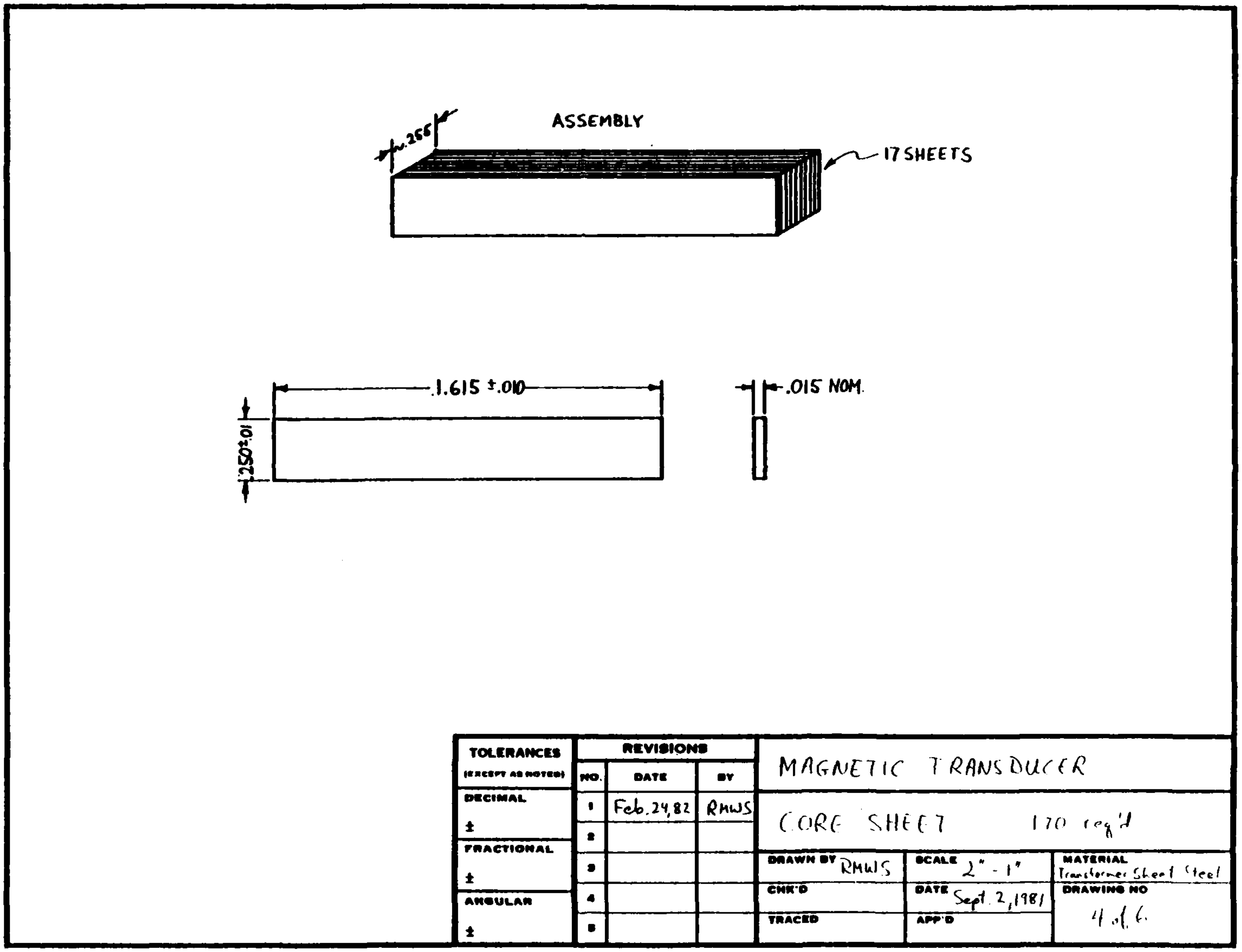

Figure 3.5. Magnetic Transducer Core Sheet

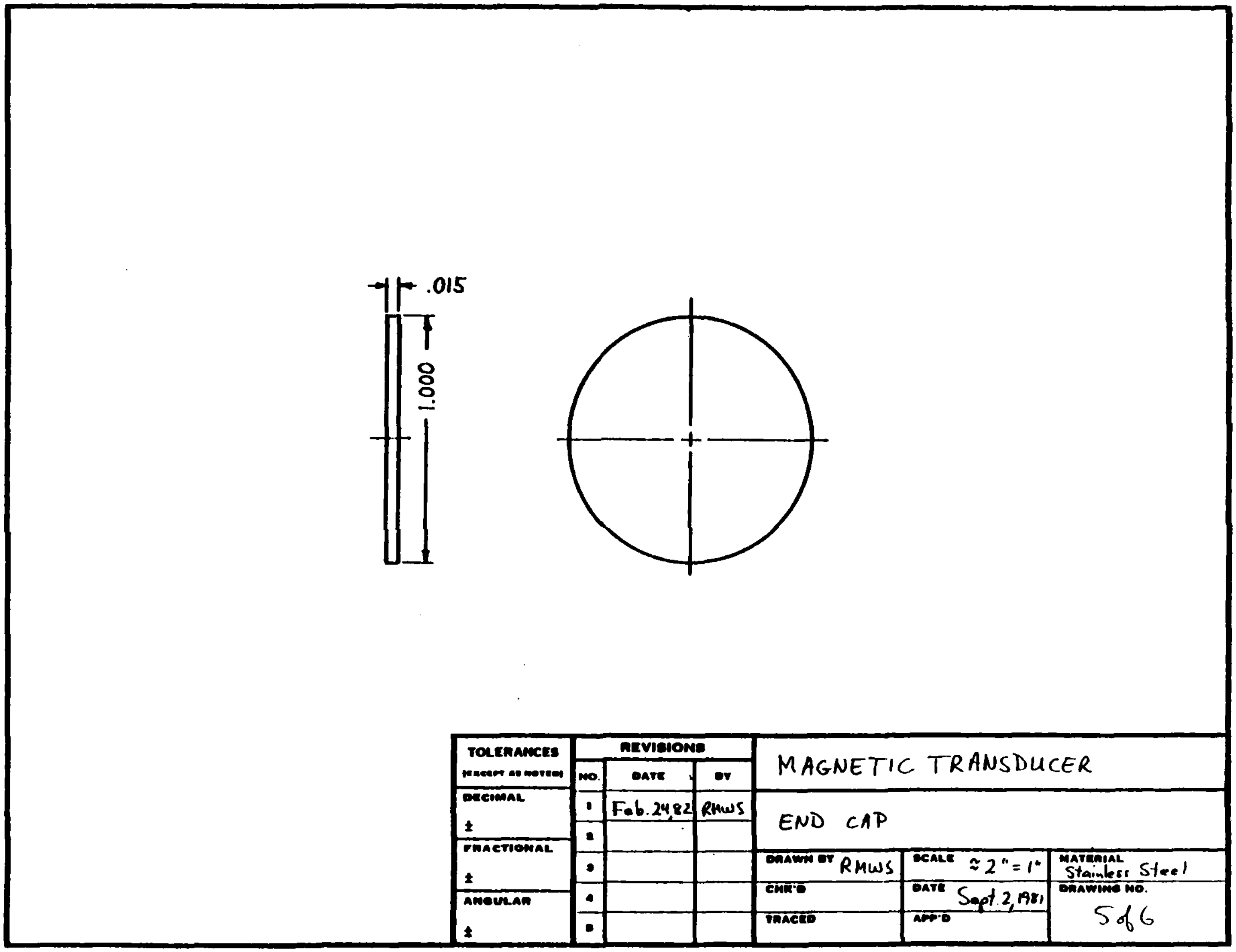

Figure 3.6. Magnetic Transducer End Cap

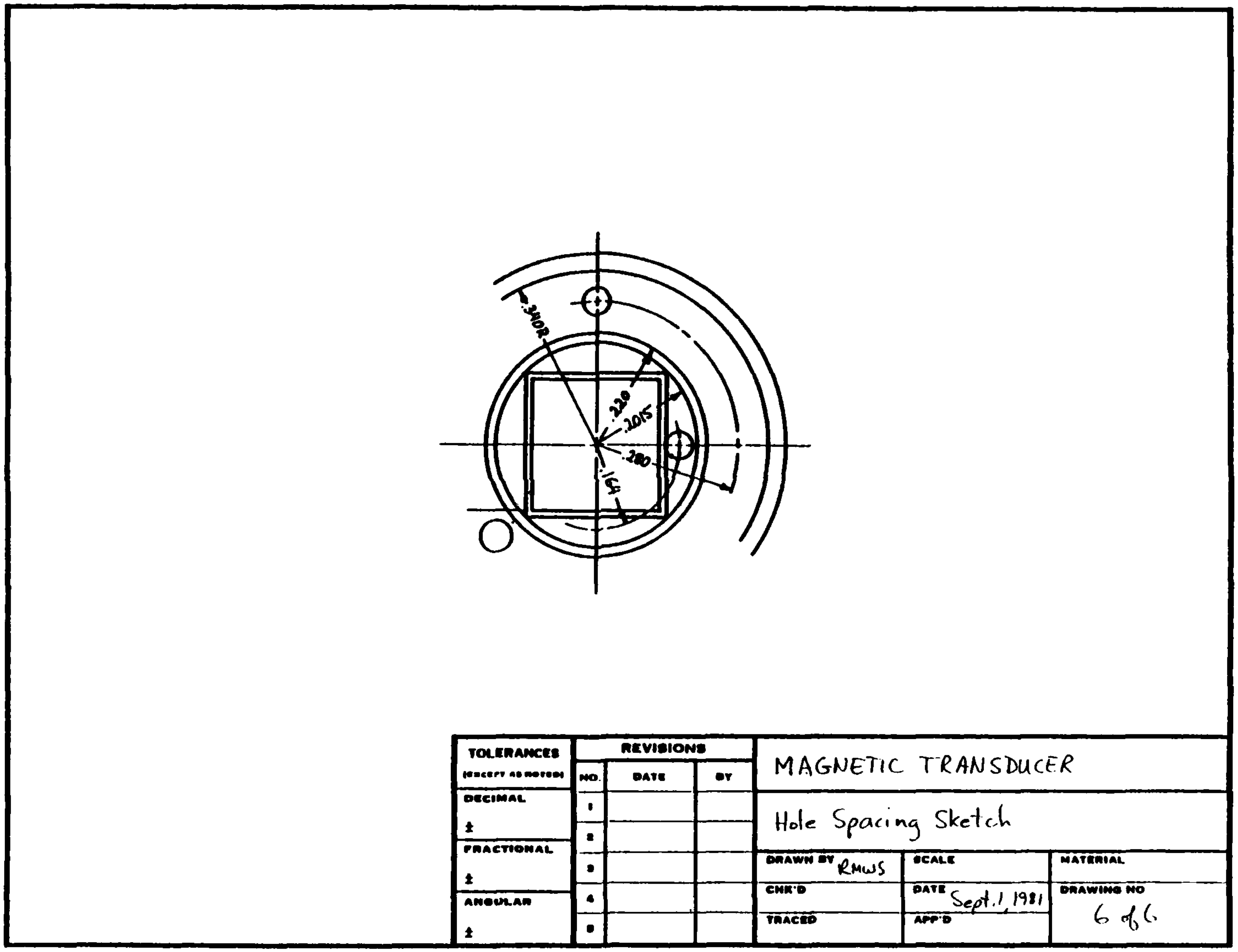

Figure 3.7 Magnetic Transducer Hole Spacing Sketch

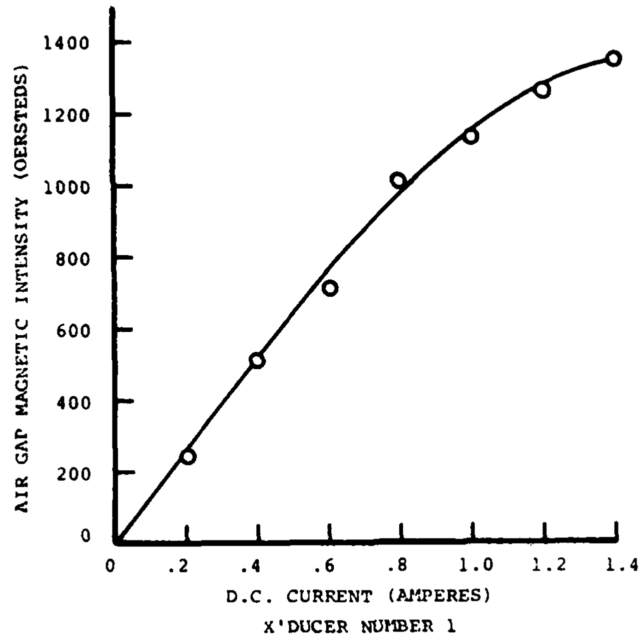

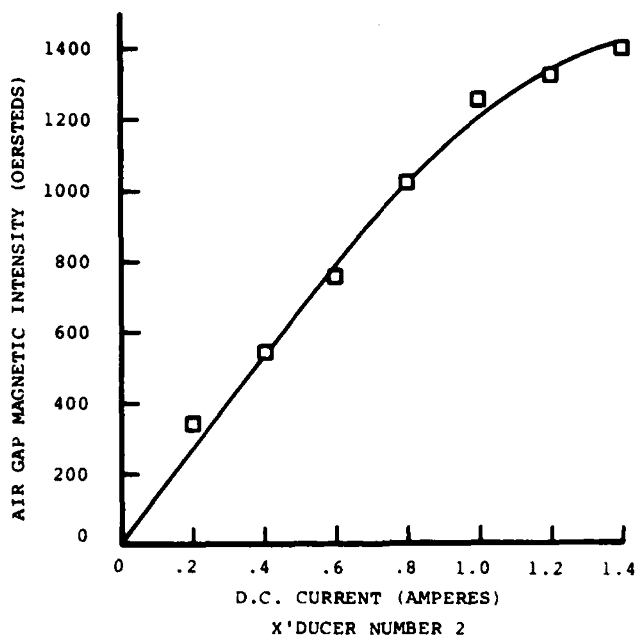

Figure 3.8. Air Gap Magnetic Intensity versus D.C. Current in Coil.

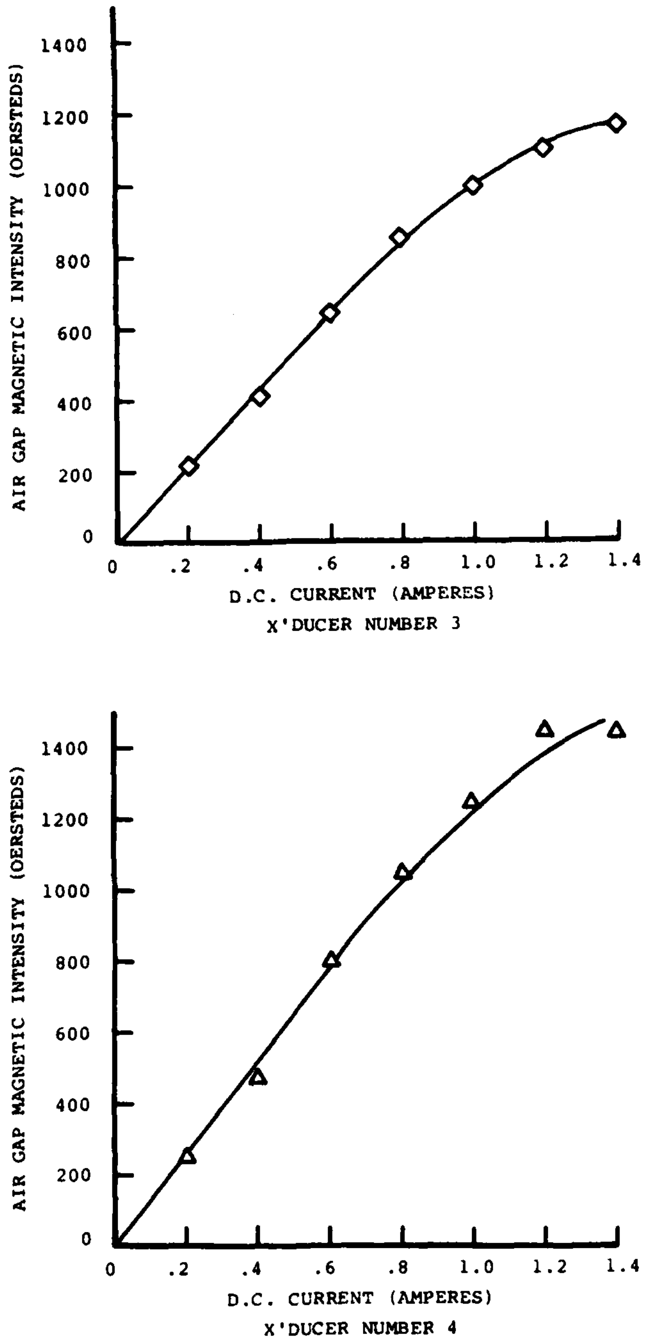

Figure 3.9. Air Gap Magnetic Intensity versus D.C. Current in Coil.

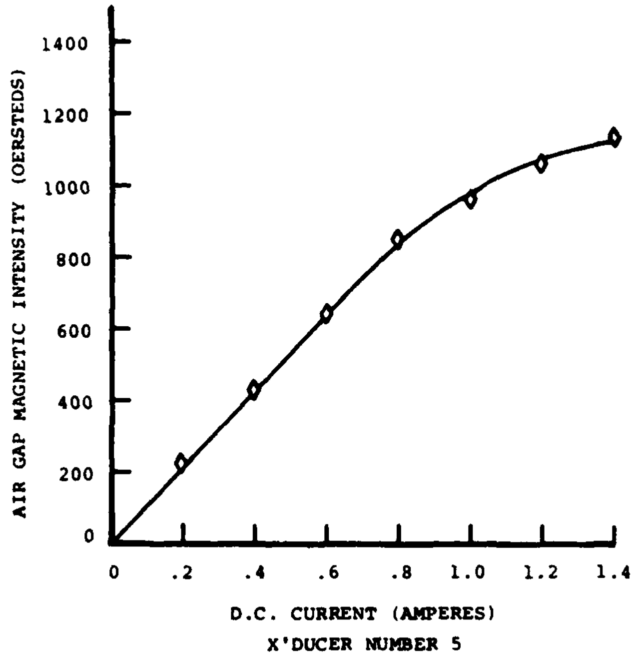

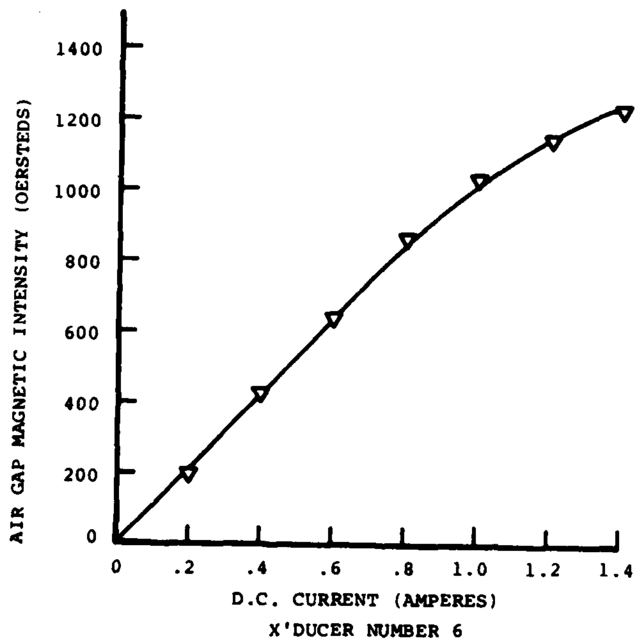

Figure 3.10. Air Gap Magnetic Intensity versus D.C. Current in Coil.

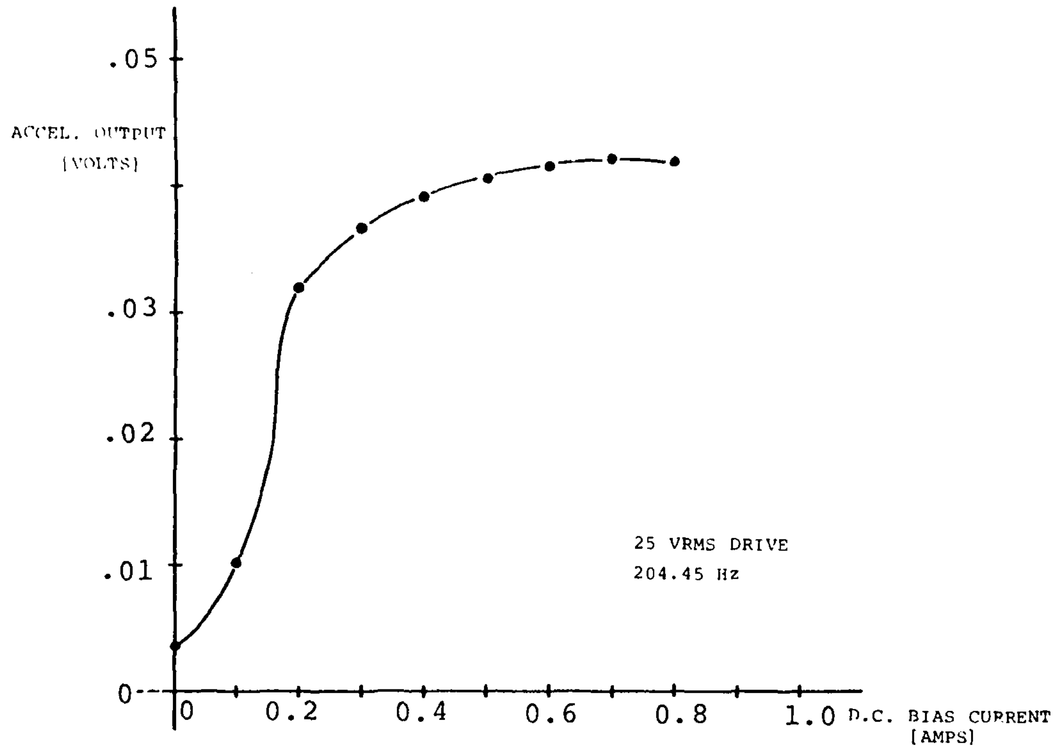

Figure 3.11. Acceleration Response versus D.C. Bias at a Constant A.C. Drive Level.

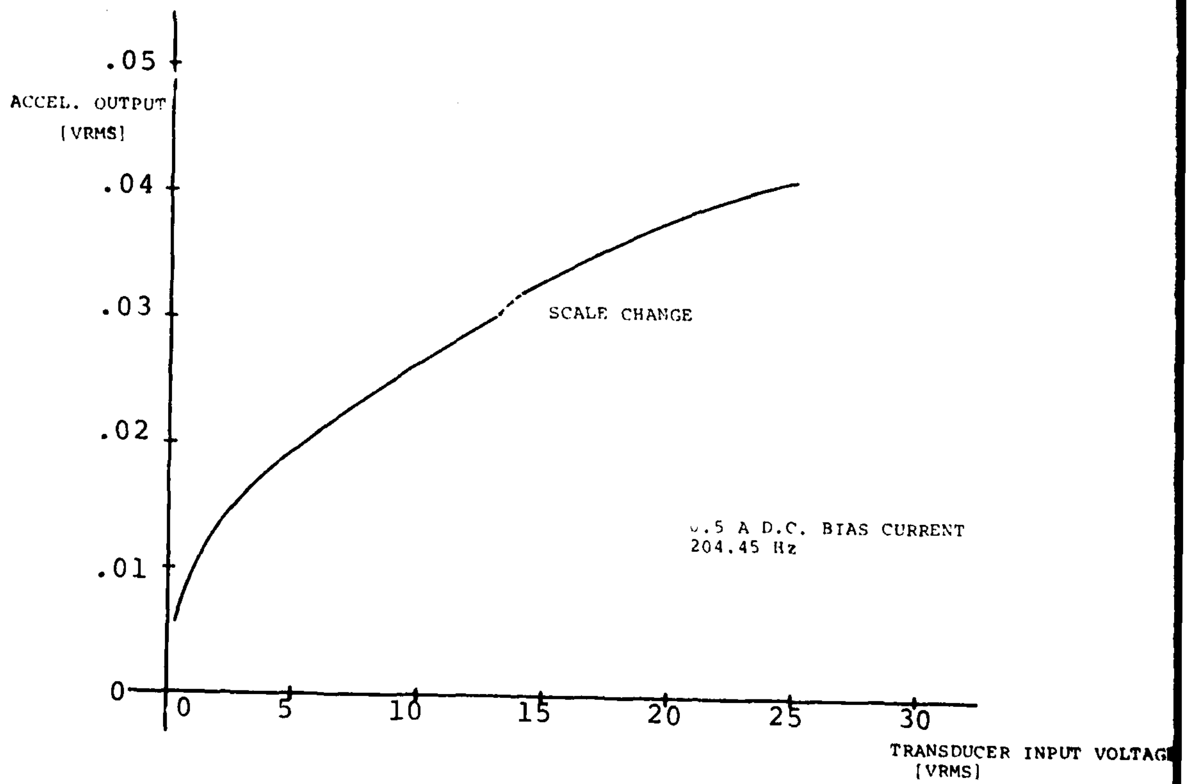

Figure 3.12. Acceleration Response versus A.C. Drive Voltage at a Constant D.C. Bias Current.

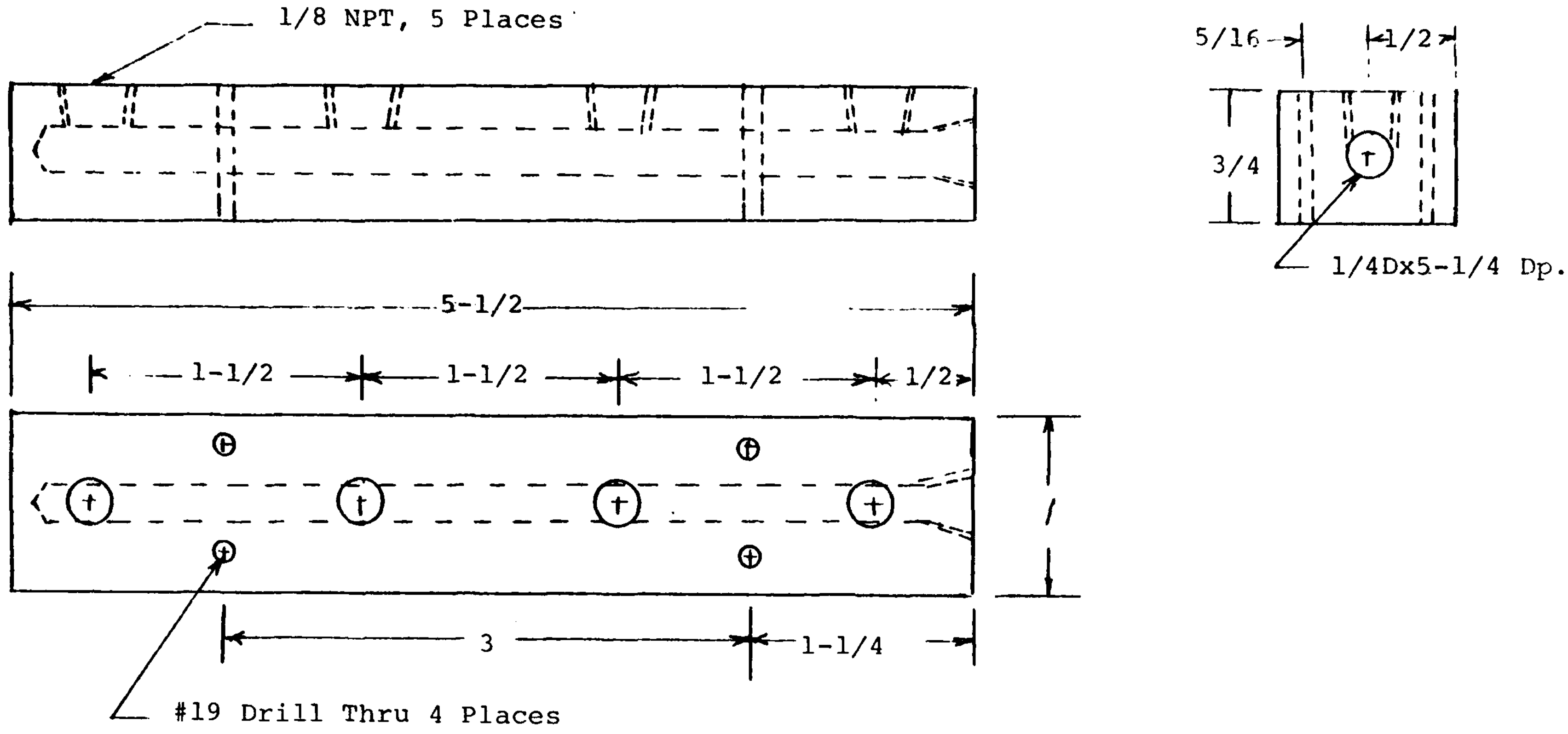

MANIFOLD COOLANT

MATERIAL: AL
2 REQUIRED

Figure 3.13. Coolant Manifold

by moisture but also by solid particulates, a larger filter-drier having 30 cubic inches desiccant and 53 square inches filter area was installed in the suction line. The larger filter-drier was placed in the suction line to trap contaminants before they enter the compressor.

A schematic diagram of the refrigerant circuit is provided in Figure 3.14. Refrigerant vapor is drawn into the compressor. The heat of compression is dissipated in the air cooled condensor and liquid refrigerant flows through the receiver and liquid line filter to the expansion valve. The expansion valve regulates the flow of liquid refrigerant to the transducers in response to the temperature of the vapor return line from the transducers which can be considered to be an evaporator. Two sets of control valves and connections have been incorporated to provide flexibility for cooling a variety of transducer configuration.

3.3.1.1. Transducer Connection

During long quiescent periods, the system will leak down to one atmosphere (0 PSI gage pressure). Connecting lines and transducers to the system could introduce ambient air to the system resulting in overburdening filter/driers. To minimize contamination, the following purge is recommended.

- Connect required number of transducers to manifolds.
- Connect supply lines loosely to supply fittings.
- Connect vapor return lines securely to return fittings.
- Open charge valve to purge room air from transducers and lines.
- Secure supply lines to fittings.
- Close charge valve.

The above procedure results in a clean system with the exception of atmospheric contamination (approximately 0.7 in ^{3}) entrapped between the supply fittings and supply valves.

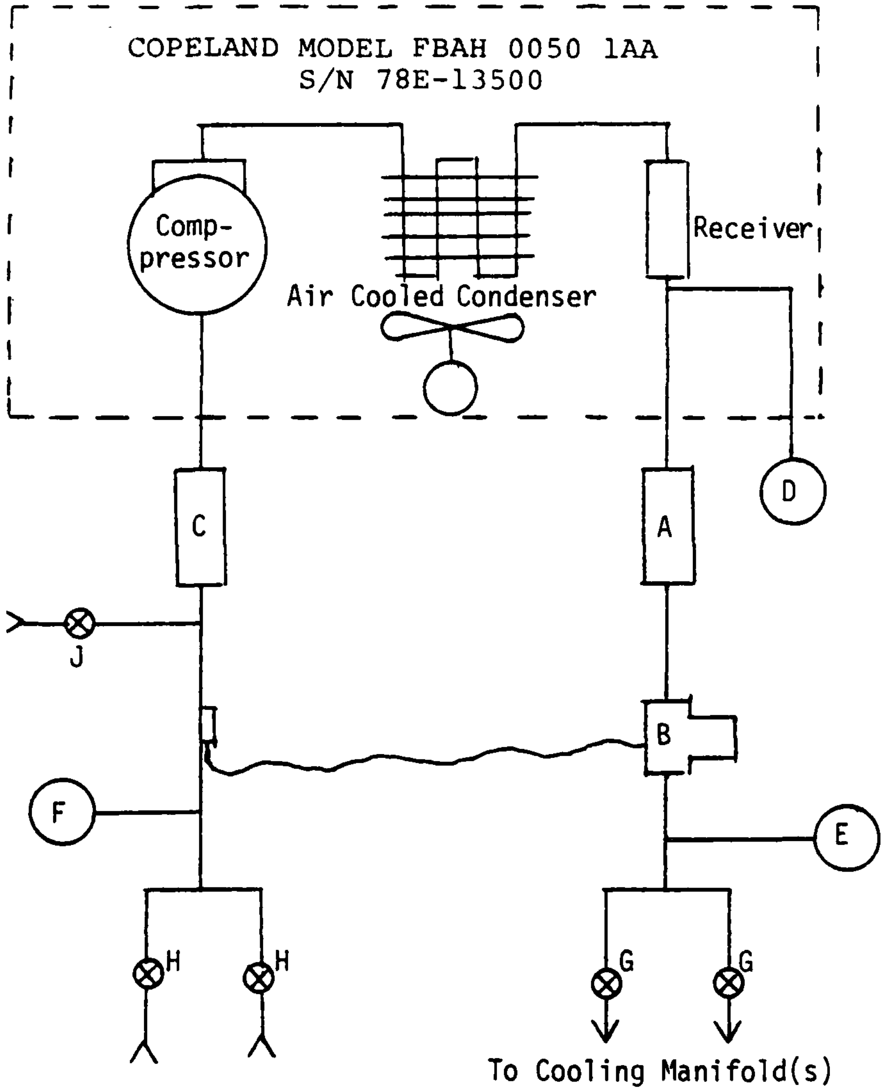

A. Filter-Drier, Sporlan, Type C082
B. Thermostatic Expansion Valve, Sporlan, Type FF-1/2-C
C. Filter-Drier, Sporlan, Type C305
D. Gauge, Head Pressure, 0-160 PSI
E. Gauge, Supply Pressure, 0-160 PSI
F. Gauge, Vapor Pressure, 0-100 PSI
G. Valve, Transducer Supply
H. Valve, Transducer Return
J. Valve, Charging

Figure 3.14. Schematic of Cooling System

3.3.1.2. Operation

The system should function satisfactorily, regardless of the number of transducers being cooled, if after turning the system on, the charge valve is opened until the HEAD PRESSURE gauge registers 120 PSI. Operation for prolonged periods may require opening the charge valves occasionally to balance the system due to slight leakage at the many mechanical connections of the system.

The following procedure is recommended for satisfactory operation of the system.

Start-up:

- Open (CCW) valve F-12 cylinder.
- Open (CCW) supply and return valves required.
- Turn on AC power switch.
- Open (CCW) charge valve until head pressure builds up to 100-120 PSI.
- Close (CW) charge valve.

During operation the supply pressure gauge should indicate 30-60 PSI and return pressure gauge should indicate 0-20 PSI.

Shut-down:

- Turn off AC power switch.
- Close (CW) supply and return valves.
- Close (CW) valve on F-12 cylinder.

3.4. DAMPING OF NASA FLUTTER BLADES

Five blades were received from the National Aeronautics and Space Administration (NASA) Lewis Research Center, Cleveland. These blades are used in the study of aerodynamic flutter (see Figure 3.15). The blades are oscillated by a variable speed cam and follower system from 0 Hz to 700 Hz to induce flutter. At certain flutter speeds, the blades were observed to be deforming in the first bending mode and subsequently developing fatigue cracks. It was requested that the UDRI perform a modal analysis on the blades and develop an appropriate damping application to evaluate the effects of additive damping on the flutter characterization of the blades.

Figure 3.16 shows the fixture which was developed to simulate the boundary conditions of the blade when mounted in the wind tunnel. The support blocks on each end have "V" grooves machined into them to keep the center line of the blade parallel to the base plate. This figure also shows the force input point (magnetic disc on upper left of blade) and the response pick-up point (accelerometer on lower left of blade) used for determining the damped and undamped modal loss factors.

Figure 3.17 shows the geometry used for the modal analysis. The small shaft would be between point 5 and 12, and the large shaft between 8 and 9. Response was measured in the Z direction at sixteen points, and the force input was applied in the negative Z direction at point number 4 by a magnetic driver connected to the DAC output of the fast Fourier transform system.

Figures 3.17 through 3.21 illustrate the first seven modes of the flutter blades superimposed on the undeformed shape, as well as the frequency associated with each mode. Mode 1, at 1,105 Hz was the primary mode of interest.

Figure 3.21 compares the measured value of the bare blade loss factor (0.0011) to the measured and predicted values of the loss factor for the chosen damping configuration (0.002-inch, 3M Company's

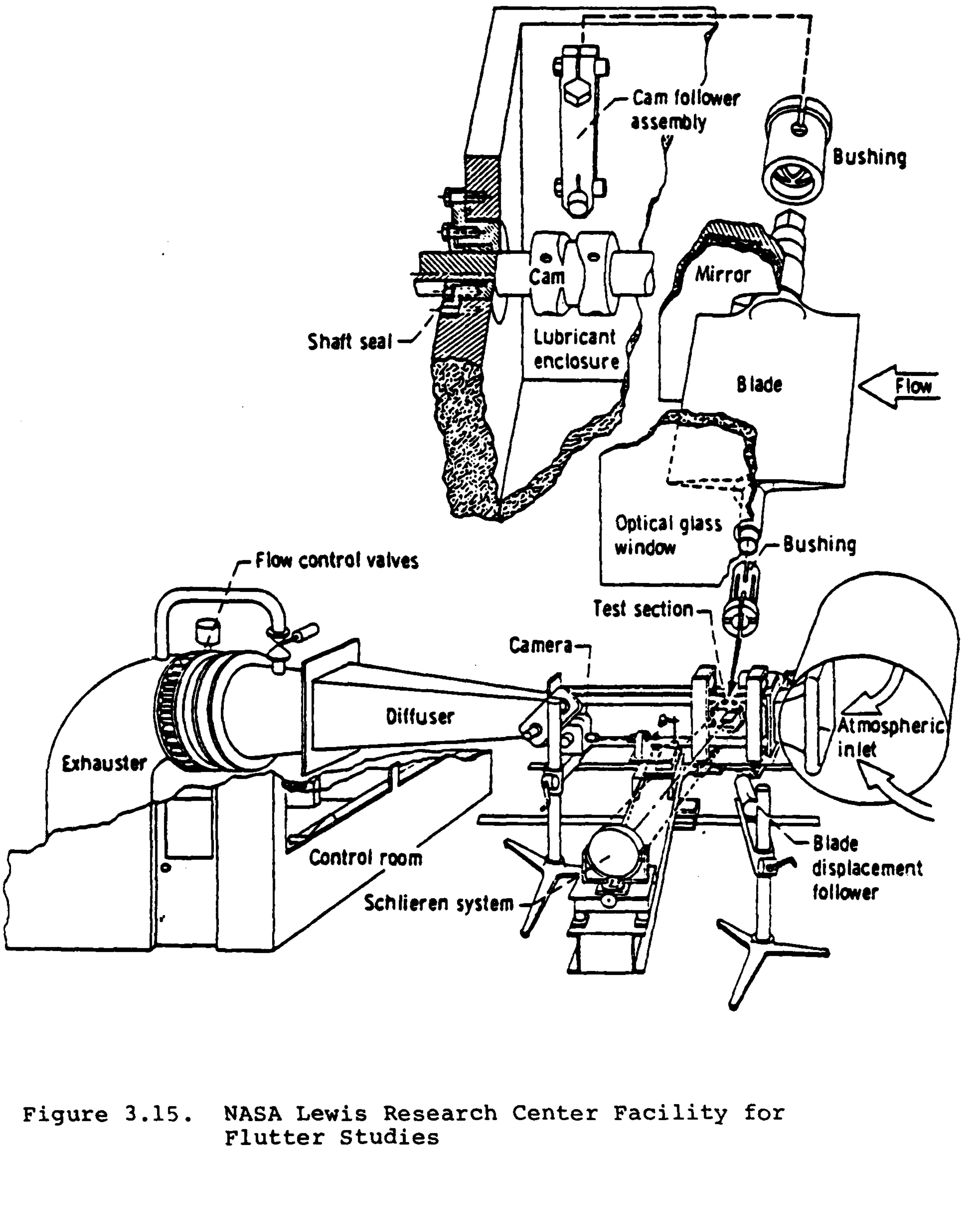

Figure 3.15. NASA Lewis Research Center Facility for Flutter Studies

Figure 3.16. Flutter Blade Test Fixture.

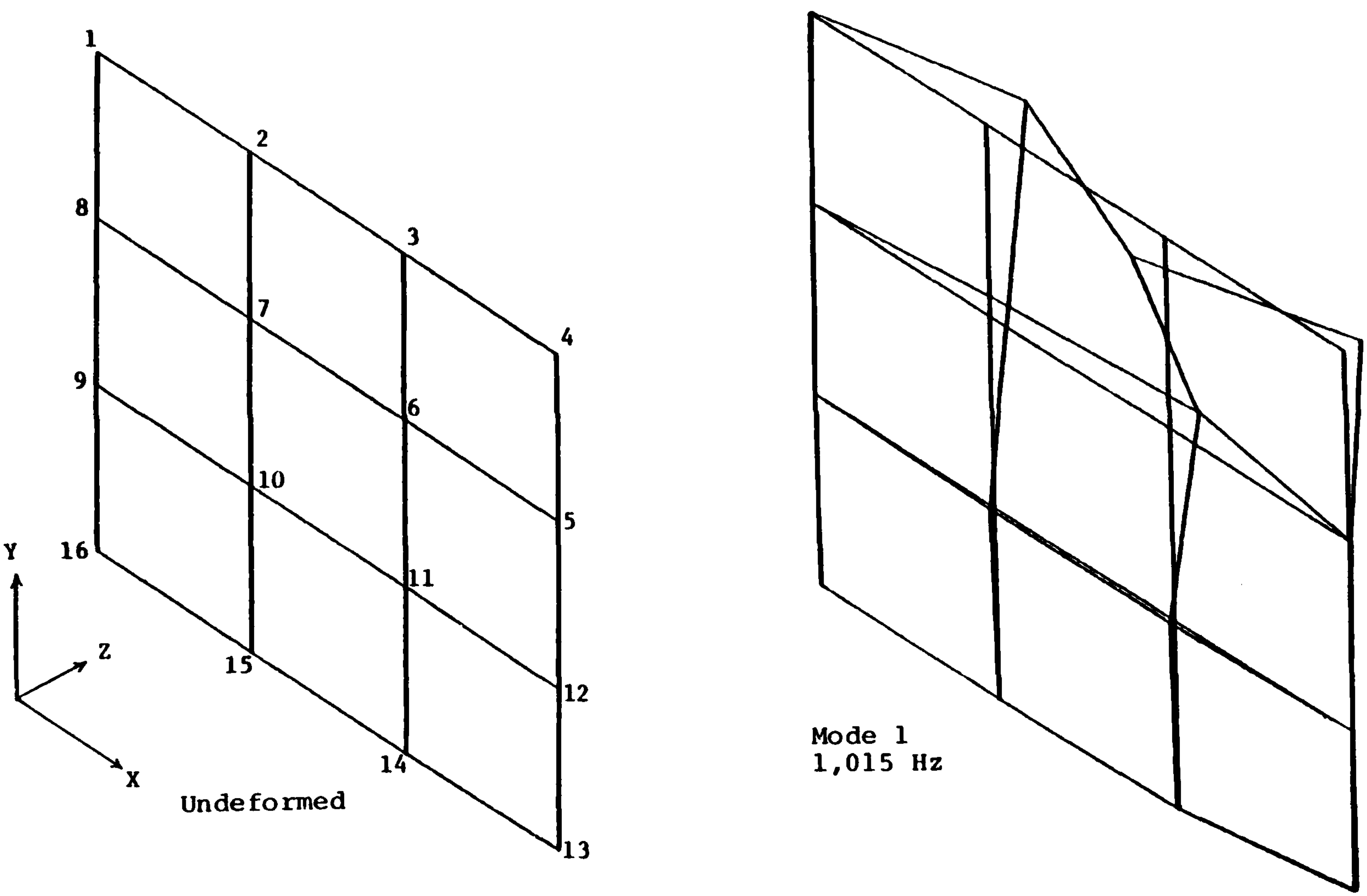

Figure 3.17. Undeformed and Mode 1 Shapes of Flutter Blade Showing Point Numbers and X-Y-Z Orientation.

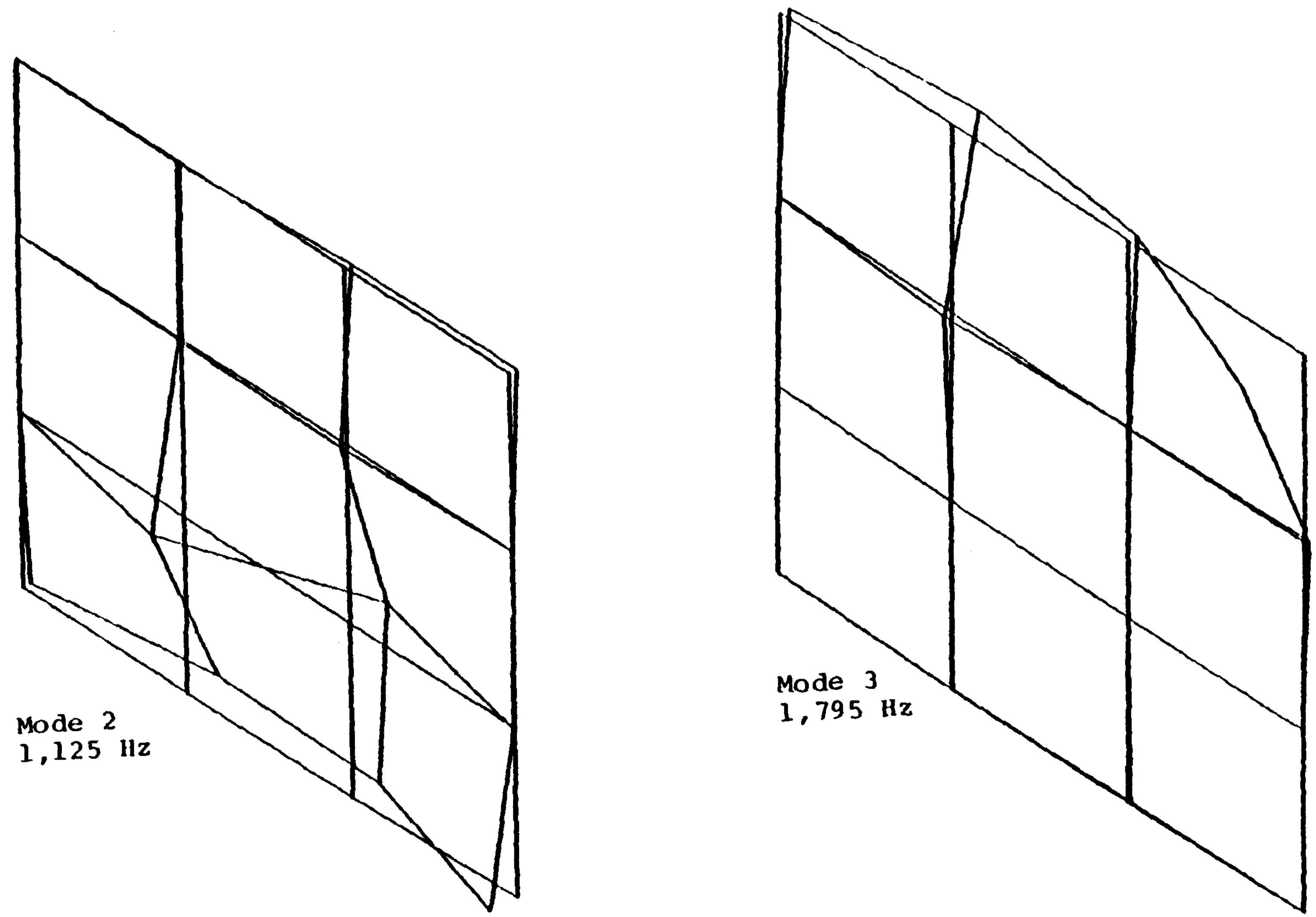

Figure 3.18. Modes 2 and 3 of Flutter Blade Superimposed Over Undeformed Shape.

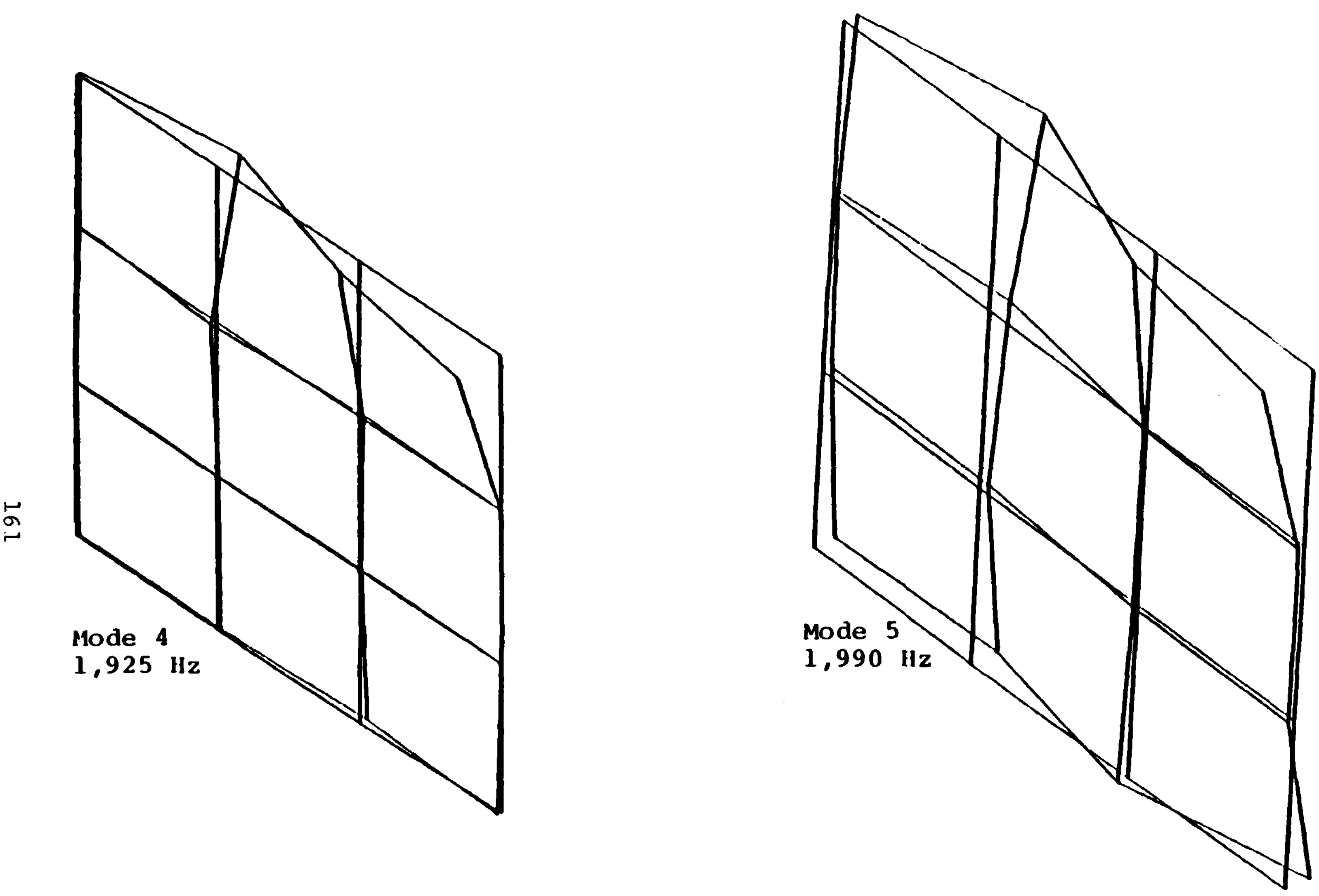

Figure 3.19. Modes 4 and 5 of Flutter Blade Superimposed Over Undeformed Shape.

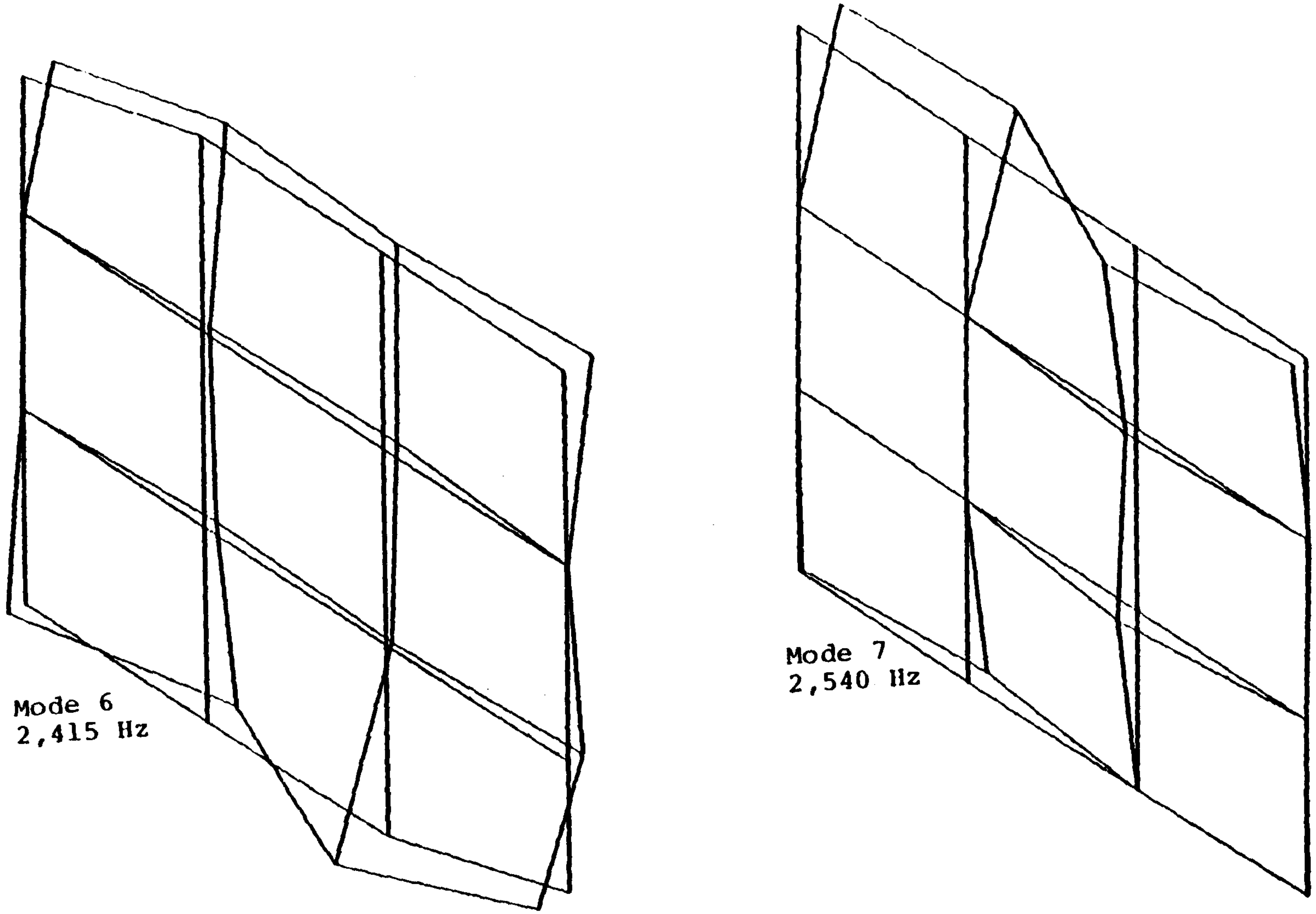

Figure 3.20. Modes 6 and 7 of Flutter Blade Superimposed Over Undeformed Shape.

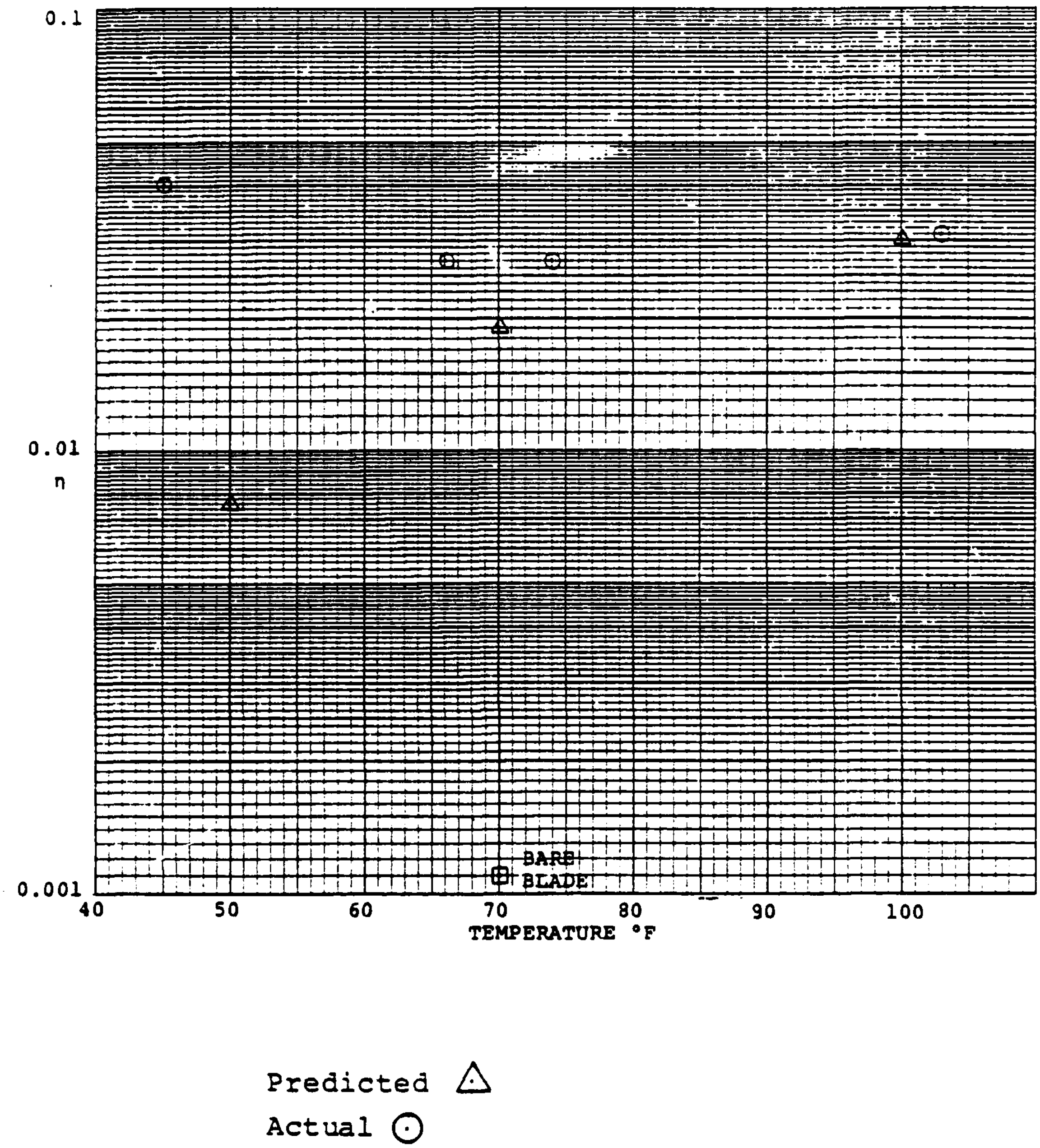

Figure 3.21. Comparison of Measured Value of Bare Blade Loss Factor to Value of Loss Factor of Chosen Damping Configuration - 0.002-inch ISD 112 and 0.005-inch Aluminum.

ISD-112 and 0.005-inch aluminum constraining layer on both sides). Although this configuration did not provide as much of a damping increase as the one in Figure 3.22, (0.005-inch ISD-112 and 0.005-inch aluminum) it is still provided over an order of magnitude increase in structural damping, and was considerably smoother and conformed better to the leading edge of the blade.

All five blades received had the 0.002 inch ISD-112/0.005 inch aluminum damping configuration applied, and were returned to NASA to be evaluated in the flutter facility.

Data received from NASA Lewis indicates that the damping wraps did not reduce the amplitude of deformation, nor did they delay the onset of flutter.

The project requires considerably more effort to be successful. One area of investigation is to determine the reason for the large difference between our measurement of the resonant frequencies of the blades, and the excitation frequency at which NASA Lewis observes flutter. Another area for investigation is the fact that the amplitude is not reduced despite a large increase in structural damping. The data supplied by NASA does not indicate that a measurement of the flutter onset condition was made. The direct measurements seem to be maximum defection during flutter. If flutter forces are high enough to over-ride the damping added, hard flutter would appear the same with or without damping; however, the onset of flutter should be delayed. The contract funding and scheduled completion date do not allow for completion of this project. This report terminates our effort on this project.

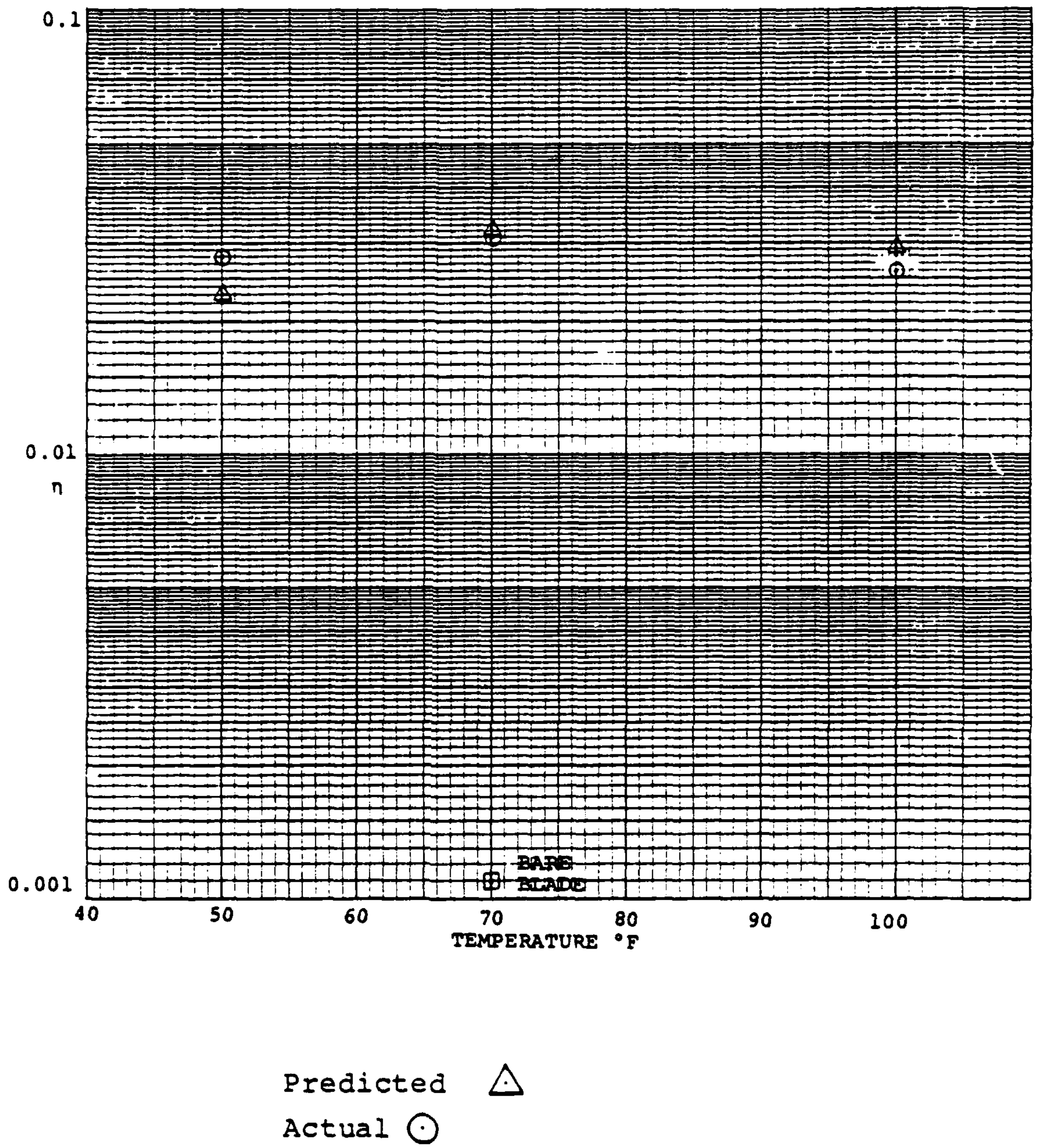

Figure 3.22. Comparison of Measured Value of Bare Blade Loss Factor to Value of Loss Factor of 0.005-inch ISD 112 and 0.005-inch Aluminum Damping Configuration.

3.5. CHARACTERIZATION OF MAGNETIC TRANSDUCERS

Four types of magnetic transducers are currently being used by the Vibration Analysis and Control Group of the UDRI: Electro Corporation model 3030HTB, Electro Corporation model 3015HTB, and two freon cooled models developed by UDRI. A test was developed to create plots of relative force output versus frequency at a constant excitation level for each of the four transducers. Two types of excitation were examined: constant current and constant voltage.

Figure 3.23 shows the test fixture that was used to analyze the force/frequency relationship of the model 3030HTB magnetic transducer. The transducer is held rigidly in position 1/16 inch above a magnetic stud mounted in a Wilcoxon Research force gage. The test set-up for the other three transducers (model 3015HTB and two UDRI freon cooled transducers) is identical, except for the transducer mounting bracket.

Figures 3.24 and 3.25 are block diagrams of the instrumentation that were used to maintain constant current and constant voltage during the tests.

The results of the tests are shown in Figures 3.26 through 3.35. Two model 3030HTB transducers were tested to check repeatability.

All four transducer models showed the same basic trends. When driven with a constant voltage, the output force drops rapidly with an increase in frequency. The frequency at which the output drops below 50 percent is approximately 520 Hz for both 3030HTB's, 560 Hz for the 3015HTB, 340 Hz for the original high temperature transducer, and 95 Hz for the new high temperature transducer. When driven with a constant current, both 3030HTB's and the 3015HTB are relatively flat (± 10%, approximately) out to 1,000 Hz. The original high temperature transducer has lost about 35 percent of its force by 1,000 Hz, and the new high temperature transducer has lost about 38 percent.

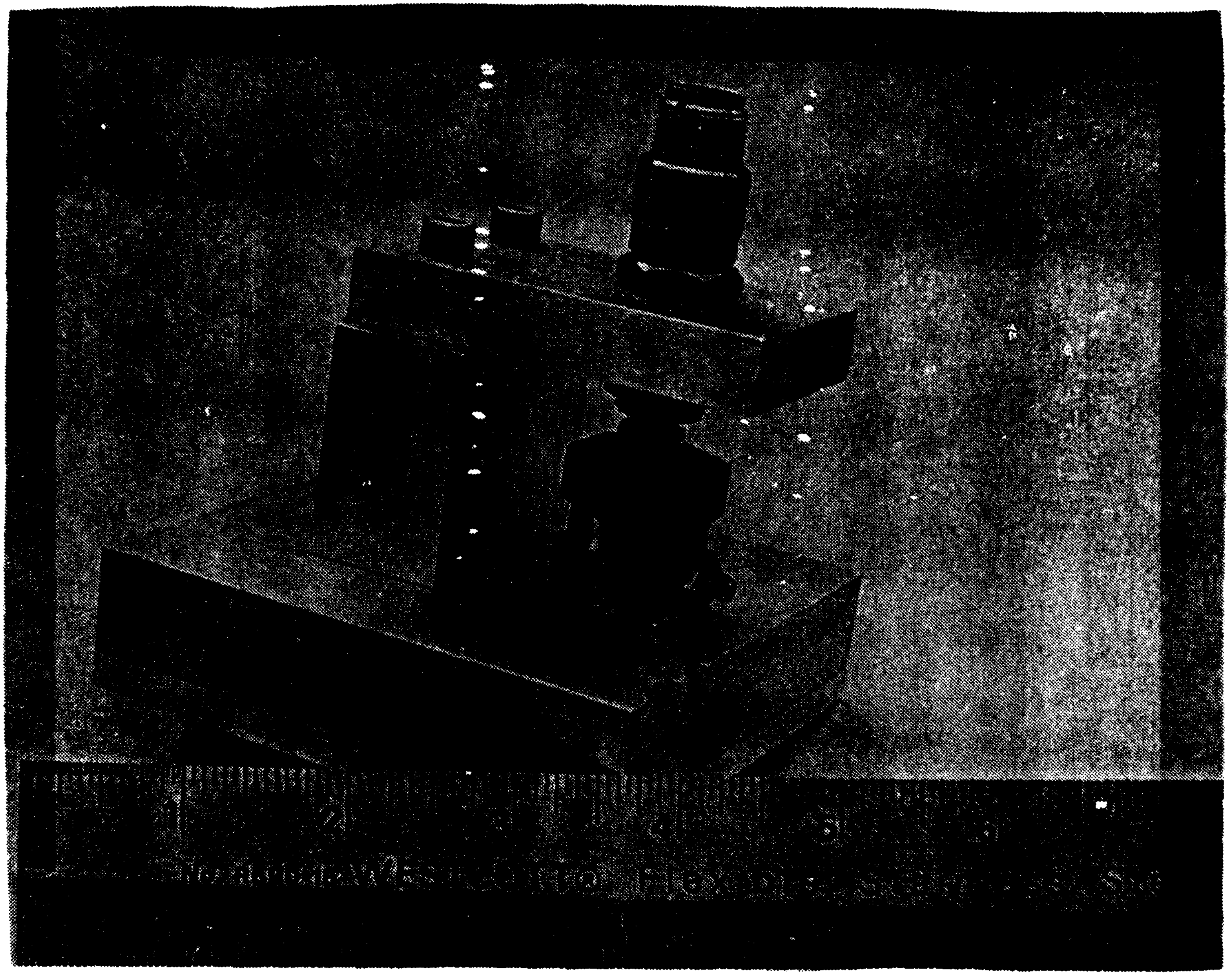

Figure 3.23. Test Fixture for Measuring the Force-Frequency Relationship of Magnetic Transducers.

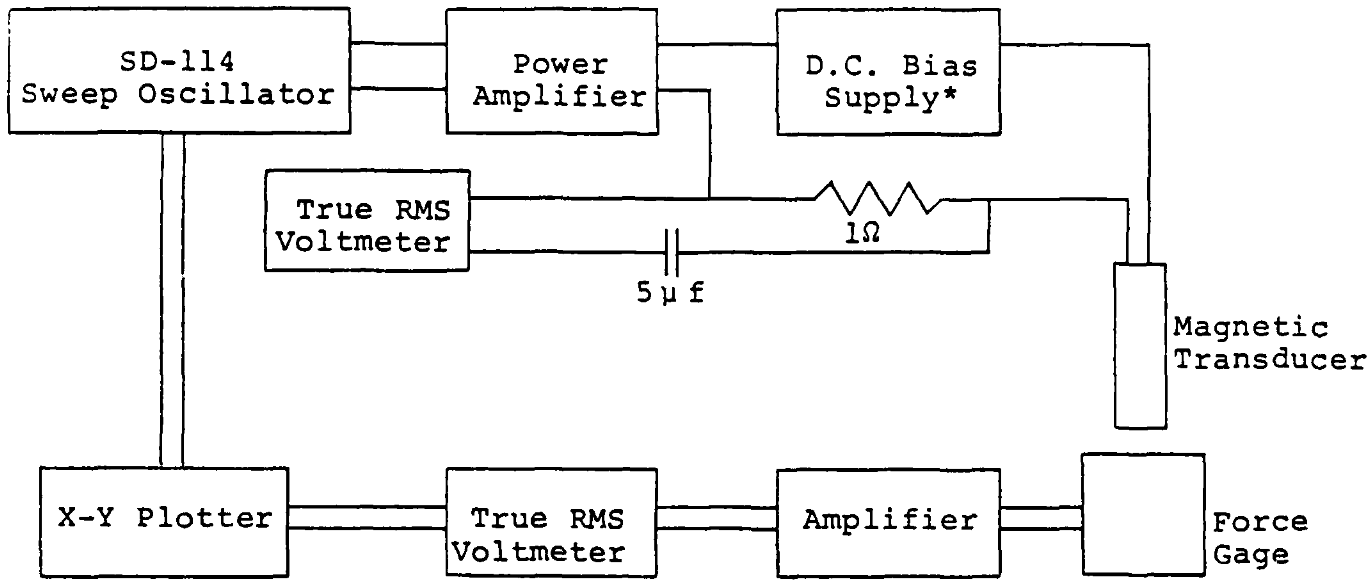

Figure 3.24. Block Diagram of Constant Current Force Gage Test.

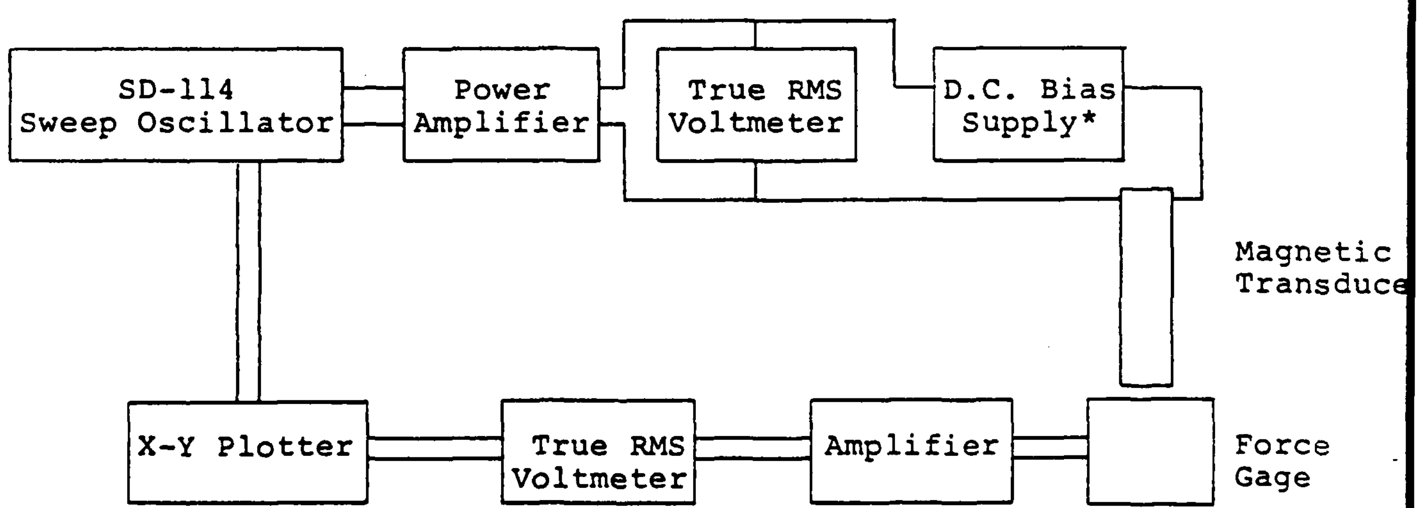

*D.C. bias supply for freon cooled transducers only.

Figure 3.25. Block Diagram of Constant Voltage Force Gage Test.

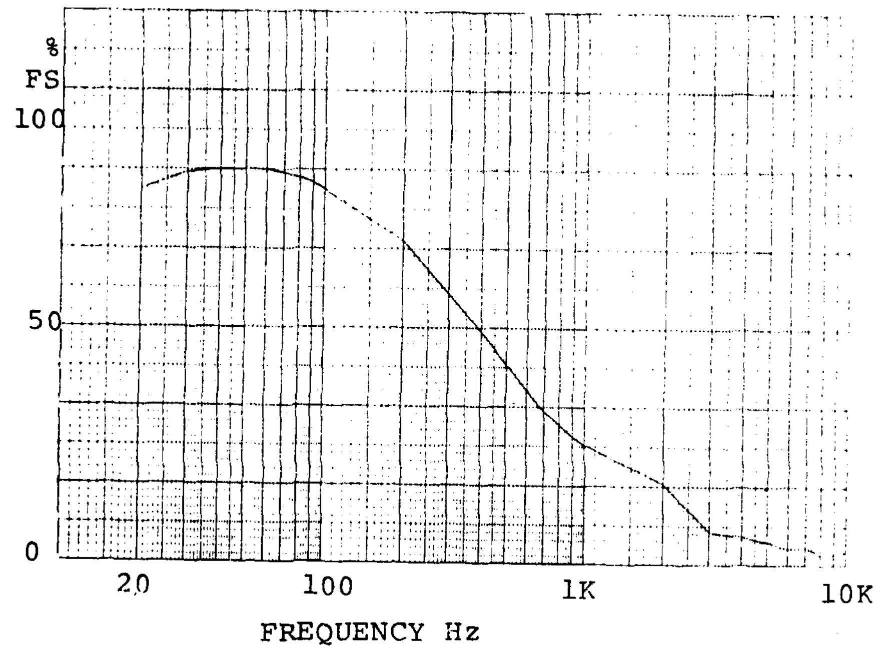

Figure 3.26. Force versus Frequency for First Model 3030 HTB, Constant Voltage, $20V_{RMS}$.

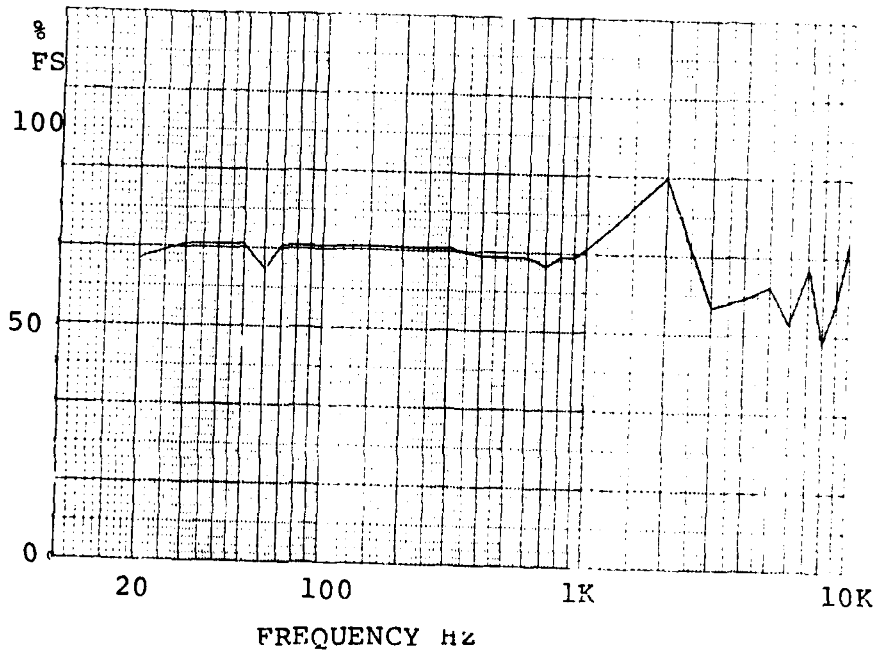

Figure 3.27. Force versus Frequency for First Model 3030 HTB, Constant Current $0.7mA_{RMS}$.

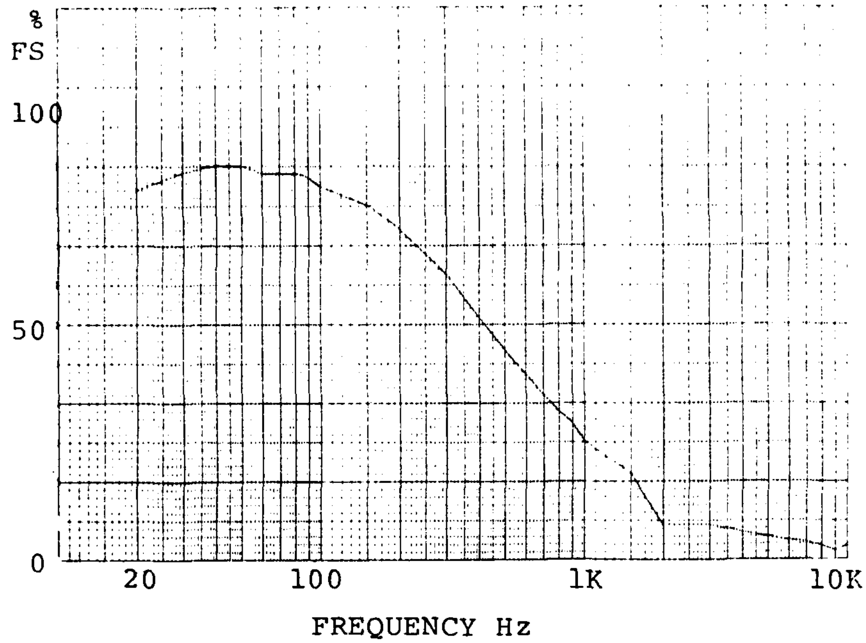

Figure 3.28. Force versus Frequency Second Model 3030 HTB, Constant Voltage, $20V_{RMS}$.

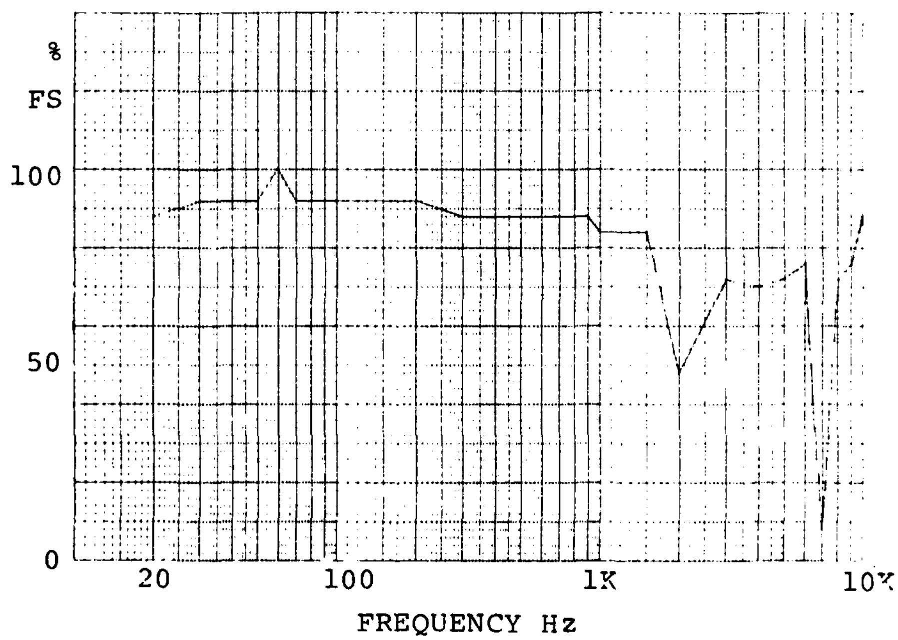

Figure 3.29. Force versus Frequency for Second Model 3030 HTB, Constant Current, $0.7mA_{RMS}$.

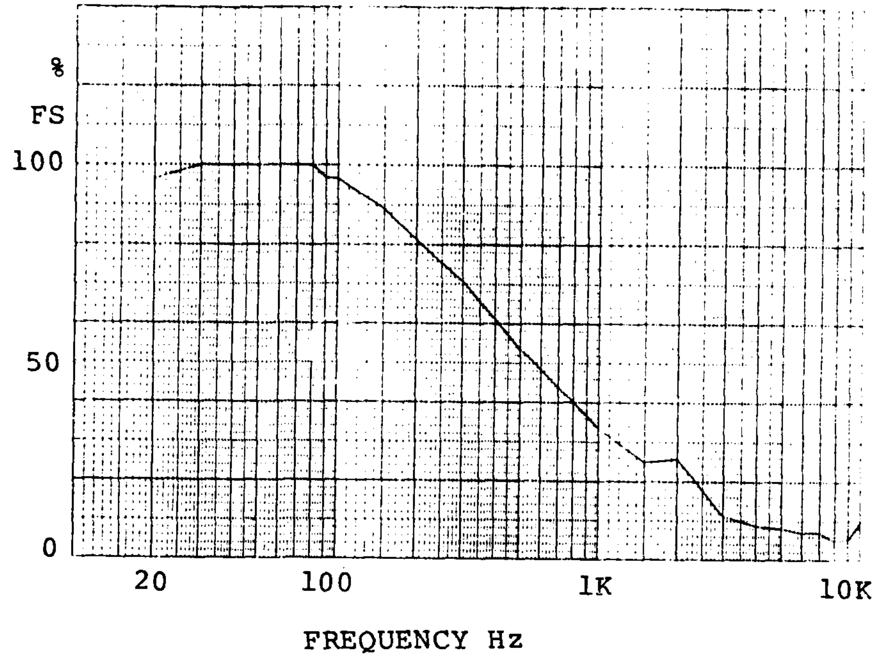

Figure 3.30. Force versus Frequency for Model 3015 HTB, Constant Voltage, $10V_{RMS}$.

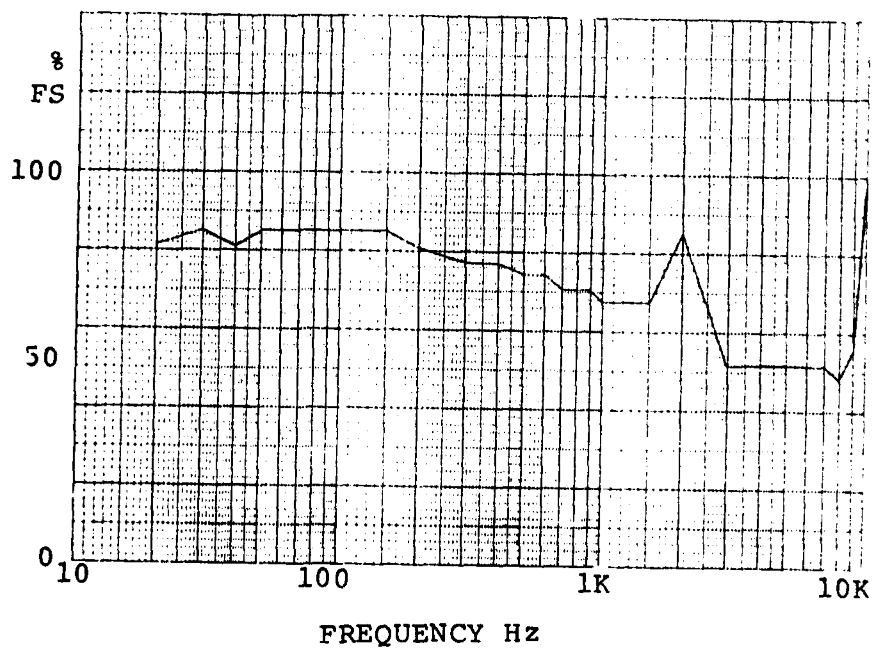

Figure 3.31. Force versus Frequency for Model 3015 HTB, Constant Current, $50MA_{RMS}$.

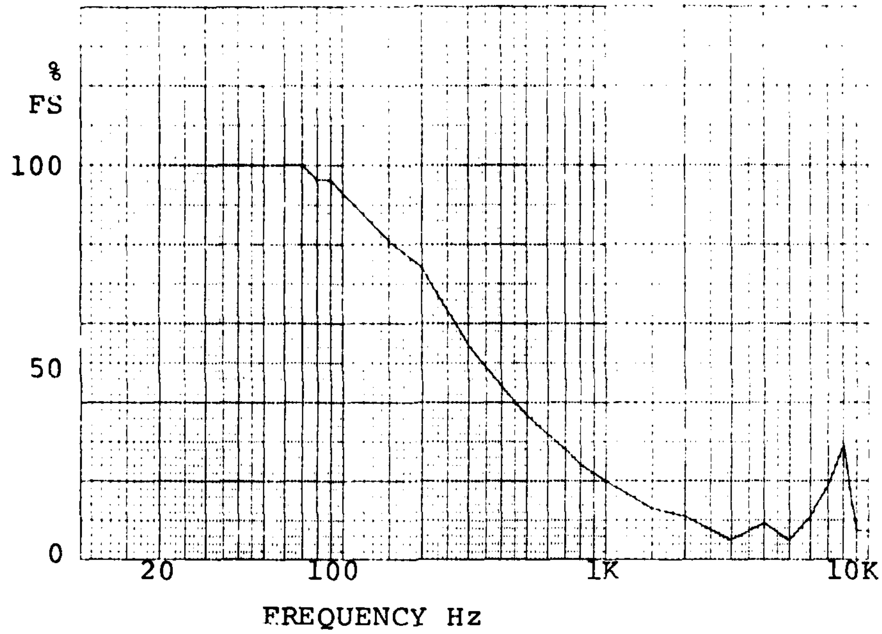

Figure 3.32. Force versus Frequency for Original High Temperature Transducer, Constant Voltage, 2.5V_{RMS}.

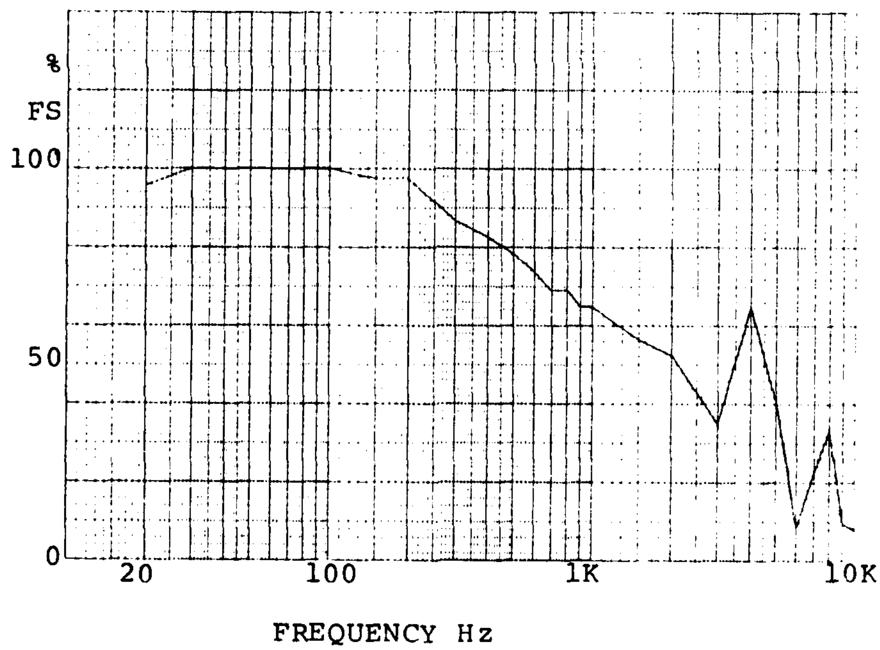

Figure 3. 33. Force versus Frequency for Original High Temperature Transducer, Constant Current, 90mA_{RMS}.

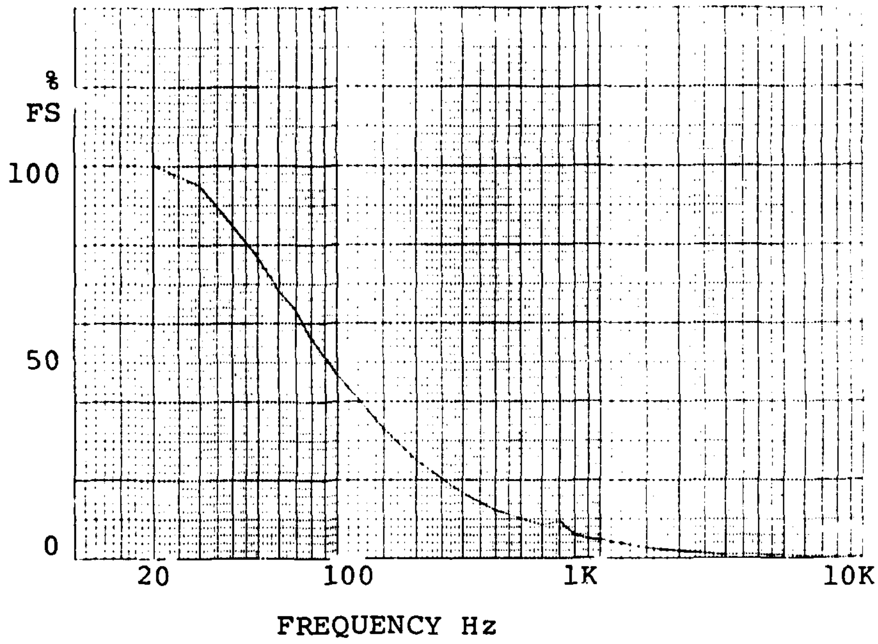

Figure 3.34. Force versus Frequency for New High Temperature Transducer, Constant Voltage, $3V_{RMS}$.

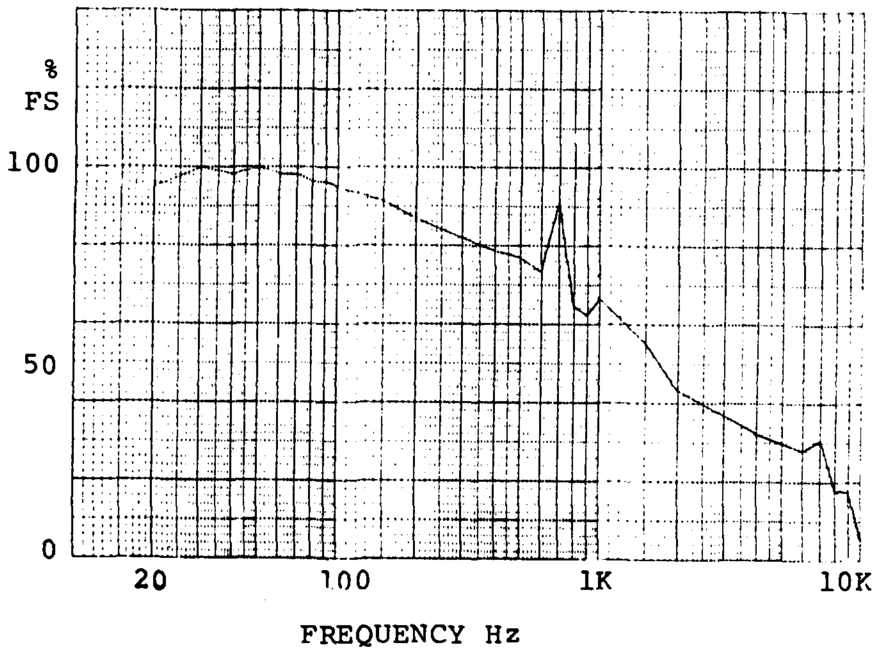

Figure 3.35. Force versus Frequency for New High Temperature Transducer, Constant Current, $15mA_{RMS}$.

REFERENCES

1. Hopkins, David M. and Michael L. Drake, "Porcelain Enamel Material Testing Procedures to Determine the Damping Properties and the Results of Selected Materials." UDR-TR-80-47, AFWAL-TR-80-4116, University of Dayton Research Institute, Dayton, Ohio, September 1980.

2. Oberst, H. and Frankenfeld, K., "Uber die Dampfung dunner Bleche durch festhaltende Belage," Acoustics, 1952, Vol. 2, pp. 181-184.

3. Sridharan, R. I., Damping in Porcelain Enamel Coatings, AFWAL-TR-74-191, Materials Laboratory, Wright-Patterson Air Force Base, Ohio, 1976 (also published as Ph.D. dissertation, University of Minnesota, 1975).

4. Bishop, R. E. D. and Johnson, V. Final Report, United States Air Force Contract Number F33615-72-C-1315 (1974).

5. Jones, D. I. G., "A Reduced Temperature Nomogram for Characterization of Damping Material Behavior," Shock and Vibration Bulletin 48, Part 2, 1978.

6. King, C. S. Jr., Computerized Processing and Graphic Representation of Viscoelastic Material Property Data, AFWAL-TR-79-4099, Materials Laboratory, Wright-Patterson Air Force Base, Ohio, 1979.

7. Rogers, L. C. and Nashif, A.D., "Computerized Processing and Empirical Representation of Viscoelastic Material Property Data and Preliminary Constrained Layer Damping Treatment Designs," Shock and Vibration Bulletin 48, 1978.

8. Soni, M. L. , "Finite Element Analysis of Vibrations of Initially Stressed Viscoelastic Structures," UDR-TR-79-113, November 1979.

9. Brockman, R. A. "MAGNA Computer Program Users's Manual," UDR-TR-80-107, November 1980.

10. Brockman, Robert A. MAGNA: A Finite Element Program for the Materially and Geometrically Nonlinear Analysis of Three-Dimensional Structures Subjected to Static and Dynamic Transient Loading, AFWAL-TR-81-3181, Wright-Patterson Air Force Base, Ohio, April 1982.

11. Brockman, Robert A. "MAGNA: Materially and Geometrically Nonlinear Analysis" UDR-TR-82-111 (to be published as an AFWAL TR), University of Dayton Research Institute, Dayton, Ohio, September 1982.

REFERENCES
(concluded)

12. Drake, Michael L. and David M. Hopkins, "Structural Analysis of TF-30 Engine Vibration Transducers V-1 and V-2," UDR-TR-81-27, University of Dayton Research Institute, Dayton, Ohio, April 1981.

APPENDIX A

DAMPING PROPERTIES OF TWELVE COMMERCIAL MATERIALS

MATERIAL CODE :246
MATERIAL :NBN 51914-50-2
LOG(FR)=LOG(F)-12(T-T0)/(525+T-T0)

NO.	MODULUS LB/IN**2	LOSS FACTOR	TEMP. DEG. F	FREQ. HZ	MODE NO.
1	2.29317E+02	1.1658	211.0	378.6	2.
2	4.20464E+02	1.3576	211.0	1004.0	3.
3	4.61599E+02	1.4762	211.0	1267.3	4.
4	5.92307E+02	1.8881	211.0	3043.0	5.
5	5.98718E+01	.7542	251.5	329.0	2.
6	8.69745E+01	1.0221	251.5	595.3	3.
7	9.38284E+01	1.3212	251.5	1737.6	4.
8	1.14750E+02	1.6211	251.5	2865.5	5.
9	1.52679E+02	1.6165	251.5	4277.4	6.
10	3.06125E+01	.6291	275.7	318.9	2.
11	4.12174E+01	.8243	275.7	877.9	3.
12	3.99604E+04	.1035	64.9	692.1	2.
13	4.67468E+04	.0793	64.9	1838.1	3.
14	4.30339E+04	.0716	64.9	3558.6	4.
15	4.30636E+04	.0712	64.9	5691.2	5.
16	5.23286E+04	.0593	64.9	8128.2	6.
17	2.66747E+04	.2512	99.8	683.3	2.
18	3.29525E+04	.1561	99.8	1848.4	3.
19	3.14354E+04	.1327	99.8	3451.8	4.
20	3.52567E+04	.1245	99.8	5475.2	5.
21	3.72806E+04	.1235	99.8	7809.8	6.
22	1.08610E+04	.4379	147.3	1696.3	3.
23	1.11806E+04	.4123	147.3	3042.9	4.
24	1.35424E+04	.4453	147.3	4767.9	5.
25	1.83267E+03	.9806	175.4	567.9	2.
26	3.62003E+03	.8162	175.4	1468.1	3.
27	4.03630E+03	.8765	175.4	2581.5	4.
28	4.42753E+02	1.3581	201.8	434.6	2.
29	7.66323E+02	1.5712	201.8	1112.8	3.
30	9.23370E+02	1.6524	201.8	2021.7	4.
31	1.61485E+02	1.1013	226.1	365.3	2.
32	2.86396E+02	1.3283	226.1	961.8	3.
33	3.41629E+02	1.4998	226.1	1825.6	4.
34	4.58896E+02	1.7020	226.1	2983.8	5.
35	3.84874E+04	.1027	74.4	691.2	2.
36	4.99247E+04	.0998	74.4	1886.1	3.
37	4.48664E+04	.0872	74.4	3561.9	4.
38	4.87990E+04	.0787	74.4	5685.5	5.
39	1.41984E+04	.3204	124.5	667.5	2.
40	1.98253E+04	.2718	124.5	1787.1	3.
41	2.06426E+04	.2368	124.5	3299.2	4.
42	2.36782E+04	.2240	124.5	5194.3	5.
43	5.70448E+03	.6810	149.5	638.8	2.
44	1.02554E+04	.4571	149.5	1685.8	3.
45	1.11092E+04	.4370	149.5	3044.4	4.
46	1.27301E+04	.4668	149.5	4730.8	5.

MATERIAL CODE :253
MATERIAL :NBN-51914-50-8
LOG(FR)=LOG(F)-12(T-T0)/(525+T-T0)

NO.	MODULUS LB/IN**2	LOSS FACTOR	TEMP. DEG. F	FREQ. HZ	MODE NO.
1	1.91720E+04	.0814	76.2	664.2	2.
2	2.33073E+04	.0735	76.2	1809.8	3.
3	2.59200E+04	.0622	76.2	3441.9	4.
4	3.12579E+04	.0560	76.2	5555.9	5.
5	2.78696E+04	.0505	76.2	7890.1	6.
6	1.46784E+04	.1316	115.1	657.0	2.
7	1.81603E+04	.1144	115.1	1779.2	3.
8	2.00665E+04	.1006	115.1	3362.0	4.
9	2.46302E+04	.0929	115.1	5417.8	5.
10	2.24903E+04	.0635	115.2	7645.0	6.
11	1.32786E+04	.1921	130.0	654.6	2.
12	1.68086E+04	.1486	130.0	1769.2	3.
13	1.82293E+04	.1240	130.0	3330.3	4.
14	2.23636E+04	.1334	130.0	5353.0	5.
15	9.12726E+03	.3031	150.7	645.7	2.
16	1.18624E+04	.2447	150.7	1727.9	3.
17	1.35163E+04	.2311	150.7	3235.6	4.
18	1.68049E+04	.1596	150.7	5171.5	5.
19	1.50680E+04	.1745	150.7	7200.2	6.
20	4.42809E+03	.5150	175.7	624.9	2.
21	6.72780E+03	.4300	175.7	1653.9	3.
22	6.59215E+03	.3189	175.7	1641.6	3.
23	7.48166E+03	.4078	175.7	3019.1	4.
24	9.78217E+03	.4003	175.7	4826.7	5.
25	1.75566E+03	.5903	201.0	575.3	2.
26	2.21306E+03	.8283	201.0	1452.1	3.
27	2.89191E+03	.6918	201.0	2613.4	4.
28	3.50388E+03	1.0737	201.0	4179.5	5.
29	3.58959E+02	1.1750	230.6	455.7	2.
30	5.55883E+02	1.3896	230.6	1142.9	3.
31	6.38674E+02	1.5899	230.6	2058.4	4.
32	3.12161E+02	1.3287	249.0	1033.0	3.
33	3.58103E+02	1.8052	249.0	1913.6	4.
34	6.81434E+02	1.1698	249.0	3182.1	5.
35	7.37758E+01	1.0172	275.0	348.1	2.
36	1.06796E+02	1.1806	275.0	929.1	3.
37	1.34665E+02	1.2582	275.0	1779.2	4.
38	1.58660E+02	1.7373	275.0	2909.6	5.
39	1.85144E+02	1.9507	275.0	4330.5	6.
40	4.15041E+01	.7260	300.2	331.2	2.
41	6.16821E+01	.9255	300.2	898.5	3.
42	7.08889E+01	1.0864	300.2	1739.7	4.
43	8.61526E+01	1.3374	300.2	2861.7	5.
44	2.04989E+02	1.1442	249.0	405.1	2.
45	9.21900E+01	1.4719	300.2	4264.3	6.

MATERIAL CODE :173
MATERIAL :ISD 468
LOG(FR)=LOG(F)-12(T-T0)/(525+T-T0)

NO.	MODULUS LB/IN**2	LOSS FACTOR	TEMP. DEG. F	FREQ. HZ	MODE NO.
1	1.44744E+02	1.2739	100.0	319.3	2.
2	3.23123E+02	1.8252	100.0	1525.7	4.
3	4.47729E+02	1.3504	100.0	2443.7	5.
4	1.15765E+02	1.2202	125.0	737.9	3.
5	1.64285E+02	1.2093	124.0	1406.8	4.
6	2.28081E+02	1.1670	124.0	2301.5	5.
7	3.92710E+01	.9164	150.0	262.0	2.
8	5.74497E+01	1.0908	150.0	700.1	3.
9	8.90162E+01	1.0086	150.0	1356.2	4.
10	1.31657E+02	.9381	150.0	2235.0	5.
11	1.47550E+02	1.1385	150.0	3326.4	6.
12	2.74272E+01	.8117	175.0	254.4	2.
13	2.87795E+01	1.2969	175.0	685.0	3.
14	6.25452E+01	.9322	175.0	1335.1	4.
15	1.04629E+02	.6829	175.0	2208.4	5.
16	1.16533E+02	.3403	175.0	3293.6	6.
17	1.87821E+01	.7415	201.0	248.2	2.
18	5.42076E+01	.5910	201.0	1324.5	4.
19	8.71397E+01	.4883	200.0	2187.9	5.
20	1.07029E+02	.5345	200.0	3267.0	6.
21	1.49559E+01	.5574	226.0	244.5	2.
22	2.04341E+01	.6977	226.0	669.9	3.
23	3.53332E+01	.5418	225.0	1308.1	4.
24	5.28142E+01	.4939	225.0	2164.7	5.
25	8.74206E+01	.3526	224.0	3237.4	6.
26	1.27060E+01	.5074	250.0	242.0	2.
27	1.59353E+01	.6221	249.0	664.1	3.
28	2.77050E+01	.4797	249.0	1297.3	4.
29	5.27142E+01	.3564	248.0	2145.0	5.
30	8.26470E+01	.2831	248.0	3212.5	6.
31	1.68737E+02	1.2539	112.0	328.8	2.
32	2.80088E+02	1.3393	112.0	832.8	3.
33	3.84461E+02	1.3169	112.0	1538.8	4.
34	4.45735E+02	1.4395	112.0	2443.6	5.
35	3.75232E+02	1.2126	87.0	389.9	2.
36	6.77920E+02	1.1773	87.0	987.0	3.
37	6.29648E+02	1.0631	75.0	423.2	2.
38	1.20090E+03	1.0249	75.0	1097.3	3.
39	2.27492E+03	.6437	50.0	476.5	2.
40	4.00537E+03	.7231	50.0	1280.2	3.
41	5.13241E+03	.7439	50.0	2387.6	4.
42	5.49405E+03	.8783	50.0	3742.4	5.
43	1.08786E+04	.3331	25.0	1368.0	3.
44	1.38469E+04	.3279	25.0	2605.4	4.
45	1.72091E+04	.3426	25.0	4187.5	5.
46	1.38899E+04	.1709	-1.0	509.9	2.
47	2.90820E+04	.1660	-1.0	2698.6	4.
48	3.18704E+04	.1554	-1.0	4380.4	5.
49	2.36967E+04	.1628	-1.0	1402.0	3.

```
MATERIAL CODE :242
MATERIAL :SOUNDCOAT #12-15-80

LOG(M)=LOG(ML)+(2LOG(MROM/ML))/(1+(FROM/FR)**N)
  T0       FROM         MROM        N          ML
             A1           A2        A3         A4
  50.0  2.0000E+03  3.5572E+02    .300   3.7710E+00

LOG(ETA)=LOG(ETAFPOL)+((SH+SL)A+(SL-SH)(1-SQRT(1+A**2)))C/2
  T0    ETAFROL     SL      SH       FROL        C
           B1       B2      B3        B4         B5
  50.0   2.100     .400   -.600  1.3000E+03   1.000

LOG(FR)=LOG(F)-12(T-T0)/(525+T-T0)
A=(LOG(FR)-LOG(FROL))/C
```

NO.	MODULUS LB/IN**2	LOSS FACTOR	TEMP. DEG. F	FREQ. HZ	MODE NO.
1	1.16447E+02	1.2324	74.6	373.4	2.
2	2.01530E+02	1.4057	74.6	989.9	3.
3	2.14822E+02	1.4658	74.6	1848.1	4.
4	3.10533E+22	1.5036	74.6	3036.8	5.
5	2.85380E+05	.0743	-48.6	1895.9	3.
6	3.31655E+04	.1006	-48.6	3507.9	4.
7	3.66620E+04	.0595	-48.6	5655.0	5.
8	4.85865E+04	.0748	-48.6	8396.9	6.
9	6.08286E+04	.4150	-24.2	1866.9	3.
10	3.63913E+04	.2358	-24.2	3399.8	4.
11	6.64097E+03	.0949	-24.2	5461.8	5.
12	3.19120E+04	.1740	-24.2	8047.0	6.
13	1.16588E+04	.7870	-3.2	661.5	2.
14	1.15560E+04	.3103	-3.2	3210.0	4.
15	1.44633E+04	.2808	-3.2	5123.3	5.
16	1.90543E+04	.2827	-3.2	7545.0	6.
17	1.55815E+04	.2933	-3.2	9705.5	7.
18	2.04753E+03	1.3453	24.4	621.5	2.
19	4.68742E+03	.9943	24.4	1664.9	3.
20	3.61125E+03	.8287	24.4	2777.3	4.
21	4.73203E+03	.7615	24.4	4368.7	5.
22	6.27109E+03	.7721	24.4	6395.0	6.
23	3.34252E+02	2.2040	49.0	493.4	2.
24	8.31178E+02	2.1800	49.0	1338.5	3.
25	6.56166E+02	2.4842	49.0	2163.1	4.
26	1.12917E+03	1.6933	49.0	3477.0	5.
27	1.27428E+03	2.6114	49.0	5152.9	6.
28	3.32787E+01	1.0090	99.2	332.1	2.
29	6.10700E+01	1.2162	99.2	913.6	3.
30	8.67561E+01	1.0039	99.2	1774.1	4.
31	1.16780E+02	1.6125	99.2	4357.7	6.
32	1.40377E+02	1.6591	99.2	6074.4	7.
33	2.05936E+01	.8500	129.6	324.6	2.
34	3.65312E+01	.9248	129.6	897.7	3.
35	5.17508E+01	.7698	129.6	1748.8	4.
36	7.10690E+01	.7859	129.6	2885.4	5.
37	6.21279E+01	1.2635	129.6	4311.0	6.
38	1.56453E+01	.7067	146.9	320.8	2.
39	2.85436E+01	.7033	146.9	889.9	3.
40	4.32734E+01	.5871	146.9	1737.3	4.
41	6.02709E+01	.5884	146.9	2869.9	5.
42	4.73040E+01	1.0533	146.6	4285.5	6.
43	9.95350E+00	.6658	174.4	316.8	2.
44	1.97764E+01	.5703	174.4	881.7	3.
45	3.25234E+01	.4215	174.4	1724.5	4.
46	4.31193E+01	.4732	174.4	2849.1	5.
47	2.17139E+01	1.3239	174.4	4257.3	6.
48	7.60635E+00	.5798	196.7	314.3	2.
49	1.64316E+01	.4374	196.7	876.3	3.
50	2.68411E+01	.3404	196.7	1715.6	4.
51	3.78929E+01	.3905	196.7	2834.5	5.

AD-A135 409 DAMPING MATERIALS FINITE ELEMENTS AND SPECIAL PROJECTS 3/3
(U) DAYTON UNIV OH RESEARCH INST M RUDDELL ET AL.
DEC 82 UDR-TR-82-110 AFWAL-TR-82-4167 F33615-79-C-5108

UNCLASSIFIED F/G 14/2 NL

END

FILMED

1-84

DTIC

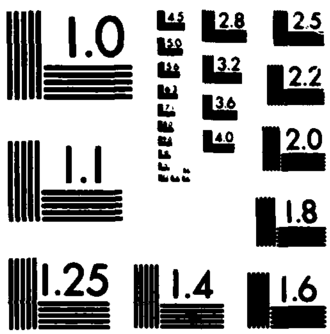

MICROCOPY RESOLUTION TEST CHART
NATIONAL BUREAU OF STANDARDS-1963-A

MATERIAL CODE :113
MATERIAL :SOUNDCOAT D-2
LOG(FR)=LOG(F)-12(T-T0)/(525+T-T0)

NO.	MODULUS LB/IN**2	LOSS FACTOR	TEMP. DEG. F	FREQ. HZ	MODE NO.
1	1.38197E+03	.2321	50.0	452.1	2.
2	1.89953E+03	.2016	50.0	1152.8	3.
3	2.20813E+03	.2317	50.0	2078.9	4.
4	2.87048E+03	.2227	50.0	3299.3	5.
5	9.15337E+02	.3137	75.0	431.8	2.
6	1.32246E+03	.2742	75.0	1090.2	3.
7	1.55997E+03	.2804	75.0	1954.6	4.
8	1.95431E+03	.3130	75.0	3073.4	5.
9	5.92246E+02	.4117	100.0	407.2	2.
10	9.39118E+02	.3538	100.0	1023.9	3.
11	1.10128E+03	.3695	100.0	1837.1	4.
12	1.32551E+03	.4052	100.0	2875.9	5.
13	3.61321E+02	.5377	125.0	376.9	2.
14	6.04950E+02	.4696	125.0	952.6	3.
15	7.46302E+02	.4902	125.0	1717.6	4.
16	8.51382E+02	.5307	125.0	2678.7	5.
17	2.25557E+02	.6636	150.0	347.3	2.
18	3.92484E+02	.5956	150.0	883.1	3.
19	4.63402E+02	.6140	150.0	1593.4	4.
20	5.52144E+02	.6353	150.0	2521.9	5.
21	1.32549E+02	.7800	175.0	315.2	2.
22	2.72481E+02	.6850	175.0	818.0	3.
23	2.89174E+02	.7229	175.0	1495.5	4.
24	3.50134E+02	.6962	175.0	2393.0	5.
25	8.39205E+01	.7927	200.0	291.0	2.
26	1.36911E+02	.7935	200.0	756.1	3.
27	1.70133E+02	.8235	200.0	1416.1	4.
28	2.48279E+02	.6955	200.0	2316.8	5.
29	1.16579E+02	.7483	185.0	307.3	2.
30	1.96471E+02	.7772	185.0	792.2	3.
31	2.49037E+02	.7413	185.0	1469.1	4.
32	3.14812E+02	.6987	135.0	2366.6	5.
33	1.74792E+02	.6939	165.0	330.6	2.
34	3.02913E+02	.6587	165.0	845.3	3.
35	4.50451E+02	.6612	165.0	2458.0	5.
36	3.06333E+02	.5767	135.0	366.4	2.
37	5.06190E+02	.4971	135.0	922.2	3.
38	6.17008E+02	.5252	135.0	1664.9	4.
39	7.39022E+02	.5508	135.0	2623.3	5.
40	5.60376E+01	.7908	225.0	273.4	2.
41	8.88386E+01	.9341	225.0	723.8	3.
42	1.10171E+02	.8751	225.0	1374.1	4.
43	3.17560E+01	.8333	250.0	257.5	2.
44	4.35442E+01	1.0809	250.0	688.6	3.
45	7.61001E+01	.7366	250.0	1338.1	4.
46	1.21179E+02	.6003	250.0	2203.4	5.
47	2.58329E+01	.7522	275.0	252.2	2.
48	3.84260E+01	.7652	275.0	681.1	3.
49	8.00051E+01	.6865	275.0	1320.9	4.
50	1.03795E+02	.5087	275.0	2183.6	5.
51	1.98603E+01	.6723	300.0	246.6	2.
52	2.66374E+01	.8064	300.0	670.9	3.
53	4.35966E+01	.6350	300.0	1302.1	4.
54	8.15666E+01	.4652	300.0	2149.8	5.
55	3.58392E+02	.6760	165.0	1536.7	4.
56	1.64413E+02	.7667	225.0	2254.3	5.

MATERIAL CODE :150
MATERIAL :SOUNDCOAT N-5
LOG(FR)=LOG(F)-12(T-T0)/(525+T-T0)

NO.	MODULUS LB/IN**2	LOSS FACTOR	TEMP. DEG. F	FREQ. HZ	MODE NO.
1	1.36935E+02	.9084	101.0	386.8	2.
2	2.54239E+02	1.1894	101.0	1028.4	3.
3	2.65411E+02	1.2844	101.0	1887.9	4.
4	4.41699E+02	1.2584	101.0	3121.8	5.
5	4.75557E+02	1.5767	101.0	4589.2	6.
6	4.73908E+02	1.8453	101.0	6317.6	7.
7	7.16611E+01	.7923	125.0	354.0	2.
8	1.13582E+02	.9705	125.0	945.5	3.
9	1.55405E+02	.8200	125.0	1814.0	4.
10	2.03572E+02	.9177	124.0	2968.3	5.
11	2.67825E+02	.9716	123.0	4438.5	6.
12	2.71227E+02	1.2094	123.0	6160.4	7.
13	9.04335E+01	.8349	115.0	364.1	2.
14	1.44316E+02	1.1073	115.0	964.9	3.
15	1.90988E+02	.9672	115.0	1837.5	4.
16	3.33662E+02	.7783	114.0	3046.3	5.
17	3.42070E+02	1.1145	114.0	4489.3	6.
18	3.40645E+02	1.4496	114.0	6214.4	7.
19	3.16552E+02	1.0404	75.0	456.1	2.
20	7.09236E+02	1.2064	75.0	1234.0	3.
21	6.09371E+02	1.6477	76.0	2113.2	4.
22	9.44399E+02	1.7610	77.0	3470.2	5.
23	1.11855E+03	1.0072	47.0	572.9	2.
24	2.89656E+03	.8456	47.0	1564.9	3.
25	3.43919E+03	.8754	47.0	2831.7	4.
26	5.03561E+03	.8900	47.0	4547.3	5.
27	1.80204E+02	.9235	88.0	405.6	2.
28	3.12402E+02	1.3987	88.0	1067.6	3.
29	3.87048E+02	1.3281	88.0	1962.8	4.
30	5.66972E+02	1.2677	88.0	3199.9	5.
31	5.83667E+02	1.1267	61.0	520.6	2.
32	1.40431E+03	1.1673	61.0	1393.6	3.
33	1.37400E+03	1.5352	61.0	2476.5	4.
34	4.07980E+01	.6433	150.0	336.3	2.
35	6.60445E+01	.7591	150.0	914.4	3.
36	1.01584E+02	.5525	149.0	1775.2	4.
37	1.40267E+02	.6210	149.0	2918.5	5.
38	1.73317E+02	.6291	148.0	4367.1	6.
39	1.69190E+02	.7960	148.0	6076.9	7.
40	2.75343E+01	.5542	175.0	327.8	2.
41	4.83538E+01	.6156	175.0	900.4	3.
42	7.98293E+01	.3855	174.0	1755.3	4.
43	1.25193E+02	.3736	173.0	2899.6	5.
44	1.35739E+02	.4240	173.0	4327.1	6.
45	1.39136E+02	.4990	173.0	6034.0	7.
46	2.13160E+01	.4547	203.0	322.8	2.
47	4.07239E+01	.3864	203.0	892.2	3.
48	7.01638E+01	.2675	202.0	1742.5	4.
49	1.14177E+02	.2311	202.0	2879.4	5.
50	1.15166E+02	.2892	201.0	4297.2	6.
51	1.16030E+02	.3460	201.0	5997.4	7.
52	6.42213E+03	.6929	25.0	644.0	2.
53	1.03534E+04	.4202	25.0	1737.8	3.
54	1.17715E+04	.3830	25.0	3254.1	4.
55	1.51449E+04	.3696	25.0	5232.1	5.
56	1.55526E+04	.1646	25.0	7413.7	6.
57	2.53984E+04	.5187	-4.0	662.8	2.
58	2.67734E+04	.2101	-4.0	1814.0	3.
59	2.47347E+04	.2116	-3.0	3441.1	4.
60	3.24514E+04	.1794	-3.0	5599.3	5.
61	6.02175E+04	.6884	-26.0	669.3	2.
62	4.52598E+04	.1534	-26.0	1841.9	3.
63	4.12833E+04	.1216	-25.0	3532.9	4.
64	4.89044E+04	.1096	-25.0	5751.0	5.

MATERIAL CODE :167
MATERIAL :SOUNDCOAT M
LOG(FR)=LOG(F)-12(T-T0)/(525+T-T0)

NO.	MODULUS LB/IN**2	LOSS FACTOR	TEMP. DEG. F	FREQ. HZ	MODE NO.
1	2.42525E+04	.0736	-43.0	1815.8	3.
2	2.26997E+04	.0771	-43.0	3434.4	4.
3	2.58881E+04	.0671	-47.0	5528.9	5.
4	1.14418E+04	.3723	-25.0	654.7	2.
5	1.69021E+04	.1667	-25.0	1785.5	3.
6	1.90516E+04	.1531	-24.0	5360.0	5.
7	3.29147E+03	.5966	-2.0	632.0	2.
8	7.48623E+03	.4589	-1.0	1704.3	3.
9	7.62153E+03	.4154	-1.0	3110.5	4.
10	1.32520E+03	1.0931	12.0	591.7	2.
11	3.84756E+03	.7513	12.0	1613.1	3.
12	3.81781E+03	.8374	12.0	2885.9	4.
13	5.15391E+02	1.5026	26.0	528.2	2.
14	1.71436E+03	1.0760	26.0	1468.0	3.
15	2.80541E+02	1.1256	37.0	449.2	2.
16	7.75331E+02	1.4739	37.0	1286.3	3.
17	1.92795E+02	.3726	50.0	411.1	2.
18	3.94817E+02	1.6847	50.0	1130.4	3.
19	8.19467E+01	.7643	76.0	361.1	2.
20	1.61586E+02	.7903	76.0	1829.9	4.
21	2.24417E+02	.9792	76.0	3005.6	5.
22	2.90125E+02	1.1941	76.0	4484.9	6.
23	2.96576E+02	1.5013	76.0	6221.9	7.
24	4.71021E+01	.5701	101.0	341.9	2.
25	7.82217E+01	.6907	100.0	927.9	3.
26	1.06918E+02	.5034	99.0	1792.2	4.
27	1.58031E+02	.5231	99.0	2954.7	5.
28	1.90029E+02	.6341	99.0	4408.8	6.
29	2.02324E+02	.7472	99.0	6141.3	7.
30	3.44049E+01	.4912	126.0	333.8	2.
31	6.01467E+01	.4971	126.0	913.9	3.
32	8.96375E+01	.3265	126.0	1774.5	4.
33	1.32011E+02	.3119	126.0	2926.8	5.
34	1.56424E+02	.3648	126.0	4371.3	6.
35	1.62849E+02	.4295	126.0	6093.0	7.
36	4.90002E+01	.3554	153.0	903.6	3.
37	7.66605E+01	.2309	151.0	1760.4	4.
38	1.14754E+02	.2128	150.0	2906.9	5.
39	1.35559E+02	.2382	150.0	4342.9	6.
40	1.39950E+02	.2789	150.0	6056.8	7.
41	1.71588E+04	.1474	-50.0	661.1	2.
42	2.82523E+02	1.8558	51.0	1924.2	4.
43	4.51966E+02	1.9689	51.0	3178.6	5.
44	1.37544E+02	1.0269	76.0	965.5	3.
45	4.90002E+01	.3554	152.0	903.6	3.
46	1.57890E+04	.1484	-24.0	3335.6	4.

MATERIAL CODE : 56
MATERIAL :SOUNDFOIL NO. LT 12
LOG(FR)=LOG(F)-12(T-T0)/(525+T-T0)

NO.	MODULUS LB/IN**2	LOSS FACTOR	TEMP. DEG. F	FREQ. HZ	MODE NO.
1	3.07659E+01	.3219	150.0	320.7	2.
2	6.12631E+01	.2276	150.0	839.4	3.
3	1.14388E+02	.1354	149.0	1741.0	4.
4	1.96493E+02	.1081	149.0	2880.5	5.
5	1.77958E+02	.2137	149.0	5994.5	7.
6	3.99431E+01	.3768	125.0	324.8	2.
7	7.39665E+01	.2946	124.0	896.8	3.
8	1.26618E+02	.1798	124.0	1752.0	4.
9	2.11875E+02	.1460	124.0	2897.0	5.
10	2.34931E+02	.1588	124.0	4327.1	6.
11	2.09861E+02	.2446	124.0	6025.4	7.
12	4.92422E+01	.4326	102.0	328.8	2.
13	8.56473E+01	.3577	102.0	903.8	3.
14	1.40552E+02	.2210	102.0	1762.3	4.
15	2.26061E+02	.1825	102.0	2911.2	5.
16	2.43566E+02	.1987	102.0	4345.8	6.
17	2.21140E+02	.2677	102.0	6051.5	7.
18	7.51459E+01	.4931	74.0	339.3	2.
19	1.26759E+02	.4619	74.0	920.3	3.
20	1.75570E+02	.2768	74.0	1780.5	4.
21	2.58391E+02	.2546	74.0	2937.0	5.
22	2.92935E+02	.2760	74.0	4379.1	6.
23	2.71881E+02	.3359	74.0	6092.4	7.
24	1.26754E+02	.4453	51.0	353.3	2.
25	1.82586E+02	.4521	51.0	939.8	3.
26	2.20772E+02	.3530	51.0	1801.0	4.
27	3.19996E+02	.3623	51.0	2966.1	5.
28	3.39562E+02	.4903	51.0	6134.7	7.
29	2.94325E+02	.6365	26.0	976.0	3.
30	3.26244E+02	.5839	26.0	1840.0	4.
31	4.54733E+02	.6536	26.0	3020.1	5.
32	5.49069E+02	.6911	26.0	4490.8	6.
33	5.42371E+02	.8129	26.0	6220.5	7.
34	3.74300E+02	.7923	1.0	416.4	2.
35	5.64580E+02	1.0279	1.0	1059.6	3.
36	6.16863E+02	1.0406	1.0	1936.7	4.
37	8.59293E+02	1.2397	1.0	3162.4	5.
38	3.08857E+04	1.0474	-48.0	696.9	2.
39	5.45188E+04	.4635	-47.0	1903.8	3.
40	2.90043E+04	.2270	-47.0	3444.9	4.
41	5.27786E+04	.1760	-47.0	8265.0	6.
42	2.45532E+05	.9333	-74.0	704.3	2.
43	1.13237E+05	.0852	-74.0	1933.9	3.
44	4.02024E+04	.0422	-73.0	3540.2	4.
45	5.28064E+04	.1030	-73.0	5756.7	5.
46	4.30205E+04	.2126	-47.0	5641.5	5.
47	2.06555E+02	.1305	149.0	4303.3	6.
48	3.60048E+02	.4125	51.0	4416.4	6.

MATERIAL CODE :143
MATERIAL :E A R ISODAMP C-1002
LOG(FR)=LOG(F)-12(T-T0)/(525+T-T0)

NO.	MODULUS LB/IN**2	LOSS FACTOR	TEMP. DEG. F	FREQ. HZ	MODE NO.
1	5.20603E+03	.6780	102.0	1313.1	4.
2	4.26871E+03	1.1675	102.0	2172.5	5.
3	2.30022E+03	1.1242	125.0	1301.8	4.
4	4.92657E+03	1.4912	75.0	670.0	3.
5	1.22005E+04	.7336	75.0	1334.3	4.
6	1.35836E+04	.9020	75.0	2216.8	5.
7	8.19569E+03	1.9207	75.0	3296.5	6.
8	2.67686E+04	.8180	49.0	247.1	2.
9	4.55422E+04	.6946	49.0	717.7	3.
10	6.12754E+04	.6206	49.0	1443.5	4.
11	6.86048E+04	.6340	49.0	2417.5	5.
12	6.39118E+04	.7635	49.0	3599.5	6.
13	1.29962E+05	.3625	25.0	285.5	2.
14	1.64315E+05	.3003	25.0	835.0	3.
15	1.86141E+05	.2657	25.0	1678.2	4.
16	1.96223E+05	.2509	25.0	2808.9	5.
17	1.66677E+05	.2619	25.0	4164.7	6.
18	2.66147E+05	.1016	-2.5	327.8	2.
19	3.10423E+05	.0830	-2.5	955.6	3.
20	3.25371E+05	.0750	-2.5	1899.0	4.
21	3.27172E+05	.0721	-2.5	3150.2	5.
22	3.18634E+05	.0712	-2.5	4680.7	6.
23	1.84762E+05	.2149	11.0	303.5	2.
24	2.22589E+05	.1811	11.0	886.0	3.
25	2.43880E+05	.1590	11.0	1774.7	4.
26	2.48580E+05	.1439	11.0	2952.3	5.
27	2.39244E+05	.1592	11.0	4379.5	6.
28	6.47091E+04	.5828	35.0	262.2	2.
29	8.46395E+04	.5112	35.0	759.3	3.
30	1.14305E+05	.4411	35.0	2567.9	5.
31	1.09409E+05	.4508	35.0	3823.5	6.
32	3.39782E+05	.0295	-27.0	348.2	2.
33	4.03962E+05	.0307	-26.0	2010.5	4.
34	3.94629E+05	.0266	-26.0	3311.1	5.
35	3.75201E+05	.0285	-26.0	4885.0	6.
36	1.04933E+05	.4530	35.0	1531.9	4.
37	3.91050E+05	.0259	-27.0	1015.1	3.

MATERIAL CODE :143
MATERIAL :E A R EXODAMP C-2003
LOG(FR)=LOG(F)-12(T-T0)/(525+T-T0)

NO.	MODULUS LB/IN**2	LOSS FACTOR	TEMP. DEG. F	FREQ. HZ	MODE NO.
1	4.87892E+04	1.1889	102.0	203.4	2.
2	1.12477E+05	.7779	102.0	579.2	3.
3	1.68393E+05	.6110	102.0	1157.7	4.
4	2.08269E+05	.5752	102.0	1944.0	5.
5	2.14538E+05	.6406	102.0	2928.7	6.
6	6.88590E+04	.6952	125.0	1841.9	5.
7	6.13893E+04	.5744	125.0	2763.8	6.
8	3.06356E+05	.4896	75.0	222.6	2.
9	4.35238E+05	.3870	75.0	644.7	3.
10	5.22810E+05	.3448	75.0	1293.3	4.
11	5.91735E+05	.3238	75.0	2181.6	5.
12	6.10289E+05	.3229	75.0	3291.0	6.
13	8.45937E+05	.1622	49.0	256.5	2.
14	9.68118E+05	.1332	49.0	734.2	3.
15	1.06250E+06	.1136	49.0	1464.7	4.
16	1.12851E+06	.1075	49.0	2456.9	5.
17	1.14222E+06	.1017	49.0	3695.0	6.
18	6.42865E+05	.2433	60.0	244.6	2.
19	7.67675E+05	.2058	60.0	702.6	3.
20	8.51819E+05	.1840	60.0	1401.6	4.
21	9.19185E+05	.1722	60.0	2355.7	5.
22	9.49542E+05	.1593	60.0	3556.3	6.
23	1.38474E+05	.7326	87.0	210.3	2.
24	2.36247E+05	.5659	87.0	606.0	3.
25	3.05297E+05	.4975	87.0	1212.8	4.
26	3.66945E+05	.4600	87.0	2048.1	5.
27	3.86314E+05	.5030	87.0	3094.3	6.
28	1.19881E+06	.0490	25.0	275.6	2.
29	1.28567E+06	.0433	26.0	780.7	3.
30	1.37546E+06	.0378	26.0	1552.1	4.
31	4.71331E+04	.7871	125.0	1102.9	4.
32	1.42853E+06	.0359	26.0	2593.1	5.
33	1.44183E+06	.0336	26.0	3897.5	6.
34	1.43358E+04	.7853	151.0	1085.1	4.
35	2.45104E+04	.6067	150.0	1803.7	5.
36	1.43252E+04	1.2211	150.0	2702.7	6.
37	4.07566E+03	1.1498	175.0	1076.1	4.
38	1.55257E+04	.4077	174.0	1789.0	5.
39	3.55801E+03	1.9651	173.0	2680.0	6.
40	9.64921E+03	.4342	199.0	1774.8	5.

MATERIAL CODE :187
MATERIAL :BUTYL 268
LOG(FR)=LOG(F)-12(T-T0)/(525+T-T0)

NO.	MODULUS LB/IN**2	LOSS FACTOR	TEMP. DEG. F	FREQ. HZ	MODE NO.
1	9.41375E+01	.3393	149.0	336.7	2.
2	1.30928E+02	.4752	149.0	911.5	3.
3	2.28952E+02	.3768	149.0	1772.7	4.
4	3.59465E+02	.3963	149.0	2918.3	5.
5	5.46321E+02	.2645	148.0	4347.1	6.
6	7.22289E+02	.2597	148.0	6058.1	7.
7	1.16592E+02	.5104	124.0	342.9	2.
8	1.72307E+02	.6281	124.0	924.2	3.
9	2.73461E+02	.5836	124.0	1790.3	4.
10	4.38440E+02	.5238	124.0	2948.6	5.
11	8.10048E+02	.4556	123.0	6103.2	7.
12	1.75233E+02	.7517	100.0	356.9	2.
13	2.51811E+02	.9552	100.0	946.1	3.
14	3.87139E+02	.9020	100.0	1824.0	4.
15	5.49625E+02	.8355	100.0	2989.2	5.
16	6.73620E+02	1.1193	99.0	4414.5	6.
17	1.23764E+03	.7035	99.0	6229.0	7.
18	4.78645E+02	1.2767	74.0	1003.8	3.
19	6.56359E+02	1.3527	74.0	1897.5	4.
20	8.99073E+02	1.5622	74.0	3092.6	5.
21	6.59879E+02	1.3309	49.0	455.9	2.
22	1.12088E+03	1.7620	49.0	1170.4	3.
23	1.68698E+03	1.6410	25.0	586.3	2.
24	3.42449E+03	1.3600	25.0	1483.0	3.
25	4.50293E+02	1.1050	62.0	414.4	2.
26	7.08681E+02	1.5348	62.0	1063.9	3.
27	8.71675E+02	1.8594	62.0	1966.9	4.
28	1.03375E+03	2.2492	62.0	3154.3	5.
29	9.14249E+02	1.7123	35.0	511.1	2.
30	2.10642E+03	1.6380	35.0	1350.1	3.
31	6.41378E+03	.9901	.0	672.9	2.
32	1.12947E+04	.8810	.0	1770.5	3.
33	1.41135E+04	1.0108	.0	3267.7	4.
34	1.84280E+04	1.0811	-24.0	718.4	2.
35	3.28453E+04	.8253	-24.0	1947.9	3.
36	4.86650E+04	.5892	-23.0	3690.5	4.
37	5.44430E+04	.5339	-23.0	5856.8	5.
38	1.16020E+05	.1661	-51.0	2017.5	3.
39	1.27531E+05	.1508	-50.0	3864.7	4.
40	1.23065E+05	.1146	-50.0	6202.7	5.
41	3.18518E+02	.9627	74.0	387.6	2.

MATERIAL CODE :124
MATERIAL :BUTYL 268
LOG(FR)-LOG(F)-12(T-T0)/(525+T-T0)

NO.	MODULUS LB/IN**2	LOSS FACTOR	TEMP. DEG. F	FREQ. HZ	MODE NO.
1	1.33338E+04	.1726	122.0	256.5	2.
2	1.31689E+04	.2898	122.0	713.6	3.
3	1.40601E+04	.2819	122.0	1403.7	4.
4	1.43731E+04	.4710	122.0	3479.1	6.
5	1.56887E+04	.2058	101.0	253.1	2.
6	1.62684E+04	.2293	101.0	719.0	3.
7	1.70094E+04	.3488	101.0	1413.9	4.
8	1.74572E+04	.5656	101.0	3507.2	6.
9	1.48720E+04	.7978	101.0	4884.1	7.
10	1.93943E+04	.2596	75.0	260.6	2.
11	2.19016E+04	.3692	75.0	728.1	3.
12	2.50730E+04	.4135	75.0	1436.9	4.
13	2.55386E+04	.4950	75.0	2383.0	5.
14	2.77607E+04	.6549	75.0	5002.0	7.
15	2.68746E+04	.4160	49.0	264.5	2.
16	3.26943E+04	.4988	49.0	742.7	3.
17	4.42937E+04	.5796	49.0	2460.9	5.
18	3.23654E+04	1.0380	49.0	5052.2	7.
19	4.67638E+04	.5111	23.0	273.5	2.
20	6.16608E+04	.5678	23.0	777.9	3.
21	7.76262E+04	.5550	23.0	1561.1	4.
22	8.16876E+04	.6158	23.0	2600.9	5.
23	9.39921E+04	.6653	23.0	3950.6	6.
24	2.57505E+04	.5021	23.0	5467.2	7.
25	8.73608E+04	.5121	-2.0	290.1	2.
26	1.12351E+05	.5465	-2.0	834.9	3.
27	1.24384E+05	.5509	-2.0	1659.9	4.
28	1.51612E+05	.6399	-2.0	2836.9	5.
29	1.45883E+05	.4805	-17.0	311.7	2.
30	1.92243E+05	.5397	-17.0	912.1	3.
31	2.74383E+05	.6373	-17.0	3195.2	5.
32	1.88167E+05	.5054	-26.0	326.1	2.
33	2.54772E+05	.5349	-26.0	967.8	3.
34	3.19268E+05	.5707	-26.0	2001.2	4.
35	3.72056E+05	.4154	-40.0	380.6	2.
36	4.83680E+05	.3495	-40.0	1142.1	3.
37	5.51786E+05	.3161	-40.0	2326.3	4.
38	5.49974E+05	.3308	-40.0	3847.5	5.
39	5.91388E+05	.3155	-40.0	5951.1	6.
40	5.67371E+05	.2242	-40.0	8199.1	7.
41	5.09526E+05	.3013	-51.0	415.4	2.
42	5.95930E+05	.2484	-51.0	1215.1	3.
43	6.42335E+05	.2161	-51.0	2437.1	4.
44	6.81418E+05	.2089	-50.0	4110.1	5.
45	6.70604E+05	.0667	-50.0	6130.1	6.
46	7.00624E+05	.0654	-50.0	8689.0	7.
47	7.95437E+05	.0714	-75.0	476.9	2.
48	8.68351E+05	.0617	-75.0	1370.8	3.
49	8.89855E+05	.0613	-75.0	2707.5	4.
50	8.99098E+05	.0551	-75.0	4498.6	5.
51	9.13933E+05	.0247	-104.0	499.6	2.
52	9.81137E+05	.0247	-104.0	1429.6	3.
53	1.00018E+06	.0196	-104.0	2817.5	4.
54	1.00909E+06	.0187	-104.0	4680.1	5.
55	9.70297E+05	.0198	-104.0	6901.0	6.
56	9.33021E+05	.0196	-118.0	503.4	2.
57	4.09676E+04	.5198	49.0	1477.3	4.
58	2.48165E+05	.5862	-17.0	1886.0	4.
59	1.00377E+06	.0166	-118.0	1441.9	3.
60	1.03047E+06	.0158	-118.0	2847.5	4.
61	1.03647E+06	.0152	-117.0	4725.6	5.
62	1.01358E+06	.0148	-117.0	7008.4	6.

APPENDIX B

TABULAR DATA OF TESTS PERFORMED ON ISD-110

MATERIAL CODE :292
MATERIAL :ISD-110
LOG(FR)=LOG(F)-12(T-T0)/(525+T-T0)

NO.	MODULUS LB/IN**2	LOSS FACTOR	TEMP. DEG. F	FREQ. HZ	MODE NO.
1	6.59496E+04	.0758	.0	1809.3	3.
2	7.75242E+04	.0703	.0	4636.4	5.
3	6.40430E+04	.1051	10.0	3005.1	4.
4	6.39517E+04	.1022	10.0	4457.3	5.
5	4.78021E+04	.1364	20.0	1682.5	3.
6	5.39275E+04	.1431	20.0	2872.5	4.
7	5.92529E+04	.1546	20.0	4257.2	5.
8	3.96074E+04	.1851	30.0	1613.7	3.
9	4.49448E+04	.1904	30.0	2735.7	4.
10	4.87309E+04	.2105	30.0	4041.1	5.
11	2.08695E+04	.1936	40.0	631.1	2.
12	3.19013E+04	.2432	40.0	1523.9	3.
13	1.71544E+04	.2818	50.0	605.1	2.
14	2.49537E+04	.3166	50.0	1430.0	3.
15	2.92716E+04	.3488	50.0	2442.4	4.
16	3.23394E+04	.3425	50.0	3651.1	5.
17	1.34532E+04	.4223	60.0	574.4	2.
18	1.86141E+04	.4234	60.0	1324.8	3.
19	9.15213E+03	.5453	70.0	521.7	2.
20	1.39418E+04	.5422	70.0	1228.5	3.
21	1.51444E+04	.5605	70.0	2070.9	4.
22	1.56020E+04	.5546	70.0	3094.6	5.
23	5.69478E+03	.7041	80.0	460.4	2.
24	8.62967E+03	.8539	80.0	1093.8	3.
25	9.12739E+03	.7853	80.0	1861.1	4.
26	3.39902E+03	1.1844	90.0	409.1	2.
27	4.42303E+03	1.5488	90.0	955.2	3.
28	5.57129E+03	1.1165	90.0	1715.3	4.
29	8.68837E+03	.9961	90.0	2813.9	5.
30	1.83373E+03	1.9517	100.0	359.7	2.
31	3.33620E+03	1.2905	100.0	897.4	3.
32	2.57761E+03	1.7264	100.0	1571.9	4.
33	4.07161E+03	1.6717	100.0	2592.9	5.
34	1.21731E+03	1.4938	110.0	323.4	2.
35	1.87686E+03	1.3196	110.0	825.8	3.
36	1.68607E+03	1.7155	110.0	1522.2	4.
37	2.94994E+03	1.3740	110.0	2526.8	5.
38	1.08525E+03	1.2315	120.0	783.9	3.
39	1.02417E+03	1.6707	120.0	1483.5	4.
40	1.24180E+03	1.8193	120.0	2433.3	5.
41	3.62190E+02	1.3285	130.0	279.2	2.
42	8.71741E+02	1.1442	130.0	771.4	3.
43	5.34784E+02	3.0413	130.0	2392.5	5.
44	3.43434E+02	1.8067	140.0	742.5	3.
45	8.44893E+01	2.0550	160.0	263.0	2.
46	1.56794E+02	1.7852	160.0	730.2	3.
47	7.21701E+01	2.3247	180.0	723.7	3.
48	7.44801E+04	.0734	.0	3125.1	4.
49	5.59567E+04	.1026	10.0	1745.3	3.
50	5.06584E+02	2.4397	130.0	1452.9	4.
51	2.21433E+02	1.7399	150.0	734.5	3.
52	5.04811E+01	2.5033	170.0	260.9	2.

MATERIAL CODE :310
MATERIAL :ISD-110
LOG(FR)=LOG(F)-12(T-T0)/(525+T-T0)

NO.	MODULUS LB/IN**2	LOSS FACTOR	TEMP. DEG. F	FREQ. HZ	MODE NO.
1	3.74246E+04	.0535	.0	869.9	2.
2	5.54597E+04	.0577	.0	2249.1	3.
3	7.89653E+04	.0894	.0	6277.3	5.
4	3.36404E+04	.0766	10.0	859.4	2.
5	4.64644E+04	.1073	10.0	2127.7	3.
6	3.05362E+04	.0997	20.0	849.4	2.
7	4.21079E+04	.1046	20.0	2149.8	3.
8	6.01367E+04	.1664	20.0	5896.9	5.
9	2.39723E+04	.1329	30.0	824.7	2.
10	3.54489E+04	.1439	30.0	2084.0	3.
11	2.32874E+04	.1923	40.0	322.2	2.
12	3.01066E+04	.2040	40.0	2021.0	3.
13	2.46807E+04	.2585	50.0	1941.6	3.
14	9.79735E+03	.3426	60.0	713.3	2.
15	1.81530E+04	.3409	60.0	1816.0	3.
16	8.82361E+03	.3414	70.0	696.6	2.
17	1.42512E+04	.4693	70.0	1722.0	3.
18	6.51511E+03	.5232	80.0	657.7	2.
19	1.04962E+04	.5876	90.0	1600.3	3.
20	1.72662E+04	.9879	80.0	4423.5	5.
21	4.59468E+03	.7137	90.0	611.0	2.
22	7.35736E+03	.6201	90.0	1474.3	3.
23	1.50613E+04	.9557	90.0	4248.4	5.
24	2.81517E+03	.2712	100.0	539.5	2.
25	4.03881E+03	1.1945	100.0	1277.7	3.
26	1.38235E+04	.9890	100.0	4157.6	5.
27	1.97986E+03	1.0135	110.0	492.2	2.
28	2.99264E+03	1.1816	110.0	1181.5	3.
29	1.32393E+04	.6814	110.0	4086.1	5.
30	1.22464E+03	1.1382	120.0	435.7	2.
31	2.05244E+03	1.1810	120.0	1086.4	3.
32	8.04326E+02	1.1235	130.0	395.0	2.
33	1.24720E+03	1.2632	130.0	998.3	3.
34	4.70359E+02	1.1596	140.0	359.2	2.
35	6.72475E+02	1.3438	140.0	928.8	3.
36	7.83220E+02	1.4976	140.0	1756.4	4.
37	3.09897E+02	1.0961	150.0	340.1	2.
38	4.39635E+02	1.3344	150.0	898.4	3.
39	5.46042E+02	1.5358	150.0	1723.5	4.
40	8.66611E+02	1.3380	150.0	2847.4	5.
41	2.04048E+02	1.0508	160.0	326.8	2.
42	3.15248E+02	1.8875	160.0	881.5	3.
43	3.26673E+02	1.7765	160.0	1692.7	4.
44	4.62334E+02	1.7065	160.0	2791.4	5.
45	1.47984E+02	.9825	170.0	319.3	2.
46	2.44363E+02	1.1074	170.0	870.2	3.
47	2.35352E+02	1.6813	170.0	1677.2	4.
48	3.12044E+02	1.6998	170.0	2765.9	5.
49	1.66171E+02	1.7277	180.0	1665.7	4.
50	2.00954E+02	1.8631	180.0	2747.4	5.
51	1.21291E+02	1.6734	190.0	1657.4	4.
52	1.01097E+02	1.5682	200.0	1652.5	4.
53	9.43946E+01	2.2088	200.0	2725.7	5.

MATERIAL CODE :283
MATERIAL :ISD-110
LOG(FR)=LOG(F)-12(T-T0)/(525+T-T0)

NO.	MODULUS LB/IN**2	LOSS FACTOR	TEMP. DEG. F	FREQ. HZ	MODE NO.
1	1.36335E+05	.0309	-140.8	13.6	1.
2	1.34885E+05	.0312	-137.2	13.5	1.
3	1.33000E+05	.0324	-133.6	13.4	1.
4	1.30969E+05	.0332	-130.0	13.3	1.
5	1.29084E+05	.0344	-126.4	13.2	1.
6	1.28068E+05	.0343	-122.8	13.2	1.
7	1.27633E+05	.0355	-119.2	13.1	1.
8	1.23282E+05	.0370	-115.6	12.9	1.
9	1.18931E+05	.0402	-108.4	12.7	1.
10	1.17045E+05	.0421	-104.8	12.6	1.
11	1.09213E+05	.0496	-86.8	12.2	1.
12	1.07763E+05	.0506	-83.2	12.1	1.
13	1.02397E+05	.0525	-79.6	12.0	1.
14	1.01962E+05	.0541	-76.0	11.9	1.
15	1.00511E+05	.0555	-72.4	11.7	1.
16	9.86257E+04	.0575	-68.8	11.6	1.
17	9.52898E+04	.0590	-65.2	11.4	1.
18	9.32593E+04	.0609	-61.6	11.3	1.
19	8.99234E+04	.0647	-58.0	11.1	1.
20	8.65875E+04	.0689	-54.4	10.9	1.
21	8.36868E+04	.0739	-50.8	10.7	1.
22	7.97708E+04	.0801	-47.2	10.5	1.
23	7.68700E+04	.0877	-43.6	10.3	1.
24	7.35341E+04	.0983	-40.0	10.1	1.
25	6.86029E+04	.1130	-36.4	9.8	1.
26	6.48319E+04	.1320	-32.8	9.5	1.
27	6.13510E+04	.1370	-29.2	9.3	1.
28	5.84502E+04	.1340	-25.6	9.1	1.
29	5.46792E+04	.1330	-22.0	8.8	1.
30	5.22136E+04	.1350	-18.4	8.6	1.
31	4.93128E+04	.1410	-14.8	8.4	1.
32	4.52518E+04	.1490	-11.2	8.1	1.
33	4.16258E+04	.1600	-7.6	7.8	1.
34	3.81449E+04	.1700	-4.0	7.5	1.
35	3.48091E+04	.1840	-.4	7.2	1.
36	3.24885E+04	.1980	3.2	7.0	1.
37	2.88625E+04	.2130	6.8	6.6	1.
38	2.62518E+04	.2310	10.4	6.4	1.
39	2.27709E+04	.2500	14.0	6.0	1.
40	2.00152E+04	.2730	17.6	5.7	1.
41	1.79847E+04	.2950	21.2	5.4	1.
42	1.52290E+04	.3180	24.8	5.1	1.
43	1.26618E+04	.3450	28.4	4.8	1.
44	1.11244E+04	.3760	32.0	4.6	1.
45	9.18089E+03	.4120	35.6	4.3	1.
46	7.44044E+03	.4560	39.2	4.0	1.
47	5.94655E+03	.5110	42.8	3.7	1.
48	4.68472E+03	.5690	46.4	3.5	1.
49	3.69846E+03	.6190	50.0	3.3	1.
50	2.85724E+03	.6730	53.6	3.1	1.
51	2.24808E+03	.7040	57.2	3.1	1.
52	1.72595E+03	.7430	60.8	2.9	1.
53	1.35900E+03	.7360	64.4	2.8	1.
54	9.90608E+02	.7540	68.0	2.7	1.
55	7.49345E+02	.7350	71.6	2.7	1.
56	5.17725E+02	.7010	75.2	2.6	1.
57	1.94351E+02	.5730	82.4	2.5	1.
58	7.58547E+01	.4590	86.0	2.5	1.
59	1.15595E+05	.0430	-101.2	12.5	1.
60	1.13129E+05	.0450	-97.6	12.4	1.
61	1.11679E+05	.0460	-94.0	12.3	1.
62	1.11244E+05	.0474	-90.4	12.3	1.
63	3.42289E+02	.6240	78.8	2.6	1.
64	1.20816E+05	.0388	-112.0	12.8	1.

MATERIAL CODE :291
MATERIAL :ISD-110
LOG(FR)=LOG(F)-12(T-T0)/(525+T-T0)

NO.	MODULUS LB/IN**2	LOSS FACTOR	TEMP. DEG. F	FREQ. HZ	MODE NO.
1	3.07480E+05	.0254	-94.0	35.0	1.
2	2.88625E+05	.0266	-85.0	35.0	1.
3	2.77022E+05	.0292	-76.0	35.0	1.
4	2.75572E+05	.0306	-67.0	35.0	1.
5	2.50915E+05	.0360	-58.0	35.0	1.
6	2.27709E+05	.0424	-49.0	35.0	1.
7	2.19007E+05	.0480	-40.0	35.0	1.
8	2.07404E+05	.0555	-31.0	35.0	1.
9	1.87099E+05	.0636	-22.0	35.0	1.
10	1.66793E+05	.0706	-13.0	35.0	1.
11	1.47938E+05	.0820	-4.0	35.0	1.
12	1.23427E+05	.0924	5.0	35.0	1.
13	8.21830E+04	.1420	14.0	35.0	1.
14	6.48319E+04	.2070	23.0	35.0	1.
15	3.61144E+04	.2440	32.0	35.0	1.
16	1.68244E+04	.2950	41.0	35.0	1.
17	1.43587E+04	.4300	50.0	35.0	1.
18	3.30685E+05	.0222	-94.0	11.0	1.
19	3.08930E+05	.0244	-85.0	11.0	1.
20	2.94427E+05	.0260	-76.0	11.0	1.
21	2.94427E+05	.0280	-67.0	11.0	1.
22	2.71221E+05	.0322	-58.0	11.0	1.
23	2.42213E+05	.0376	-49.0	11.0	1.
24	2.23353E+05	.0456	-40.0	11.0	1.
25	2.10305E+05	.0532	-31.0	11.0	1.
26	1.91450E+05	.0608	-22.0	11.0	1.
27	1.71145E+05	.0718	-13.0	11.0	1.
28	1.53740E+05	.0870	-4.0	11.0	1.
29	1.33290E+05	.1050	5.0	11.0	1.
30	1.01962E+05	.1470	14.0	11.0	1.
31	4.84426E+04	.1700	23.0	11.0	1.
32	3.93052E+04	.2060	32.0	11.0	1.
33	1.78396E+04	.3090	41.0	11.0	1.
34	1.40252E+04	.4700	50.0	11.0	1.

APPENDIX C

J-85 AFTERBURNER LINER FOLLOW-UP TEST DATA SHEETS

Project J-85 Afterburner Liner Follow-up Experiment No. 01

1) Substrate Hastelloy X Alloy base Cobalt
Mfr. Huntington Alloy Density 8.23 g/cc Thickness 0.47625 cm.

2) Material Base J85-1 Additives None
Mfr. UDRI Density 2.82 g/cc Thickness 0.0194 cm.

3) Overcoat 1 None Additives
Mfr. Density Thickness

4) Overcoat 2 Additives
Mfr. Density Thickness

5) Overcoat 3 Additives
Mfr. Density Thickness

Overall Pretest Description gray-blue tint overall

Overall Posttest Description coating discolored with rough surface

THERMAL HISTORY

Temperature °C	815	815								
Duration (hrs.)	4.3	4.2								

CONDITION	REMARKS
• Creep from edge	None
• Flake from edge	None
• Peel from edge	None
• Gravity flow	Some evidence
• Downstream flow	Some evidence
• Seep through overcoat	N.A.
• Devitrification	Very evident over entire surface.
•	

Remarks Composition = Corning 0010 + 10% AL_2O_3 1% Co_2O_3

Project J-85 ABL Follow-up Experiment No. 02

1) Substrate Hastelloy X Alloy base Cobalt
Mfr. Huntington Alloy Density 8.23 g/cc Thickness 0.47625 cm.

2) Material Base J-85-2 Additives None
Mfr. UDRI Density 2.82 g/cc Thickness 0.0198 cm.

3) Overcoat 1 None Additives
Mfr. Density Thickness

4) Overcoat 2 Additives
Mfr. Density Thickness

5) Overcoat 3 Additives
Mfr. Density Thickness

Overall Pretest Description dark gray tint

Overall Posttest Description glossy but with signs of deterioration in some spots.

THERMAL HISTORY

Temperature °C	815	815								
Duration (hrs.)	4.3	4.2								

CONDITION REMARKS

- Creep from edge Some
- Flake from edge None
- Peel from edge None
- Gravity flow Very little
- Downstream flow None
- Seep through overcoat N.A.
- Devitrification Some obvious evidence in certain areas.
-

Remarks Composition = Corning 0010 + 10% AL_2O_3 + 6% Na_2O + 1% Co_2O_3

Project J-85 ABL Follow-up — Experiment No. 03

1) Substrate Hastelloy — Alloy base Cobalt
Mfr. Huntington Alloy — Density 8.23 g/cc — Thickness 0.47625 cm

2) Material Base J-85-3 — Additives None
Mfr. UDRI — Density 2.82 g/cc — Thickness 0.0148

3) Overcoat 1 None — Additives
Mfr. — Density — Thickness

4) Overcoat 2 — Additives
Mfr. — Density — Thickness

5) Overcoat 3 — Additives
Mfr. — Density — Thickness

Overall Pretest Description: dark gray overall

Overall Posttest Description: dark gray with some debonding occurring

THERMAL HISTORY

Temperature °C	815	815								
Duration (hrs.)	4.3	4.2								

CONDITION	REMARKS
• Creep from edge	Not obvious
• Flake from edge	In spots
• Peel from edge	Some debonding from substrate in evidence
• Gravity flow	Negligible
• Downstream flow	None
• Seep through overcoat	N.A.
• Devitrification	Not certain
•	

Remarks: Composition = Corning 0010 + 12.5% AL_2O_3 + 2% Co_2O_3

Project J-85 ABL Follow-up Experiment No. 04

1) Substrate Hastelloy X Alloy base Cobalt
Mfr. Huntington Alloy Density 8.23 g/cc Thickness 0.47625 cm.

2) Material Base J-85-4 Additives None
Mfr. UDRI Density 2.82 g/cc Thickness 0.0203 cm

3) Overcoat 1 None Additives
Mfr. Density Thickness

4) Overcoat 2 Additives
Mfr. Density Thickness

5) Overcoat 3 Additives
Mfr. Density Thickness

Overall Pretest Description

Overall Posttest Description Most of coating came off substrate sometime during second exposure period

THERMAL HISTORY

Temperature °C	815	815								
Duration (hrs.)	4.3	4.2								

CONDITION REMARKS

- Creep from edge
- Flake from edge
- Peel from edge
- Gravity flow
- Downstream flow
- Seep through overcoat
- Devitrification
- Debonding Approximately 80% of coating came off during test

Remarks

Project J-85 ABL Follow-up Experiment No. 05

1) Substrate Hastelloy X Alloy base Cobalt
Mfr. Huntington Alloy Density 8.23 g/cc Thickness 0.47625 cm.

2) Material Base J-85-5 Additives None
Mfr. UDRI Density 2.82 g/cc Thickness 0.0148

3) Overcoat 1 None Additives
Mfr. Density Thickness

4) Overcoat 2 Additives
Mfr. Density Thickness

5) Overcoat 3 Additives
Mfr. Density Thickness

Overall Pretest Description

Overall Posttest Description Coating came off substrate sometime during second exposure period.

THERMAL HISTORY

Temperature °C	815	815								
Duration (hrs.)	4.3	4.2								

CONDITION REMARKS

- Creep from edge
- Flake from edge
- Peel from edge
- Gravity flow
- Downstream flow
- Seep through overcoat
- Devitrification
- Debonding 100% of coating came off during test

Remarks

Project Enamel Development Experiment No. 06

1) Substrate Hastelloy X Alloy base Cobalt
Mfr. Huntington Alloys Density 8.23 g/cc Thickness 0.47625 cm.

2) Material Base 8871 Additives None
Mfr. Corning Density ______ Thickness ______

3) Overcoat 1 None Additives ______
Mfr. ______ Density ______ Thickness ______

4) Overcoat 2 None Additives ______
Mfr. ______ Density ______ Thickness ______

5) Overcoat 3 None Additives ______
Mfr. ______ Density ______ Thickness ______

Overall Pretest Description smooth, blue-gray

Overall Posttest Description gray-blue with mottled surface

THERMAL HISTORY

Temperature °C	540	540								
Duration (hrs.)	4.3	4.2								

CONDITION	REMARKS
• Creep from edge	Some
• Flake from edge	Some
• Peel from edge	None
• Gravity flow	None
• Downstream flow	None
• Seep through overcoat	N.A.
• Devitrification	30%-60% of surface
•	

Remarks ______

Project Enamel Development Experiment No. 07

1) Substrate Hastelloy Alloy base Cobalt
Mfr. Huntington Alloys Density 8.23 g/cc Thickness 0.47625 cm.

2) Material Base 8871 Additives + 3%
Mfr. Corning Density Thickness

3) Overcoat 1 None Additives
Mfr. Density Thickness

4) Overcoat 2 None Additives
Mfr. Density Thickness

5) Overcoat 3 None Additives
Mfr. Density Thickness

Overall Pretest Description Blue-gray with smooth, glossy surface

Overall Posttest Description gray-blue with some bubbles and general mottled appearance; dark blue where flaking had occurred.

THERMAL HISTORY

Temperature °C	540	540								
Duration (hrs.)	4.3	4.2								

CONDITION	REMARKS
• Creep from edge	Some
• Flake from edge	Much in evidence (likely from thermal shock)
• Peel from edge	None
• Gravity flow	None
• Downstream flow	None
• Seep through overcoat	N.A.
• Devitrification	Over 50% of surface
•	

Remarks

Project Enamel Development Experiment No. 08

1) Substrate Hastelloy X Alloy base Cobalt
Mfr. Huntington Alloys Density 8.23 g/cc Thickness 0.47625 cm

2) Material Base Sulfate 2 Additives None
Mfr. UDRI Density Thickness

3) Overcoat 1 None Additives
Mfr. Density Thickness

4) Overcoat 2 Additives
Mfr. Density Thickness

5) Overcoat 3 Additives
Mfr. Density Thickness

Overall Pretest Description White-blue, evenly smooth

Overall Posttest Description Whitish-gray, mottled surface

THERMAL HISTORY

Temperature °C	399									
Duration (hrs.)	2.0									

CONDITION REMARKS

- Creep from edge Some
- Flake from edge None
- Peel from edge None
- Gravity flow Negligible
- Downstream flow Negligible
- Seep through overcoat N.A.
- Devitrification 85-95% after 2 hours
-

Remarks Test terminated after 2 hours with much evidence of reactive attack.

Project Enamel Development Experiment No. 09

1) Substrate Hastelloy X Alloy base Cobalt
Mfr. Huntington Alloys Density 8.23 g/cc Thickness 0.47625 cm

2) Material Base Lead 1 Additives None
Mfr. UDRI Density Thickness

3) Overcoat 1 None Additives
Mfr. Density Thickness

4) Overcoat 2 None Additives
Mfr. Density Thickness

5) Overcoat 3 None Additives
Mfr. Density Thickness

Overall Pretest Description Smooth glossy gray

Overall Posttest Description Lighter gray with dull, mottled surface

THERMAL HISTORY

Temperature °C	635	635	635	635	635					
Duration (hrs.)	4.0	4.0	8.0	8.0	4.0					

CONDITION REMARKS

- Creep from edge Some
- Flake from edge Some
- Peel from edge None
- Gravity flow Negligible
- Downstream flow Negligible
- Seep through overcoat N.A.
- Devitrification Much in evidence
- Bubbling Some evidence in spots

Remarks Material showed degradation over entire surface.

Project Enamel Development Experiment No. 010

1) Substrate Hastelloy X Alloy base Cobalt
Mfr. Huntington Alloys Density 8.23 g/cc Thickness 0.47625 cm.

2) Material Base Lead 2 Additives None
Mfr. UDRI Density Thickness

3) Overcoat 1 None Additives
Mfr. Density Thickness

4) Overcoat 2 None Additives
Mfr. Density Thickness

5) Overcoat 3 None Additives
Mfr. Density Thickness

Overall Pretest Description Dark gray with smooth, glossy surface

Overall Posttest Description Gray-white with rough mottled surface

THERMAL HISTORY

Temperature °C	635	635	635	635	635					
Duration (hrs.)	8.0	8.0	4.0	4.0	4.0					

CONDITION	REMARKS
• Creep from edge	Some
• Flake from edge	Some
• Peel from edge	None
• Gravity flow	Negligible
• Downstream flow	Negligible
• Seep through overcoat	N.A.
• Devitrification	85-100% of surface area
• Bubbling	Some evidence over entire surface

Remarks Degradation began after 1st 8 hours of exposure. Degradation seemed to proceed steadily afterwards.

Project J-85 ABL Follow-up Experiment No. 011

1) Substrate Hastelloy X Alloy base Co
Mfr. Huntington Alloys Density 9.13 g/cc Thickness 0.1875 cm.

2) Material Base J-85-14 Additives None
Mfr. UDRI Density 2.64 g/cc Thickness ≃.018 cm.

3) Overcoat 1 1252 Additives None
Mfr. O-Hommel Density Thickness ≃.005 cm

4) Overcoat 2 None Additives
Mfr. Density Thickness

5) Overcoat 3 None Additives
Mfr. Density Thickness

Overall Pretest Description Bluish-white with evidence of white spots (sputter) over lower 30% of surface

Overall Posttest Description No significant change after 30 hours

THERMAL HISTORY

Temperature °C	675	675	675	675	675	675				
Duration (hrs.)	12.0	4.0	4.0	4.0	4.0	2.0				

CONDITION REMARKS

- Creep from edge A small amount
- Flake from edge Some apparent after 4 hours (due to thermal shock)
- Peel from edge None
- Gravity flow None
- Downstream flow None
- Seep through overcoat Some evidence in spots
- Devitrification None obvious after 30 hours
- Open cavitation "pock marks" of small dimension in spots

Remarks Composition = 74.5% SiO_2 + 10.75% CaO + 6.375% Na_2O + 6.375% $KHCO_3$ + 2% Co_2O_3

Project Enamel Development Experiment No. 012

1) Substrate Inconel 600 Alloy base Co
Mfr. Inco Density Thickness

2) Material Base AMB5 Additives None
Mfr. UDRI Density Thickness

3) Overcoat 1 None Additives
Mfr. Density Thickness

4) Overcoat 2 None Additives
Mfr. Density Thickness

5) Overcoat 3 None Additives
Mfr. Density Thickness

Overall Pretest Description Uniform smooth, glossy, dark gray

Overall Posttest Description Surface rough with partial loss of gloss, "bubbling" on surface, lighter gray color

THERMAL HISTORY

Temperature °C	630	630	630	630	630	630	630			
Duration (hrs.)	4.0	4.0	4.0	4.0	4.0	4.0	4.0			

CONDITION	REMARKS
• Creep from edge	Some
• Flake from edge	Some
• Peel from edge	Negligible
• Gravity flow	Negligible
• Downstream flow	Negligible
• Seep through overcoat	N.A.
• Devitrification	About 10% visually evident
• "Bubbling"	About 75% coverage after 28 hours

Remarks Some deterioration seen after 20 hours; testing terminated after 28 hours due to notable changes in overall appearance.

Project Enamel Development | Experiment No. 013

1) Substrate Inco 600 | Alloy base Co
Mfr. Inco | Density | Thickness

2) Material Base Sulfate 3 | Additives None
Mfr. UDRI | Density | Thickness

3) Overcoat 1 None | Additives
Mfr. | Density | Thickness

4) Overcoat 2 None | Additives
Mfr. | Density | Thickness

5) Overcoat 3 None | Additives
Mfr. | Density | Thickness

Overall Pretest Description Blueish-white with globular appearance with smooth surface overall, without gloss (flat)

Overall Posttest Description Whitish-blue with smooth surface

THERMAL HISTORY

Temperature °C	399									
Duration (hrs.)	2.0									

CONDITION	REMARKS
• Creep from edge	
• Flake from edge	
• Peel from edge	
• Gravity flow	
• Downstream flow	
• Seep through overcoat	
• Devitrification	80 to 95% after 2 hours
•	

Remarks Test terminated after 2 hours, with no obvious signs of reactive attack. Surface, however, was mostly devitrified.

Project Enamel Development Experiment No. 014

1) Substrate Inconel 600 Alloy base Co
Mfr. Inco Density Thickness

2) Material Base Sulfate S-7 Additives None
Mfr. UDRI Density Thickness

3) Overcoat 1 None Additives
Mfr. Density Thickness

4) Overcoat 2 None Additives
Mfr. Density Thickness

5) Overcoat 3 None Additives
Mfr. Density Thickness

Overall Pretest Description Milky-white with foamy appearance, smooth and glossy

Overall Posttest Description Lime-white with dull, mottled surface

THERMAL HISTORY

Temperature °C	399									
Duration (hrs.)	2.0									

CONDITION REMARKS

- Creep from edge Some
- Flake from edge None
- Peel from edge None
- Gravity flow Some in evidence
- Downstream flow Negligible
- Seep through overcoat N.A.
- Devitrification 90-100% total
-

Remarks Test terminated after 2 hours. No obvious sign of degradation by reaction,but almost complete devitrification.

Project Enamel Development Experiment No. 015

1) Substrate Inconel 600 Alloy base Co
Mfr. Density Thickness

2) Material Base Sulfate S-11 Additives None
Mfr. UDRI Density Thickness

3) Overcoat 1 None Additives
Mfr. Density Thickness

4) Overcoat 2 None Additives
Mfr. Density Thickness

5) Overcoat 3 None Additives
Mfr. Density Thickness

Overall Pretest Description Clear violet with some platelet structure visible, surface smooth.

Overall Posttest Description Milky-violet with much evidence of devitrification and phase-separation

THERMAL HISTORY

Temperature °C	399									
Duration (hrs.)	2.0									

CONDITION	REMARKS
• Creep from edge	None
• Flake from edge	Some in evidence
• Peel from edge	None
• Gravity flow	Some evidence over entire surface
• Downstream flow	Negligible
• Seep through overcoat	N.A.
• Devitrification	Much evidence over entire surface
•	

Remarks Surface mottled and rough with cracks (possible due to migration of material over substrate)

Project Enamel Development Experiment No. 016

1) Substrate Inconel 600 Alloy base Co
Mfr. ______ Density ______ Thickness ______

2) Material Base Sulfate S-11 Additives None
Mfr. UDRI Density ______ Thickness ______

3) Overcoat 1 None Additives ______
Mfr. ______ Density ______ Thickness ______

4) Overcoat 2 None Additives ______
Mfr. ______ Density ______ Thickness ______

5) Overcoat 3 None Additives ______
Mfr. ______ Density ______ Thickness ______

Overall Pretest Description Clear-violet with some evidence of platelet structure, surface relatively smooth

Overall Posttest Description Milky-white with trace of violet tint, much evidence of devitrification and phase separation

THERMAL HISTORY

Temperature °C	399									
Duration (hrs.)	2.0									

CONDITION	REMARKS
• Creep from edge	None
• Flake from edge	None
• Peel from edge	None
• Gravity flow	Some in evidence
• Downstream flow	Some in evidence
• Seep through overcoat	N.A.
• Devitrification	Very noticeable over entire surface
•	

Remarks Surface mottled and rough with surface cracks (possibly due to migration of material over substrate)

APPENDIX D

MAGNA COMPUTER PROGRAM

MAGNA is a proprietary computer program of the University of Dayton. User's manuals can be obtained from the Air Force (Reference 10), or a more recent version (Reference 11) can be obtained from the University of Dayton. This program is currently available to Government personnel and Government contractors for use on the ASD CYBER computer system. The program also is available on a time share basis on the CRAY-1 computer of

United Information Services, Inc.
2525 Washington
Kansas City, Missouri 64114

Separate annual lease agreements can be arranged through the Director of the University of Dayton Research Institute, Dayton, Ohio 45469.

☆U.S.Government Printing Office: 1983 — 759-062/564

END

FILMED

1-84

DTIC